Synthesis and Functionalization of Three-Dimensional Covalent Organic Frameworks

by

Xingjian Ma

A dissertation submitted in partial fulfillment
of the requirements for the degree of
Doctor of Philosophy
(Chemical Engineering)
in The University of Michigan
2019

Doctoral Committee:

Associate Professor Timothy F. Scott, Chair
Professor Brian J. Love
Associate Professor Sunitha Nagrath
Professor Robert M. Ziff

Xingjian Ma

xjma@umich.edu

ORCID ID: 0000-0001-9454-4065

DEDICATION

This dissertation is dedicated to

Mom and Dad

Xinyi

For their endless love and support

ACKNOWLEDGEMENTS

First, I would like to thank my PhD advisor Professor Timothy F. Scott, for his constant guidance, support, and encouragement throughout my doctoral studies at the University of Michigan. I am especially thankful for his understanding of my foray into consulting and his patience with all the research difficulties I have encountered. I would also like to express my gratitude to my dissertation committee members, Professor Sunitha Nagrath, Professor Robert Ziff and Professor Brian Love for their constructive feedback for my project.

I must emphasize how lucky I am to have extremely supportive and encouraging lab mates including Dr. Scott Zavada, Dr. Joseph Furgal, Dr. Tao Wei, Dr. Dowon Ahn, Dr. Megan Dunn, Dr. Harry van der Laan, Samuel Leguizamon, Abdulla Alqubati, Austin Bingham, Alex Commisso, Futianyi Wang, Dr. Jae Hwan Jung, Dr. Junting Li, Sameer Sathe, Dan Li, Nathan Wood, and Aishwarya Chandrashekar. I want to thank them for building the family atmosphere of our Polymer Dojo and I really appreciate their camaraderie and friendship over these last five years. I am especially appreciative of the mentorship from Scott, Tao, and Megan during my early years in the group, and for their invaluable advice on research and life. I would also like to mention Harry and Alex for maintaining a safe lab environment and Sam and Abdulla for their efforts towards ensuring smooth daily operation and cleanliness of our lab.

I have had the fortune of working with two excellent undergraduate researchers, Sari B. Goldstein and Kristin Lewis, who assisted me with many tasks associated with my research. I want to mention Sari specifically for helping me with hundreds of scandium triflate COF synthesis trials that ultimately led to a breakthrough.

I want to thank my fellow Chemical Engineering graduate students who have assisted me with the various instruments I have needed during my studies, including Doug Montjoy, who helped me with scanning electron microscopy (SEM), and Jiwoong Kang, Zixuan Wang, and Xiaowen Zhao for helping me with BET surface area measurements. I would also like to thank Dr. Daniel Holmes from the Chemistry Department at Michigan State University for running Solid-state Cross-Polarization Magic Angle Spinning Carbon-13 Nuclear Magnetic Resonance (CP/MAS ^{13}C NMR) on my samples. I am also grateful for the staff members of the Chemical Engineering department, particularly Susan Hamlin, Barbara Perry, Kelly Raickovich, Jennifer Downey, and Shelley Fellers for their assistance with chemical purchases and many other things.

I have had the fortune of befriending some amazing individuals during my time at Michigan. Tingwen Lo, Tianhui Ma, Yufei Wei, and Xiaowen Zhao were all in my Chemical Engineering cohort, and their companionship have been invaluable these last five years, and I am glad Yufei and Xiaowen will be in Indianapolis with me as I embark on a new adventure. In addition, I am deeply grateful to have met my dearest friends Jiji Ahn, Jonathan Bezenah, Chansoo Lee, Kristina Oberly, and Rohan Jalalizadeh, who started out as a board game group but have evolved into a second family that has been an instrumental source of motivation and support.

I must express my eternal gratitude to my parents, for their endless love, understanding, and support of all my decisions and endeavors. I am also thankful for having my sister, Xinyi, live with me for the past three years and help me create a slice of home on the other side of the world in Ann Arbor.

TABLE OF CONTENTS

LIST OF FIGURES

LIST OF SCHEMES

LIST OF TABLES

ABSTRACT

Covalent organic frameworks (COFs) are an emerging class of cross-linked porous crystalline polymers constructed exclusively from rigid building blocks linked together by covalent interactions. Compared to conventional nanoporous materials, COFs possess a unique and highly desirable combination of attributes that are conducive to a variety of applications. Three-dimensional (3D) COFs are, in general, characterized by superior internal surface areas and pore sizes than their two-dimensional (2D) counterparts, and these two attributes are vital for many applications such as gas separation, gas storage, and catalysis. Unfortunately, 3D COFs are also significantly more difficult to construct, and the synthesis, application, and fundamental understanding of 3D COFs lag those of 2D COFs as a result. Thus, improving synthetic accessibility, practical utility, and basic understanding of 3D COFs is vital for realizing their full potential as controllable crystalline nanoporous materials.

This dissertation details the design and execution of an improved synthetic method to afford the archetypal imine-linked 3D COF-300, catalyzed by Lewis acidic scandium triflate ($Sc(OTf)_3$), that allows the reduction of reaction temperature from 120°C to room temperature. A systematic investigation of temperature, catalyst loading, and water content as reaction variables elucidates the contribution of each factor towards the reaction equilibrium and facilitates identification of reaction conditions that result in the most crystalline framework formation, which is determined by powder X-ray diffraction (PXRD). Fourier transform infrared spectroscopy

(FTIR) and Brunauer–Emmett–Teller (BET) surface area measurements confirm that COFs obtained *via* $Sc(OTf)_3$ possess comparable properties as those produced by the conventional solvothermal method.

In addition, the synthesis of several functionalized aldehyde monomers is conducted utilizing a range of chemistries, and they were subsequently employed for functionalized COF-300 synthesis to embed reactive sites into the COF backbone for post-synthetic modification (PSM). The functionalized COFs are consistently amorphous despite systematic variations in reaction conditions under both solvothermal and $Sc(OTf)_3$ catalyzed regimes, and decreasing ratios of functionalized to unfunctionalized aldehydes corresponded to increasingly crystalline frameworks. Steric hindrance is likely the culprit preventing rearrangement into crystalline structures. Lastly, the reduction of imine bonds in COF-300 to amides, multiphase synthesis of COF-300, and high-pressure transformation of COF-300 are explored as alternative methods of synthesis and functionalization.

The combination of these findings provides valuable insight into the imine formation and exchange process and tuning the equilibrium through reaction parameter adjustments, unlocking new synthetic possibilities in the field of 3D COFs *via* the utilization of a much more effective catalyst. In addition, the limitation of functionalized 3D COF syntheses due to steric hindrance is established and will inform future design efforts.

Chapter 1
Introduction

1.1 Original Publication Information

Ma, X. & Scott, T. F. Approaches and challenges in the synthesis of three-dimensional covalent-organic frameworks. *Communications Chemistry* **1**, 98 (2018).

Modifications have been made to the original document to adapt the content to this dissertation.

1.2 Covalent Organic Frameworks

Nanoporous materials have received tremendous interest in recent years owing to their specific and exceptional attributes, notably permanent porosity and large and accessible internal surface areas[1–5]. Conventional nanoporous materials that find wide usage as adsorbents and heterogeneous catalysts and catalyst supports, such as zeolites and activated carbon, are based on inorganic building blocks; nevertheless, research interest in nanoporous materials bearing organic components has expanded rapidly[1,5,6] owing to the exquisite structural and functional control such components provide and flexibility they afford for materials design specifically tailored towards the intended application[5]. A large number of such nanoporous organic polymers have been fabricated in recent years, including polymers of intrinsic microporosity (PIMs)[5,6], porous polymer networks (PPNs)[7], and conjugated microporous polymers (CMPs)[8–10]. These materials are uniformly amorphous and composed of multifunctional building blocks linked by covalent bonds,

and many studies have demonstrated their synthesis and utility[7,11–13]. Unfortunately, the amorphous nature of these materials can yield significant pore size dispersities, inhibiting their utilization in certain applications such as size- and shape-based gas separation and storage[2,11].Crystallinity, in contrast, is characterized by ordered structure and uniform porosity, ideal attributes for gas separation and storage, catalysis, and optoelectronic devices[2,14]. Metal-organic frameworks (MOFs) is one such class of crystalline nanoporous materials that has been extensively investigated. MOFs are constructed from metal ions or clusters linked by organic ligands through coordination bonds, thus possessing both the chemical and structural tunability of the organic ligands, the coordination possibilities of various metal ions, and the uniform porosity and high surface area of a crystalline nanoporous material[3,15–17]. Examples of this class of materials necessarily contain a large amount of potentially toxic or reactive metal centers, and their relatively weak coordination bonds exhibit varying stability under high humidity and temperature, conditions ubiquitous in industrial applications[18–21].

A particularly exciting development in this field was the landmark synthesis of covalent-organic frameworks (COFs) by Yaghi and co-workers in 2005[22]. In this seminal work, two COFs were synthesized from the self-condensation of 1,4-benzenediboronic acid (COF-1) or co-condensation with hexahydroxy triphenylene (COF-5), establishing the first class of crystalline nanoporous organic frameworks linked exclusively by covalent bonds. Although the strength of covalent bonds contributes to significantly improved stability, the general irreversibility of kinetically controlled reactions prevents the molecular rearrangement necessary to form a crystalline structure. Fortunately, the addition products of several covalent bond-forming reactions are known to either revert to the constituent reactants or rearrange under specific reaction conditions. These ‘dynamic’ covalent reactions, utilizing reversible covalent bonds which can be

formed and broken rapidly under appropriate conditions, are capable of obtaining thermodynamic equilibrium as opposed to kinetically-controlled chemistries, thereby ensuring a mechanism for error-correction and facilitating the assembly of the most stable covalent structure, equivalent to conventional self-assembly with non-covalent, intermolecular interactions[19]. In contrast with the aforementioned amorphous nanoporous polymers and MOFs, COFs offer a unique combination of chemical modularity and structural diversity, crystallinity, high surface area, tunable pore size, thermal stability, and low density[3,11,14,23].

1.3 Two-dimensional versus Three-dimensional COFs

Based on the dimensionality of the covalent connectivity, COFs can be classified as either two-dimensional (2D) COFs or three-dimensional (3D) COFs. Two dimensional COFs are fabricated from planar building blocks, and the framework is restricted to 2D sheets, which can then be stacked to form a layered eclipsed structure through π-orbital overlap, generating ordered, one-dimensional channels that are well-suited for charge transport[1,3]. In contrast, 3D COFs are synthesized from aplanar (typically tetrahedral) building blocks to form highly porous networks which are similar in structure to MOFs and have been found to possess exceptionally high surface areas (>5,000 m^2/g) and low densities (<0.13 g/cm^3)[24], making them attractive synthetic targets. Indeed, although studies examining 3D COF applications remain sparse, several simulation and experimental studies have assessed the gas storage capacity of 3D COFs and predicted or empirically demonstrated performance equal to or exceeding the best-performing MOFs owing to their exceptional porosity, surface area, and low density[25–30]. In addition, the promising performance of 3D COFs as superb adsorbents has also been shown[31]. Despite the attractive attributes of 3D COFs, research efforts have predominantly focused on their more synthetically-accessible 2D counterparts. The first synthesis of 3D COFs, reported in 2007 again by Yaghi and

co-workers, brought a new dimension to the field[32]. There have since been many reports describing new 2D COF structures[33,34], novel synthetic strategies such as microwave synthesis[35], flow synthesis[36–38], and vapor-assisted synthesis[39,40], and construction and modification of 2D COFs towards applications including catalysis[41,42], membrane fabrication[43], and gas storage[44]. In comparison, there have been only a handful of new 3D COF structures reported, and little beyond structural explorations and preliminary applications. This dissertation focuses on the more synthetically-challenging 3D COFs, whose superior inherent properties are quite appealing for a variety of applications, and the lack of research progress in recent years leave much room for investigation.

1.4 3D COF Linkages

Whereas a variety of dynamic covalent bond-forming reactions have been employed for the synthesis of 2D COFs, only a few have been utilized for constructing 3D structures. Consequently, the linkages that govern 3D COFs can be generally categorized as boron–oxygen linkages, imine linkages, and other linkage types. A list of linkage chemistries that have been reported to date for 3D COFs is shown in Figure 1.1.

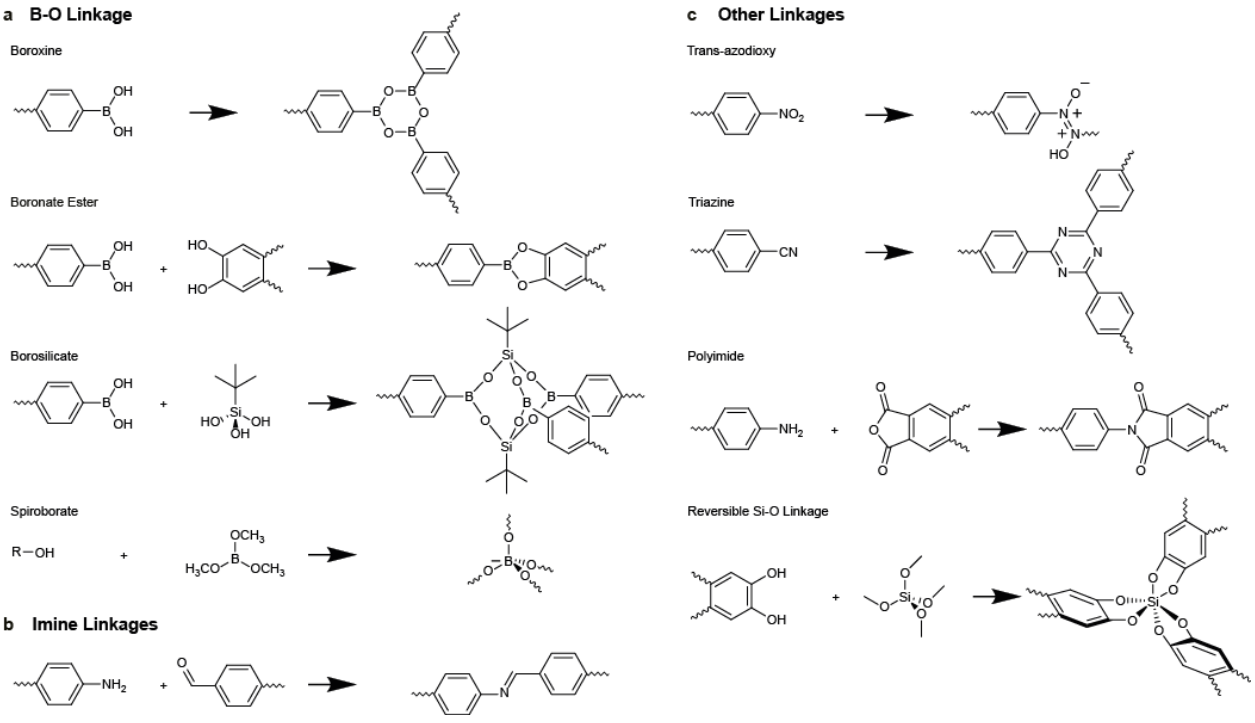

Figure 1.1. Reported synthetic approaches and accompanying linkages used to generate 3D COFs. a) Reported B-O linkages, including boroxine ring, boronate ester ring, borosilicate cage, and spiroborate linkage. b) the imine linkage. c) Other reported linkages, including trans-azodioxy linkage, triazine linkage, polyimide linkage, and reversible Si-O linkage.

1.4.1 Boron-oxygen Linkages

Most early 3D COF structures were formed utilizing boron-oxygen (B–O) linkages. The first 3D COFs, COF-102, COF-103, COF-105, and COF-108, were synthesized from the self-condensation of boronic acids into boroxine rings and co-condensation with catechol into boronate ester rings (Figure 1.2a-b). These syntheses were performed under solvothermal conditions from suspensions of precursors in a mixture of mesitylene/dioxane, resulting in the lowest density crystals known at the time (COF-108, 0.17 g/cm^3) and Brunauer-Emmett-Teller (BET) surface areas (COF-103, 4210 m^2/g) far exceeding those of porous carbons, silicates, 2D COFs, and PIMs, and comparable to some of the highest reported for MOFs (MOF-177, 4500 m^2/g)[32]. Although

rapid microwave synthesis and purification was later successfully demonstrated for both 2D and 3D boroxine and boronate ester linked COFs, this approach has not received significant further study for 3D COFs, and the solvothermal approach has emerged as the prevalent method for 3D COF synthesis[32,45]. In addition to boroxine and boronate ester linkages, a borosilicate cage was also utilized as a linkage for the synthesis of COF-202 (Figure 1.2c)[46].

The exceptionally low densities and high surface areas of these 3D COFs makes them highly promising gas storage candidates. Indeed, grand canonical Monte Carlo (GCMC) simulations on H_2 binding for 2D and 3D COFs containing B–O linkages, which was confirmed experimentally for COF-105, predicted that 3D COFs outperform 2D COFs in hydrogen storage capacity by a factor of 2.5-3, attributable to higher surface area and free volume in the three-dimensional variants[26]. 3D COFs were also expected to significantly outperform the best-performing MOFs in H_2 gravimetric uptake owing to reduced densities and comparable volumetric storage capacity, while doping with lithium ions was anticipated to further increase storage capacity[26–28]. Subsequent experimental investigation of the H_2 storage capacity of these COFs confirmed that these 3D COFs demonstrate best-in-class H_2 saturation uptake (72.4 mg/g for COF-102), far exceeding 2D COFs (39.2 mg/g for COF-10) and comparable to MOFs (72.4 mg/g for MOF-5) at 77 K. The same study also showed that 3D COFs perform remarkably in the storage of methane and carbon dioxide, comparing favorably to other nanoporous materials including zeolites and MOFs, and that larger intrinsic surface area (or pore volume) generally correlate to higher uptake capacity for these gases[30]. Further theoretical studies predicted that COF-102 and COF-103 outperform other 2D and 3D COFs and the benchmark MOF-177 in volumetric uptake and delivery amount of methane at high pressure[25]; however, 3D COFs were predicted to exhibit only average hydrogen storage capacity compared to other MOFs, and required the introduction

of stronger H_2 interaction sites in the COF material for improved performance[29,47]. In addition to small gas molecules, the organometallic host-guest chemistry of COF-102 was also examined by infiltration of metallocenes, and similarities between MOFs and COFs as hosts for organometallics was demonstrated[48].

More recently, metalation of a 3D COF containing B–O linkage was also demonstrated utilizing dehydrobenzoannulene (DBA), a planar triangular macrocycle that can complex with low oxidation state transition metals, as a building block. The synthesized DBA-3D-COF 1 (Figure 1.2d) possesses the highest BET surface area (5083 m^2/g) and lowest density (0.13 g/cm^3) reported to date for a COF, and subsequent metalation of the COF with nickel resulted in retention of crystallinity and minimal reduction in surface area and pore volume[24]. In addition, a 3D, γ-cyclodextrin-based COF (CD-COF) was synthesized utilizing a unique tetrakis(spiroborate) linkage, marking the first instance of a 3D anionic COF constructed from flexible aliphatic building blocks (Figure 1.3a)[49].

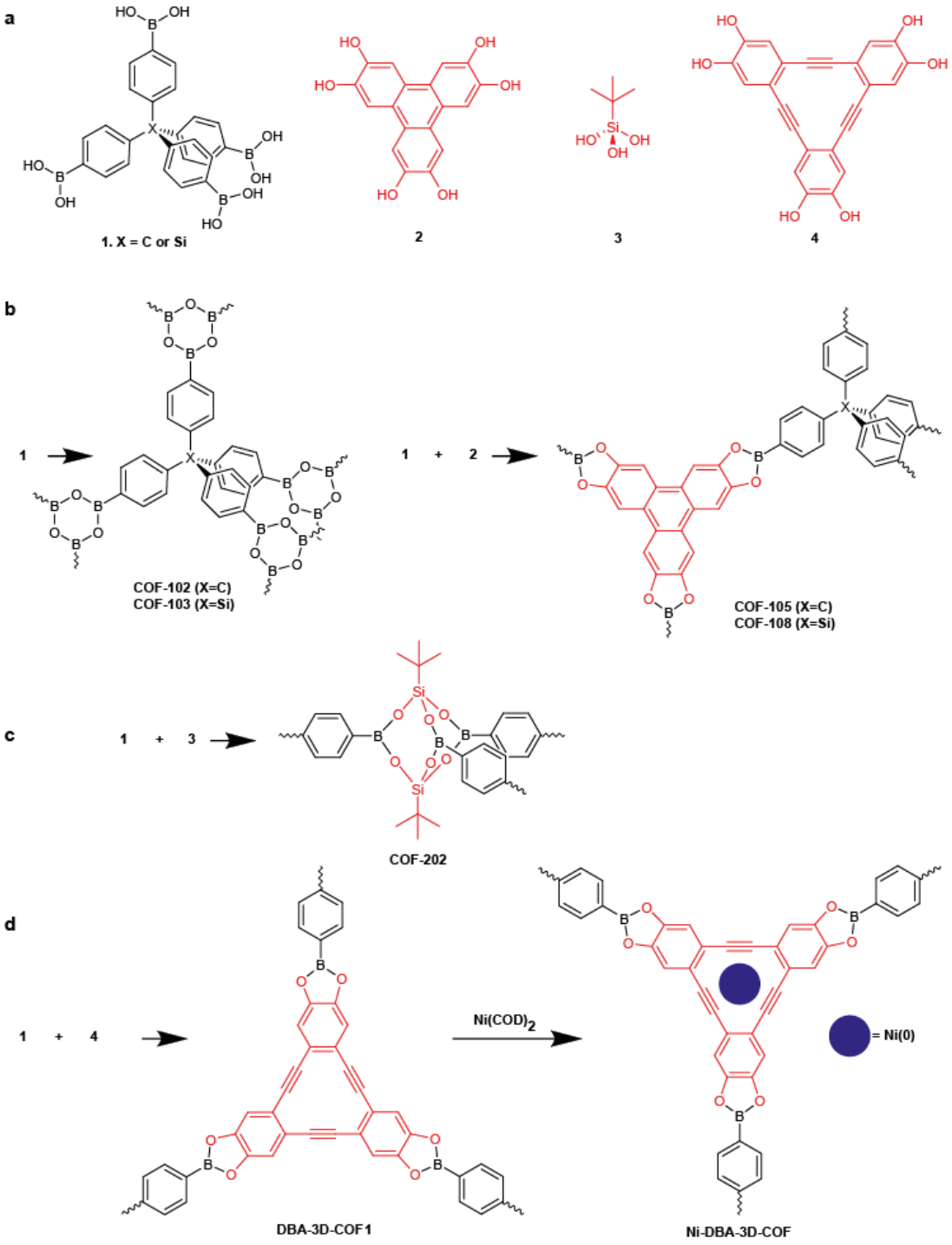

Figure 1.2. Precursors and structures of 3D COFs containing B–O linkages. a) Building blocks employed for B–O linked 3D COF construction. b) Synthetic pathway of COF-102, COF-103, COF-105, and COF-108, the first reported 3D COFs, based on boroxine and boronate ester linkages[32]. c) Synthetic pathway of COF-202, the only 3D COF based on a borosilicate cage linkage[46]. d) Synthetic approach for DBA-3D-COF, utilizing a planar triangular catechol-functionalized macrocycle and boronate ester linkage to metalate Ni and obtain Ni-DBA-3D-COF[24].

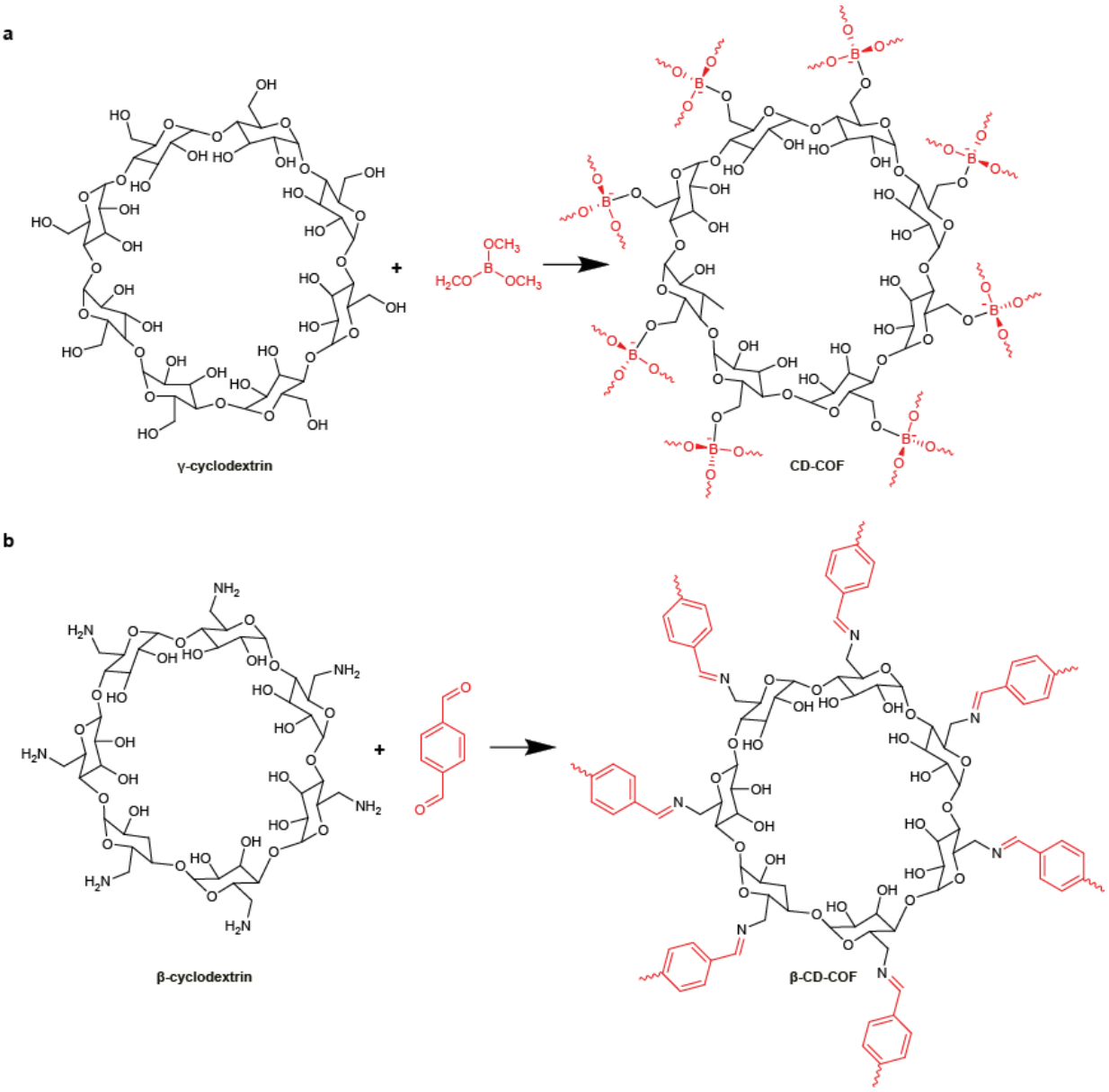

Figure 1.3. Synthetic scheme for 3D COFs constructed from flexible aliphatic cyclodextrin. a) Synthetic pathway of 3D anionic CD-COF, the first 3D COF constructed from γ-cyclodextrin utilizing a unique B-O based spiroborate linkage[49]. b) Synthetic pathway of 3D β-CD-COF constructed from β-cyclodextrin and imine linkage[50].

1.4.2 Imine Linkages

Although many of the early 3D COFs relied on B–O linkages, these linkages suffer from poor hydrolytic and oxidative stability, limiting their practical utility, and there has been a notable trend away from such linkages towards more robust nitrogen-containing linkage chemistries for COF design and synthesis[51]. Imine linkages, synthesized from multi-functional, amine- and aldehyde-bearing precursors, currently dominate the field of 3D COFs owing to their excellent thermal and chemical stability. Owing to these factors, imine-linked 3D COFs are of particular interest to this dissertation and are the sole focus of this research.

The first imine-linked 3D COF, COF-300, was reported by Yaghi and coworkers in 2009, and is synthesized from tetrakis-(4-aminophenyl)methane (TAPM) and terephthalaldehyde (Figure 1.4b). COF-300 possesses a 5-fold interpenetrated diamond structure (**dia-c5** topology), is stable up to 490°C, and is insoluble in water and common organic solvents[52]. It was later reported that by first aging the reaction mixture prior to synthesis, an interpenetration isomer **dia-c7** COF-300 possessing a seven-fold interpenetrated diamond structure, was obtained[53]. The two isomers exhibited identical covalent bonding at the atomic level and thermal stability but were structurally different as revealed by X-ray diffractometry. Ma et al. recently reported the construction of single crystal COF-300 by employing a large excess of aniline as a nucleation inhibitor to prevent immediate precipitation of amorphous networks and increase the reversibility of imine bond formation and dissociation[54]. They showed that crystal size could be controlled by adjusting aniline concentration and were able to obtain single COF-300 crystals of up to 100 μm in size after 30-40 days. Single-crystal X-ray diffraction (SCXRD) characterization allowed the resolution of ambiguity in the interpenetration and revealed that COF-300 exhibits a sevenfold interpenetrated structure, and that previous assessment of five-fold interpenetration was owing to

structural contortion. SCXRD measurements also revealed that hydration of COF-300 led to structural distortion and a drastic 34% reduction in unit-cell volume, which may be attributed to hydrogen bonding between water molecules and the imine bonds. The authors also synthesized COF-303, an analog of COF-300 with a reversed imine condensation between a tetratopic aldehyde and diamine, and demonstrated that the switch in imine bond direction was not differentiable by conventional powder X-ray diffraction (PXRD), but could be detected by SCXRD[54]. COF-300 has also been utilized in conjunction with the zirconium-carboxylate-based MOF UiO-66 to fabricate a composite laminate where a COF-300 layer was grown on top of a prefabricated UiO-66 membrane. These composite membranes demonstrated excellent H_2 permeability as well as a highly enhanced H_2/CO_2 selectivity, far surpassing that of the parent UiO-66 membrane[55]. Additionally, layer-by-layer synthesis of COF-300/silica composites was recently demonstrated to afford particles with potential utility as a chromatographic stationary phase[56]. Yaghi and coworkers also reported COF-320, essentially an extended version of COF-300 constructed from a biphenyl dialdehyde linker, and determined its single-crystal structure using 3D rotation electron diffraction (Figure 1.4c)[57]. COF-320 was later utilized for the encapsulation of a common ionic liquid, 1-ethyl-3-methylimidazolium bis(trifluoromethylsulfonyl) imide, in its pores[58].

Since the first report on COF-300, TAPM has been utilized as the tetrahedral amine building block of choice for a range of new 3D COF structures. The first instance of a dynamic 3D COF, LZU-301, was synthesized from condensation of TAPM with (3,3′-bipyridine)-6,6′-dicarbaldehyde (Figure 1.4d). As the bipyridine analog of COF-320, LZU-301 exhibits symmetry breaking and lattice expansion upon THF solvation, which the authors attributed to the conformation change of the –C=N– bond, serving as a ‘molecular pedal’ in the crystal structure[59].

Lin et al. synthesized a pyrene-based 3D COF by condensing TAPM with 1,3,6,8-tetrakis(4-formylphenyl)pyrene (Figure 1.4e), resulting in a novel structure that featured selective adsorption of CO_2 over N_2 and emitted yellow-green luminescence, marking the first report of a fluorescent 3D COF[60]. Two porphyrin-based 3D COFs, 3D-Por-COF and 3D-CuPor-COF, were synthesized from the condensation of TAPM with porphyrin-based tetraaldehydes (Figure 1.4f) and exhibited photocatalytic activity towards the generation of highly reactive singlet oxygen under visible light irradiation[61]. A 3D chiral COF, CCOF-5, was synthesized by condensation of TAPM with a chiral tetraaldehyde, which subsequently underwent imine oxidation to afford an amide-linked framework, CCOF-6, that retained the crystallinity and permanent porosity of the parent COF (Figure 1.4g). Although both CCOF-5 and CCOF-6 could be used as chiral stationary phases (CSP) for high performance liquid chromatography (HPLC), CCOF-6 exhibited superior resolution performance in addition to improved acid and base stability compared to CCOF-5[62].

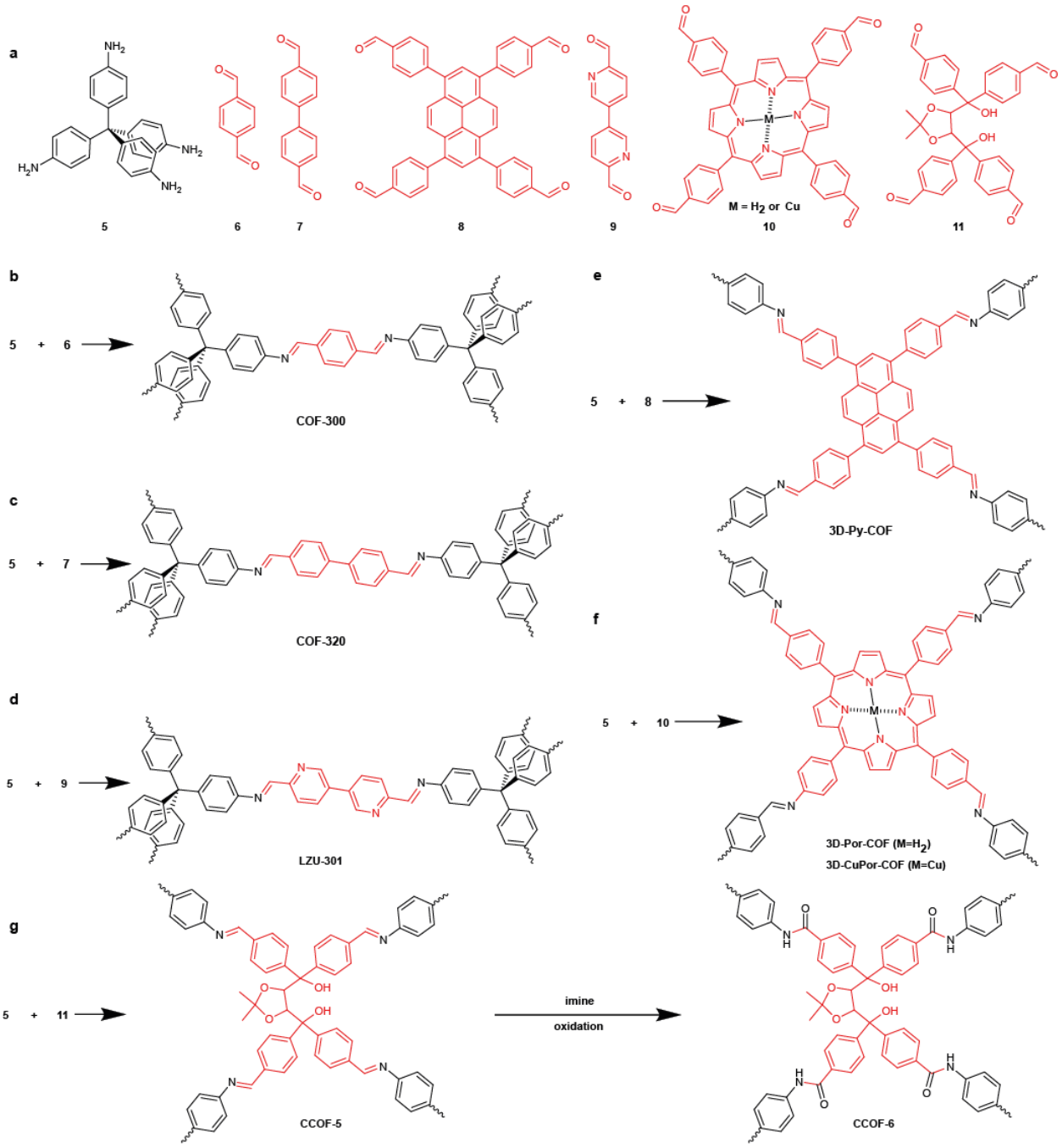

Figure 1.4. Building blocks and synthetic schemes for imine-linked 3D COFs constructed from tetrakis-(4-aminophenyl)methane (TAPM, 5). a) Aldehyde building blocks employed alongside TAPM for synthesis of imine-linked 3D COFs. Synthetic pathway of b) COF-300, the first imine-linked 3D COF[52], c) COF-320[57], d) LZU-301, the first 3D COF exhibiting dynamic behavior[59], e) 3D-Py-COF, the first pyrene-based and first fluorescent 3D COF[60], f) porphyrin-based 3D-Por-COF and 3D-CuPor-COF[61], and g) chiral COFs CCOF-5 and CCOF-6[62].

An alternative tetrahedral amine commonly used for 3D COF synthesis is 1,3,5,7-tetraaminoadamantane (TAA). Li et al. co-condensed TAA with the heterobifunctional 4-formylphenylboronic acid and its fluorinated derivative to obtain DL-COF-1 and DL-COF-2, respectively (Figure 1.5a), the first 3D COFs to feature dual linkages (imine and boroxine). The bifunctional catalytic capabilities of these two COFs were then demonstrated through acid-base catalyzed one-pot cascade reactions utilizing acidic sites supplied by the boroxine ring and basic sites from the imine bond[63]. While the hydrolytic and oxidative stability of the imine linkage is higher compared to B–O linkages found in earlier 3D COFs, they can be further improved by enol-keto tautomerization without affecting the COF structure. This was demonstrated by the Yan group, who reported the first instance of a 3D *β*-ketoenamine COF, BF-COF-2, in addition to the imine-linked BF-COF-1 (Figure 1.5b-c). These COFs were strongly alkaline owing to the high pK_a of the alkyl amine building blocks (TAA) employed, and the excellent catalytic activity and size selectivity of these COFs for the Knoevenagel condensation reaction was shown[64]. Recently, an alternative adamantane-based tetrahedral amine, 1,3,5,7-tetrakis(4-aminophenyl)-adamantane (TAPA), was employed for 3D COF synthesis, undergoing reaction with terephthalaldehyde to form COF-DL229 (Figure 1.5d). In comparison with COF-300, COF-DL229 possesses higher BET surface area (1762 m^2/g vs. 1360 m^2/g) owing to the more extended radiating arms of TAPA compared with TAPM. Additionally, COF-DL229 achieved an exceptional iodine uptake capacity of 82.4 wt% in iodine vapor adsorption experiments while simultaneously exhibiting retentiveness and quick release capabilities. The authors also noted that the exclusively organic skeleton of COFs in general are ‘soft’ and observed reduced crystallinity and iodine uptake in recycled COF-DL229, attributed to local structural deformation to fit solid iodine within the pores upon adsorption[31].

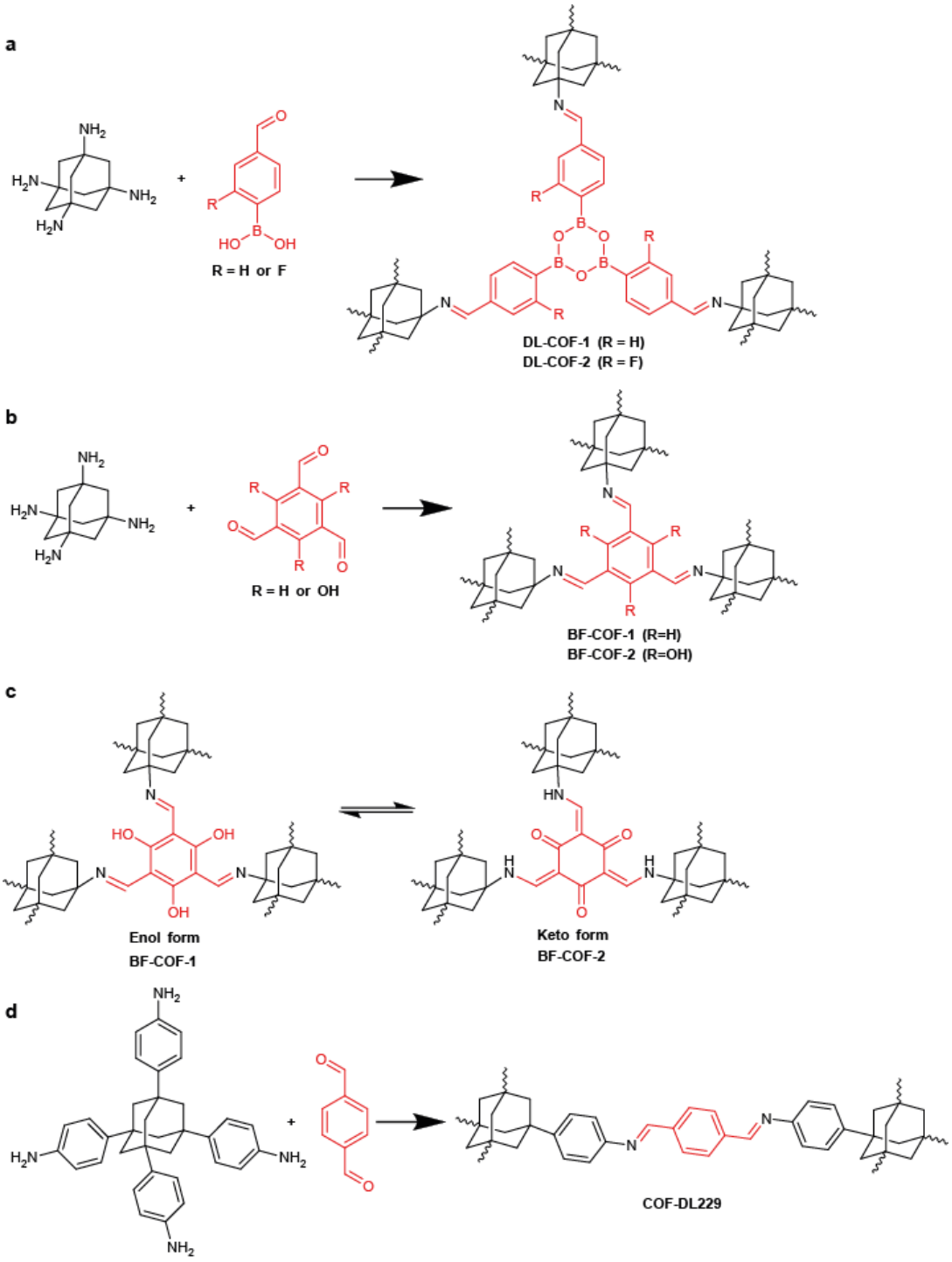

Figure 1.5. Imine-linked 3D COFs synthesized from adamantane-containing tetraamines. a) Synthetic approach for DL-COF-1 and DL-COF-2 from 1,3,5,7-tetraaminoadamantane (TAA) featuring both imine and boroxine ring linkages[63]. b) Synthetic pathway of based functionalized BF-COF-1 and BF-COF-2 from TAA[64]. c) Enol-keto tautomerization of BF-COF-2, which retains crystallinity and structural integrity[64]. d) Synthetic pathway of COF-DL229 from 1,3,5,7-tetrakis(4-aminophenyl)-adamantane[31].

Utilizing imine chemistry, Yaghi's group fabricated the first woven COF, COF-505, by employing an aldehyde-functionalized derivative of the copper bis-phenanthroline complex (Figure 1.6a). They weaved helical organic threads that complexed to Cu(I) ions as points of registry and demonstrated that the structure and topology of COF-505 was retained through demetalation and remetalation, although the demetalated COF-505 did exhibit reduced crystallinity[65]. This work was followed by the synthesis of woven COF-112 from a homogeneous solution, utilizing the gradual *in situ* deprotection of *tert*-butyloxycarbonyl- (Boc) protected amine groups to facilitate the formation of nuclei directly from solution and direct growth into crystalline frameworks and avoid precipitation of amorphous insoluble intermediates, while conventional heterogeneous one-pot synthesis resulted in only amorphous materials (Figure 1.6b). Synthesis of a prototype 2D imine COF, LZU-1, utilizing the same protected amine species under rapid microwave heating resulted in nanocrystals with a surface area (729 m^2/g) more than 1.5 times that of the original report (457 m^2/g), and the fabrication of LZU-1 thin films on silicon substrates was also demonstrated through homogeneous synthesis[66]. An imine-linked 3D COF based on β-cyclodextrin (β-CD-COF) was also synthesized (Figure 1.3b)[50].

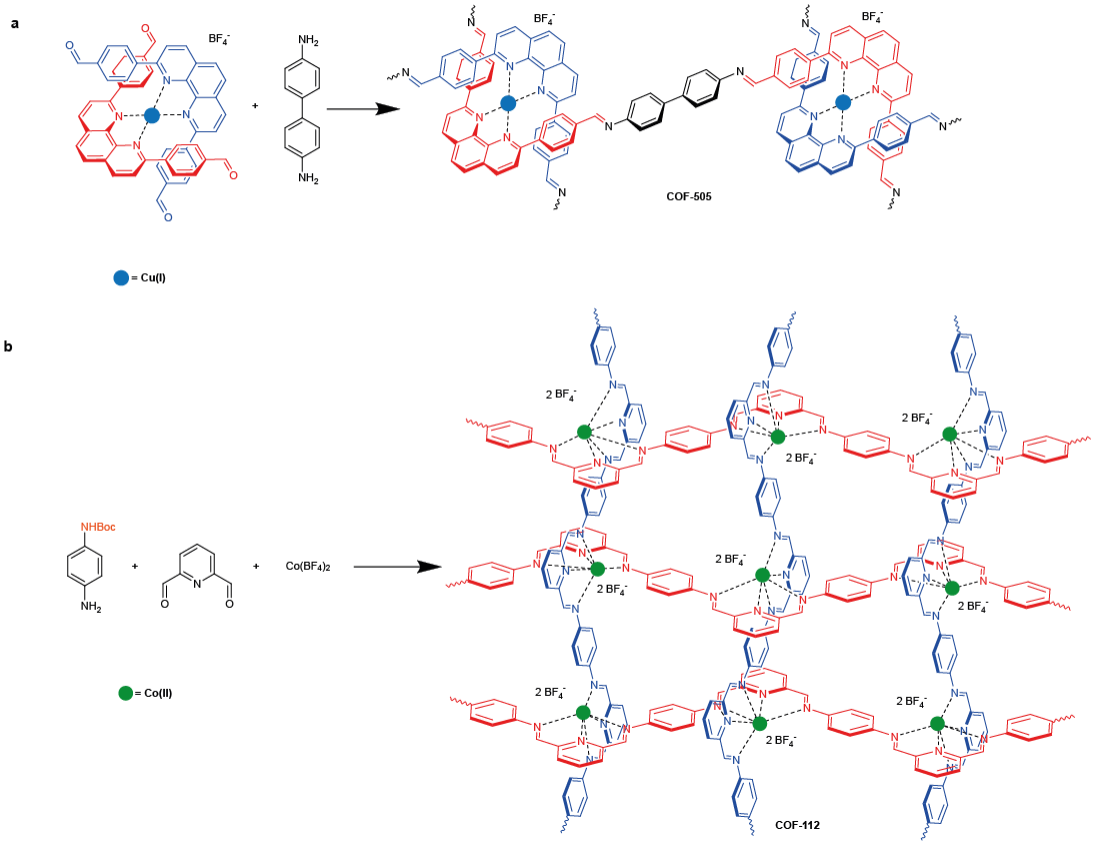

Figure 1.6. Synthetic schemes for woven COFs. a) Synthetic scheme of woven COF-505 [65]. b) Synthetic approach of woven COF-112 utilizing *in situ* deprotection of Boc-protected amine monomer to avoid precipitation of amorphous intermediates and to form crystalline frameworks[66].

Recently, Guan et al. demonstrated the fast ionothermal synthesis of 3D COFs under ambient temperature and pressure, synthesizing three 3D ionic liquid-containing COFs (3D-IL-COFs) from tetrakis(4-formylphenyl)methane (TFPM) and diamines instead of the more prevalent tetraamine and dialdehyde combination (Figure 1.7). By utilizing the ionic liquid 1-butyl-3-methylimidazolium bis((trifluoromethyl)sulfonyl)imide as both solvent and catalyst for the imine formation reaction, the authors were able to synthesize crystalline solids at ambient temperature and pressure within 12 hours, significantly faster than the 3-7 days required for the conventional

solvothermal method. The ionic liquid can be reused without activity loss, and the 3D-IL-COFs were determined to contain 8-12% ionic liquid in their pores, which contributed to the high adsorption selectivity for CO_2/N_2 and CO_2/CH_4[67]. This works presents an exciting new stage in 3D COF synthesis, and will be discussed in greater detail in Section 1.6

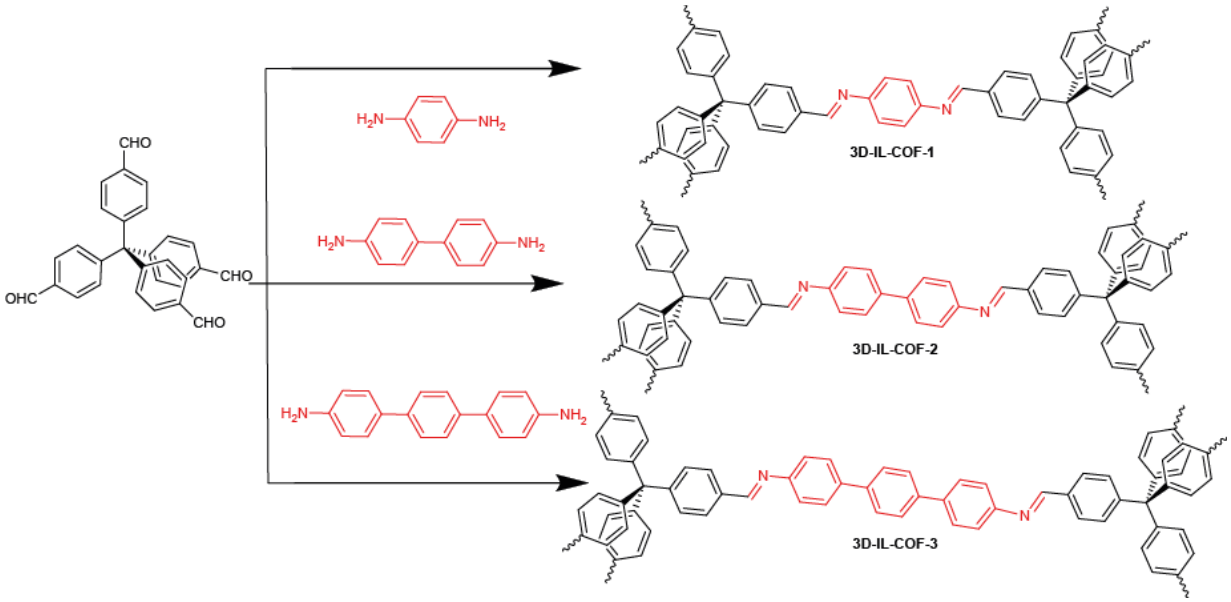

Figure 1.7. Synthetic scheme 3D COFs obtained through ionothermal synthesis. 3D-IL-COFs 1-3 were synthesized from tetrakis-(4-formylphenyl)methane and aromatic diamines of varying lengths under ambient temperature and pressure using ionothermal reaction conditions [67].

1.4.3 Other Linkages

In addition to the B–O and imine linkages, a handful of other linkages have also been utilized for constructing 3D COFs (Figure 1.8). Beaudoin et al. reported COFs constructed using reversible self-addition polymerizations of nitroso groups to form *trans*-azodioxy linkages, resulting in covalent nitroso polymer networks NPN-1, NPN-2, and NPN-3 (Figure 1.8a)[68]. Ren et al. reported the first 3D covalent triazine framework (CTF), a class of porous polymers related

to COFs, which exhibited reasonable BET surface area (1152 m^2/g) but was not crystalline Figure 1.8b)[69]. The Yan group synthesized two polyimide COFs, PI-COF-4 and PI-COF-5, by condensation of TAA and TAPM with pyromellitic dianhydride (Figure 1.8c). These PI-COFs possessed high BET surface area (2430 m^2/g for PI-COF-4 and 1876 m^2/g for PI-COF-5) and pore widths (13 Å and 10 Å respectively) and were thus examined for controlled drug delivery. The authors found that *in vitro* release rate of drugs in COFs was directly related to pore size and geometry, and that the two drug-loaded PI-COFs exhibited good release control, achieving ca. 95% release of initial loading after about 6 days, compared to the typical 2-hour biological half-life. This marked the first time COFs were utilized for drug delivery[70]. Yahiaoui et al. recently reported the first synthesis of a three-coordinated anionic 3D COF, based on novel reversible Si–O chemistry and resulting in a topology that had not been previously reported for 3D COFs (Figure 1.8d). This work also marked the first instance of a 3D COF that did not require tetrahedral building blocks[71]. Several other linkages, including hydrazones, azines, and imides, have been utilized for the synthesis of 2D COFs, but have yet to be explored for 3D COFs[51]. Compared to the imine linkage, these alternative linkages have seen limited utility for 3D COFs and are therefore not explored in this dissertation.

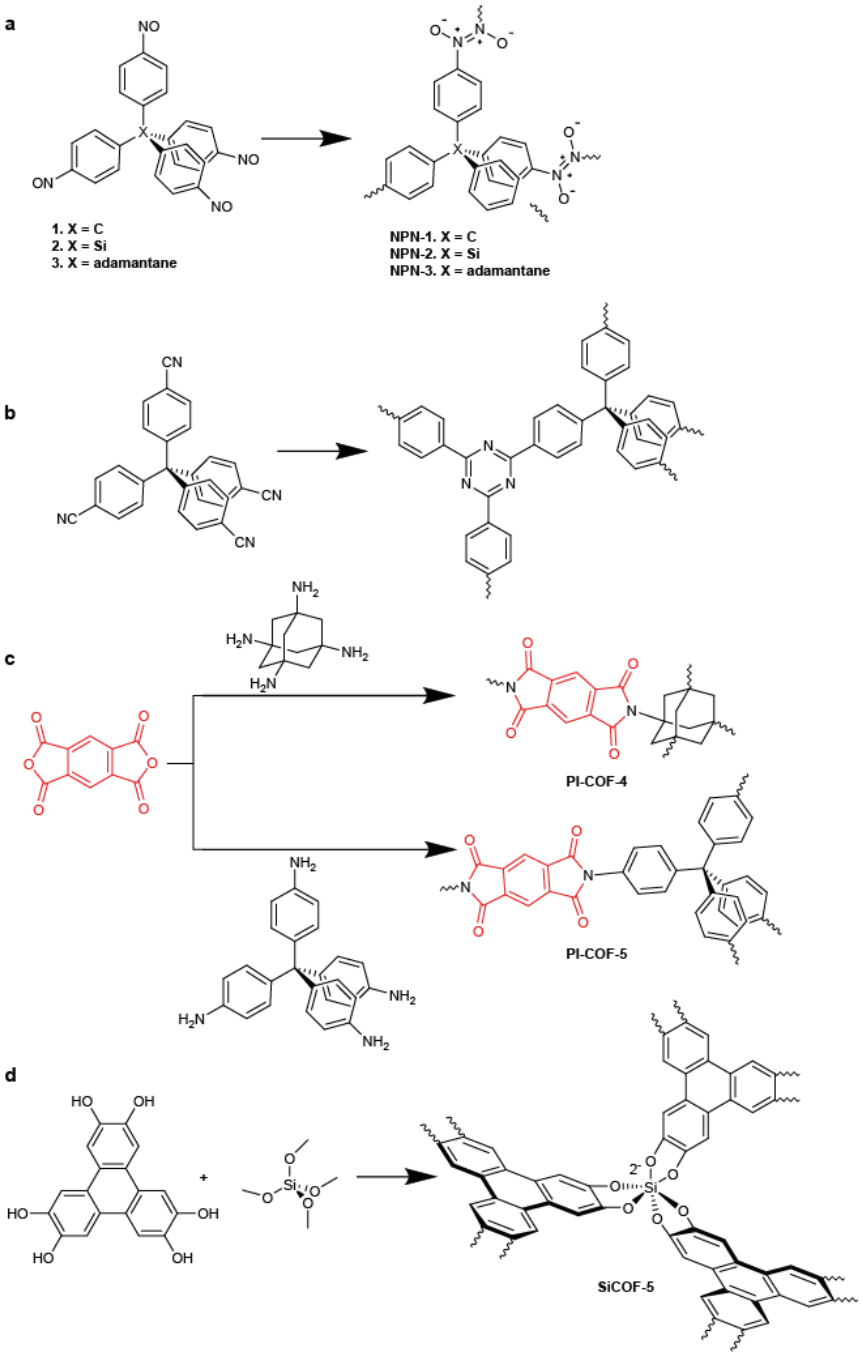

Figure 1.8. Synthesis schemes for 3D COFs based on alternative linkages. a) Construction of nitroso polymer frameworks NPN-1, NPN-2, and NPN-3, which were polymerized utilizing *trans*-azodioxy linkage to obtain a large number of uniform single crystals[68]. b) Synthetic pathway of the first 3D covalent triazine framework, a class of amorphous porous polymers related to COFs[69]. c) Synthesis of the first polyimide 3D COFs, PI-COF-4 and PI-COF-5, from 1,3,5,7-tetraaminoadamantane and tetrakis-(4-aminophenyl)methane , respectively, and pyromellitic dianhydride as a linear linker[70]. d) Synthetic approach of the first three-coordinated 3D COF, SiCOF-5, utilizing tetramethoxysilane (TMOS) and 2,3,6,7,10,11-hexahydroxytriphenylene (HHTP) and reversible Si–O covalent interactions [71].

1.5 Functionalization and Modification of 3D COFs

The organic nature of COFs affords facile chemical tunability, leading to immense structural and functional diversity compared to their inorganic counterparts. As such, modification and functionalization of the COF structure becomes a crucial step towards tailored applications and is a focus of this dissertation. Excluding the use of different monomers or alternative linkages, post-synthetic modification (PSM) is the most common approach to COF functionalization. A common PSM method is embedding reactive functionalities into constituent monomers and applying subsequent chemistry to those groups upon completion of the initial COF synthesis. Using this approach, Dichtel and coworkers carried out a series of interior functionalization studies on COF-102. Utilizing a monomer-truncation strategy, they co-condensed the tetrahedral boronic acid building block of COF-102 with a truncated version in which one of the four arylboronic acid groups was replaced with a dodecyl or allyl group, obtaining internally-functionalized COF structures with the truncated moieties distributed throughout the material that retains the crystallinity and high surface area of COF-102 (Figure 1.9a)[72]. The introduced allyl group was subject to post-synthetic functionalization using thiol–ene chemistry, achieving full conversion of the allyl group while retaining crystallinity and permanent porosity (Figure 1.9b)[73]. Dichtel and coworkers also explored the functionalization of COF-102 utilizing the monofunctional tolylboronic acid instead of the trigonal truncated monomers of the previous studies (Figure 1.9c), and found that COF-102-tolyl crystallized even in the presence of up to 36 equivalents of tolylboronic acid relative to the tetra-boronic acid and demonstrated incorporation of up to 36 mol% of tolylboronic acid into the framework while maintaining crystallinity and porosity, which the authors postulated as a fundamental limit for the COF-102 structure[74]. In comparison, PSM of imine-linked 3D COFs has been scarce. The demonstrated the synthesis of a carboxylated, imine-

linked 3D-COOH-COF by performing PSM on a 3D hydroxy-functionalized COF by Lu et al. (Figure 1.9d)[75] is the only example of embedding reactive functionalities into the backbone of an imine-linked 3D COF. The many works in the PSM of imine-linked 2D COFs utilizing this method suggests significant potential for the similar functionalization of 3D COFs, which is explored in-depth in this dissertation. Aside from embedding reactive groups, an alternative PSM technique for imine-linked COFs is the direct modification of the imine bond. For example, Han et al. converted their imine-linked 3D COF CCOF-5 into an amide-linked CCOF-6 by oxidation of the imine bonds, achieving enhanced chemical stability compared to its predecessor (Figure 1.4g)[62]. Reversible enol-keto tautomerization has also been shown by the Yan group in the conversion between BF-COF-1 and BF-COF-2 (Figure 1.5c)[64].

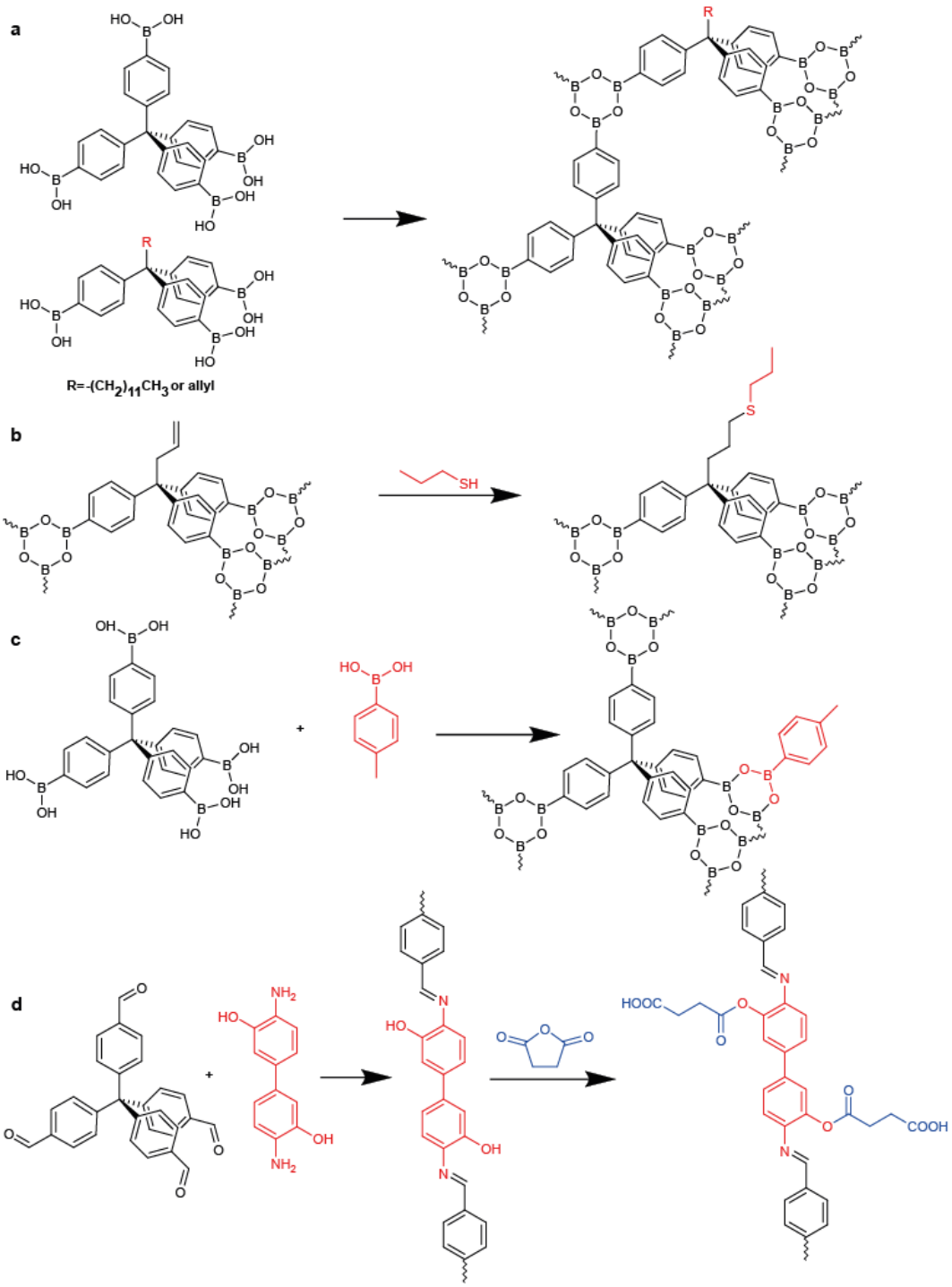

Figure 1.9. Synthetic schemes for the internal functionalization of model framework COF-102. a) Functional group incorporation into COF framework through the use of a truncated version of the tetrahedral boronic acid building block[72]. b) Post-synthetic functionalization of a reactive allyl group, initially introduced by a truncated monomer, *via* the radical-mediated thiol–ene addition reaction[73]. c) Functionalization using monofunctional tolylboronic acid[74]. d) Preparation of 3D carboxy-functionalized 3D-COOH-COF through post-synthetic modification of hydroxy-functionalized 3D-OH-COF[75].

Several other chemistries have been employed for PSM of 2D COFs, including copper(I)-catalyzed azide-alkyne cycloaddition[76,77], acylation of phenol groups[44], and the ring-opening of succinic anhydride with phenol groups to form carboxylic acids[78]; these chemistries are wholly transferrable to 3D COFs. Some alternative PSM techniques have also been implemented in 2D COFs. For example, Chen et al. highlighted the ability to lock 2D COF networks with hydrogen bonds by introducing hydroxy groups into the terephthalaldehyde linker, which subsequently form hydrogen bonds with imine-centered nitrogen atoms[79]. Structural modification of COFs has also been achieved through induction of *cis*-*trans* isomerization to facilitate a reversible conformation change. Zhang et al. demonstrated this concept utilizing the *trans*-*cis* photoisomerization of azobenzene, using an azobenzene diboronic acid to produce a boronate ester-linked 2D Azo-COF that underwent photoisomerization under 365 nm UV irradiation[80]. The dynamic behavior of the 3D LZU-301, highlighted in the previous section, can be similarly attributed to an imine bond conformation change[59]. An important consideration for applying PSM to 3D COFs is the reaction site accessibility within the pores. Modification of internal structure of 3D frameworks requires ready access of reactant species to internal functionalization sites, which may impose additional barriers for the translation of 2D COF PSM techniques to their three-dimensional counterparts. In contrast, PSM techniques developed for 3D MOFs, such as the introduction of polymerizable methacrylamide functionalities into MOF UiO-66[16] or the removal of photolabile *o*-nitrobenzyl pendant groups[81], could be more readily implemented in 3D COFs.

1.6 Challenges in 3D COF Development

1.6.1 Disparity between 2D and 3D Frameworks

Although there have been notable advances in the field of 3D COFs, progress persistently lags that of 2D COFs. For example, several dynamic covalent linkages that have been employed for synthesizing 2D COFs, such as hydrazones and azines, have yet to see similar utilization for 3D COFs[51]. Moreover, compared to the more abundant and systematic studies on the synthesis, modification, and application of 2D COFs, the current research in 3D COFs revolves around the synthesis and characterization of novel structures and preliminary applications that arise from the unique traits of each structure. This discrepancy is one of the key motivations in the exclusive focus on 3D COFs in this dissertation.

1.6.2 Addressing the Crystallization Problem

A major factor behind this COF development disparity is the so-called 'crystallization problem', originating from the inherent conflict between the use of robust covalent bonds to form stable crystalline frameworks, which necessitates the formation of reversible or rearrangeable linkages to facilitate error-correction, and the tendency of covalent bonds to form irreversible interactions[82]. Even in these dynamic covalent bond-forming reactions, the kinetic trapping of amorphous networks often occurs owing to the bulkiness and rigidity of the monomeric precursors impeding proximity between reactive groups, precluding further network rearrangement into the desired crystalline framework. Indeed, in contrast to 2D COFs where reaction sites are readily accessed and van der Waals interactions from π-orbital overlap provide additional driving force outside of covalent bonds towards the stacked layer structure, the synthesis of 3D COFs relies solely on inaccessible covalent interactions for the rearrangement of its rigid building blocks[62].

Nevertheless, as the synthesis of contemporary 3D COFs have relied primarily on boronic acid and imine condensation reactions, the formation of stoichiometric quantities of water provides a convenient factor in the mediation of the reaction equilibrium, which can be accomplished by using water immiscible solvents or controlling reactor pressure[82].

To date, the synthesis of 3D COFs has primarily been performed under heating, commonly at 120°C but even at temperatures of up to 160°C[70], either *via* the predominant solvothermal approach for extended periods or under rapid microwave heating, providing additional energy for covalent bond rearrangement as well as the necessary mobility for the COF building blocks to achieve the desired connectivity. This is essentially a 'brute force' method to overcome the crystallization problem, and these reaction conditions impose limitations on the utility of 3D COFs. Reactions that proceed over multiple days may be too slow for industrial relevance, and heating to high temperatures reduces functional group compatibility and precludes certain applications such as the encapsulation of folded biomacromolecules. The development of milder conditions capable of rapidly yielding crystalline materials will be key to unlocking the potential of 3D COFs for a broader range of applications, and researchers have just begun to explore various means of overcoming the crystallization problem outside extended heating.

In the case of imine-linked COFs, a mechanistic study of the 2D TAPB-PDA COF has revealed that the amine and aldehyde monomers very quickly precipitate into amorphous networks, which then slowly rearrange into crystalline networks after extended heating, demonstrating imine exchange as the rate limiting step in COF formation[83]. An acid catalyst, commonly acetic acid, is often employed to promote imine formation and exchange[19]; however, acetic acid is a relatively inefficient catalyst for transamination[84]. Lewis acidic rare earth metal triflates are promising alternative catalysts owing to their effectiveness in mediating imine exchange reactions, tolerance

of both aqueous and organic environments, and functional group compatibility[84]. These metal triflates, particularly scandium triflate ($Sc(OTf)_3$), have recently been shown to catalyze the formation of crystalline 2D imine-linked COFs at room temperature in as little as 10 minutes while yielding improved material properties such as BET surface area (2175 m^2/g vs. <1000 m^2/g from the solvothermal method)[84]. Although similar studies have yet to be described for 3D COFs, the utilization of improved catalysts, such as metal triflates, for network rearrangement is a promising approach towards milder reaction conditions. Of course, the reduced driving force for 3D COF network formation suggests that the directly applicability of conditions identified for the 2D TAPB-PDA COF (2% $Sc(OTf)_3$ loading, 10 minutes at room temperature)[84] is unlikely, and some combination of elevated temperature, extended reaction duration, and higher catalyst loading may be required to induce formation of a crystalline, imine-based 3D network. Interestingly, whereas low rare earth metal triflate concentrations catalyze imine rearrangement reactions, at raised concentrations these compounds no longer act catalytically and instead affect the reaction equilibrium to favor the precursor reactants[85], an attribute likely to find synthetic utility in mediating framework crystallinity and post-synthetic modification.

Notably, the room temperature synthesis of 3D COFs has recently been demonstrated. Guan et al. employed ionothermal synthesis to obtain highly crystalline, imine-linked 3D COFs in as little as three minutes at ambient temperature and pressure utilizing an ionic liquid as both solvent and catalyst[67]. Although these results hold promise, several aspects of this approach remain subject to optimization. The 3D-IL-COFs synthesized in this study contained 8-12% ionic liquid in their pores, potentially contributing to their relatively low internal surface areas. For example, 3D-IL-COF-1 exhibited a BET surface area of 517 m^2/g[67], whereas COF-300, whose structure differed from 3D-IL-COF-1 only by the directionality of the imine bonds, offered a BET

surface area of 1360 m^2/g[52], suggesting that this ionothermal synthetic approach may compromise the internal surface area of 3D COFs, one of their most important characteristics. Moreover, applications of 3D COFs invariably revolve around host-guest interactions within the pores, and the apparent retention of ILs presents an additional complication in the compatibility of the guest species. Finally, the applicability of this approach to generic imine-based frameworks still needs to be demonstrated. Whereas the three 3D-IL-COFs synthesized in this paper possessed similar structures, differing only by the number of the phenyl rings in the linear diamine linker[67], further investigation is necessary to determine the breadth of ionothermal synthesis utility. In a separate study, Ma et al. also demonstrated the ability to synthesize single crystalline COF-300 at room temperature by utilizing aniline as a nucleation inhibitor and extending the reaction duration to 30-40 days and elucidated greater insight into the COF structure through single crystal analysis[54]. Unfortunately, the extended reaction times required by this strategy would likely curtail adoption of the resultant 3D COFs for industrial applications.

The lack of control over the rapid precipitation of amorphous intermediates during COF synthesis can lead to kinetic trapping of said intermediates, preventing the rearrangement necessary to form a crystalline structure. Limiting the concentration of available monomers in the reaction through controlled addition of reactants or through *in situ* deprotection or generation or reactant species can contribute to reaction rate control, mediating the rate of crystal nucleation and growth, and ultimately overcoming kinetic trapping. The Dichtel group reported the successful growth of the first discrete colloidal 2D boronate ester-linked COF-5 particles *via* gradual monomer addition, whereas faster addition led predominantly to the formation of new particles with smaller crystalline domains[86]. Similarly, Yuan et al. demonstrated the use of heterogeneous SiO_2 seeds coated with a thin layer of amorphous Schiff-base polymer from which the imine-linked

2D COF-LZU1 network was grown, suppressing the rapid precipitation of amorphous materials and promoting crystallization. The frameworks were obtained in significantly shorter timeframe than conventional solvothermal methods and exhibited high crystallinity and surface area after the SiO_2 particles were etched away[87]. Additionally, interfacial crystallization, multiple demonstrations of which have been reported for 2D COFs[88,89], may be applicable to 3D COFs. For example, Li et al. demonstrated a novel approach to yield high-quality 2D COF nanosheets at the interface of two miscible organic solvents, each of which contained one of the two constituent monomers in solution, by adding a low-density solvent interlayer as a buffer between the two main solvent layers[90]. Alternatively, *in situ* deprotection can also control monomer release rate and precipitation, an approach that even enables the use of precursor monomers bearing multiple, covalently coreactive functional group types. *In situ* deprotection of catechol was previously reported for the incorporation of insoluble and unstable building blocks in boronate ester COF synthesis[91], and *in situ* deprotection of certain reactant functional groups can curtail the condensation reaction rate and hence mediate the rate of precipitation to avoid kinetic trapping[92]. Yaghi's group recently applied this concept to woven 3D COFs, employing *in situ* deprotection of Boc protected amine monomers to slow down the initial imine condensation and synthesize the woven COF-112 homogeneously without the precipitation of amorphous intermediates, using trifluoroacetic acid (TFA) as a dual-role catalyst. This approach also afforded greater control over COF morphology, allowing the synthesis of uniform nanocrystals and thin films based on 2D imine-linked COF LZU-1[66]. Similarly, Yahiaoui et al. utilized the *in situ* generation of silicon source tetramethoxysilane (TMOS) by gradual disproportionation of methyltrimethoxysilane to synthesize SiCOF-5, while direct condensation of constituent monomers HHTP and TMOS did not yield a crystalline framework[71]. Establishing more precise control over the monomer

availability in the reaction system, either through slow addition, heterogeneous nucleation, or *in situ* deprotection or generation of constituent species, will likely prove indispensable to circumvent kinetic trapping for a broad range of 3D COF syntheses.

1.6.3 Deficient Systematic Understanding

Another notable issue that has plagued the COF community is the fragmentary understanding of both their inherent structure and the contributions of COF synthetic conditions, particularly for 3D COFs. To date, most 3D COF synthetic efforts have yielded amorphous or polycrystalline products, and their crystalline morphologies have been determined by PXRD; however, elucidation of the precise structure, including atomic positions, interpenetration, and pore guest arrangement, has proven challenging. This dilemma may be resolved by the construction of single crystals of 3D COFs, enabling a more definitive understanding of their structure *via* SCXRD[54]. Beaudoin et al. synthesized monocrystalline COFs by utilizing reversible, self-addition polymerization of tetrahedral nitroso compounds to afford diamondoid azodioxy networks which were then subject to SCXRD characterization, enabling elucidation of the location and bonding of essentially every atom[68]. Ma et al. further demonstrated the characterization utility of single crystalline COFs by employing single crystals of COF-300 to resolve prior ambiguity regarding their degree of interpenetration as well as structural distortion upon hydration[54]. These reports represent an important direction in the field of 3D COFs, and continued emphasis on single crystalline 3D COF synthesis will enable definitive resolution of their structures.

The influence of 3D COF synthetic conditions remains poorly understood. Duncan et al. conducted a study on the kinetic and thermodynamic factors in imine-linked 3D COF synthesis, and found that acetic acid is a crucial component of the reaction, acting as both a catalyst and a

co-solvent[19]. In addition, they evaluated the suitability of a range of organic solvents for synthesis and reported that DMF and THF were the most suitable solvents for obtaining highly cross-linked materials, although the polymer networks they obtained remained amorphous[19]. Dichtel's mechanistic study of the crystallization process of 2D imine-linked COFs provided the first real insight into the synthetic process, and successfully elucidated the mechanism of rapid amorphous precipitation followed by gradual rearrangement into crystalline structures. In addition, the crucial role of acetic acid and water in inducing crystallinity and maintaining high yields was shown[83]. Li et al. used a kinetic Monte Carlo model to describe the nucleation and growth of 2D COF-5 from solution which agrees with experimentally measured growth kinetics and showed that nucleation and growth processes could be described by the same model, which could lead to informed 2D COF syntheses and improved control over nucleation and growth[93]. Similar insight into 3D COF synthesis would offer improved understanding and control of the crystallization process.

Other than the aforementioned reaction conditions, additional factors affecting the synthesis of 3D COFs need further elucidation. For example, whereas COF-300 is typically synthesized from a suspension of starting materials, homogeneous starting conditions were reported to yield the best results in a boronate ester 3D COF synthesis[24,52]. A controlled variable study comparing 3D COF synthesis from a suspension or homogeneous solution would inform the influence of these initial conditions. Additionally, COF-300 synthesis has required freeze-pump-thaw degassing and subsequent reaction vessel flame sealing prior to heating[52], where raised pressure through sealing the reaction vessel has been touted as key to obtaining a crystalline solid[82]. This methodology has been universally adopted for 3D COFs synthesized by the solvothermal method; however, overpressure has proven unnecessary for the synthesis of COFs containing B–O linkages, as an open reaction vessel with a reflux condenser attached for collecting water

achieved similar results as a sealed reaction vessel in microwave synthesis[45]. Since water plays a similar role in mediating the reaction equilibrium in both boronic acid condensation and imine condensation, one might conclude that a sealed reaction vessel serves as a convenient method for retaining water in the system, but it is not the only way of doing so. Even if the use of a sealed reaction vessel is desired, degassing is potentially unnecessary. Again, controlled variable experiments comparing 3D COF synthesis from a degassed and pressurized versus simply a sealed reaction system, are required to assess this hypothesis, and if confirmed these findings can contribute to simplification of the established 3D COF synthetic process.

1.6.4 Limited Topologies and Building Blocks

A second reason behind the disparity of studies on 2D and 3D COFs is the limited variety of available molecular building blocks and consequent network topologies[60,71]. Compared to 2D COFs, which can be constructed from a variety of ditopic and tritopic linkers, 3D COFs have, with the recent exception of the three-coordinated SiCOF-5 with **srs** topology, utilized tetrahedral building blocks and adopted a topology belonging to one of five nets (**dia, bor, ctn, rra,** or **pts**) [49,60,71]. The chemical diversity of these building blocks is similarly limited, as many 3D COFs based on B–O linkages have been synthesized from tetra(4-dihydroxyborylphenyl)methane, and the majority of imine-linked 3D COFs employed TAPM and TAA as precursors[82].

From a geometry perspective, tetrahedral nodes are the most direct method of sustaining an infinite 3D cross-linked network. Though employing a non-planar tritopic linker would also result in a non-planar structure, growth in the z-direction may be finite and would not necessarily assemble into a true 3D framework. Employing higher functionality linkers would conceivably yield 3D frameworks with higher degrees of cross-linking; however, limited functional group

accessibility, steric hindrance, and kinetic trapping, which, as discussed earlier, are already present when utilizing tetratopic linkers, would become increasingly prevalent and further impede the synthetic accessibility of crystalline structures. As such, tetratopic linkers are ubiquitously employed as the most straightforward way to sustain an infinite 3D cross-linked network around a tetrahedral node, while avoiding increased steric hindrance and kinetic trapping from monomers with higher order functionalities. This limit in topology and building block diversity has limited the number of attainable 3D COF structures, and novel building block structures must be discovered in addition to employing different linkages and COF structure modifications to access increased compositional and structural complexity.

1.6.5 Controlling Network Interpenetration

Interpenetration, where the empty space described by the crystalline framework accommodates one or more additional networks[94] and which can adversely affect pore volume and impact internal surface area[95], is another aspect of 3D COFs that requires improved understanding and synthetic control. Whereas interpenetration in 3D COFs has typically been determined by structural modeling and unit cell indexing and is reported as an inherent characteristic, efforts to better understand, characterize, and even modify degrees of interpenetration have been recently reported. For example, the synthesis of an interpenetration isomer was reported for COF-300, representing a preliminary attempt towards modifying the extent of interpenetration in a 3D COF[53]. More sophisticated approaches to control COF interpenetration might be derived from techniques successfully implemented in MOF syntheses, such as temperature and monomer concentration control[96], organic bond structure alteration[95], rational design of organic building blocks[97], and incorporation of space-filling, photolabile protecting groups that could be post-synthetically

cleaved[81]. These techniques inform the potential for reducing or preventing interpenetration in 3D COFs and could conceivably be translated to 3D COF synthetic approaches to fully realize their potential as crystalline, controllably porous materials.

1.7 Overview of Subsequent Chapters

This dissertation details attempts to develop improved 3D COF synthetic methods, establish alternative approaches to synthesis, modify 3D COFs for potential applications, and gain systematic and fundamental understanding of 3D COF synthesis. These efforts address the most pressing challenges in 3D COF development today highlighted in Section 1.6 . The remaining chapters of this dissertation are organized as follows:

Chapter 2 discusses the synthesis of tetrahedral monomers crucial for imine-linked 3D COF construction and the novel degassing solution developed for easier COF fabrication. This improved procedure was applied to the synthesis of two previously reported COFs and a new framework. The insight and synthetic improvements from this chapter and the COF-300 synthesized informs the COF syntheses and modifications in subsequent chapters and serves as the foundation for further investigation.

Chapter 3 features the development of a novel synthetic method for imine-linked 3D COFs utilizing a new catalyst, the Lewis acidic rare earth metal triflate scandium triflate, which allows the successful synthesis of crystalline COF-300 at room temperature. A systematic investigation of how different synthetic parameters impact reaction equilibrium and product crystallinity provides much-needed fundamental understanding of the COF synthetic process. Additionally,

in-situ deprotection of acetyl groups in COF-300 synthesis employing scandium triflate as a dual-role catalyst and the ionothermal synthesis of COF-300 is explored.

Chapter 4 details the efforts to synthesize four different functionalized aldehyde linkers utilizing three different chemistries and subsequent COF syntheses utilizing these linkers to embed reaction functionalities into the COF backbone. A systematic investigation of reaction conditions is conducted to induce the formation of crystalline functionalized COFs utilizing both the solvothermal approach and the scandium triflate catalyzed approach highlighted in Chapter 3.

Chapter 5 describes three alternative approaches to the synthesis and modification of COF-300, namely post-synthetic reduction of imine bonds for further functionalization, multiphase synthesis, and high-pressure processing.

Chapter 6 provides an overall summary and conclusion for this dissertation, as well as suggestions for future work.

1.8 References

1. Huang, N., Wang, P. & Jiang, D. Covalent organic frameworks: a materials platform for structural and functional designs. *Nat. Rev. Mater.* **1**, 16068 (2016).
2. Dogru, M. & Bein, T. On the road towards electroactive covalent organic frameworks. *Chem. Commun.* **50**, 5531–5546 (2014).
3. Feng, X., Ding, X. & Jiang, D. Covalent organic frameworks. *Chem. Soc. Rev.* **41**, 6010–6022 (2012).
4. Zhu, L. & Zhang, Y.-B. Crystallization of Covalent Organic Frameworks for Gas Storage Applications. *Molecules* **22**, 1149 (2017).
5. McKeown, N. B. & Budd, P. M. Polymers of intrinsic microporosity (PIMs): organic materials for membrane separations, heterogeneous catalysis and hydrogen storage. *Chem. Soc. Rev.* **35**, 675–683 (2006).
6. McKeown, N. B. Polymers of Intrinsic Microporosity. *Int. Sch. Res. Not.* **2012**, e513986 (2012).
7. Yuan, D., Lu, W., Zhao, D. & Zhou, H.-C. Highly Stable Porous Polymer Networks with Exceptionally High Gas-Uptake Capacities. *Adv. Mater.* **23**, 3723–3725 (2011).
8. Jiang, J.-X. *et al.* Conjugated Microporous Poly(aryleneethynylene) Networks. *Angew. Chem. Int. Ed.* **46**, 8574–8578 (2007).
9. Cooper, A. I. Conjugated Microporous Polymers. *Adv. Mater.* **21**, 1291–1295 (2009).
10. Jiang, J.-X. *et al.* Synthetic Control of the Pore Dimension and Surface Area in Conjugated Microporous Polymer and Copolymer Networks. *J. Am. Chem. Soc.* **130**, 7710–7720 (2008).

11. Ding, S.-Y. & Wang, W. Covalent organic frameworks (COFs): from design to applications. *Chem. Soc. Rev.* **42**, 548–568 (2013).

12. Yao, S., Yang, X., Yu, M., Zhang, Y. & Jiang, J.-X. High surface area hypercrosslinked microporous organic polymer networks based on tetraphenylethylene for CO2 capture. *J. Mater. Chem. A* **2**, 8054 (2014).

13. Zhang, Y. & Riduan, S. N. Functional porous organic polymers for heterogeneous catalysis. *Chem Soc Rev* **41**, 2083–2094 (2012).

14. Bisbey, R. P. & Dichtel, W. R. Covalent Organic Frameworks as a Platform for Multidimensional Polymerization. *ACS Cent. Sci.* (2017). doi:10.1021/acscentsci.7b00127

15. Li, J.-R., Sculley, J. & Zhou, H.-C. Metal–Organic Frameworks for Separations. *Chem. Rev.* **112**, 869–932 (2012).

16. Zhang, Y. *et al.* Photoinduced Postsynthetic Polymerization of a Metal–Organic Framework toward a Flexible Stand-Alone Membrane. *Angew. Chem.* **127**, 4333–4337 (2015).

17. Zhou, H.-C., Long, J. R. & Yaghi, O. M. Introduction to Metal–Organic Frameworks. *Chem. Rev.* **112**, 673–674 (2012).

18. Zhu, Y., Long, H. & Zhang, W. Imine-Linked Porous Polymer Frameworks with High Small Gas (H-2, CO2, CH4, C2H2) Uptake and CO2/N-2 Selectivity. *Chem. Mater.* **25**, 1630–1635 (2013).

19. Duncan, N. C., Hay, B. P., Hagaman, E. W. & Custelcean, R. Thermodynamic, kinetic, and structural factors in the synthesis of imine-linked dynamic covalent frameworks. *Tetrahedron* **68**, 53–64 (2012).

20. Czaja, A. U., Trukhan, N. & Müller, U. Industrial applications of metal–organic frameworks. *Chem. Soc. Rev.* **38**, 1284–1293 (2009).

21. Ben, T. *et al.* Targeted Synthesis of a Porous Aromatic Framework with High Stability and Exceptionally High Surface Area. *Angew. Chem. Int. Ed.* **48**, 9457–9460 (2009).

22. Côté, A. P. *et al.* Porous, Crystalline, Covalent Organic Frameworks. *Science* **310**, 1166–1170 (2005).

23. Zhao, W., Xia, L. & Liu, X. Covalent organic frameworks (COFs): perspectives of industrialization. *CrystEngComm* **20**, 1613–1634 (2018).

24. Baldwin, L. A., Crowe, J. W., Pyles, D. A. & McGrier, P. L. Metalation of a Mesoporous Three-Dimensional Covalent Organic Framework. *J. Am. Chem. Soc.* **138**, 15134–15137 (2016).

25. Mendoza-Cortés, J. L., Han, S. S., Furukawa, H., Yaghi, O. M. & Goddard, W. A. Adsorption Mechanism and Uptake of Methane in Covalent Organic Frameworks: Theory and Experiment. *J. Phys. Chem. A* **114**, 10824–10833 (2010).

26. Han, S. S., Furukawa, H., Yaghi, O. M. & Goddard, W. A. Covalent Organic Frameworks as Exceptional Hydrogen Storage Materials. *J. Am. Chem. Soc.* **130**, 11580–11581 (2008).

27. Klontzas, E., Tylianakis, E. & Froudakis, G. E. Hydrogen Storage in 3D Covalent Organic Frameworks. A Multiscale Theoretical Investigation. *J. Phys. Chem. C* **112**, 9095–9098 (2008).

28. Cao, D., Lan, J., Wang, W. & Smit, B. Lithium-Doped 3D Covalent Organic Frameworks: High-Capacity Hydrogen Storage Materials. *Angew. Chem. Int. Ed.* **48**, 4730–4733 (2009).

29. Tylianakis, E., Klontzas, E. & Froudakis, G. E. Multi-scale theoretical investigation of hydrogen storage in covalent organic frameworks. *Nanoscale* **3**, 856–869 (2011).

30. Furukawa, H. & Yaghi, O. M. Storage of Hydrogen, Methane, and Carbon Dioxide in Highly Porous Covalent Organic Frameworks for Clean Energy Applications. *J. Am. Chem. Soc.* **131**, 8875–8883 (2009).

31. Wang Chang *et al.* A 3D Covalent Organic Framework with Exceptionally High Iodine Capture Capability. *Chem. – Eur. J.* **24**, 585–589 (2017).

32. El-Kaderi, H. M. *et al.* Designed Synthesis of 3D Covalent Organic Frameworks. *Science* **316**, 268–272 (2007).

33. Huang, N., Ding, X., Kim, J., Ihee, H. & Jiang, D. A Photoresponsive Smart Covalent Organic Framework. *Angew. Chem. Int. Ed.* **54**, 8704–8707 (2015).

34. Alahakoon, S. B. *et al.* An azine-linked hexaphenylbenzene based covalent organic framework. *Chem. Commun.* **52**, 2843–2845 (2016).

35. Ritchie, L. K., Trewin, A., Reguera-Galan, A., Hasell, T. & Cooper, A. I. Synthesis of COF-5 using microwave irradiation and conventional solvothermal routes. *Microporous Mesoporous Mater.* **132**, 132–136 (2010).

36. Singh, V., Jang, S., Vishwakarma, N. K. & Kim, D.-P. Intensified synthesis and post-synthetic modification of covalent organic frameworks using a continuous flow of microdroplets technique. *NPG Asia Mater.* **10**, e456 (2018).

37. Bisbey, R. P., DeBlase, C. R., Smith, B. J. & Dichtel, W. R. Two-dimensional Covalent Organic Framework Thin Films Grown in Flow. *J. Am. Chem. Soc.* **138**, 11433–11436 (2016).

38. Peng, Y. *et al.* Room Temperature Batch and Continuous Flow Synthesis of Water-Stable Covalent Organic Frameworks (COFs). *Chem. Mater.* **28**, 5095–5101 (2016).

39. Jiang, Y. *et al.* Green, scalable and morphology controlled synthesis of nanofibrous covalent organic frameworks and their nanohybrids through a vapor-assisted solid-state approach. *J. Mater. Chem. A* **2**, 8201–8204 (2014).

40. Medina, D. D. *et al.* Room Temperature Synthesis of Covalent–Organic Framework Films through Vapor-Assisted Conversion. *J. Am. Chem. Soc.* **137**, 1016–1019 (2015).

41. Ding, S.-Y. *et al.* Construction of Covalent Organic Framework for Catalysis: Pd/COF-LZU1 in Suzuki–Miyaura Coupling Reaction. *J. Am. Chem. Soc.* **133**, 19816–19822 (2011).

42. Pachfule, P., Kandambeth, S., Díaz, D. D. & Banerjee, R. Highly stable covalent organic framework–Au nanoparticles hybrids for enhanced activity for nitrophenol reduction. *Chem. Commun.* **50**, 3169–3172 (2014).

43. Valentino, L., Matsumoto, M., Dichtel, W. R. & Mariñas, B. J. Development and Performance Characterization of a Polyimine Covalent Organic Framework Thin-Film Composite Nanofiltration Membrane. *Environ. Sci. Technol.* **51**, 14352–14359 (2017).

44. Zhao, S. *et al.* Channel-wall functionalization in covalent organic frameworks for the enhancement of CO2 uptake and CO2/N2 selectivity. *RSC Adv.* **6**, 38774–38781 (2016).

45. Campbell, N. L., Clowes, R., Ritchie, L. K. & Cooper, A. I. Rapid Microwave Synthesis and Purification of Porous Covalent Organic Frameworks. *Chem. Mater.* **21**, 204–206 (2009).

46. Hunt, J. R., Doonan, C. J., LeVangie, J. D., Côté, A. P. & Yaghi, O. M. Reticular Synthesis of Covalent Organic Borosilicate Frameworks. *J. Am. Chem. Soc.* **130**, 11872–11873 (2008).

47. Liu, X.-Y. *et al.* Effect of metal catalyst on the mechanism of hydrogen spillover in three-dimensional covalent-organic frameworks. *Chin. Phys. B* **26**, 027302 (2017).

48. Kalidindi, S. B., Yusenko, K. & Fischer, R. A. Metallocenes@COF-102: organometallic host–guest chemistry of porous crystalline organic frameworks. *Chem. Commun.* **47**, 8506–8508 (2011).

49. Zhang, Y. *et al.* Three-Dimensional Anionic Cyclodextrin-Based Covalent Organic Frameworks. *Angew. Chem. Int. Ed.* **56**, 16313–16317 (2017).

50. Wang, R.-Q., Wei, X.-B. & Feng, Y.-Q. β-Cyclodextrin Covalent Organic Framework for Selective Molecular Adsorption. *Chem. – Eur. J.* **24**, 10979–10983 (2018).

51. DeBlase, C. R. & Dichtel, W. R. Moving Beyond Boron: The Emergence of New Linkage Chemistries in Covalent Organic Frameworks. *Macromolecules* **49**, 5297–5305 (2016).

52. Uribe-Romo, F. J. *et al.* A Crystalline Imine-Linked 3-D Porous Covalent Organic Framework. *J. Am. Chem. Soc.* **131**, 4570–4571 (2009).

53. Ma, T. *et al.* Observation of Interpenetration Isomerism in Covalent Organic Frameworks. *J. Am. Chem. Soc.* (2018). doi:10.1021/jacs.8b03169

54. Ma, T. *et al.* Single-crystal x-ray diffraction structures of covalent organic frameworks. *Science* **361**, 48–52 (2018).

55. Das, S. & Ben, T. A [COF-300]-[UiO-66] composite membrane with remarkably high permeability and H2/CO2 separation selectivity. *Dalton Trans.* **47**, 7206–7212 (2018).

56. Qian, H.-L., Yang, C. & Yan, X.-P. Layer-by-layer preparation of 3D covalent organic framework/silica composites for chromatographic separation of position isomers. *Chem. Commun.* (2018). doi:10.1039/C8CC06621C

57. Zhang, Y.-B. *et al.* Single-Crystal Structure of a Covalent Organic Framework. *J. Am. Chem. Soc.* **135**, 16336–16339 (2013).

58. Xin, Y., Wang, C., Wang, Y., Sun, J. & Gao, Y. Encapsulation of an ionic liquid into the nanopores of a 3D covalent organic framework. *RSC Adv.* **7**, 1697–1700 (2017).

59. Ma, Y.-X. *et al.* A Dynamic Three-Dimensional Covalent Organic Framework. *J. Am. Chem. Soc.* **139**, 4995–4998 (2017).

60. Lin, G., Ding, H., Yuan, D., Wang, B. & Wang, C. A Pyrene-Based, Fluorescent Three-Dimensional Covalent Organic Framework. *J. Am. Chem. Soc.* **138**, 3302–3305 (2016).

61. Lin, G. *et al.* 3D Porphyrin-Based Covalent Organic Frameworks. *J. Am. Chem. Soc.* **139**, 8705–8709 (2017).

62. Han, X., Huang, J., Yuan, C., Liu, Y. & Cui, Y. Chiral 3D Covalent Organic Frameworks for High Performance Liquid Chromatographic Enantioseparation. *J. Am. Chem. Soc.* (2018). doi:10.1021/jacs.7b12110

63. Li, H. *et al.* Three-Dimensional Covalent Organic Frameworks with Dual Linkages for Bifunctional Cascade Catalysis. *J. Am. Chem. Soc.* **138**, 14783–14788 (2016).

64. Fang, Q. *et al.* 3D Microporous Base-Functionalized Covalent Organic Frameworks for Size-Selective Catalysis. *Angew. Chem. Int. Ed.* **53**, 2878–2882 (2014).

65. Liu, Y. *et al.* Weaving of organic threads into a crystalline covalent organic framework. *Science* **351**, 365–369 (2016).

66. Zhao, Y. *et al.* A Synthetic Route for Crystals of Woven Structures, Uniform Nanocrystals, and Thin Films of Imine Covalent Organic Frameworks. *J. Am. Chem. Soc.* **139**, 13166–13172 (2017).

67. Guan, X. *et al.* Fast, Ambient Temperature and Pressure Ionothermal Synthesis of Three-Dimensional Covalent Organic Frameworks. *J. Am. Chem. Soc.* **140**, 4494–4498 (2018).

68. Beaudoin, D., Maris, T. & Wuest, J. D. Constructing monocrystalline covalent organic networks by polymerization. *Nat. Chem.* **5**, 830–834 (2013).

69. Ren, S. *et al.* Porous, Fluorescent, Covalent Triazine-Based Frameworks Via Room-Temperature and Microwave-Assisted Synthesis. *Adv. Mater.* **24**, 2357–2361 (2012).

70. Fang, Q. *et al.* 3D Porous Crystalline Polyimide Covalent Organic Frameworks for Drug Delivery. *J. Am. Chem. Soc.* **137**, 8352–8355 (2015).

71. Yahiaoui, O. *et al.* 3D Anionic Silicate Covalent Organic Framework with srs Topology. *J. Am. Chem. Soc.* **140**, 5330–5333 (2018).

72. Bunck, D. N. & Dichtel, W. R. Internal Functionalization of Three-Dimensional Covalent Organic Frameworks. *Angew. Chem. Int. Ed.* **51**, 1885–1889 (2012).

73. Bunck, D. N. & Dichtel, W. R. Postsynthetic functionalization of 3D covalent organic frameworks. *Chem. Commun.* **49**, 2457–2459 (2013).

74. Brucks, S. D., Bunck, D. N. & Dichtel, W. R. Functionalization of 3D covalent organic frameworks using monofunctional boronic acids. *Polymer* **55**, 330–334 (2014).

75. Lu, Q. *et al.* Postsynthetic Functionalization of Three-Dimensional Covalent Organic Frameworks for Selective Extraction of Lanthanide Ions. *Angew. Chem.* **130**, 6150–6156 (2018).

76. Huang, N., Krishna, R. & Jiang, D. Tailor-Made Pore Surface Engineering in Covalent Organic Frameworks: Systematic Functionalization for Performance Screening. *J. Am. Chem. Soc.* **137**, 7079–7082 (2015).

77. Nagai, A. *et al.* Pore surface engineering in covalent organic frameworks. *Nat. Commun.* **2**, 536 (2011).

78. Huang, N., Chen, X., Krishna, R. & Jiang, D. Two-Dimensional Covalent Organic Frameworks for Carbon Dioxide Capture through Channel-Wall Functionalization. *Angew. Chem. Int. Ed.* **54**, 2986–2990 (2015).

79. Chen, X. *et al.* Locking Covalent Organic Frameworks with Hydrogen Bonds: General and Remarkable Effects on Crystalline Structure, Physical Properties, and Photochemical Activity. *J. Am. Chem. Soc.* **137**, 3241–3247 (2015).

80. Zhang, J. *et al.* A novel azobenzene covalent organic framework. *CrystEngComm* **16**, 6547–6551 (2014).

81. Deshpande, R. K., Waterhouse, G. I. N., Jameson, G. B. & Telfer, S. G. Photolabile protecting groups in metal–organic frameworks: preventing interpenetration and masking functional groups. *Chem. Commun.* **48**, 1574–1576 (2012).

82. Waller, P. J., Gándara, F. & Yaghi, O. M. Chemistry of Covalent Organic Frameworks. *Acc. Chem. Res.* **48**, 3053–3063 (2015).

83. Smith, B. J., Overholts, A. C., Hwang, N. & Dichtel, W. R. Insight into the crystallization of amorphous imine-linked polymer networks to 2D covalent organic frameworks. *Chem. Commun.* **52**, 3690–3693 (2016).

84. Matsumoto, M. *et al.* Rapid, Low Temperature Formation of Imine-Linked Covalent Organic Frameworks Catalyzed by Metal Triflates. *J. Am. Chem. Soc.* **139**, 4999–5002 (2017).

85. Giuseppone, N., Schmitt, J.-L., Schwartz, E. & Lehn, J.-M. Scandium(III) Catalysis of Transimination Reactions. Independent and Constitutionally Coupled Reversible Processes. *J. Am. Chem. Soc.* **127**, 5528–5539 (2005).

86. Evans, A. M. *et al.* Seeded growth of single-crystal two-dimensional covalent organic frameworks. *Science* **361**, 52–57 (2018).

87. Yuan, Y.-C., Sun, B., Cao, A.-M., Wang, D. & Wan, L.-J. Heterogeneous nucleation and growth of highly crystalline imine-linked covalent organic frameworks. *Chem. Commun.* **54**, 5976–5979 (2018).

88. Matsumoto, M. *et al.* Lewis-Acid-Catalyzed Interfacial Polymerization of Covalent Organic Framework Films. *Chem* **4**, 308–317 (2018).

89. Dey, K. *et al.* Selective Molecular Separation by Interfacially Crystallized Covalent Organic Framework Thin Films. *J. Am. Chem. Soc.* **139**, 13083–13091 (2017).

90. Li, Y. *et al.* Growth of high-quality covalent organic framework nanosheets at the interface of two miscible organic solvents. *Nanoscale Horiz.* **3**, 205–212 (2018).

91. Spitler, E. L. & Dichtel, W. R. Lewis acid-catalysed formation of two-dimensional phthalocyanine covalent organic frameworks. *Nat. Chem.* **2**, 672–677 (2010).

92. Wei, T., Furgal, J. C. & Scott, T. F. In situ deprotection and dynamic covalent assembly using a dual role catalyst. *Chem. Commun.* **53**, 3874–3877 (2017).

93. Li, H. *et al.* Nucleation and Growth of Covalent Organic Frameworks from Solution: The Example of COF-5. *J. Am. Chem. Soc.* **139**, 16310–16318 (2017).

94. Öhrström, L. Let's Talk about MOFs—Topology and Terminology of Metal-Organic Frameworks and Why We Need Them. *Crystals* **5**, 154–162 (2015).

95. Prasad, T. K. & Suh, M. P. Control of Interpenetration and Gas-Sorption Properties of Metal–Organic Frameworks by a Simple Change in Ligand Design. *Chem. – Eur. J.* **18**, 8673–8680 (2012).

96. Zhang, J., Wojtas, L., Larsen, R. W., Eddaoudi, M. & Zaworotko, M. J. Temperature and Concentration Control over Interpenetration in a Metal−Organic Material. *J. Am. Chem. Soc.* **131**, 17040–17041 (2009).

97. Farha, O. K., Malliakas, C. D., Kanatzidis, M. G. & Hupp, J. T. Control over Catenation in Metal−Organic Frameworks via Rational Design of the Organic Building Block. *J. Am. Chem. Soc.* **132**, 950–952 (2010).

Chapter 2
Synthesis of Tetrahedral Monomers and Imine-linked 3D COFs

2.1 Abstract

Tetra-functional amine and aldehyde monomers derived from tetraphenylmethane are successfully synthesized and characterized by ^{1}H-NMR, ^{13}C-NMR, and mass spectrometry. The synthetic procedure for producing 3D imine-linked COFs is adapted from published procedure, and an innovative reaction setup is employed to improve the usability and safety of the degas and reaction process by removing the need for flame sealing and breaking the glass tubes post synthesis. Crystalline COF-300 and COF-320 are successfully synthesized using this adapted procedure and characterized *via* PXRD, FTIR, and SEM, and the synthesis and characterization of a novel COF structure, the tetraamine-tetraaldehyde COF, is explored. The synthesis of 3D COFs is a complex and opaque process, and the insights gained from these processes are invaluable for improving the consistency and reproducibility of subsequent COF syntheses. In addition, COF-300, as an archetypal 3D imine-linked COF, serves as the basis of further investigation of 3D COF synthesis and modification of COF structure, which are detailed in the later chapters.

2.2 Introduction

Compared to two-dimensional (2D) COFs, three-dimensional (3D) COFs in general possess superior attributes including higher internal surface areas, greater porosity, and lower

density, which provide great appeal for applications such as gas storage, adsorption, and catalysis[1]. Despite the many attractive traits of 3D COFs, investigations into the structural diversity and potential applications of these 3D frameworks remain sparse in comparison to those of their 2D counterparts, whose synthetic accessibility is greatly aided by the π-orbital overlap between the stacking 2D layers that provides additional driving force towards forming an ordered crystalline structure. As such, greater research effort in 3D COFs is needed to unlock the full potential of their highly appealing attributes[1].

While early research efforts on 3D COFs revolved around structures based on boron-oxygen linkages, the research focus in the field has shifted firmly to imine-linked structures in the past five years. Compared to B-O linkages such as boroxine rings and boronate ester rings, the imine bond exhibits much greater stability towards hydrolysis and oxidation, and there has been a notable trend away from B-O linkages towards the more robust imine linkage in the overall COF field[2]. COF-300 was the first reported imine-linked 3D COF[3] and remains the archetypal, most structurally simple, and most studied[4–7] imine-linked 3D COF. As such, synthesis of tetrakis(4-aminophenyl)methane (TAPM), the tetrahedral amine monomer that constitutes COF-300, and subsequent synthesis of COF-300 itself utilizing TAPM and terephthalaldehyde is carried out to serve as a framework for improved understanding of the COF synthetic process, which is quite difficult and unpredictable compared to conventional monomer or polymer synthesis and governed by empirical approaches rather than theoretical or mechanistic studies. In addition, COF-300 could serve as an excellent representative platform through which further investigations into synthetic improvements, modification, and functionalization of 3D imine-linked COFs could be conducted. Once tetrakis(4-aminophenyl)methane is successfully synthesized, it can also be used to synthesize the structurally similar COF-320, which differs from COF-300 by the length of the linear

dialdehyde linker, employing 4-4'-biphenyldicarboxyaldehyde instead of terephthalaldehyde. Lastly, a tetrahedral aldehyde monomer, tetrakis(4-formylphenyl)methane, is synthesized and used alongside tetrakis(4-aminophenyl)methane to explore the synthesis of a novel tetraamine-tetraaldehyde COF.

2.3 Experimental

2.3.1 General Experimental Procedure

All chemicals and reagents, unless specified, were purchased from commercial sources, including Fisher Scientific, Sigma-Aldrich, Alfa Aesar, and Oakwood Chemicals, and used as received without any further purification. ^{1}H NMR spectra were recorded on a Varian Inova 500 instrument (500 MHz). ^{13}C NMR spectra were recorded on a Varian MR400 instrument (400 MHz). Chemical shifts were measured in δ (ppm) relative to residual solvent signals as internal standards ($CDCl_3$: 7.24 for ^{1}H, 77.23 for ^{13}C; d^6-DMSO: 2.49 for ^{1}H). Electronic Impact (EI) mass spectrometry spectra were collected on a Micromass AutoSpec Ultima Magnetic Sector Mass Spectrometer. Powder X-ray Diffraction (PXRD) spectra were collected using a Rigaku 600 Miniflex XRD instrument and a 5mm zero background sample holder. Fourier Transform Infrared (FTIR) spectroscopy was performed on a Thermo Scientific Nicolet 6700 FTIR spectrometer equipped with a Spectra-Tech diffusive reflectance unit. Scanning Electron Microscopy (SEM) images were collected using a Philips XL 30 SEM instrument.

2.3.2 Monomer Synthesis

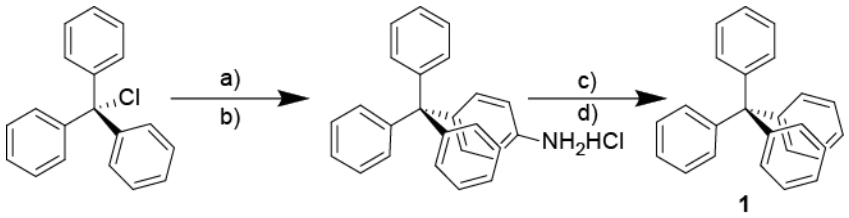

Scheme 2.1. Synthesis of tetraphenylmethane (1). Reagents and conditions: a) aniline, 190°C; b) 2N HCl/MeOH, reflux; c) H_2SO_4/EtOH, isoamylnitrite, -10°C; d) 50% H_3PO_2, reflux.[8]

Tetraphenylmethane (1). This synthesis procedure was adapted from a published approach[8]. Chlorotriphenylmethane (10 g, 35.9 mmol) and aniline (8.5 mL, 93.3 mmol) were mixed and heated to 190°C for 15 min under rigorous stirring. After cooling to room temperature, the violet solids were ground to powder and re-dissolved in a mixture of 2N aqueous hydrochloric acid solution (40 ml) and methanol (60 ml). The solution was heated to 80°C for 30 min. After cooling to room temperature, the resulting violet solid was filtered, washed with water, and dried *in vacuo*.

After drying, the solid was dissolved in ethanol (130 ml) and concentrated aqueous sulfuric acid solution (20 ml) and cooled to -10°C. 15 ml of isoamylnitrite was added to dropwise, and the mixture was stirred for 30 minutes. Then, 30 ml of 50% hypophosphorous acid was added dropwise at -10°C, and the reaction was subsequently heated to 50°C for 2 h. An olive color solid was collected by filtration, washed with dimethylformamide (100 ml), water (100 ml), and ethanol (100 ml) to yield compound **1** as an olive color solid (9.85 g, 90% yield).

Characterization data: ^{1}H NMR ($CDCl_3$, δ ppm): 7.16-7.26 (m, 20 H, Ar).

^{13}C NMR ($CDCl_3$, δ ppm): 65.0 (1C, $C_q(Ar)_4$), 125.9 (4C, C_p-Ar), 127.5 (8C, C_m-Ar), 131.2 (8C, C_o-Ar), 146.8 (4C, C_q-Ar).

m/z (70 eV, EI+): 320 (M^+), 243 (M^+-C_6H_5), 165 ($C_{13}H_9^+$).

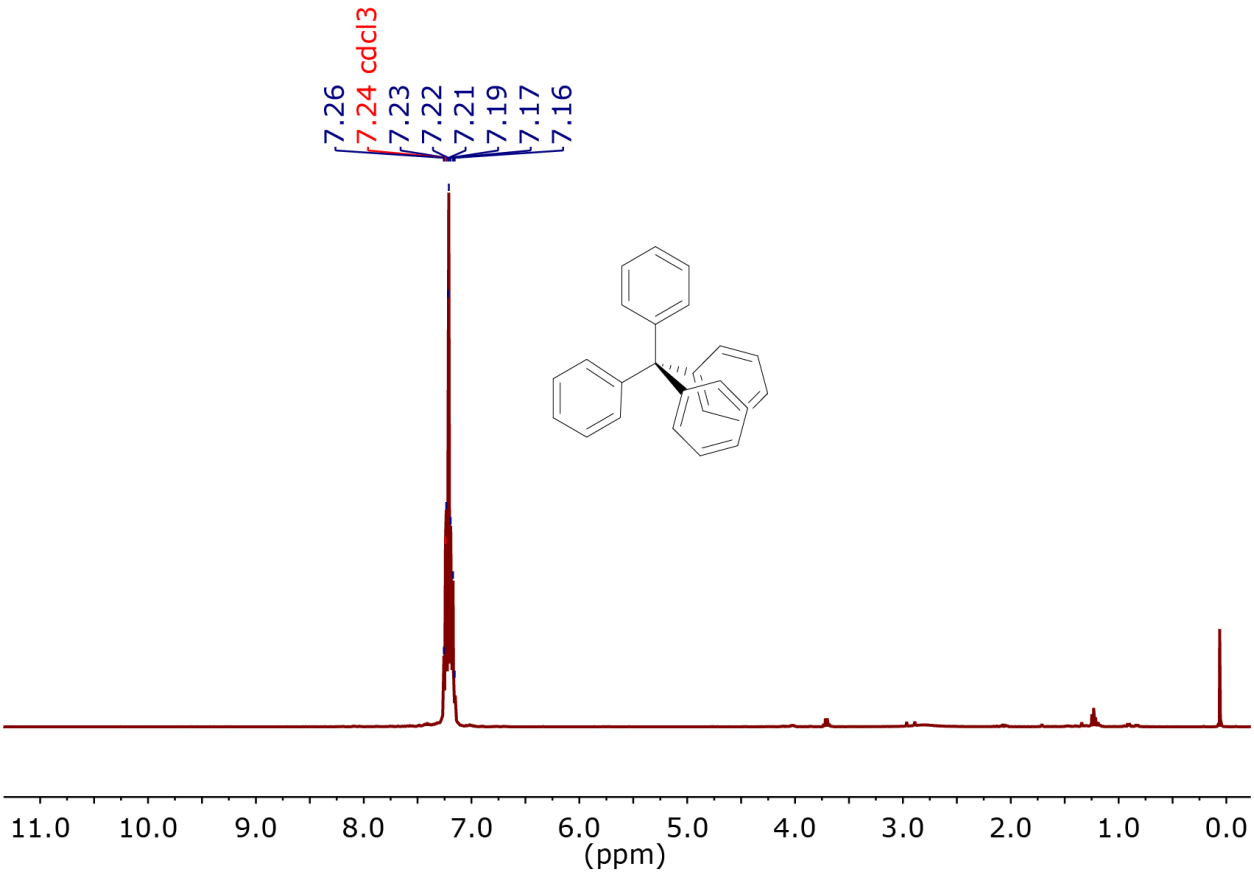

Figure 2.1. ^{1}H NMR spectrum of tetraphenylmethane.

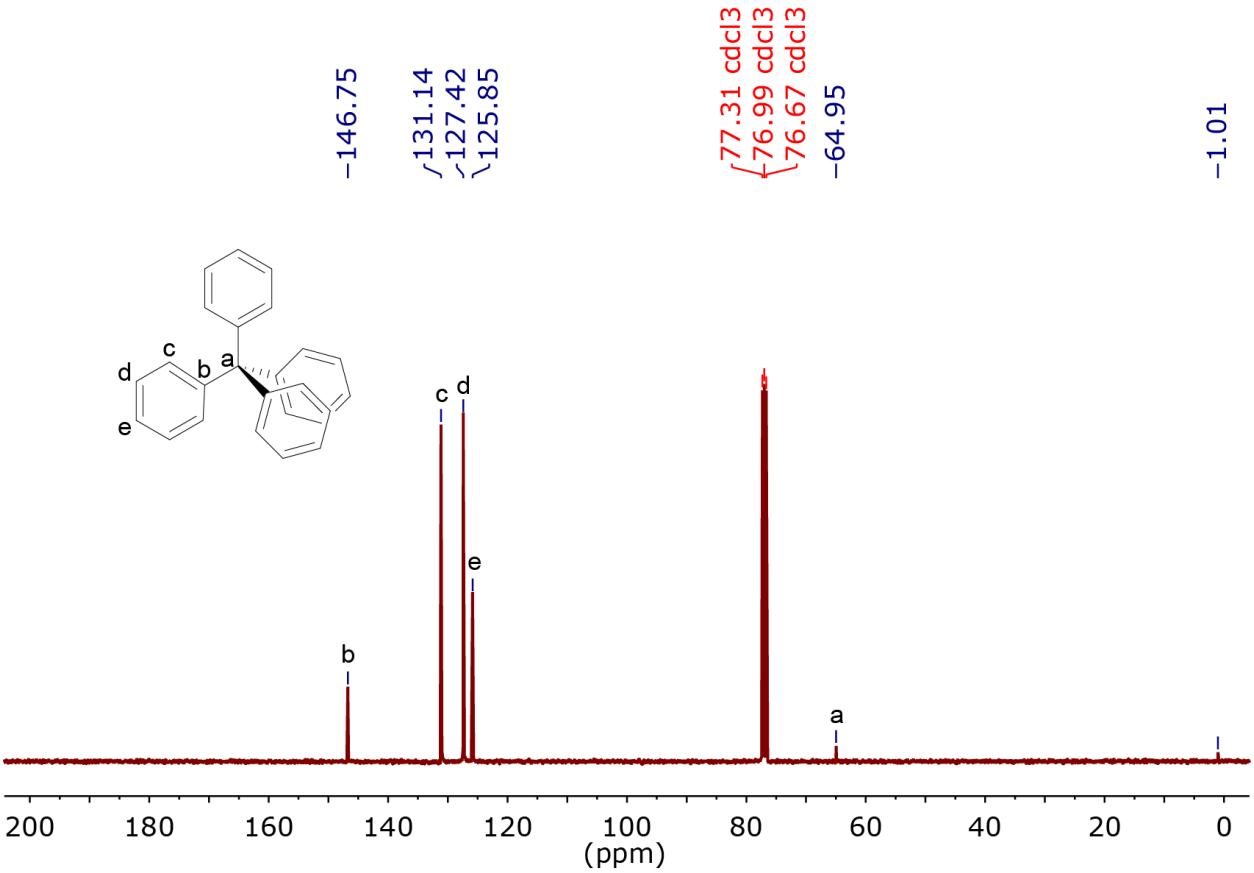

Figure 2.2. ^{13}C NMR spectrum of tetraphenylmethane.

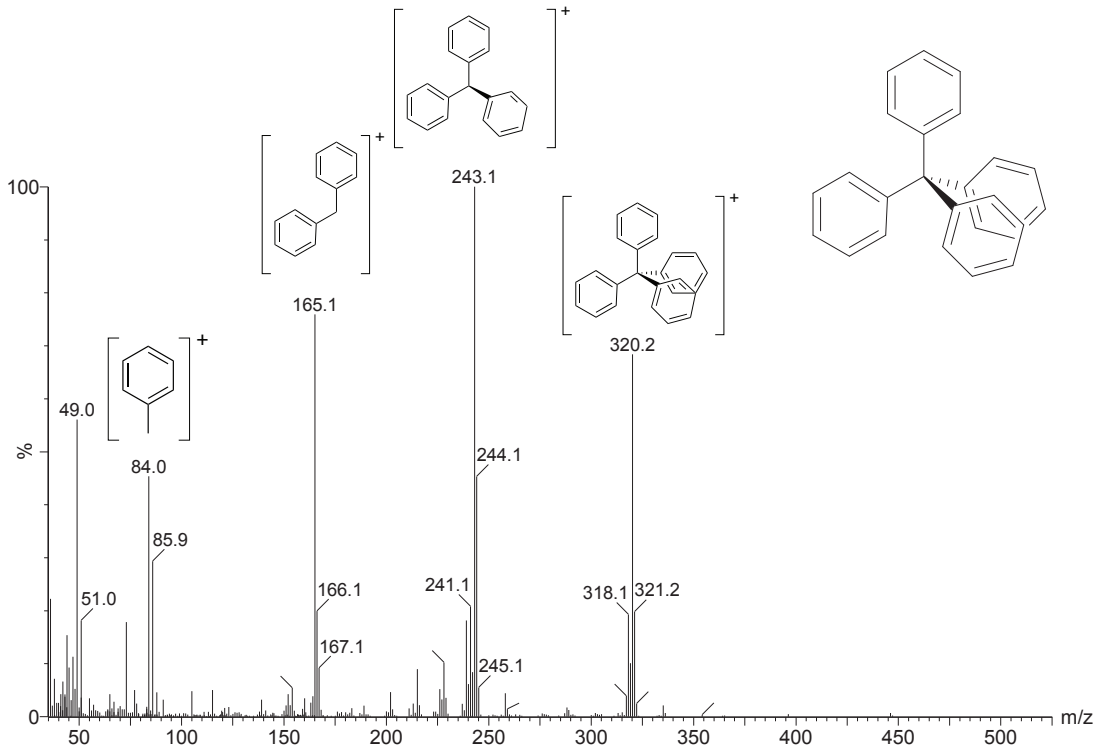

Figure 2.3. EI mass spectra of tetraphenylmethane.

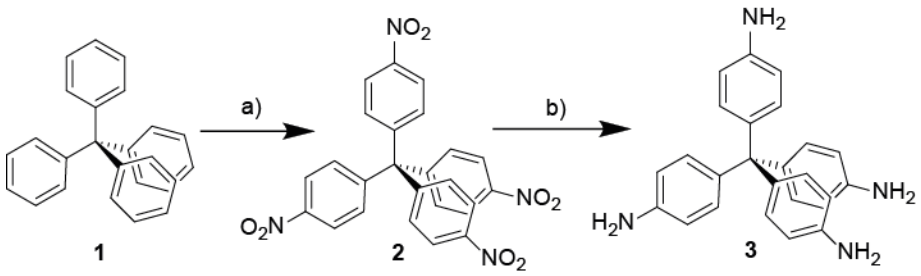

Scheme 2.2. Synthesis of tetrakis(4-aminophenyl)methane (3). Reagents and conditions: a) fuming nitric acid, Ac_2O/AcOH, AcOH, -5°C; b) Raney Ni, $N_2H_4 \cdot H_2O$, reflux.

Tetrakis-(4-nitrophenyl)methane (2). The synthesis procedure for compound **2** was adapted from a published approach[9]. Compound **1** (4.8g, 15.0 mmol) was slowly added to fuming nitric

acid (25 ml) stirred rigorously in a salt/ice bath of ~-5°C. Then, a mixture of acetic anhydride and glacial acetic acid (1:2, 25 ml) was added slowly to the mixture. After stirring at -5°C for 15 min, glacial acetic acid (80 ml) was added, and the suspension was further stirred for 5 min. The mixture was filtered on a glass frit, washed with acetic acid (2 x 100 ml), methanol (2 x 100 ml), and chilled tetrahydrofuran (2 x 50 ml) and dried *in vacuo* to afford a cream color solid (3.2 g, 43% yield).

Characterization data: ^{1}H NMR (d^{6}-DMSO, δ ppm): 8.21 (d, 8H, Ar), 7.58 (d, 8H, Ar).

^{13}C NMR (d^{6}-DMSO, δ ppm): 65.7 (1C, C_q(Ar)$_4$), 124.2 (8C, C_m-Ar), 131.9 (8C, C_o-Ar), 146.5 (4C, C_q-Ar), 151.5 (4C, C_p-Ar).

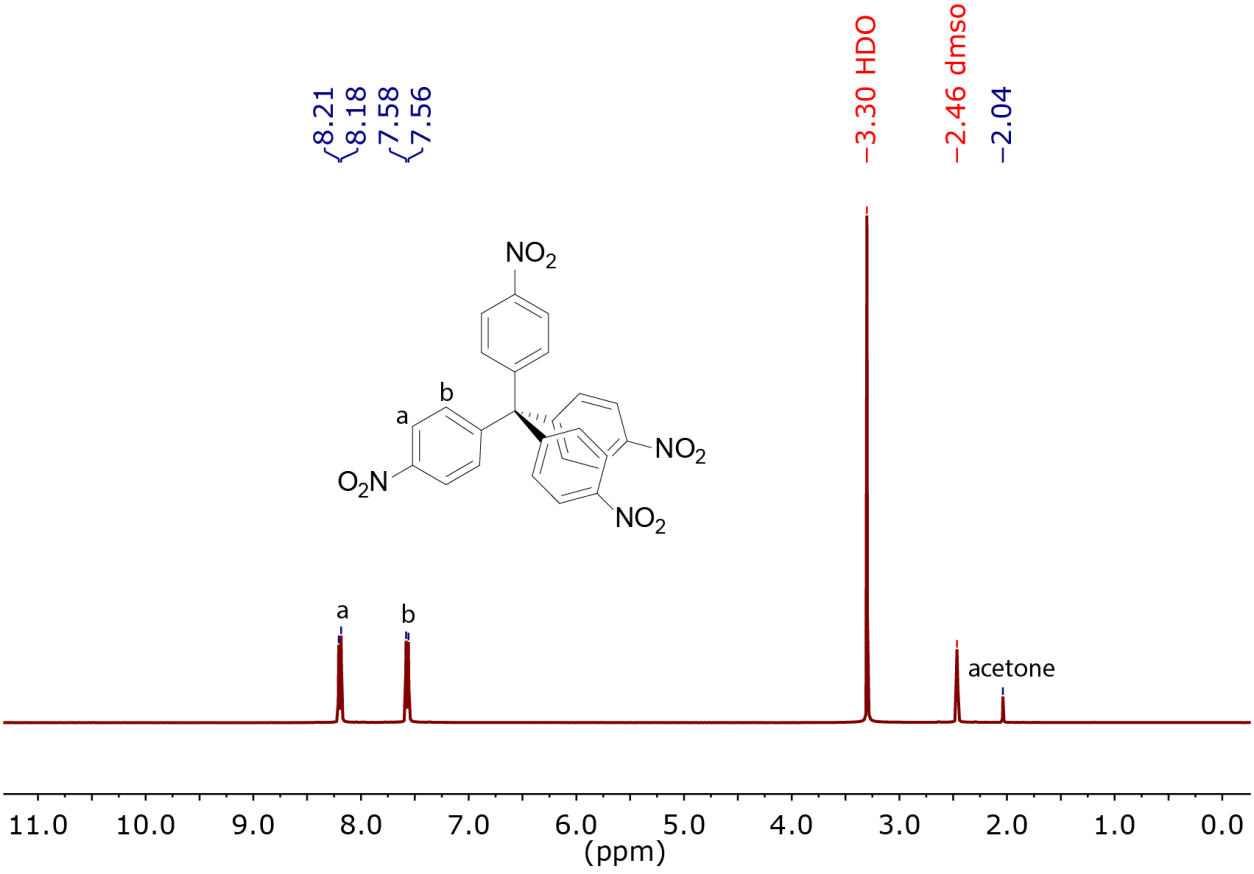

Figure 2.4. ^{1}H NMR spectrum of tetrakis(4-nitrophenyl)methane.

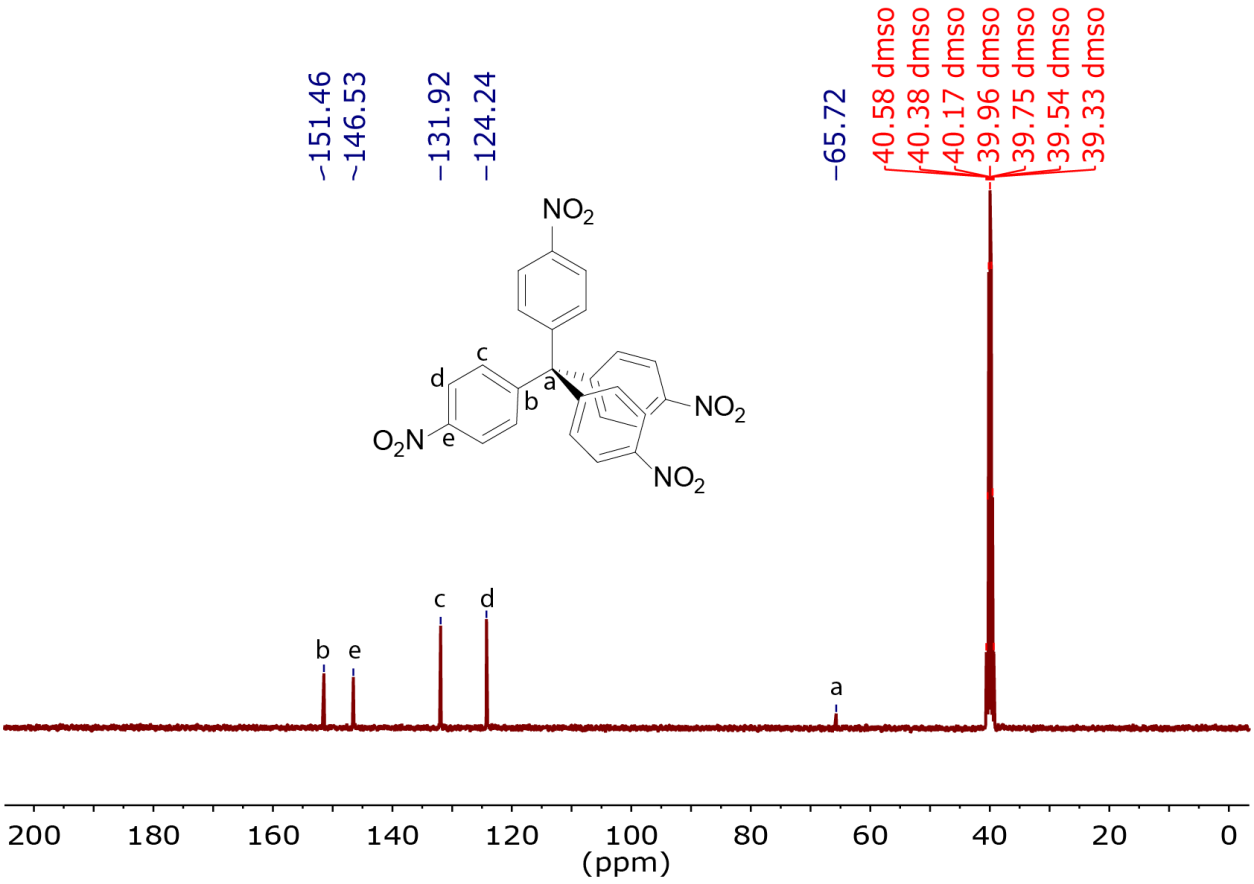

Figure 2.5. ^{13}**C NMR spectrum of tetrakis(4-nitrophenyl)methane.**

Tetrakis(4-aminophenyl)methane (3). The synthesis procedure for compound **3** was adapted from a published approach[9]. Compound **2** (1.5 g, 3 mmol) was dissolved in tetrahydrofuran (100 ml), and Raney nickel (10 g) was added to the solution while stirring under nitrogen. Hydrazine monohydrate (2 g, 0.04 mol) was slowly added via syringe, and the mixture was refluxed for 4 h. The mixture was filtered while hot and washed with ethanol. The filtrate was dried *in vacuo*. The crude product was subsequently washed with ethanol (50 ml) and dried *in vacuo* to afford **3** as a white solid (0.92 g, 81% yield).

Characterization data: ^{1}H NMR (d^{6}-DMSO, δ ppm): 6.67 (d, 8H, Ar), 6.39 (d, 8H, Ar), 4.84 (s, 8H, -NH_2).

^{13}C NMR (d^{6}-DMSO, δ ppm): 61.6 (1C, C_q(Ar)$_4$), 113.0 (8C, C_m-Ar), 131.5 (8C, C_o-Ar), 136.3 (4C, C_p-Ar), 146.1 (4C, C_q-Ar).

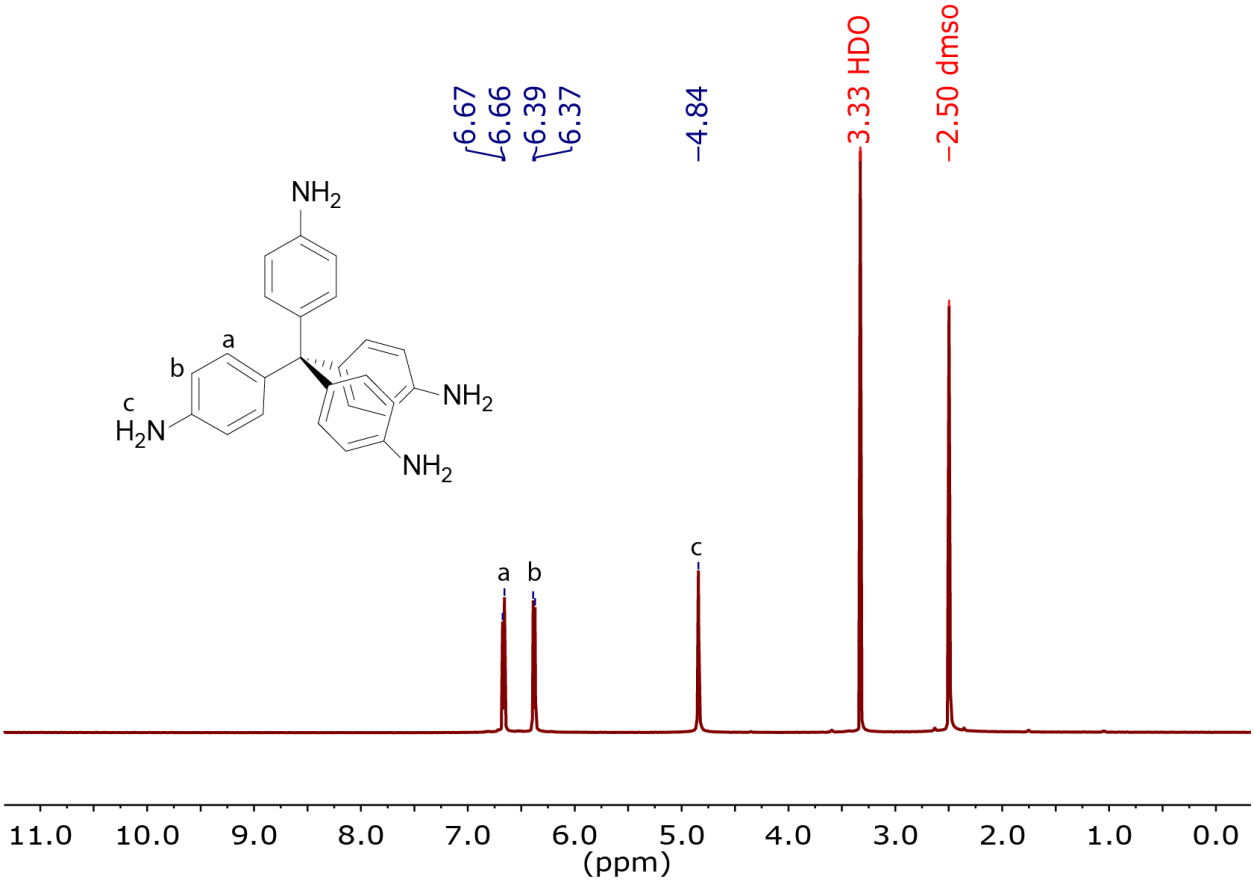

Figure 2.6. ^{1}H NMR spectrum of tetrakis(4-aminophenyl)methane.

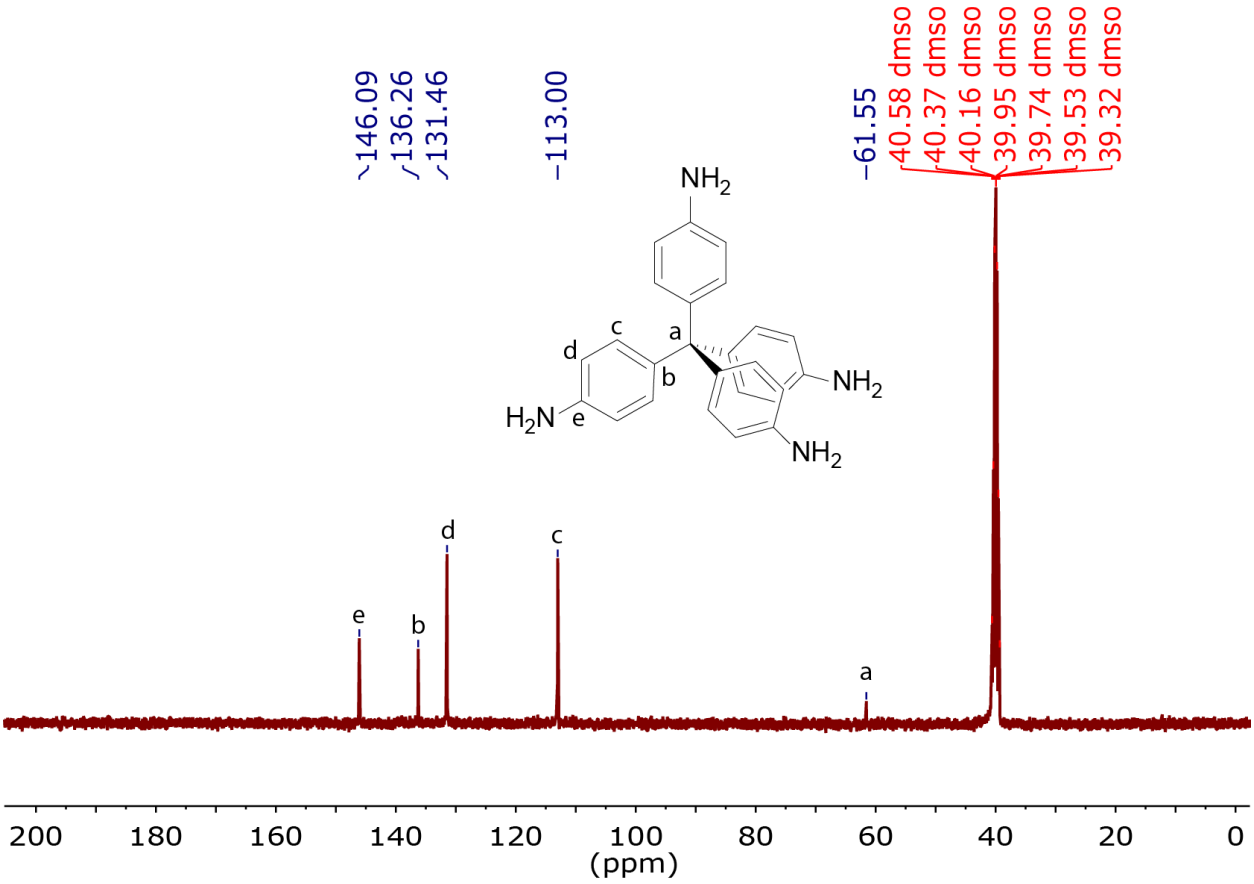

Figure 2.7. ^{13}C NMR spectrum of tetrakis(4-aminophenyl)methane.

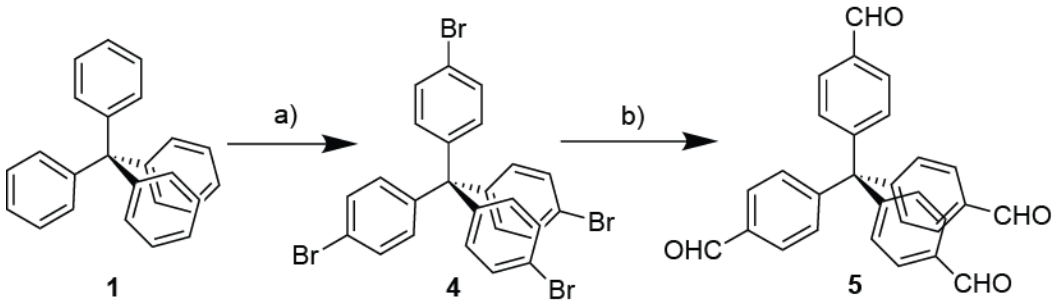

Scheme 2.3. Synthesis of tetrakis(4-formylphenyl)methane (5). Reagents and conditions: (a) Br_2, EtOH, -78°C; b) anhydrous THF, n-BuLi, anhydrous DMF, -78°C.

Tetrakis(4-bromophenyl)methane (4). The synthesis procedure for compound **4** was adapted from a published approach[8]. Compound **1** (5 g, 15.6 mmol) was deposited in a 250 ml three-neck

round bottom flask equipped with magnetic stirrer and outlet adapter connected to a sodium hydroxide quenching solution. Neat bromine (8.8 ml, 172 mmol) was added dropwise while stirring continuously. The dark orange slurry was stirred for an additional 20 min, cooled to -78°C, and diluted with ethanol (100 ml). The reaction mixture was allowed to warm to room temperature overnight. The precipitated solid was isolated by filtration and washed with saturated aqueous sodium metabisulfite solution and water. The solid was boiled in a mixture of ethanol and chloroform (1:1 v/v, 200 ml) for 10 min and cooled to room temperature. The mixture was filtered and dried *in vacuo* to afford compound **4** as a yellow solid (8.9 g, 90% yield).

Characterization data: ^{1}H NMR ($CDCl_3$, δ ppm): 7.39 (d, 8H, Ar), 7.00 (d, 8H, Ar).

^{13}C NMR ($CDCl_3$, δ ppm): 63.6 (1C, $C_q(Ar)_4$), 120.8 (4C, C_p-Ar), 131.1 (8C, C_m-Ar), 132.3 (8C, C_o-Ar), 144.4 (4C, C_q-Ar).

m/z (70 eV, EI+): 636 (M^+), 557 (M^+-Br), 479 (M^+-Br_2), 400 (M^+-Br_3), 321 (M^+-Br_4).

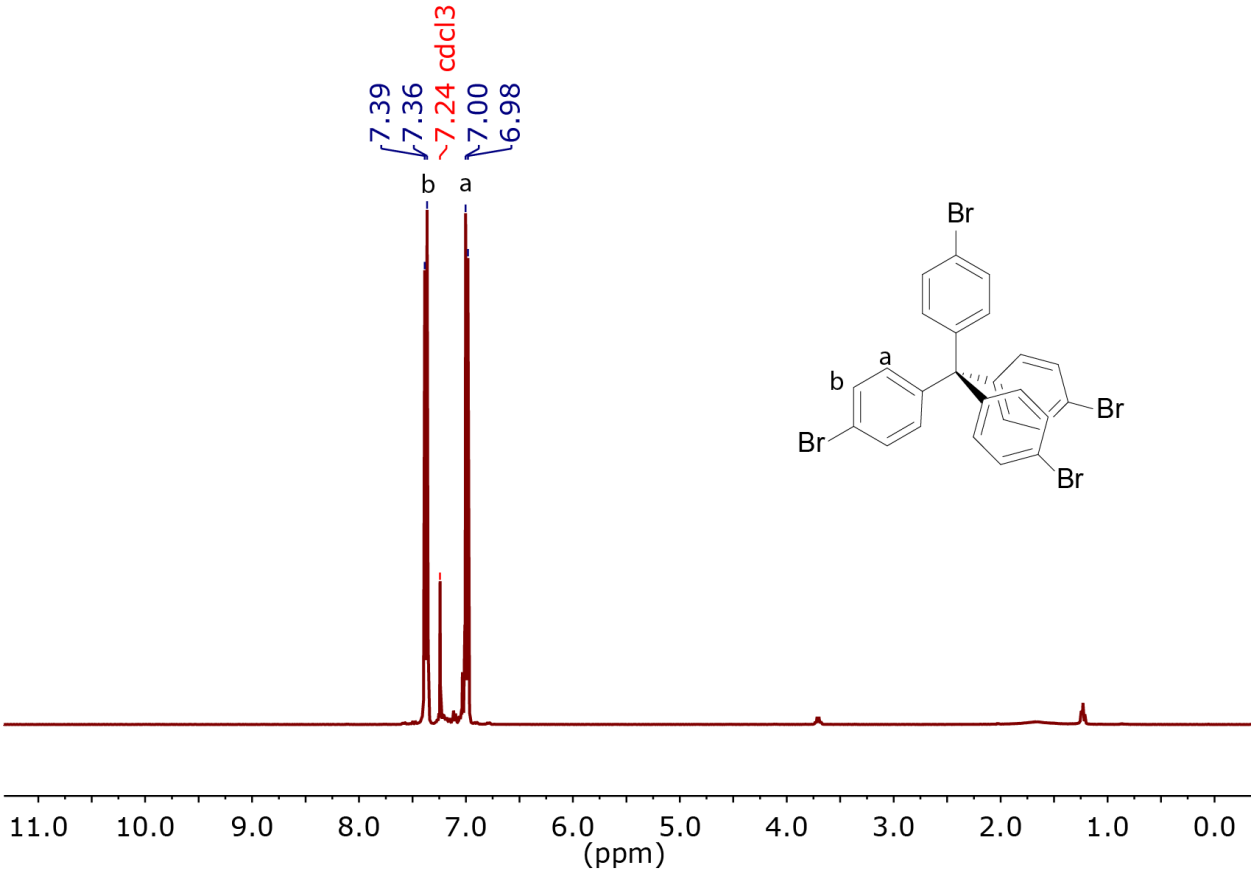

Figure 2.8. ^{1}H NMR spectrum of tetrakis(4-bromophenyl)methane.

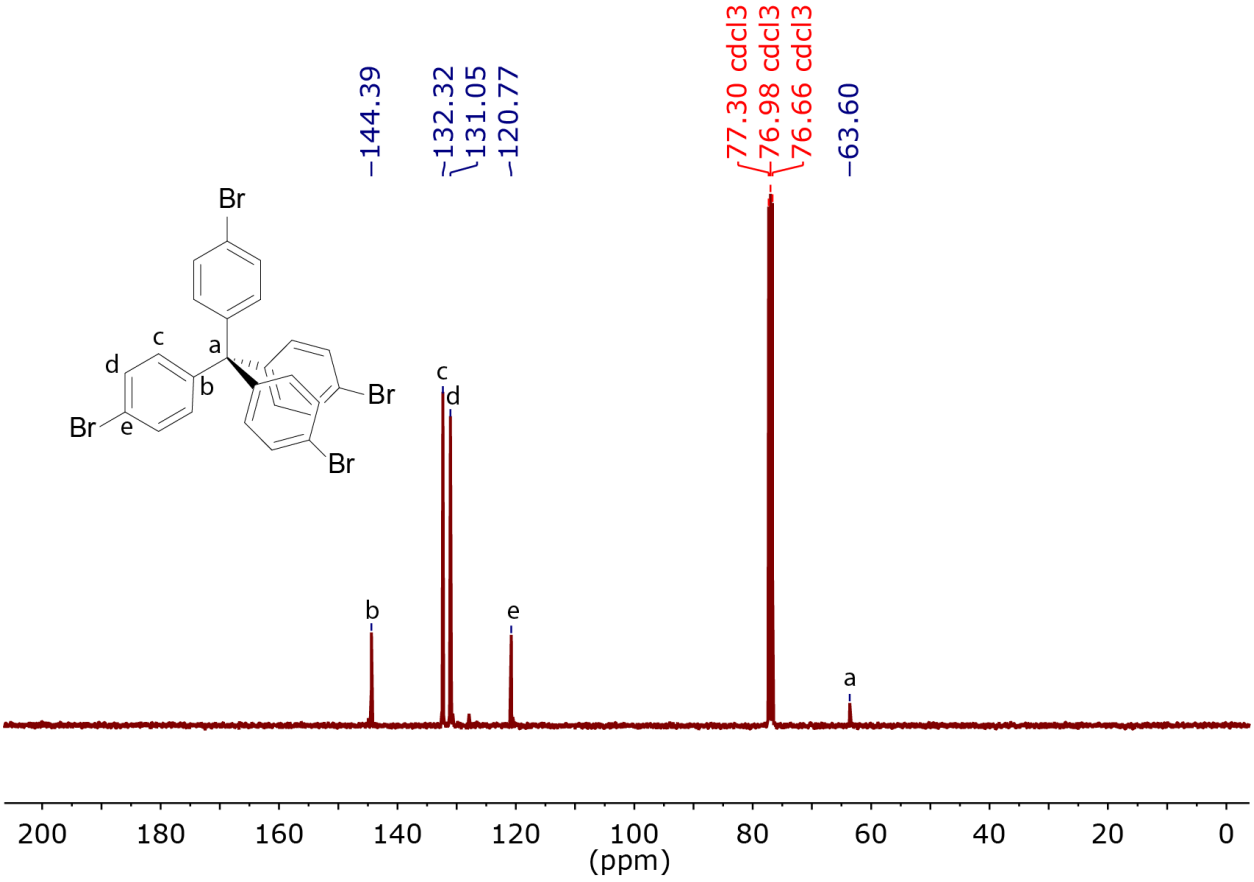

Figure 2.9. ^{13}C NMR spectrum of tetrakis(4-bromophenyl)methane.

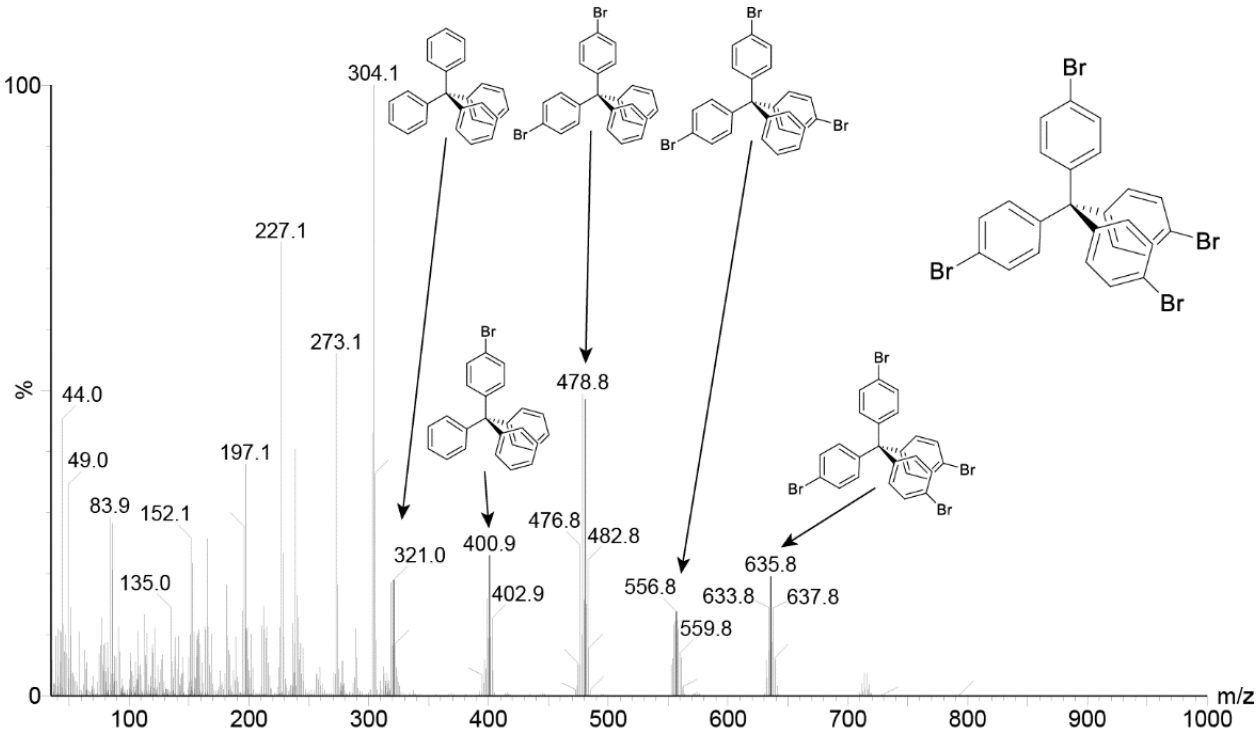

Figure 2.10. EI mass spectrum of tetrakis(4-bromophenyl)methane.

Tetrakis(4-formylphenyl)methane (5). Compound **4** (4 g, 6.3 mmol) was added to an oven-dried and septum-sealed 500 ml two-neck round bottom flask equipped with magnetic stirrer. The flask was purged with an argon balloon equipped with drying tube to remove air and moisture. Anhydrous tetrahydrofuran (200 ml) was added by syringe, and the solution was cooled to -78°C. n-Butyllithium (25 ml, 62.5 mmol) was added dropwise, and the reaction was stirred for 30 min at -78°C. Anhydrous dimethylformamide (10 ml, 129 mmol) was added, and the mixture was allowed to warm up to room temperature overnight. The reaction was quenched with 1M aqueous hydrochloric acid solution (100 ml) and extracted with ethyl acetate. The organic layer was washed with water, dried over magnesium sulfate, filtered, and dried *in vacuo*.

Characterization data: ^{1}H NMR ($CDCl_3$, δ ppm): 9.96 (s, 4H, -CHO), 7.88 (d, 8H, Ar), 7.50 (d, 8H, Ar).

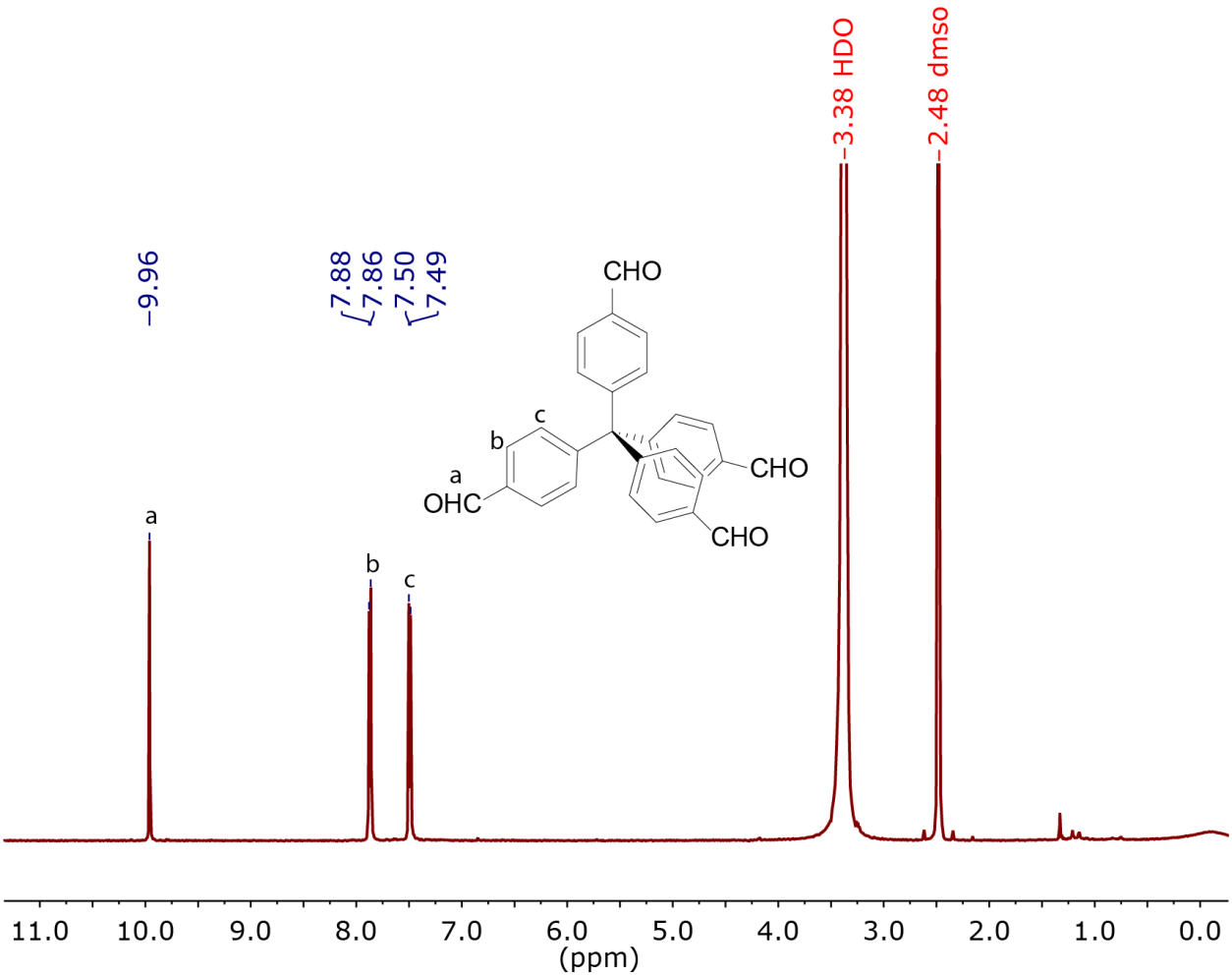

Figure 2.11. ^{1}H NMR spectrum of tetrakis(4-formylphenyl)methane.

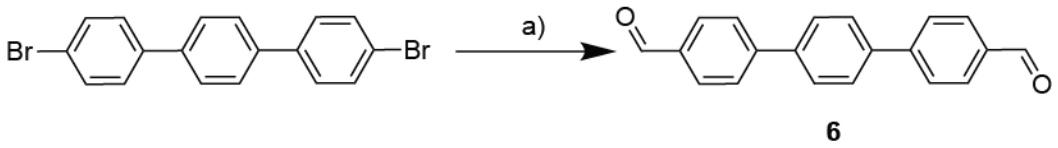

6

Scheme 2.4. Synthesis of [1,1':4',1''-terphenyl]-4,4''-dicarbaldehyde. Reagents and conditions: (a) anhydrous THF, n-BuLi, anhydrous DMF, -78°C.

[1,1':4',1''-terphenyl]-4,4''-dicarbaldehyde (5). 4,4''-dibromo-1,1':4',1''-terphenyl (0.5 g, 1.29 mmol) was added to an oven-dried and septum-sealed 250 ml two-neck round bottom flask equipped with magnetic stirrer. The flask was purged with an Ar balloon equipped with drying

tube to remove air and moisture. Anhydrous tetrahydrofuran (100 ml) was added by syringe, and the solution was cooled to -78°C. n-Butyllithium (5 ml, 12.5 mmol) was added dropwise, and the reaction was stirred for 30 min at -78°C. Anhydrous dimethylformamide (2 ml, 25.8 mmol) was added, and the mixture was allowed to warm up to room temperature overnight. The reaction was quenched with 1 M aqueous hydrochloric acid solution (20 ml) and extracted with ethyl acetate. The organic layer was washed with water, dried over magnesium sulfate, filtered, and dried *in vacuo*.

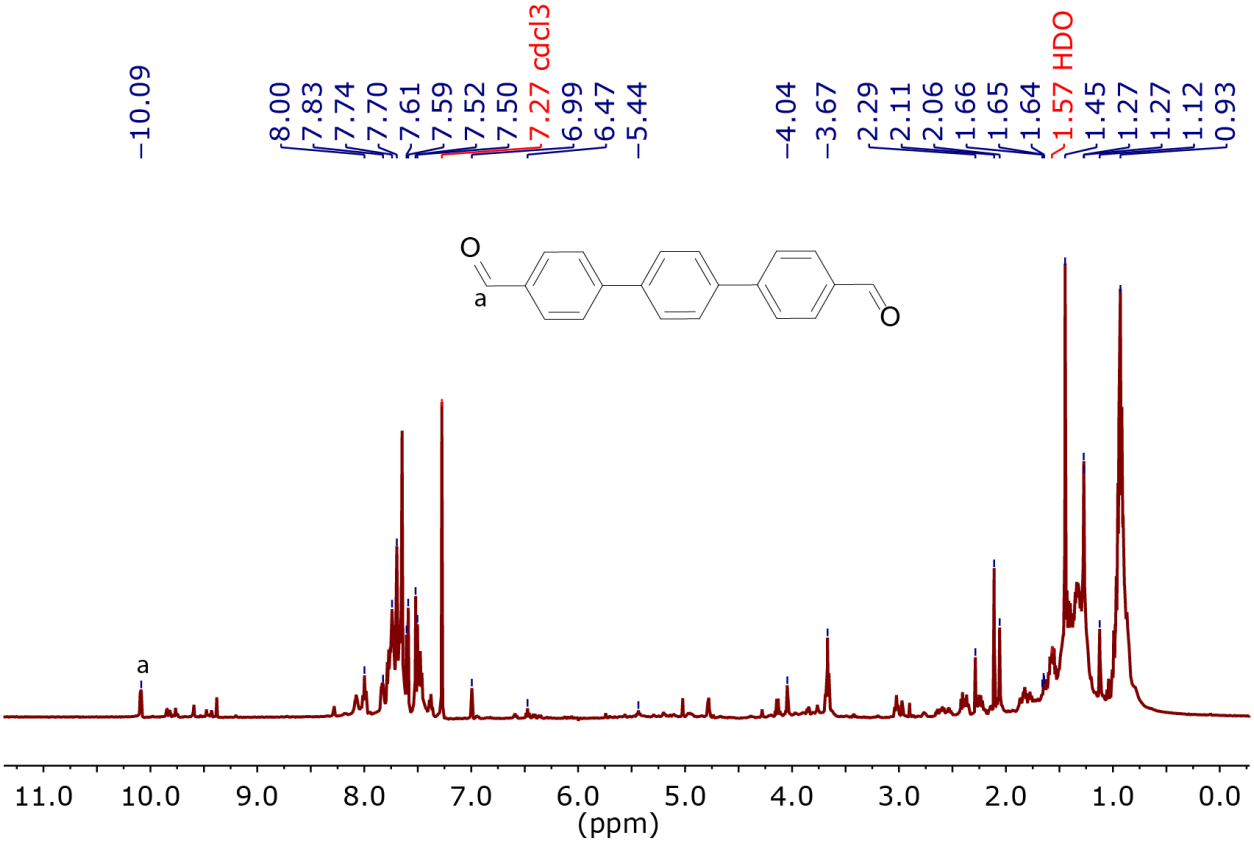

Figure 2.12. ^{1}H NMR spectrum of [1,1':4',1''-terphenyl]-4,4''-dicarbaldehyde.

2.3.3 Imine-linked 3D COF Synthesis

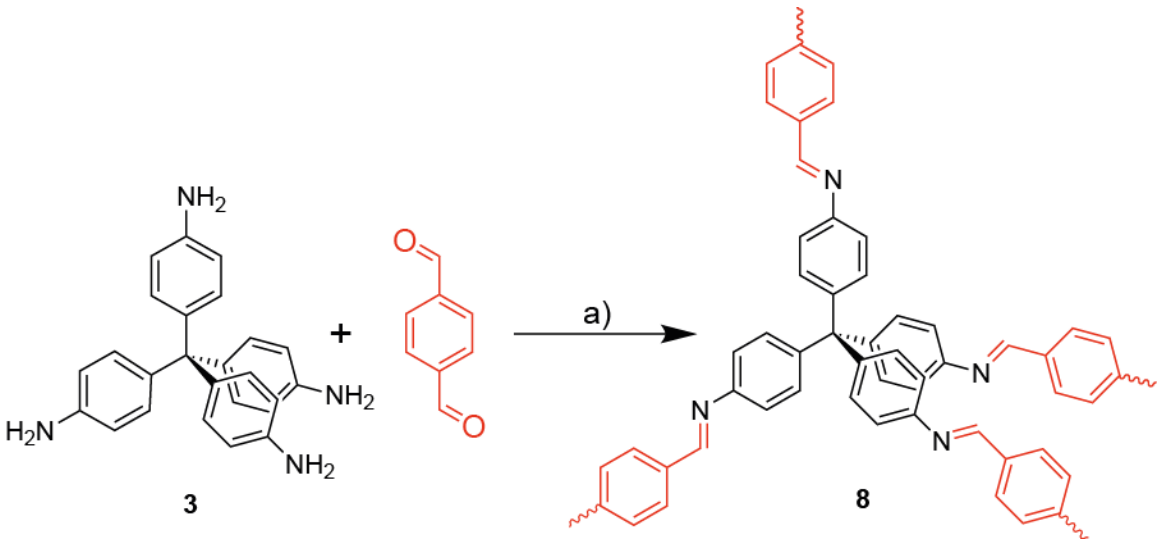

Scheme 2.5. Synthesis of COF-300 (8). Reagents and conditions: a) 1,4-dioxane, AcOH (aq), 120°C, 72 h.

COF-300 (8). The synthesis procedure for **8** was adapted from a published approach[3]. A 48 ml "glass bomb" heavy wall pressure vessel was charged with compound **3** (40 mg. 0.105 mmol), terephthalaldehyde (28.2 mg, 0.210 mmol), 1,4-dioxane (2 ml) and 3 M aqueous acetic acid solution (0.4 ml). The bomb reactor was sealed with an upside-down septum and degassed at 77 K through three freeze-pump-thaw cycles and backfilled with nitrogen. After degassing, the septum was quickly removed and replaced by the threaded cap with O-ring to seal the vessel, and the reactor was heated to 120°C for 72 h. The solids were filtered, washed with 1,4-dioxane and tetrahydrofuran, and immersed in tetrahydrofuran for 24 h, during which the solvent was exchanged for fresh tetrahydrofuran several times. The solids were then isolated by filtration and dried *in vacuo* to afford **8** as a yellow solid.

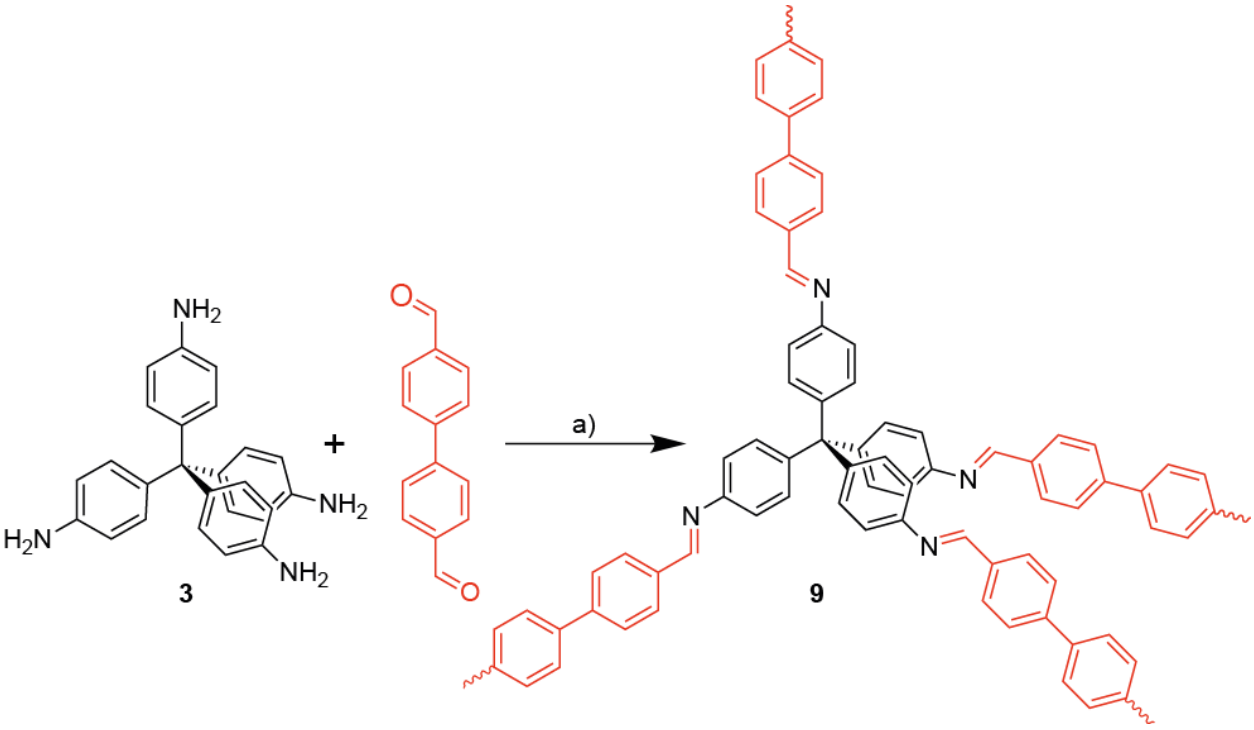

Scheme 2.6. Synthesis of COF-320 (9). Reagents and conditions: a) 1,4-dioxane, AcOH (aq), 120°C, 72 h.

COF-320 (9). The synthesis procedure for **9** was adapted from a published approach[10]. A 48 ml "glass bomb" heavy wall pressure vessel was charged with compound **3** (40 mg. 0.105 mmol), 4,4-biphenyldicarbaldehyde (37.4 mg, 0.178 mmol), 1,4-dioxane (2 ml) and 3M aqueous acetic acid solution (0.4 ml). The bomb reactor was sealed with an upside-down septum and degassed at 77 K through three freeze-pump-thaw cycles and backfilled with nitrogen. After degassing, the septum was quickly removed and replaced by the threaded cap with O-ring to seal the vessel, and the reactor was heated to 120°C for 72 h. The solids were filtered, washed with 1,4-dioxane and tetrahydrofuran, and immersed in tetrahydrofuran for 24 h, during which the solvent was exchanged for fresh tetrahydrofuran several times. The solids were then isolated by filtration and dried *in vacuo* to afford **9** as a yellow solid.

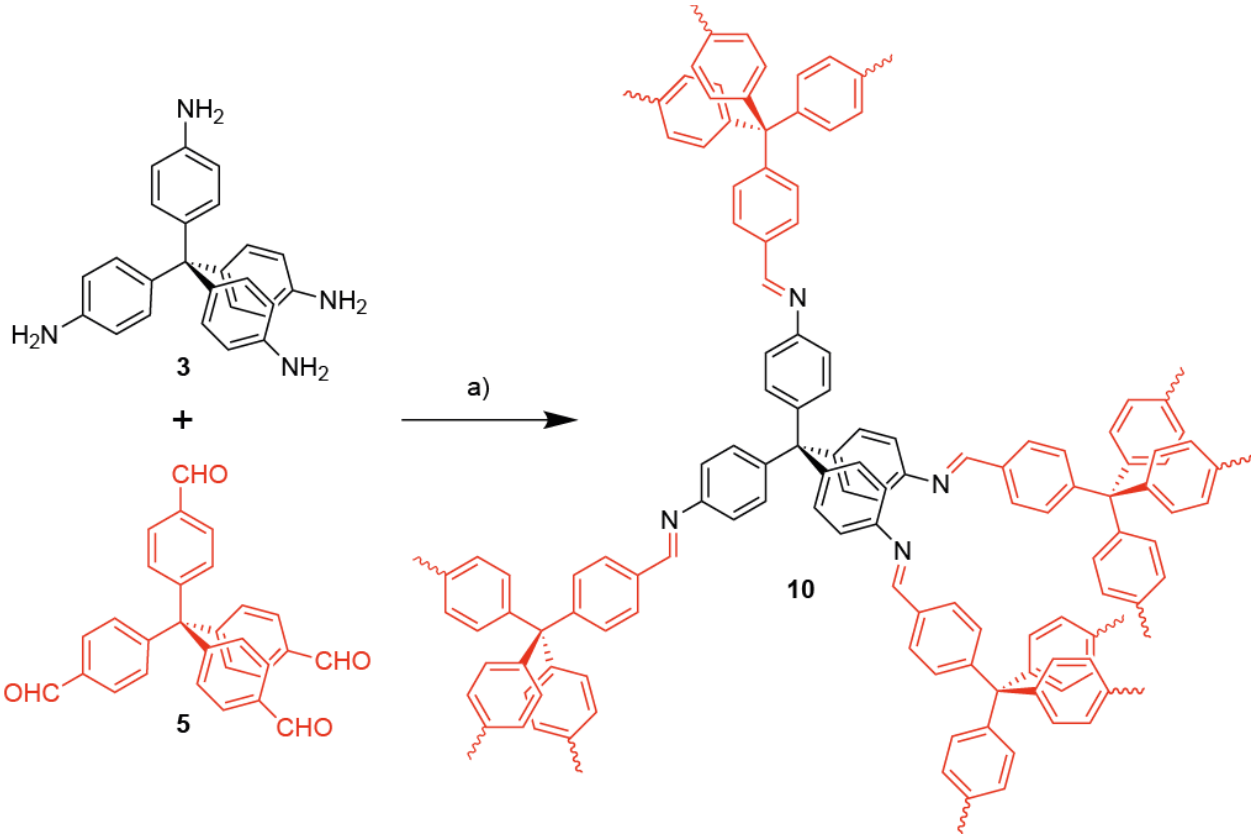

Scheme 2.7. Synthesis of tetraamine-tetraaldehyde COF (10). Reagents and conditions: a) 1,4-dioxane, AcOH (aq), 120°C, 72 h.

Tetraamine-tetraaldehyde COF (10). The synthesis procedure for **9** was adapted from published approaches for COF-300 and COF-320[3,10]. A 48 ml "glass bomb" heavy wall pressure vessel was charged with compound **3** (40 mg. 0.105 mmol), compound **5** (45.4 mg, 0.105mmol), 1,4-dioxane (2 ml) and 3M aqueous acetic acid solution (0.4 ml). The bomb reactor was sealed with an upside-down septum and degassed at 77 K through three freeze-pump-thaw cycles and backfilled with nitrogen. After degassing, the septum was quickly removed and replaced by the threaded cap with O-ring to seal the vessel, and the reactor was heated to 120°C for 72 h. The solids were filtered, washed with 1,4-dioxane and tetrahydrofuran, and immersed in tetrahydrofuran for 24 h, during

which the solvent was exchanged for fresh tetrahydrofuran several times. The solids were then isolated by filtration and dried *in vacuo* to afford **10** as a yellow solid.

2.4 Results and Discussion

2.4.1 Monomer Synthesis

The synthesis of compound **1**, the common precursor for all tetrahedral monomers subsequently employed for COF synthesis, was the first step of monomer synthesis. This synthesis procedure (see Scheme 2.1) began with a neat reaction between chlorotriphenylmethane and aniline at an elevated temperature of 190°C, which presented two unique challenges. First, a temperature of 190°C was difficult to achieve using an oil bath. The mineral oil baths commonly used for heating reactions start to degrade beyond 120°C, and as the reaction was heated to higher temperatures, the increasing temperature gradient between the reaction and ambient air caused increased heat loss and a stagnation of reaction temperature at approximately 180°C. This was resolved by using silicone oil, which is stable up to 250°C, and wrapping aluminum foil around the entire reaction setup, including reaction vessel and oil bath, to provide improved insulation against heat loss. Second, the neat reaction between chlorotriphenylmethane and aniline caused the reaction mixture to agglomerate into a large purple solid slab at the bottom of the round bottom flask became irremovable from said flask, which necessitated chiseling the slab into pieces small enough to be removed through the neck of the flask and grinding them into powder before re-dissolving in hydrochloric acid and methanol for the subsequent reaction. These adaptations also allowed the reaction to be scaled up, and compound **1** was successfully synthesized at up to 50 g scale at ~90% yield.

Synthesis of compound **2** initially resulted in yields of lower than 20% following the original procedure of adding fuming nitric acid slowly to compound **1**. After numerous optimization studies, it was discovered that reversing the order of addition and adding compound **1** slowly to fuming nitric acid provided a modest increase in yield, up to 43% (see Scheme 2.2). Tetrahydrofuran also forms an inclusion compound with compound **2**[9], and even washing with tetrahydrofuran chilled to below -10°C resulted in non-negligible product loss leading to reduced yield. Unfortunately, removing the tetrahydrofuran wash produced an impure product that led to impurities in the subsequent formation of amine **3** and caused reduced crystallinity in COFs **8** and **9**, and no alternative effective purification procedure was discovered, so the chilled tetrahydrofuran wash step remained part of the purification procedure for the preparation of **2**. The conversion of **2** into amine **3** sometimes produced product exhibiting a brown or pink tinge, so an additional ethanol wash step was incorporated to remove those colored impurities.

The bromination of compound **1** to form tetrabromine **4** was a relatively straightforward reaction. The conversion of bromine **4** to aldehyde **5**, however, was inconsistent (see Scheme 2.3). n-Butyllithium is a difficult catalyst to employ and any amount of moisture in the system would significantly reduce its effectiveness. In addition, incomplete conversion of all four bromines often occurred, causing low yield and necessitating separation by column chromatography. After several syntheses, only a small amount of aldehyde **5** was obtained for the synthesis of tetraamine-tetraaldehyde COF **10**.

The synthesis of [1,1':4',1"-terphenyl]-4,4"-dicarbaldehyde (**6**), as shown in Scheme 2.4, was conducted following the same procedure as the conversion of bromine **4** to aldehyde **5**. Unfortunately, after several attempts the desired product was not obtained in significant quantity or high purity. As shown by the NMR spectrum in Figure 2.12, while an aldehyde peak is observed

at a chemical shift of 10.09, there is an abundance of unidentifiable peaks in the 7.0-8.0 region commonly associated with aromatic protons, as well as throughout the 0 to 4.0 region commonly associated with aliphatic protons. This is a convincing indicator that the reaction did not proceed as expected, given that the structure of aldehyde **6** does not contain any aliphatic protons. After several attempts, a pure product could not be obtained in any quantity, and the corresponding terphenyl imine-linked 3D COF was not synthesized.

2.4.2 COF-300 Synthesis and Characterization

COF-300 (**8**) was synthesized by making certain adaptations to the common solvothermal approach reported in literature[3]. In published procedures, the reaction was conducted in a pyrex tube, which was charged with reactants, catalyst, and solvent, degassed *via* three freeze-thaw-pump degas cycles, flame sealed using a blow torch to reduce the length of the tube and seal the top with melted glass, and then heated to 120°C for three days. There were two main issues with this approach: 1) pyrex tubes are not designed for vacuum degassing and lacked suitable adapters for vacuum line attachment; and 2) flame sealing the pyrex tubes increases the difficulty of removing the contents from the tubes post reaction, and both using a blow torch for flame sealing and smashing the tubes to remove the product could present safety hazards. In addition, this approach renders the tube single-use, which is not environment-friendly and quite wasteful. As such, an alternative reaction setup for COF synthesis that would allow easy removal of product and straightforward degassing procedures was sought. A Schlenk tube was initially considered due to its great compatibility with vacuum lines, but its very narrow neck restricted the removal of product post reaction. Heavy wall glass pressure vessel, or glass "bomb reactors", were selected due to its screw-on cap with an O-ring that facilitated ease of sealing and product removal. There

was no method to carry out the degassing procedure through the plastic cap, so an alternative solution was developed. Instead of the plastic cap, the reactor was sealed with an upside-down rubber septum, which fit snugly over the neck of the vessel, after adding all reaction components. The reactor could then be vacuum degassed using a syringe and needle attached to the vacuum line and pumped using a balloon with a syringe and needle attached. Argon gas was used in place of nitrogen, which, possessing a larger density than air, remained in the vessel and insulated the contents of the reactor from air as the septum was quickly removed and replaced with the screw-on cap, thus achieving freeze-thaw-pump degassing of the reactor while maintaining an air-free environment in the vessel conducive to product removal post synthesis.

The synthesis of COF-300 was carried out according to Scheme 2.5, and successful synthesis was confirmed by several characterization methods. FTIR spectroscopy of the product confirmed the disappearance of the amine peak (3395 cm^{-1}) and the aldehyde peak (1720 cm^{-1}) and the appearance of what could be attributed as characteristic imine stretching at 1616 cm^{-1} and 1196 cm^{-1} compared to the starting materials, amine **3** and terephalaldehyde (Figure 2.13). Powder X-ray diffraction (PXRD) results show a crystalline structure, with diffraction peaks in agreement with previously published results (Figure 2.14);[3] in addition, no diffraction peaks from starting materials were observed in the PXRD spectrum of COF-300 (Figure 2.15). SEM images were taken, showing oblong rice-shaped crystals (Figure 2.16). Combined, these spectra confirm the successful synthesis of crystalline COF-300. In addition, optimization studies found that neither extending the reaction duration (Figure 2.17) nor scaling the reaction up seven-fold (Figure 2.18) result in observable changes in crystallinity.

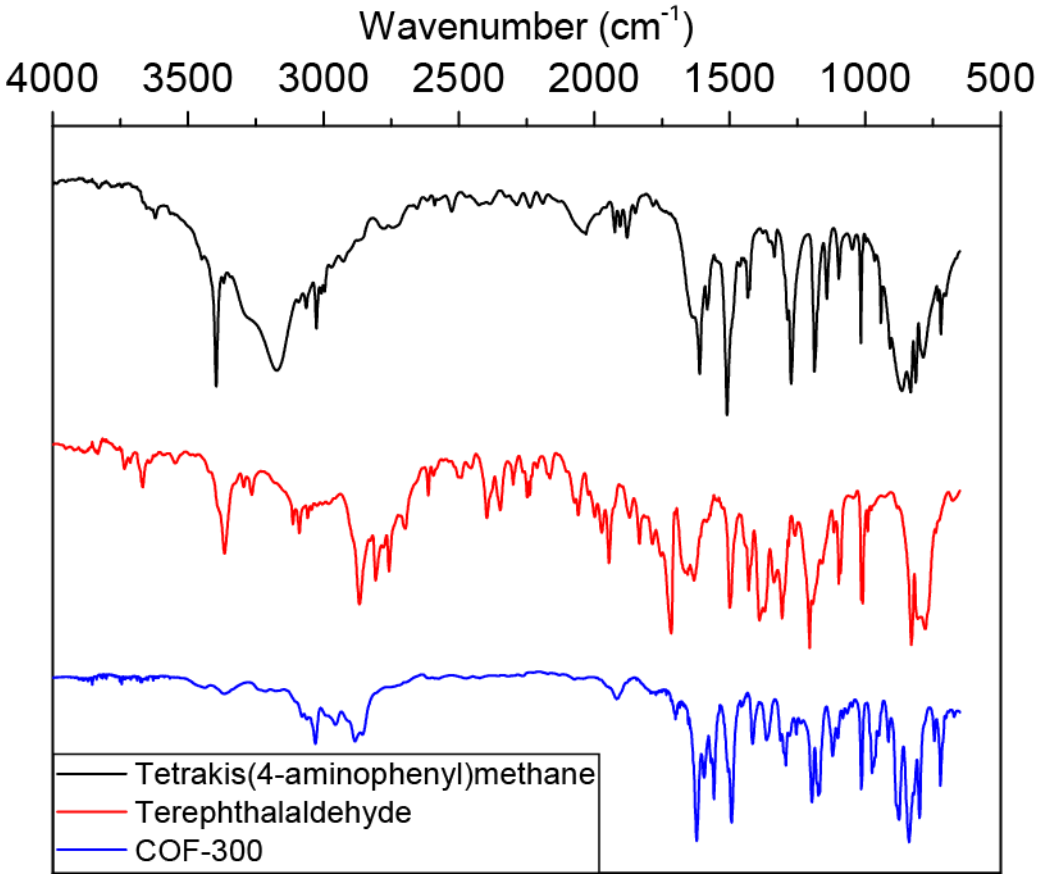

Figure 2.13. FTIR spectrum of COF-300 compared to starting materials tetrakis(4-aminophenyl)methane (3) and terephthalaldehyde.

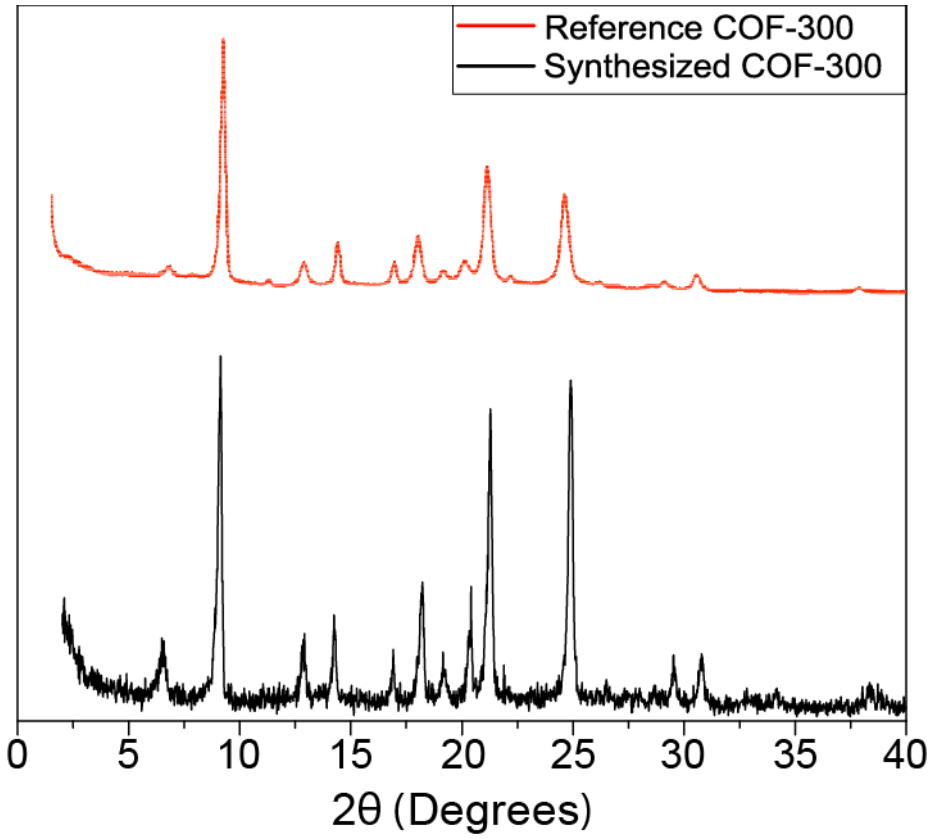

Figure 2.14. PXRD spectrum of COF-300 compared to literature reference spectrum[3].

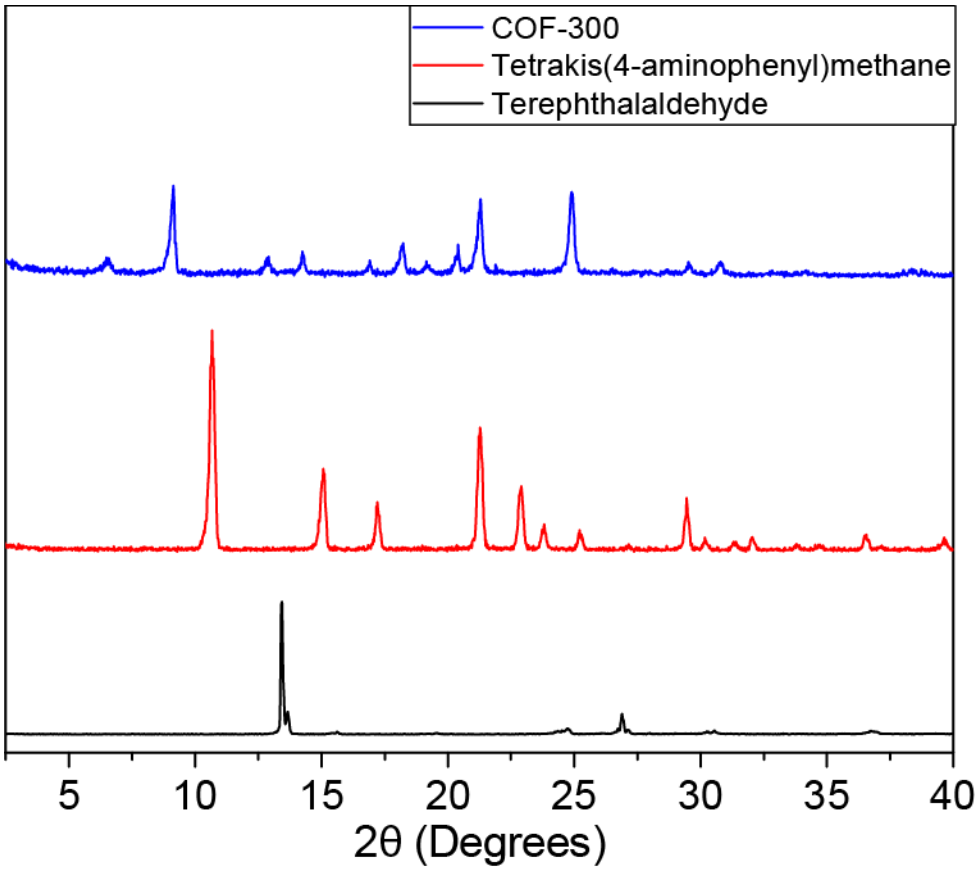

Figure 2.15. PXRD spectrum of COF-300 compared to starting materials tetrakis(4-aminophenyl)methane (3) and terephthalaldehyde.

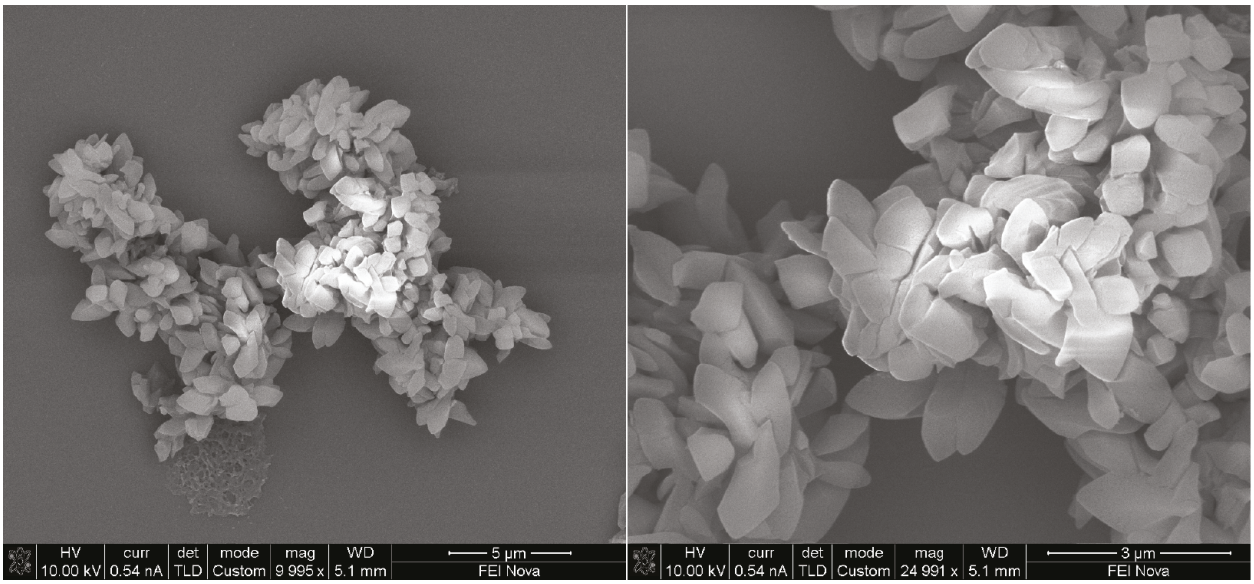

Figure 2.16. SEM images of COF-300 particles.

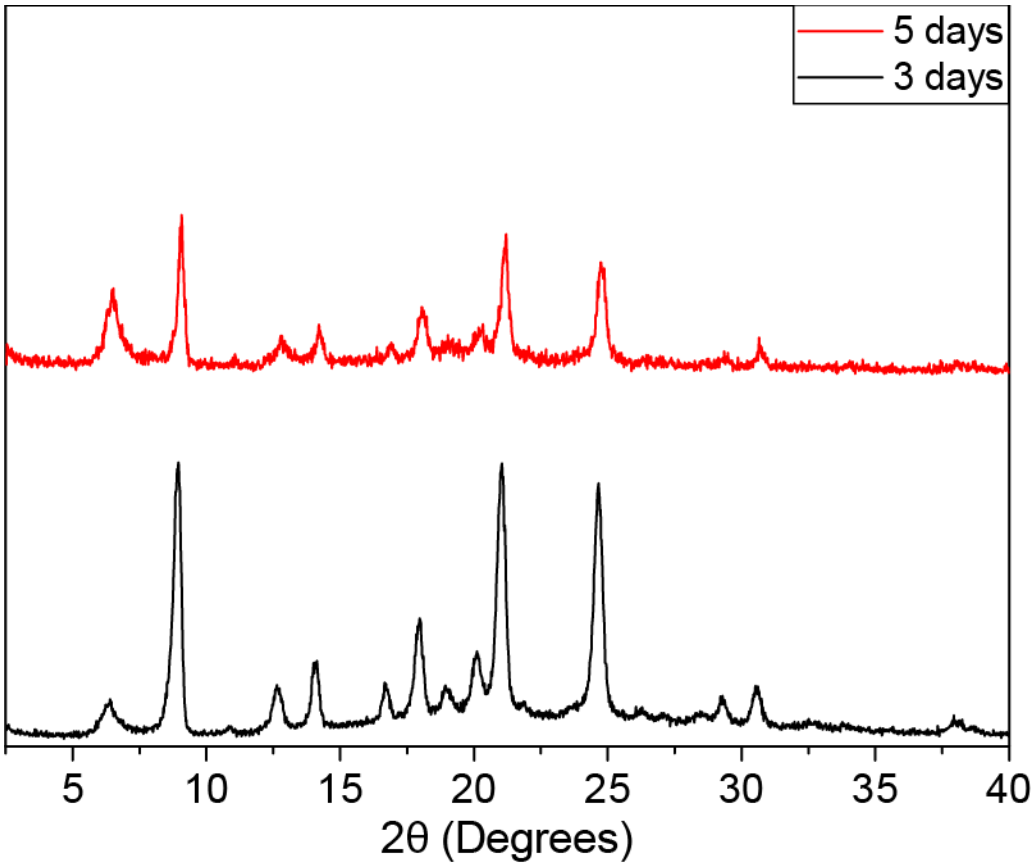

Figure 2.17. PXRD spectra comparison of COF-300 heated over five days and the literature standard of three days.

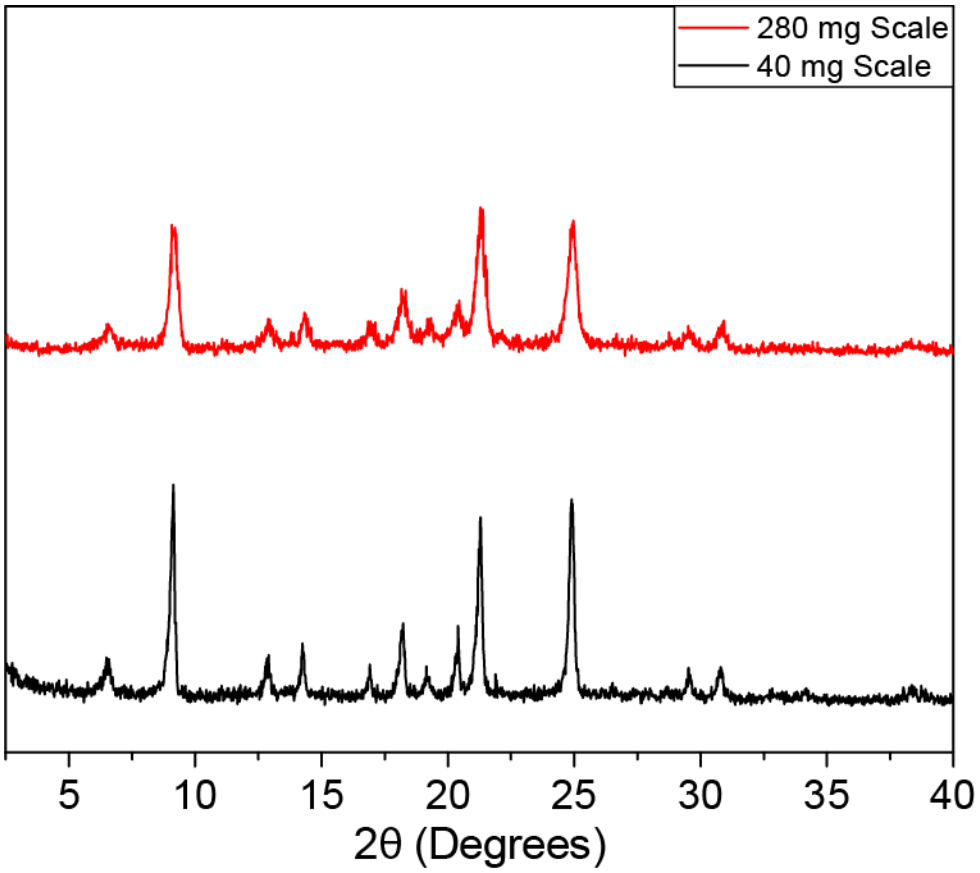

Figure 2.18. PXRD spectra comparison of COF-300 synthesized at 40 mg and 280 mg scales by starting material tetrakis(4-aminophenyl)methane.

2.4.3 COF-320 Synthesis and Characterization

The synthesis of COF-320 (**9**) was carried out according to Scheme 2.6 utilizing the same reaction setup employed for COF-300, and successful synthesis was confirmed by several characterization methods. FTIR spectroscopy confirmed the disappearance of the amine peak (3395 cm^{-1}) and the aldehyde peak (1698 cm^{-1}) and the appearance of the characteristic imine stretching at 1623 cm^{-1} and 1202 cm^{-1} compared to the starting materials, amine **3** and 4,4'-biphenyldicarboxaldehyde (Figure 2.19). PXRD results show a mostly crystalline structure, indicating some amount of amorphous materials; in addition, no diffraction peaks from starting

materials were observed in the PXRD spectrum of COF-320 (Figure 2.20). SEM images were taken, showing oblong rice-shaped crystals (Figure 2.21); however, compared to the images of COF-300 in Figure 2.16, these crystals are more aggregated and less clearly defined, again indicating a moderate degree of crystallinity and a mixture of crystalline and amorphous elements. Combined, these spectra confirm the successful synthesis of moderately crystalline COF-320.

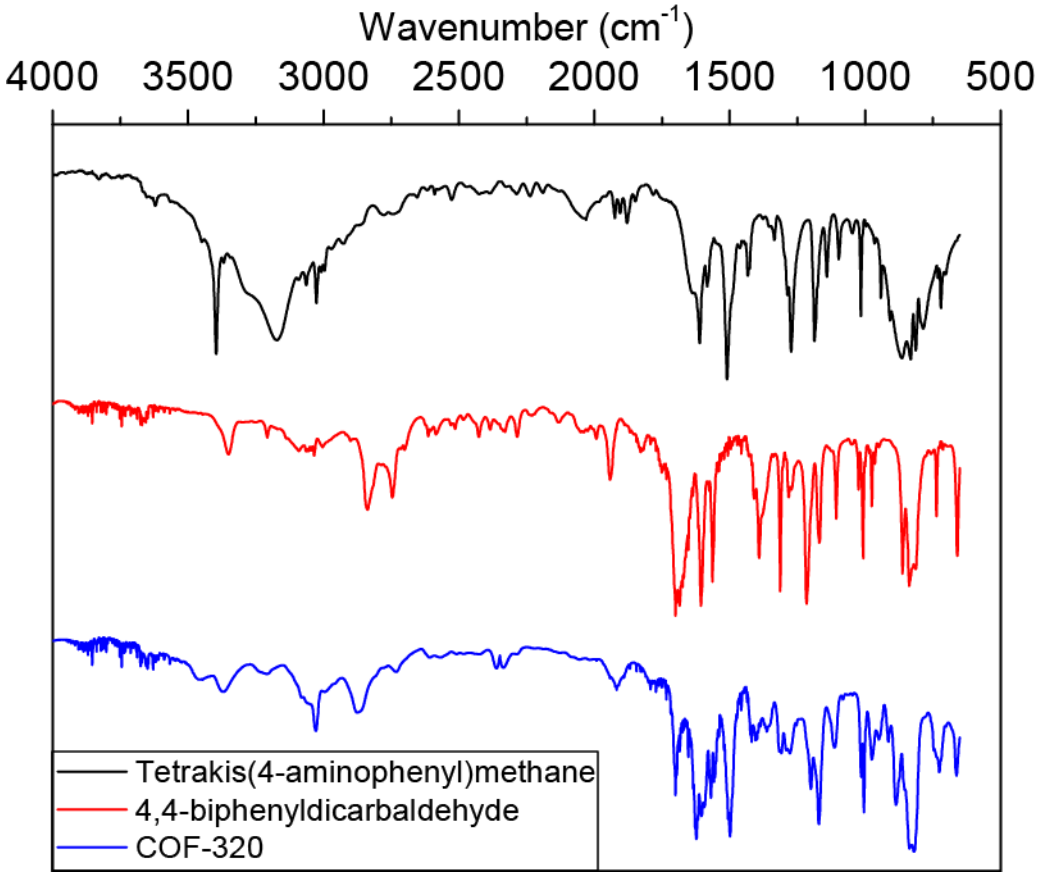

Figure 2.19. FTIR spectrum of COF-320 compared to starting materials tetrakis(4-aminophenyl)methane (3) and 4,4'-biphenylcarboxyaldehyde.

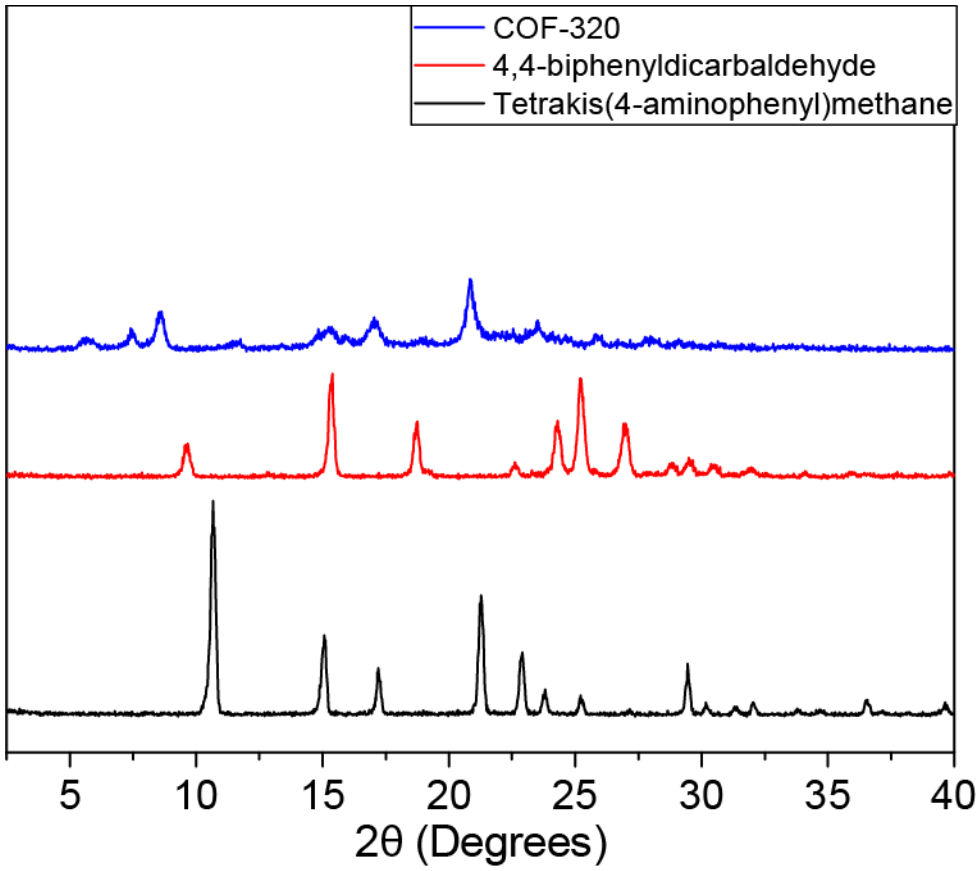

Figure 2.20. PXRD spectrum of COF-320 compared to starting materials tetrakis(4-aminophenyl)methane (3) and 4,4'-biphenylcarboxyaldehyde.

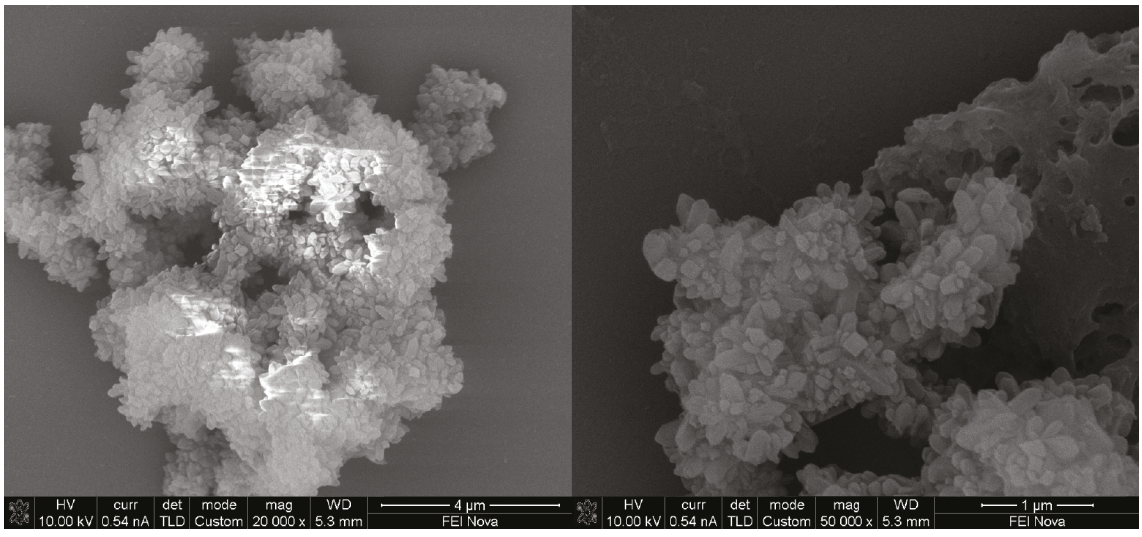

Figure 2.21. SEM images of COF-320 particles.

2.4.4 Tetraamine-tetraaldehyde COF Synthesis and Characterization

The synthesis of a novel tetraamine-tetraaldehyde COF (**10**) was carried out using amine **3** and aldehyde **5** according to Scheme 2.7 following the previously established reaction setup for COF-300 and COF-320. After several attempts, a somewhat crystalline material was obtained, as revealed by PXRD (Figure 2.22). The broad peaks and raised baseline indicate a slight degree of crystallinity with the presence of some amorphous materials, which, combined with the difficulty of synthesizing precursor aldehyde **5** consistently at high purity and acceptable yield, rendered the prospect of optimizing the crystallinity of the COF structure through iterative investigation impractical. As such, the tetraamine-tetraaldehyde COF structure was not pursued further in this dissertation research.

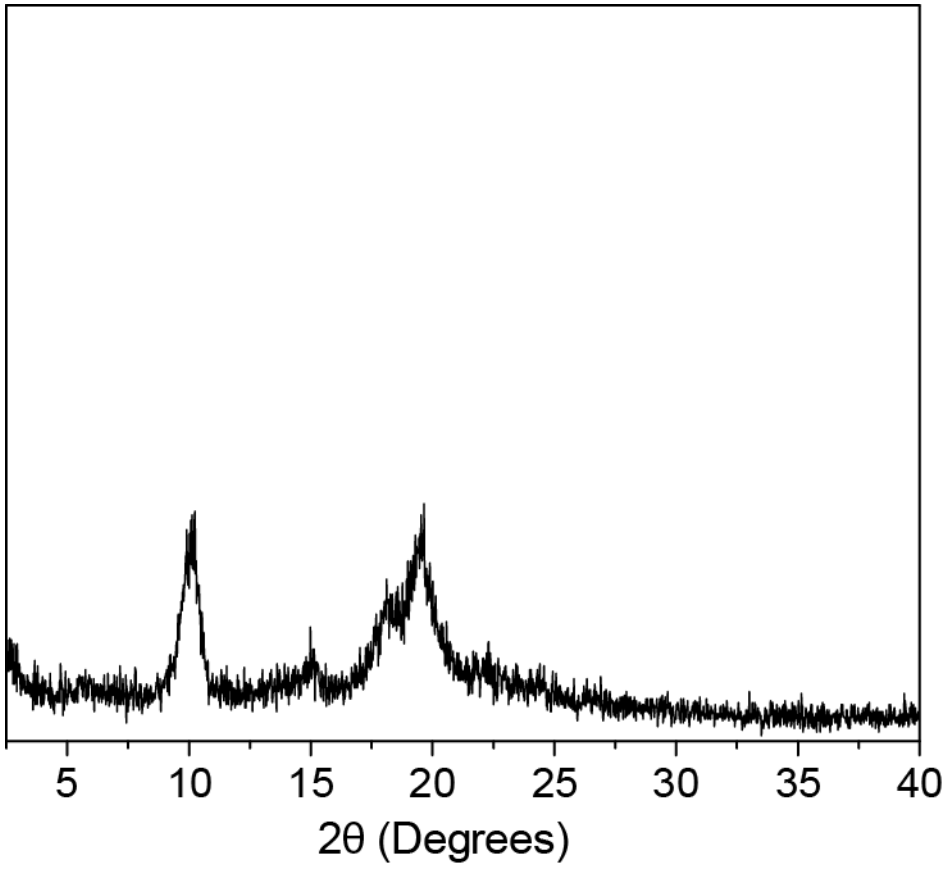

Figure 2.22. PXRD spectrum of tetraamine-tetraaldehyde COF.

2.5 Conclusions

Archetypal 3D imine-linked COFs COF-300 and COF-320 were selected as the framework for further investigation and structural alteration. Their common precursor amine monomer tetrakis(4-aminophenyl)methane was successfully synthesized and characterized *via* ^{1}H-NMR, ^{13}C-NMR, and mass spectrometry, and adaptation of the common solvothermal reaction procedures for COF synthesis from literature reduced complexity and improved usability of the operations. Utilizing tetrakis(4-aminophenyl)methane and the improved reaction setup, crystalline COF-300 and COF-320 were successfully synthesized and confirmed by FTIR and XRD and imaged by SEM. Additionally, the tetraaldehyde analog of tetrakis(4-aminophenyl)methane, tetrakis(4-formylphenyl)methane, was also synthesized and characterized, and synthesis of a novel 3D tetraamine-tetraaldehyde COF was explored, resulting in a network possessing low crystallinity. The improved procedures and successful synthesis of COF-300 will serve as a vital foundation for subsequent investigation and modification, which are detailed in the following chapters.

2.6 References

1. Ma, X. & Scott, T. F. Approaches and challenges in the synthesis of three-dimensional covalent-organic frameworks. *Commun. Chem.* **1**, 98 (2018).
2. DeBlase, C. R. & Dichtel, W. R. Moving Beyond Boron: The Emergence of New Linkage Chemistries in Covalent Organic Frameworks. *Macromolecules* **49**, 5297–5305 (2016).
3. Uribe-Romo, F. J. *et al.* A Crystalline Imine-Linked 3-D Porous Covalent Organic Framework. *J. Am. Chem. Soc.* **131**, 4570–4571 (2009).
4. Chen, Y. *et al.* Guest-Dependent Dynamics in a 3D Covalent Organic Framework. *J. Am. Chem. Soc.* **141**, 3298–3303 (2019).
5. Das, S. & Ben, T. A [COF-300]-[UiO-66] composite membrane with remarkably high permeability and H2/CO2 separation selectivity. *Dalton Trans.* **47**, 7206–7212 (2018).
6. Ma, T. *et al.* Observation of Interpenetration Isomerism in Covalent Organic Frameworks. *J. Am. Chem. Soc.* **140**, 6763–6766 (2018).
7. Ma, T. *et al.* Single-crystal x-ray diffraction structures of covalent organic frameworks. *Science* **361**, 48–52 (2018).
8. Plietzsch, O. *et al.* Four-fold click reactions: Generation of tetrahedral methane- and adamantane-based building blocks for higher-order molecular assemblies. *Org. Biomol. Chem.* **7**, 4734–4743 (2009).
9. Farha, O. K. *et al.* Synthesis, Properties, and Gas Separation Studies of a Robust Diimide-Based Microporous Organic Polymer. *Chem. Mater.* **21**, 3033–3035 (2009).

10. Zhang, Y.-B. *et al.* Single-Crystal Structure of a Covalent Organic Framework. *J. Am. Chem. Soc.* **135**, 16336–16339 (2013).

Chapter 3
Low Temperature Synthesis of Imine-linked 3D COFs Utilizing Scandium Triflate

3.1 Abstract

The synthesis of three-dimensional covalent organic frameworks (COFs) has consistently presented a challenge for investigators. Conventionally, the solvothermal method of extended heating at high temperatures exceeding 100°C in the presence of acetic acid is employed, precluding certain temperature-sensitive applications. In this chapter, an improved synthetic procedure for a representative 3D imine-linked COF, COF-300, utilizing Lewis acidic scandium triflate as the catalyst is described and the set of reaction conditions that allow the formation of a crystalline framework at room temperature is identified through systematic investigation of reaction parameters on framework crystallinity. In-situ deprotection of functional groups is investigated as an alternative method of synthesis to overcome kinetic trapping. Additionally, the ionothermal synthesis of COF-300 is explored. The synthetic methods and reaction conditions identified in this chapter can be widely adopted for the easier synthesis of imine-linked 3D COFs, and the valuable insight into the roles of various reaction parameters will contribute to the improved understanding of the COF synthetic process.

3.2 Introduction

Formation of the stable crystalline frameworks characteristic of COFs requires the usage of reversible covalent bonds to facilitate rearrangement and self-assembly; however, the tendency of covalent bonds to form irreversible interactions due to their stability significantly increases synthetic difficulty. Even in dynamic covalent-bond forming reactions, amorphous networks will frequently become kinetically trapped owing to the bulkiness and rigidity of the constituent species which limits proximity of reactant functional groups. Whereas two-dimensional (2D) COFs benefit from the additional driving force of π-orbital overlap between adjacent stacked sheets, three-dimensional (3D) COFs are constructed solely by covalent interactions and thus experience a vastly higher degree of kinetic trapping, contributing to significant synthetic challenges[1]. As such, several novel 2D COF synthesis techniques have been reported, including flow synthesis[2] and ambient temperature one-pot synthesis[3], whereas 3D COF synthesis is still dominated by solvothermal synthesis that requires heating at high temperatures in excess of 100°C for 3-5 days. For imine-linked 3D COFs, which have attracted increasing research interest over recent years compared to the earlier boron-based structures[4], acetic acid is also employed to catalyze imine hydrolysis and exchange. Two recent reports of ambient temperature imine-linked 3D COF synthesis, an ionothermal synthesis that resulted in low surface area and irremovable ionic liquid within the framework pores[5] and the utilization of a nucleation inhibitor to slowly fabricate imine-linked 3D COF single crystals at ambient temperature over 30-80 days[6], suggest the potential for reducing reaction temperature; however, solvothermal synthesis remains the default method for imine-linked 3D COFs. As such, there is a need for the development of a general and robust imine-linked 3D COF synthesis procedure that does not require reaction temperatures in excess of 100°C, a reaction duration on the order of months, or compromise the inherent properties of the COF.

Despite the prevalence of acetic acid as the catalyst of choice for solvothermal imine-linked COF synthesis, acetic acid is relatively inefficient at catalyzing imine exchange and subsequent rearrangement of amorphous networks, which is the rate limiting step in the formation of a crystalline framework[7]. In comparison, Lewis acidic rare earth metal triflates are promising as alternative catalysts owing to their effectiveness in mediating imine exchange reactions, tolerance of aqueous and organic environments, and functional group compatibility. Scandium triflate ($Sc(OTf)_3$), in particular, has been demonstrated as an effective catalyst for imine-linked 2D COF synthesis, achieving a crystalline framework in 10 minutes at room temperature[3]. This method has since been validated and utilized for the synthesis of other imine-linked 2D COFs[8] and has significantly reduced their synthetic difficulty and temperature requirement. Thus, the application of this technique to imine-linked 3D COFs holds significant appeal.

Another promising approach for mediating reaction kinetics and equilibrium and overcoming kinetic trapping is *in situ* deprotection. Protection of reactive functional groups limits the availability of said group for the reaction, which throttles the rate of reaction to the rate of deprotection and shifts the reaction equilibrium towards the monomers due to the low concentration of the deprotected reactant. Specifically, acetyl protection of aldehydes and subsequent deprotection is extremely suitable for imine chemistry owing to the ability of $Sc(OTf)_3$ to serve as a dual role catalyst and catalyze both the deprotection of the acetyl protecting groups and facilitate the imine formation and exchange reactions, which was previously demonstrated for the self-assembly of amine- and aldehyde-bearing oligomers[9]. 2-(Trimethylsilyl)ethoxycarbonyl (Teoc) protection of amines is another option whose effectiveness has been demonstrated[9].

In this chapter, acetyl protection of aldehydes and Teoc protection of amines and subsequent utilization of protected species in COF-300 synthesis was investigated. The room

temperature synthesis of COF-300 employing $Sc(OTf)_3$ as the catalyst was demonstrated, and a systematic analysis of the impact of reaction parameters on framework crystallinity and reaction equilibrium was conducted, providing much needed fundamental understanding of the synthetic process. Additionally, the ionothermal synthesis method was applied to COF-300 to evaluate the universality of this approach.

3.3 Experimental

3.3.1 General Experimental Procedure

All chemicals and reagents, unless specified, were purchased from commercial sources, including Fisher Scientific, Sigma-Aldrich, Alfa Aesar, and Oakwood Chemicals, and used as received without any further purification. ^1H NMR spectra were recorded on a Varian Inova 500 instrument (500 MHz). ^{13}C NMR spectra were recorded on a Varian MR400 instrument (400 MHz). Chemical shifts were measured in δ (ppm) relative to residual solvent signals as internal standards ($CDCl_3$: 7.24 for ^1H, 77.23 for ^{13}C; d^6-DMSO: 2.49 for ^1H). Powder X-ray Diffraction (PXRD) spectra were collected using a Rigaku 600 Miniflex XRD instrument and a 5 mm zero background sample holder. Fourier Transform Infrared (FTIR) spectroscopy was performed on a Thermo Scientific Nicolet 6700 FTIR spectrometer equipped with a Spectra-Tech diffusive reflectance unit. Nitrogen adsorption-desorption isotherms were collected on a Micromeritics ASAP 2020 instrument. Synthesis of tetrakis(4-aminophenyl)methane, the common amine precursor utilized for the synthesis of COF-300 in this chapter, was conducted according to the procedures detailed in Chapter 2, Section 2.3.2.

3.3.2 Solvothermal Synthesis of COF-300

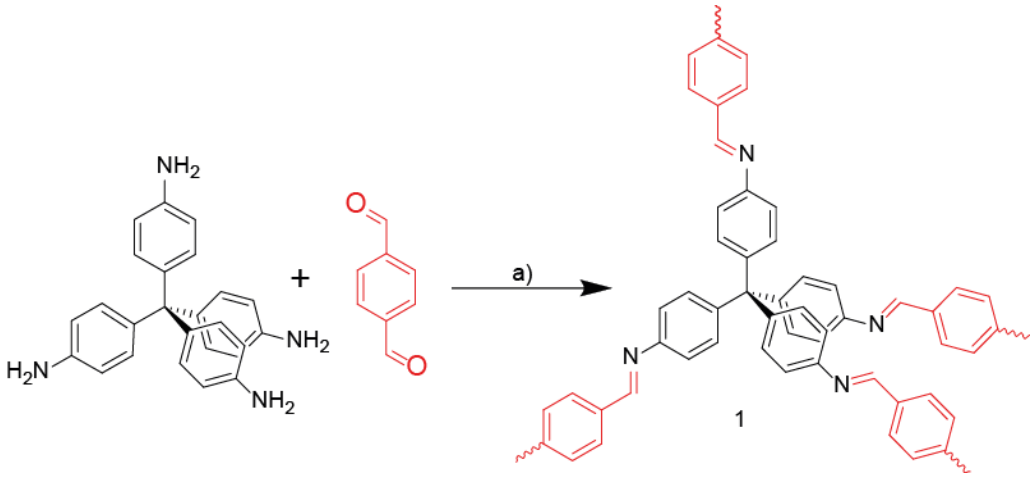

Scheme 3.1. Solvothermal synthesis of COF-300 (1). Reagents and conditions: a) 1,4-dioxane, AcOH (aq), 120°C, 72 h.

Solvothermal synthesis of COF-300 (1). The synthesis procedure for compound **1** was adapted from a published approach[10]. A 48 ml "glass bomb" heavy wall pressure vessel was charged with tetrakis(4-aminophenyl)methane (40 mg. 0.105 mmol), terephthalaldehyde (28.2 mg, 0.210 mmol), 1,4-dioxane (2 ml) and 3 M aqueous acetic acid solution (0.4 ml). The reactor was capped, sealed, and heated to 120°C for 72 hours to yield a yellow powder, which was isolated by centrifugation and immersed and washed with tetrahydrofuran to remove residual solvent and guest. This was repeated several times until the solvent became colorless. The product was then immersed in tetrahydrofuran overnight, isolated by centrifugation, and dried *in vacuo* to afford **1** as a yellow solid.

3.3.3 In-situ Deprotection and Synthesis of COF-300

3.3.3.1 Acetyl Protection and Deprotection

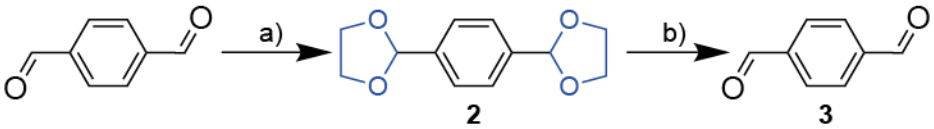

Scheme 3.2. Acetyl protection (2) and deprotection (3) of terephthalaldehyde. Reagents and conditions: a) ethylene glycol, PTSA, toluene, reflux; b) $Sc(OTf)_3$, H_2O, THF.

Acetyl protected terephthalaldehyde (2). Terephthalaldehyde (4.96 g, 0.037 mol), ethylene glycol (8.2 ml, 0.15 mol), toluene p-sulfonic acid (4 mg, 0.023 mol), and toluene (40 ml) were mixed together and refluxed overnight using a Dean-Stark trap to facilitate azeotropic distillation. The mixture was quenched with 5% aqueous sodium bicarbonate solution (8 ml), extracted with toluene, washed with di-ionized water, and dried over magnesium sulfate. The solvent was removed under reduced pressure and the product was dried *in vacuo* and recrystallized in hexanes to afford **3** as a white crystal.

Characterization data: ^{1}H NMR ($CDCl_3$, δ ppm): 7.51 (s, 4H, Ar), 5.85 (s, 2H, -CH-O2-), 4.09 (m, 8H, -O-CH_2-CH_2-O-).

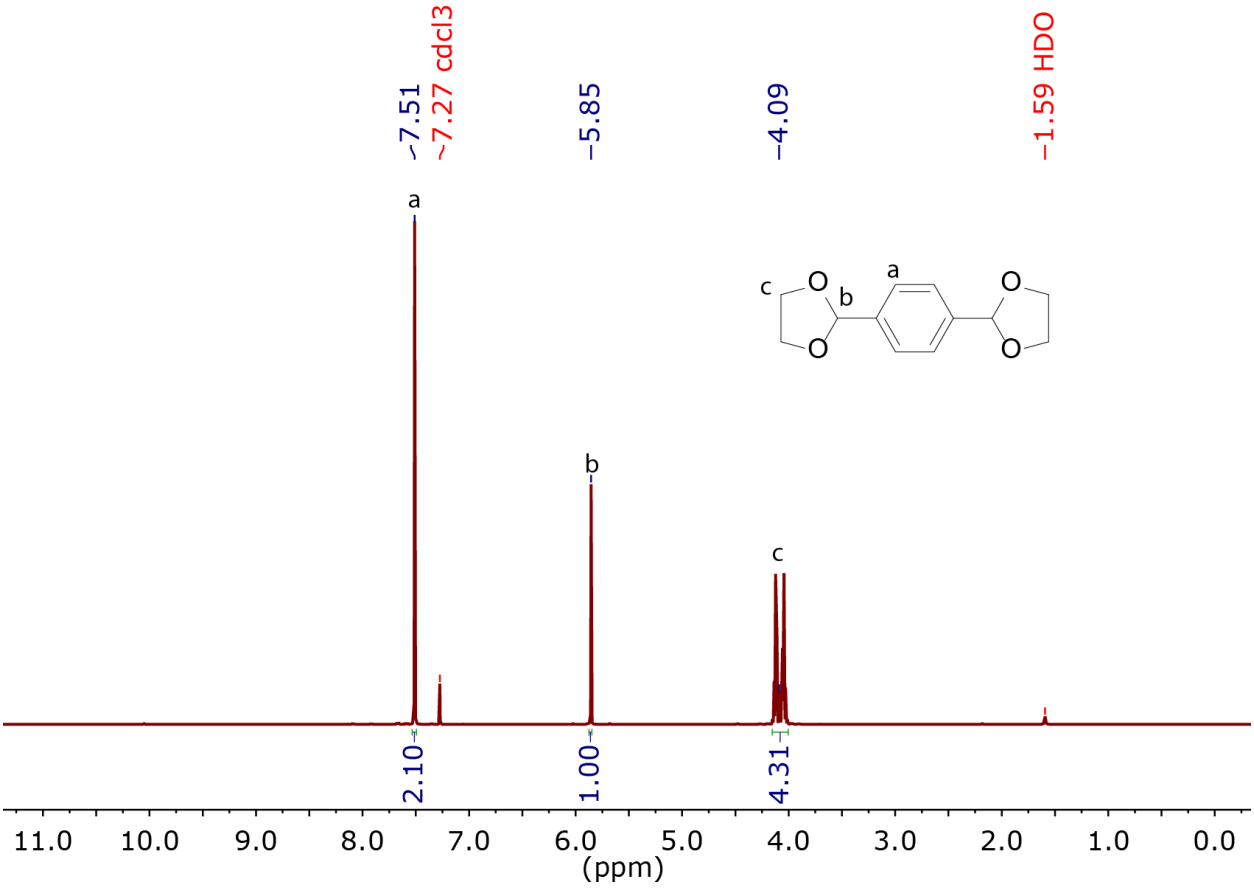

Figure 3.1. ^{1}H NMR spectrum of acetyl protected terephthalaldehyde.

Deprotection of acetyl protected terephthalaldehyde (3). Compound **2** (23 mg, 0.103 mmol), scandium triflate (10 mg, 0.021 mmol), water (0.1 ml), and tetrahydrofuran (5 ml) were stirred at room temperature overnight. The resultant mixture was analyzed by mass electrospray ionization spectrometry to assess the degree of deprotection.

m/z (ESI+): 135 $[M+H]^+$, 157 $[M+Na]^+$.

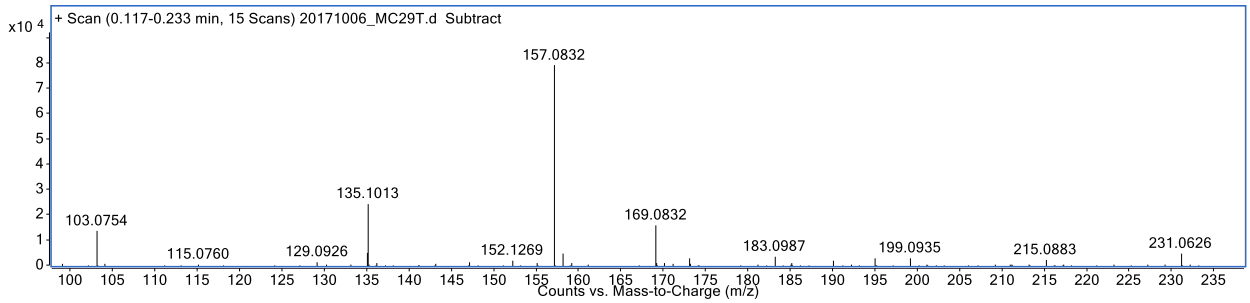

Figure 3.2. ESI mass spectrometry of the deprotection of acetyl protected terephthalaldehyde.

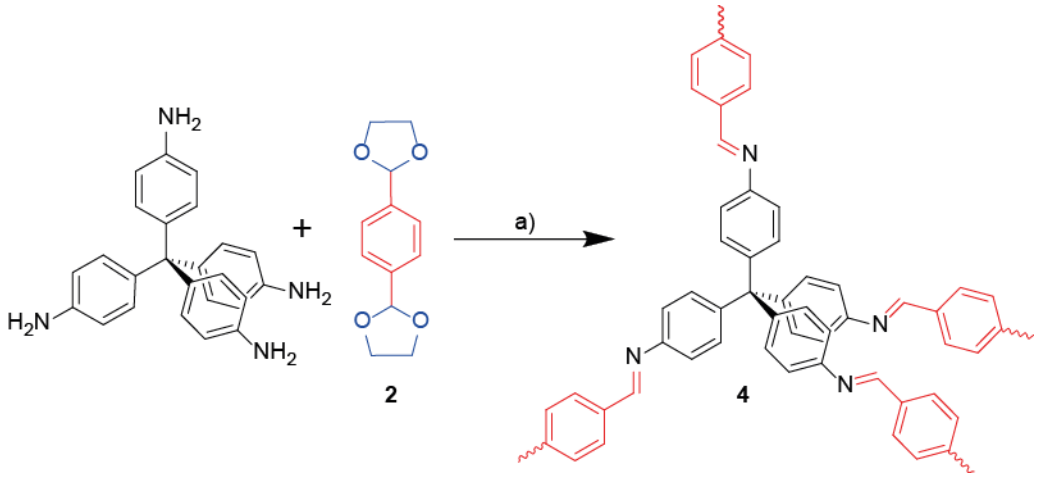

Scheme 3.3. In-situ acetyl deprotection and synthesis of COF-300 (4). Reagents and conditions: a) 1,4-dioxane, $Sc(OTf)_3$, H_2O, 70°C, 72 h.

In-situ Deprotection Synthesis of COF-300 (4). A 48 ml "glass bomb" heavy wall pressure vessel was charged with tetrakis(4-aminophenyl)methane (40 mg. 0.105 mmol), compound **2** (46.7 mg, 0.210 mmol), 1,4-dioxane (5 ml) and 84 µl of scandium triflate stock solution (0.2 M in acetonitrile, 0.0168 mmol, 0.04 equiv. per amine). The reactor was capped, sealed, and heated to 70°C for 72 hours to yield a yellow powder, which was isolated by centrifugation and immersed and washed with tetrahydrofuran to remove residual solvent and guest. This was repeated several

times until the solvent became colorless. The product was then immersed in tetrahydrofuran overnight, isolated by centrifugation, and dried *in vacuo* to afford **4** as a yellow solid.

3.3.3.2 2-(Trimethylsilyl)ethoxycarbonyl Protection

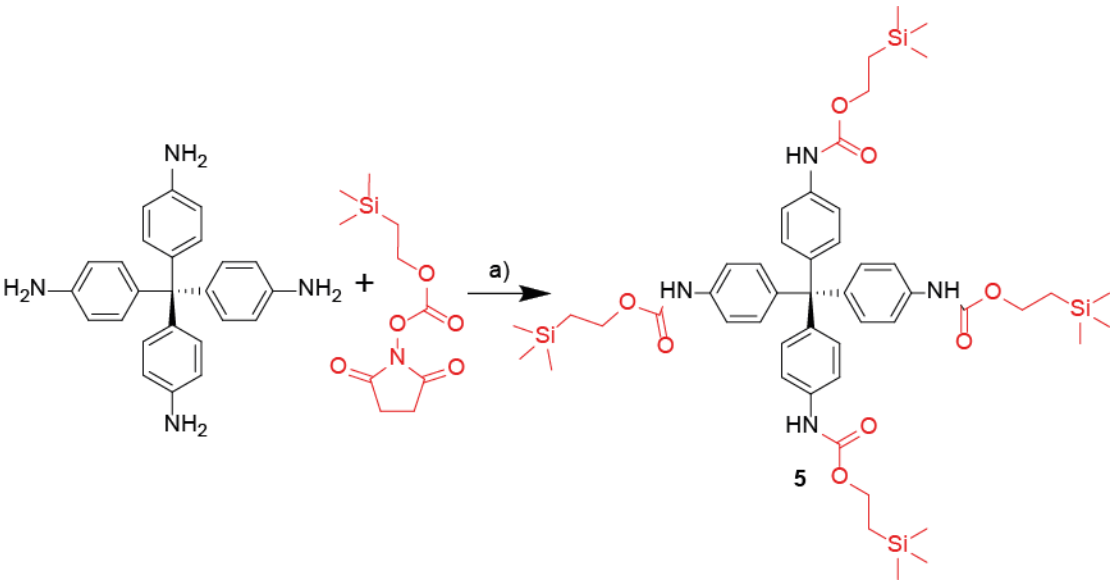

Scheme 3.4. 2-(Trimethylsilyl)ethoxycarbonyl protection of tetrakis(4-aminophenyl)methane (5). Reagents and conditions: a) Teoc, DMF, 60°C.

2-(Trimethylsilyl)ethoxycarbonyl-protected tetrakis(4-aminophenyl)methane (5). Tetrakis(4-aminophenyl)methane (100 mg, 0.526 mmol), 1-[2-(trimethylsilyl)ethoxy carbonyloxy]pyrrolidin-2,5-dione (409 mg, 3.15 mmol), and dimethylformamide (30 ml) were mixed and heated to 60°C overnight. The product was filtered and dried *in vacuo* to afford compound **5**.

Characterization data: ^{1}H NMR ($CDCl_3$, δ ppm): 7.51 (s, 4H, Ar), 5.85 (s, 2H, -CH-O2-), 4.09 (m, 8H, -O-C*H*$_2$-C*H*$_2$-O-).

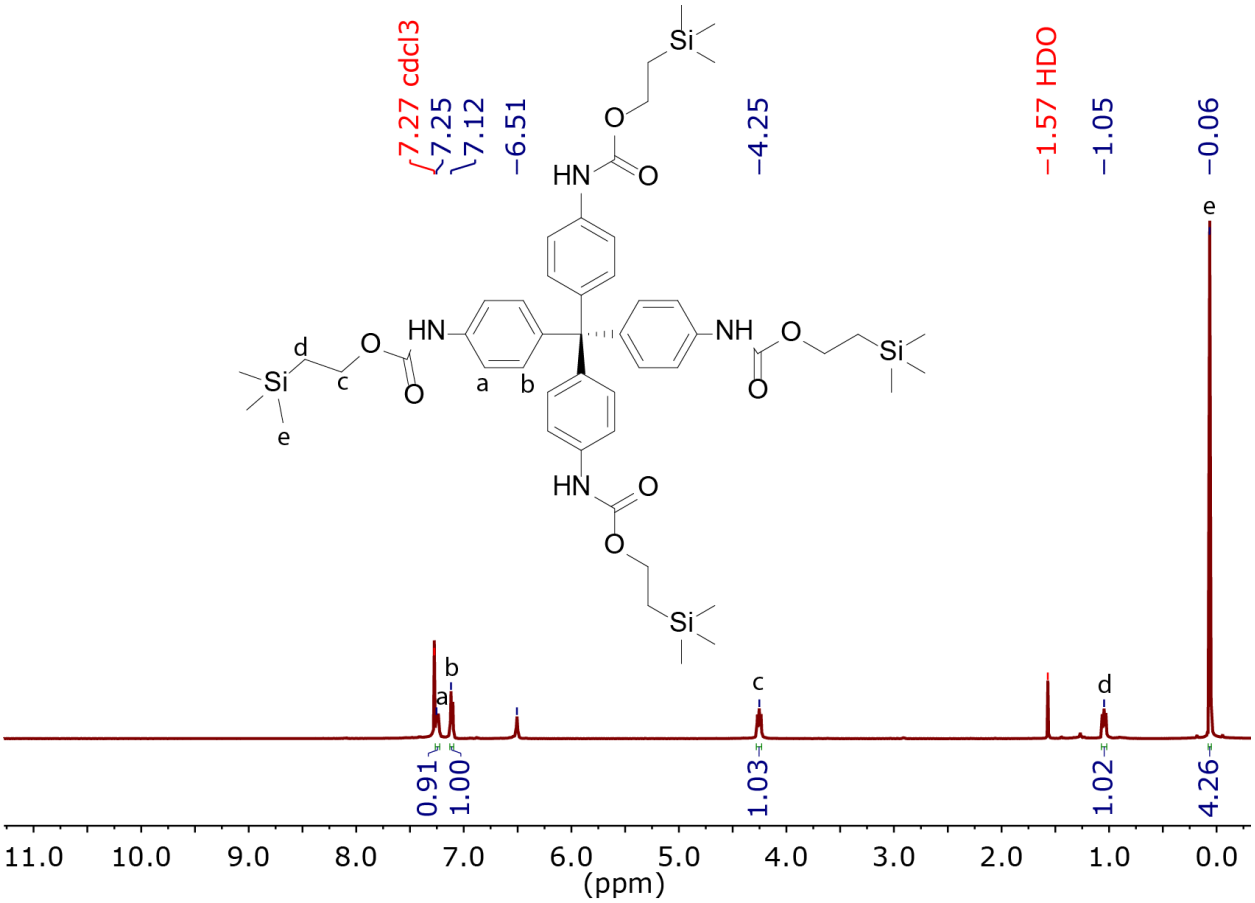

Figure 3.3. ^{1}H NMR spectrum of 2-(trimethylsilyl)ethoxycarbonyl-protected tetrakis(4-aminophenyl)methane.

3.3.4 Scandium Triflate Catalyzed Synthesis of COF-300

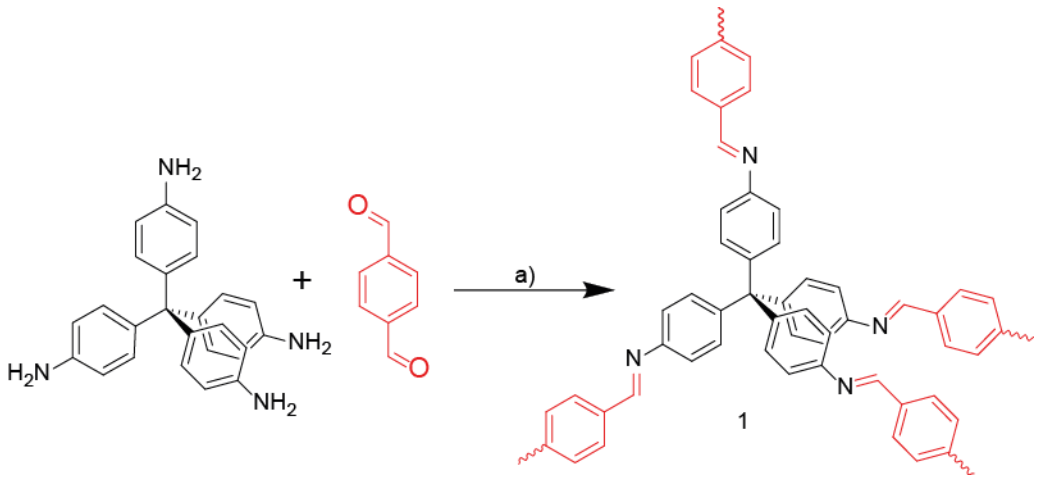

Scheme 3.5. Scandium triflate catalyzed synthesis of COF-300 (1). Reagents and conditions: a) 1,4-dioxane, $Sc(OTf)_3$, H_2O, RT, 144 h.

Scandium triflate catalyzed synthesis of COF-300 (1). A 48 ml "glass bomb" heavy wall pressure vessel was charged with tetrakis(4-aminophenyl)methane (40 mg. 0.105 mmol), terephthalaldehyde (28.2 mg, 0.210 mmol), 1,4-dioxane (5 ml), water (0.4 ml, 53 equiv. per amine) and scandium triflate stock solution (84 µl, 0.2 M in acetonitrile, 0.0168 mmol, 0.04 equiv. per amine). The reactor was capped, sealed, and either heated to 30°C, 50°C, or 70°C for 72 hours or left at room temperature for 144 hours to yield a yellow powder, which was isolated by centrifugation and immersed first in THF and then in methanol to remove residual solvent and guest. The immersions were carried out overnight, and the solvent was replaced by fresh solvent several times during the process. The yellow powder was then dried at 0.3 torr and 150°C for 24 h.

3.3.5 Ionothermal Synthesis of COF-300

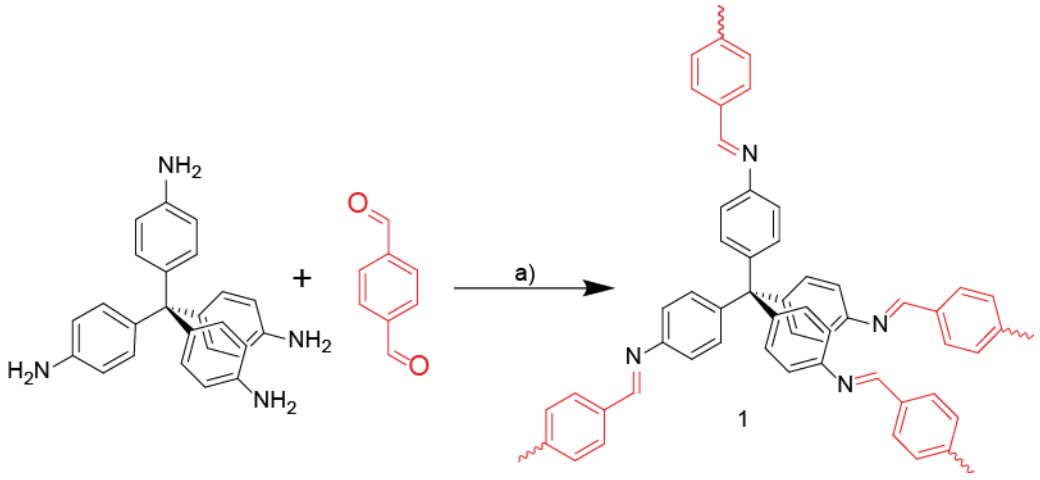

Scheme 3.6. Ionothermal synthesis of COF-300 (1). Reagents and conditions: a) [BMIm][NTf2], 48 h.

Ionothermal synthesis of COF-300 (1). Tetrakis(4-aminophenyl)methane (20 mg, 0.0525 mmol), terephthalaldehyde (14.1 mg, 0.105 mmol), and ionic liquid [BMIm][NTf2] (100 µl) were mixed together at room temperature for 48 h. The mixture was washed using acetone and ethanol to remove the ionic liquid. The product was isolated by centrifugation, washed with 1:1 acetonitrile/water, and dried via lyophilization to afford **1** as a yellow powder.

3.4 Results and Discussion

Initial attempts at $Sc(OTf)_3$ catalyzed COF-300 synthesis utilized the optimal reaction conditions previously identified for 2D imine-linked TAPB-PDA COF (0.02 equivalent $Sc(OTf)_3$, 10 minutes, room temperature)[3] in 1,4-dioxane, a proven organic solvent for COF-300 synthesis[10], which resulted in immediate precipitation and gelling of yellow amorphous frameworks that remained amorphous after one week. This suggested that the amorphous precipitates were kinetically trapped and unable to rearrange into the desired crystalline structure, either due to insufficient mobility or a shift in the forward direction of the imine formation equilibrium, reducing the reversibility of the imine bond and the ability to undergo transimination and imine metathesis. As such, establishing a suitable balance in the reaction equilibrium that would facilitate imine hydrolysis and subsequent imine exchange was necessary to overcoming kinetic trapping.

3.4.1 *In situ* Deprotection and Synthesis of COF-300

3.4.1.1 In-situ Acetyl Deprotection

As described in Section 3.2 in-situ acetyl protection and subsequent deprotection of aldehyde groups is particularly well-suited for $Sc(OTf)_3$ catalyzed imine chemistry. For imine-linked COF synthesis specifically, protecting the aldehyde groups and subsequently deprotecting them *in situ*, which is a much slower process than imine formation, would limit the concentration of the aldehyde reactant and shift the reaction equilibrium in the reverse direction towards the starting materials, providing needed driving force for imine exchange and bond rearrangement. Additionally, the slow deprotection of the aldehydes would also decrease the rate of imine

formation and provide increased opportunity for rearrangement before approaching the kinetically trapped regime.

Protection and deprotection reactions were first conducted on terephthalaldehyde (TA) as model reactions to assess the feasibility of this reaction design, following Scheme 3.2. The protection reaction proceeded smoothly and provided analytically pure compound **2**, as indicated by the ^{1}H NMR spectrum in Figure 3.1. The deprotection reaction produced similarly clean results. As shown in the mass spectrometry in Figure 3.2, the two prominent peaks (135 $[M+H]^{+}$, 157 $[M+Na]^{+}$.) both correspond to the completely deprotected species **3**. Next, **2** was mixed with tetrakis(4-aminophenyl)methane (TAPM), and in the absence of $Sc(OTf)_3$ the imine formation was unable to proceed due to the acetyl protection group, as indicated by the ESI mass spectrometry in Figure 3.4, which shows only the two peaks assigned to the starting materials TAPM (380 $[M]^{+}$) and **2** (222 $[M]^{+}$).

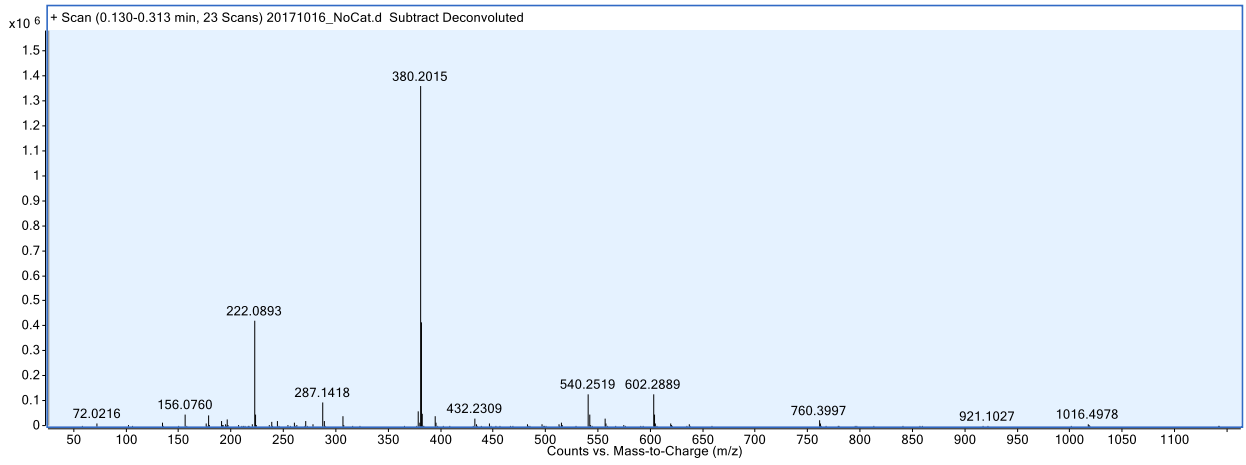

Figure 3.4. ESI mass spectrum of in-situ deprotection and synthesis of COF-300 without $Sc(OTf)_3$.

As the deprotection of TA proceeded smoothly at room temperature, experimentation on the synthesis of COF-300 utilizing in-situ deprotection of acetyl began at room temperature, and trials were conducted over an array of $Sc(OTf)_3$ loading and water content, two factors that affect the effectiveness of deprotection[9]. A summary of the room temperature reactions conducted can be found in Table 3.1.

Table 3.1. Initial room temperature experiments conducted at varying $Sc(OTf)_3$ loading and water content to explore feasibility of in-situ acetyl deprotection and synthesis of COF-300.

Sc(OTf)3 Loading (equiv. per amine)	Water Content (equiv. per amine)
0.02	40
0.02	53
0.02	265
0.02	529
0.02	992
0.04	2116
0.05	529
0.05	1058
0.05	1587
0.05	2116
0.08	529
0.08	2116
0.1	2116
0.12	2116
0.15	2116
0.15	4233
0.2	40
0.2	198
0.2	397
0.2	992
0.2	2116
0.25	2116
0.3	2116
0.35	2116
0.4	2116

Unfortunately, under no combination of conditions was a crystalline product obtained. To drive the deprotection further towards completion and facilitate imine formation, the reaction temperature was increased to 70°C, a temperature that has been demonstrated to drive deprotection and imine formation[9]. A summary of the syntheses conducted at 70°C and varying $Sc(OTf)_3$ loading and water content can be found in Table 3.2.

Table 3.2. Reactions conducted at 70°C and varying $Sc(OTf)_3$ loading and water content to explore feasibility of in-situ acetyl deprotection and synthesis of COF-300.

Sc(OTf)3 Loading (equiv. per amine)	Water Content (equiv. per amine)
0.002	59
0.002	227
0.005	59
0.005	227
0.01	59
0.01	227
0.02	11
0.02	16
0.02	29
0.02	33
0.02	40
0.02	51
0.02	59
0.02	66
0.02	88
0.02	113
0.02	132
0.02	176
0.02	198
0.02	227
0.02	265
0.02	353
0.02	529
0.04	11
0.04	59
0.04	66
0.04	113
0.04	132
0.04	227

0.04	353
0.04	529
0.05	11
0.05	16
0.05	33
0.05	51
0.05	59
0.05	198
0.05	340
0.06	11
0.06	59
0.06	59
0.06	59
0.06	59
0.06	132
0.06	227
0.06	529
0.08	227
0.1	11
0.1	28
0.1	59
0.1	132
0.1	198
0.1	227
0.1	340
0.1	353
0.1	529
0.1	567
0.1	680
0.1	794
0.12	227
0.15	340
0.2	198
0.2	340
0.2	397

Elevation of reaction temperature to 70°C was successful in facilitating the formation of crystalline frameworks, shown by the PXRD spectrum in Figure 3.5. However, even under the best-case scenario shown, the crystallinity of the in-situ deprotected COF-300 did not match that synthesized from the solvothermal method. As such, it was concluded the acetyl protection and

in-situ deprotection of aldehydes was not a viable alternative to the solvothermal method for COF synthesis.

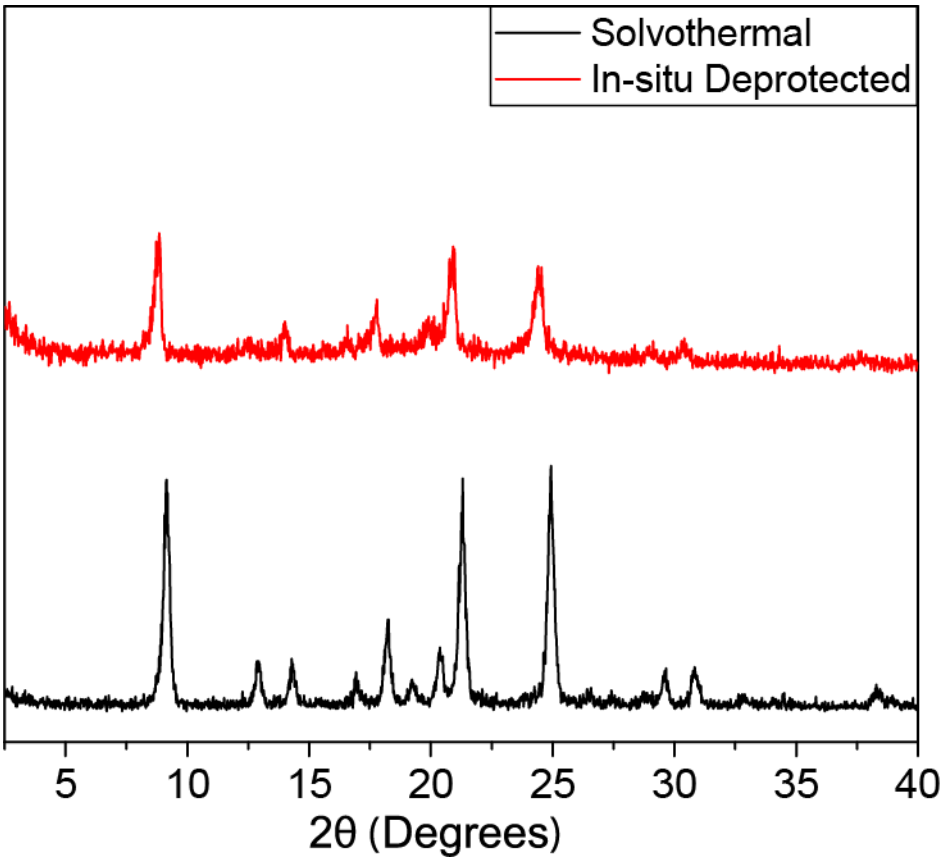

Figure 3.5. PXRD spectrum of COF-300 synthesized utilizing in-situ acetyl protection compared to that of COF-300 synthesized *via* the solvothermal method.

3.4.1.2 Teoc Protection of Amines

Aside from the acetyl protection of aldehydes, the 2-(trimethylsilyl)ethoxycarbonyl (Teoc) protection of the amine groups in TAPM was also explored as an alternative towards in-situ deprotection and was conducted following Scheme 3.4. As indicated by the ^{1}H NMR spectrum of the product in Figure 3.3, compound **5** was isolated in high purity. However, the yield and reproducibility were exceedingly low. Given that TAPM was the product of a four-step synthesis,

an additional inefficient reaction step would have been impractical for an extended systematic COF synthesis investigation similar to that of acetyl protection and deprotection. Additionally, the inability of the acetyl deprotection products to match the crystallinity of that of the solvothermal products further reduced confidence in the feasibility of this approach, and *in situ* Teoc deprotection was not further pursued.

3.4.2 Scandium Triflate Catalyzed COF-300 Synthesis

Given the difficulties experienced with *in situ* deprotection, research efforts shifted towards straight synthesis of COF-300 utilizing $Sc(OTf)_3$. As observed in preliminary attempts, the reaction became kinetically trapped easily under the more effective catalytic effects of $Sc(OTf)_3$. Therefore, a delicate balance in the reaction equilibrium was needed, such that both the forward direction of imine formation and the reverse direction of imine hydrolysis could proceed. $Sc(OTf)_3$ was an effective catalyst for imine formation, so the focus of the investigation would be providing enough driving force in the reverse direction to break the imine bonds and allow rearrangement of constituent species through imine exchange reactions into the desired crystalline structure. Additional mobility would also be helpful in overcoming kinetic trapping. To that end, the main factors which influence mobility or reaction equilibrium, reaction temperature, water content, catalyst loading, and degassing were systematically investigated to facilitate formation of crystalline frameworks and optimization of reaction conditions.

Conventional solvothermal synthesis procedure for COF-300 requires the freeze-thaw-pump degassing of the reaction vessel prior to synthesis[10]; However, the components of the imine-linked COF synthesis are not sensitive to air, and overpressure has proven unnecessary for COF synthesis[1]. A comparison of two syntheses at identical reaction conditions, one with degassing

and one without, confirms that degassing does not contribute to any noticeable difference in the crystallinity of the product, as confirmed by PXRD and is shown in Figure 3.6**.**

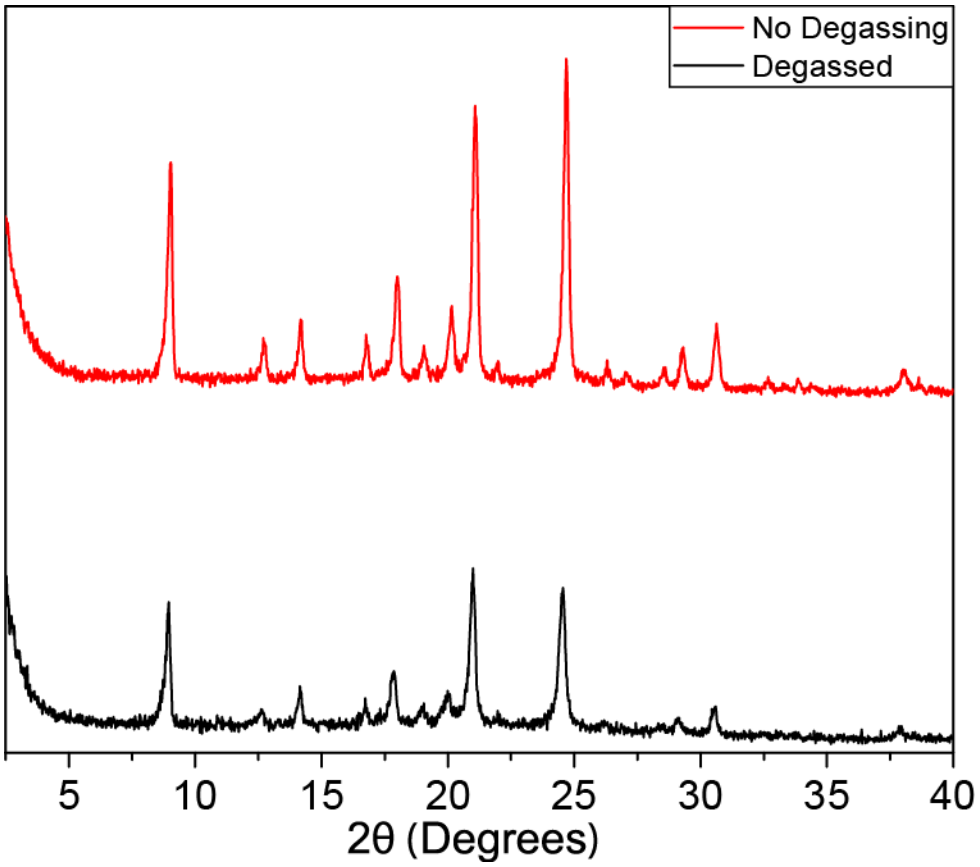

Figure 3.6. Comparison of PXRD spectrum of a degassed COF-300 sample to one without degassing.

To provide additional mobility to constituent species, syntheses were initially performed at 70°C, which has been demonstrated as a suitable temperature for $Sc(OTf)_3$ catalyzed imine-based dynamic covalent assembly[9], for 72 hours. The Lewis acidic $Sc(OTf)_3$ catalyzes both imine hydrolysis and transimination, imparting reversibility and rearrangeability to the imine bond, and as such it is reasonable to expect an optimal catalyst loading that finds the balance in reaction equilibrium between imine bond formation and rearrangement. Catalyst loading was varied

independently over a range of conditions, and highest degree of crystallinity, as characterized by PXRD, was obtained at 0.02 equiv. $Sc(OTf)_3$ per amine (Figure 3.7). Similarly, COFs possessing excellent crystallinity could be obtained at 0.04 equiv. $Sc(OTf)_3$ at 50°C and 30°C (Figure 3.8 and Figure 3.9). The reaction was then conducted at room temperature, and no crystallinity was observed after 72 hours. Extending the reaction duration to 144 hours, however, did result in crystalline products at certain catalyst loading conditions, indicating that lack of additional mobility provided by heating can be compensated by extending the reaction duration. At room temperature, 0.04 equiv. $Sc(OTf)_3$ resulted in the most crystalline structure, and increasing or decreasing the amount of catalyst resulted in diminished crystallinity owing to shifts in reaction equilibrium beyond the optimal point, as shown by the PXRD spectra in Figure 3.10. A summary of every trial conducted can be found in Table 3.3.

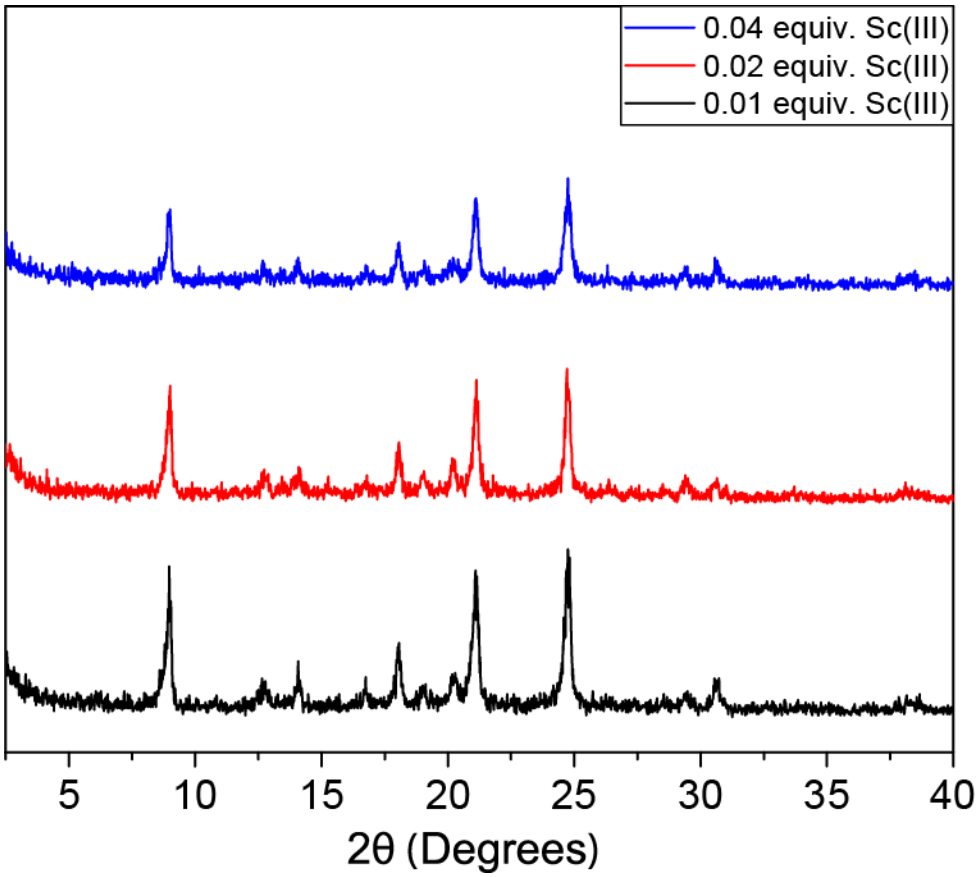

Figure 3.7. PXRD spectra of COF-300 synthesized at 70°C and 53 equiv. water per amine utilizing a range of $Sc(OTf)_3$ loading.

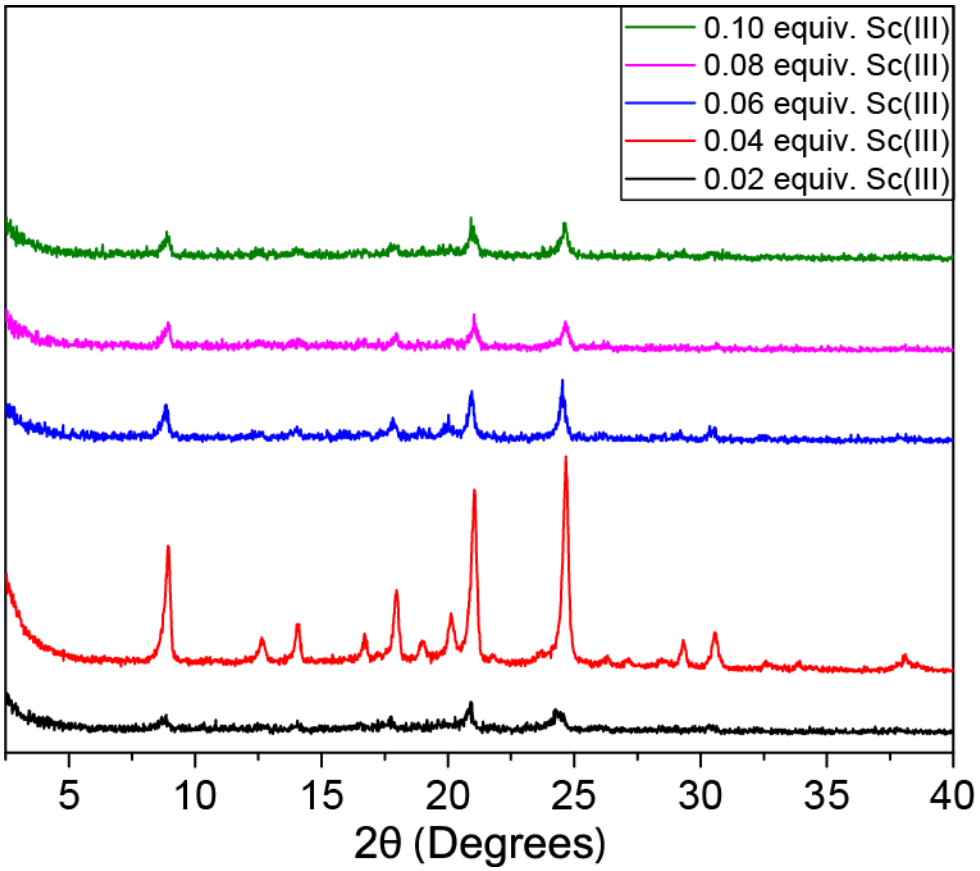

Figure 3.8. PXRD spectra of COF-300 synthesized at 50°C and 53 equiv. water per amine utilizing a range of $Sc(OTf)_3$ loading.

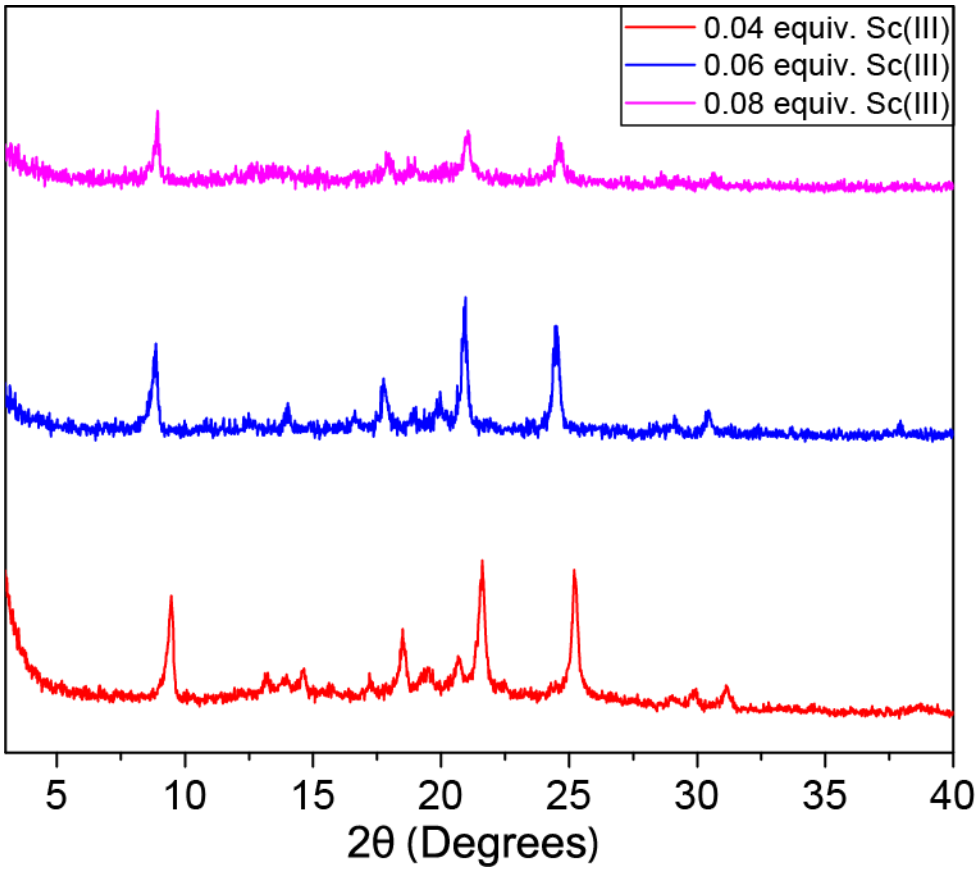

Figure 3.9. PXRD spectra of COF-300 synthesized at 30°C and 53 equiv. water per amine utilizing a range of $Sc(OTf)_3$ loading.

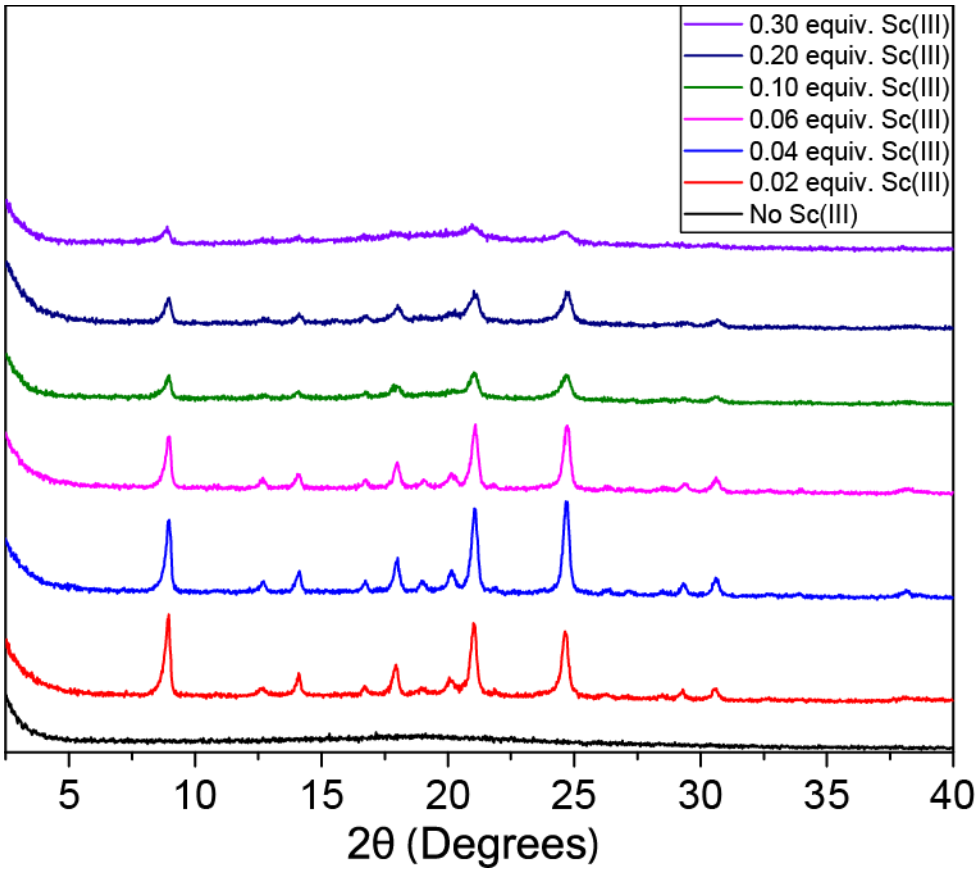

Figure 3.10. PXRD spectra of COF-300 synthesized at room temperature and 53 equiv. water per amine utilizing a range of $Sc(OTf)_3$ loading.

Table 3.3. Summary of $Sc(OTf)_3$ catalyzed COF-300 syntheses.

Temperature (°C)	$Sc(OTf)_3$ Loading (equiv. per amine)	Water Content (equiv. per amine)
70	0.005	53
70	0.01	53
70	0.02	53
70	0.04	53
70	0.06	53
70	0.005	132
70	0.01	132
70	0.02	132
50	0.02	53
50	0.04	53
50	0.06	53
50	0.08	53
50	0.1	53
30	0.04	53
30	0.06	53
30	0.08	53
RT[a]	0.02	53
RT	0.04	53
RT	0.06	53
RT	0.08	53
RT	0.1	53
RT	0.12	53
RT	0.2	53
RT	0.3	53
RT	0.04	0
RT	0.04	26
RT	0.04	53
RT	0.04	79
RT	0.04	106

The role of water in this system is to mediate the reaction equilibrium, driving the imine formation equilibrium towards imine hydrolysis and providing improved imine bond reversibility, and a range of water contents were tested at each temperature to determine the optimal condition. The presence of water proved to be crucial, as no crystalline frameworks were obtained in the

absence of water at any combination of temperature and catalyst loading. An excess of water, however, shifted the reaction equilibrium too far and likewise resulted in amorphous products. At every temperature, 53 equiv. water per amine was identified as the optimal condition, providing the XRD spectrum with the sharpest and most well-defined peaks. The comparison of PXRD spectra for samples synthesized utilizing different water content at room temperature is shown in Figure 3.11.

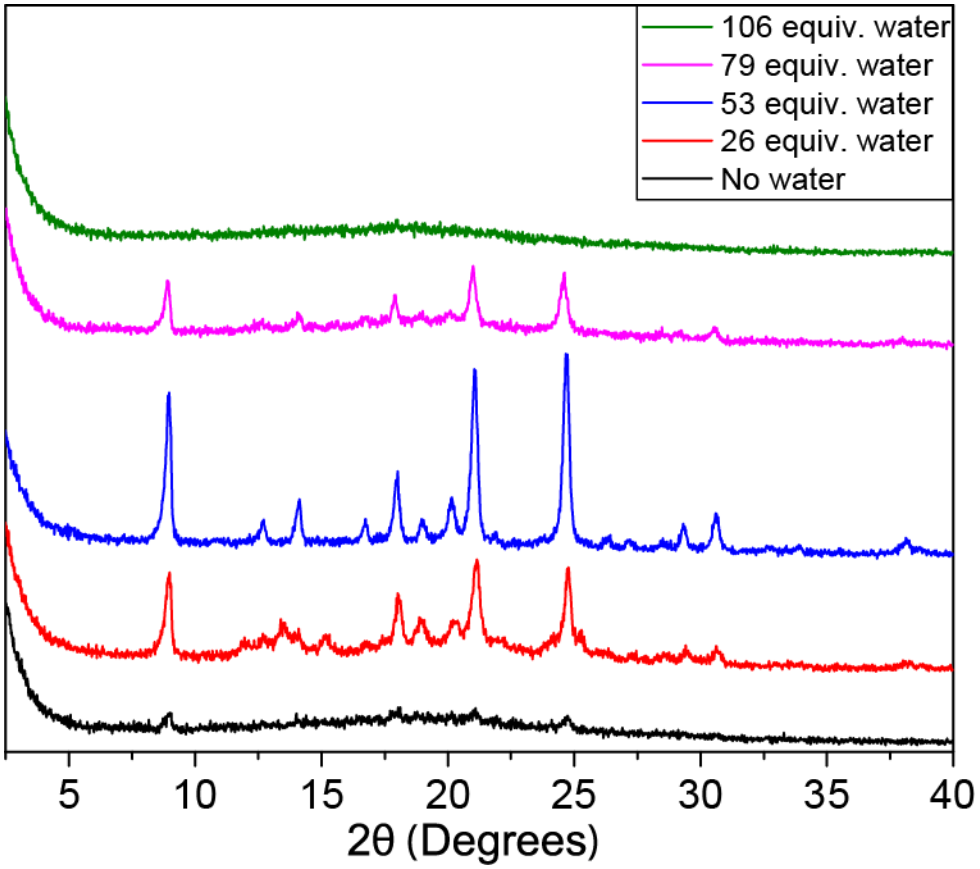

Figure 3.11. PXRD spectra of COF-300 synthesized at room temperature and 0.04 equiv. $Sc(OTf)_3$ per amine and a range of water content.

As the optimal catalyst loading and water content have been identified at each temperature, a comparison of the most crystalline COF sample obtained at each temperature was conducted to

elucidate the effects of temperature. A summary of the reaction conditions is shown in Table 3.4, and their corresponding PXRD spectra are shown in Figure 3.12. The extreme similarity of the spectra indicate that elevated temperature is not a necessary component of obtaining crystallinity but is rather a way to provide additional mobility to the constituent species and overcome kinetic trapping. The significantly higher effectiveness of $Sc(OTf)_3$ in catalyzing imine formation and exchange compared to that of acetic acid in the predominant solvothermal method leads to a lower degree of kinetic trapping, and allows for the reduction of reaction temperature from 120°C to much lower temperatures. At room temperature, the kinetics of the $Sc(OTF)_3$ catalyzed synthesis is much slower than the heated reactions, requiring twice the reaction duration to obtain a crystalline structure, but the system is not completely kinetically trapped. The excellent efficacy of $Sc(OTf)_3$ and extended reaction duration provide sufficient driving force for rearrangement and eliminates the need for elevated temperatures.

Table 3.4. Summary of optimal $Sc(OTf)_3$ catalyzed COF-300 synthesis conditions at different temperatures.

Temperature	Catalyst Loading (equiv. per amine)	Water Content (equiv. per amine)	Reaction Duration (hours)
RT	0.04	53	144
30°C	0.04	53	72
50°C	0.04	53	72
70°C	0.02	53	72

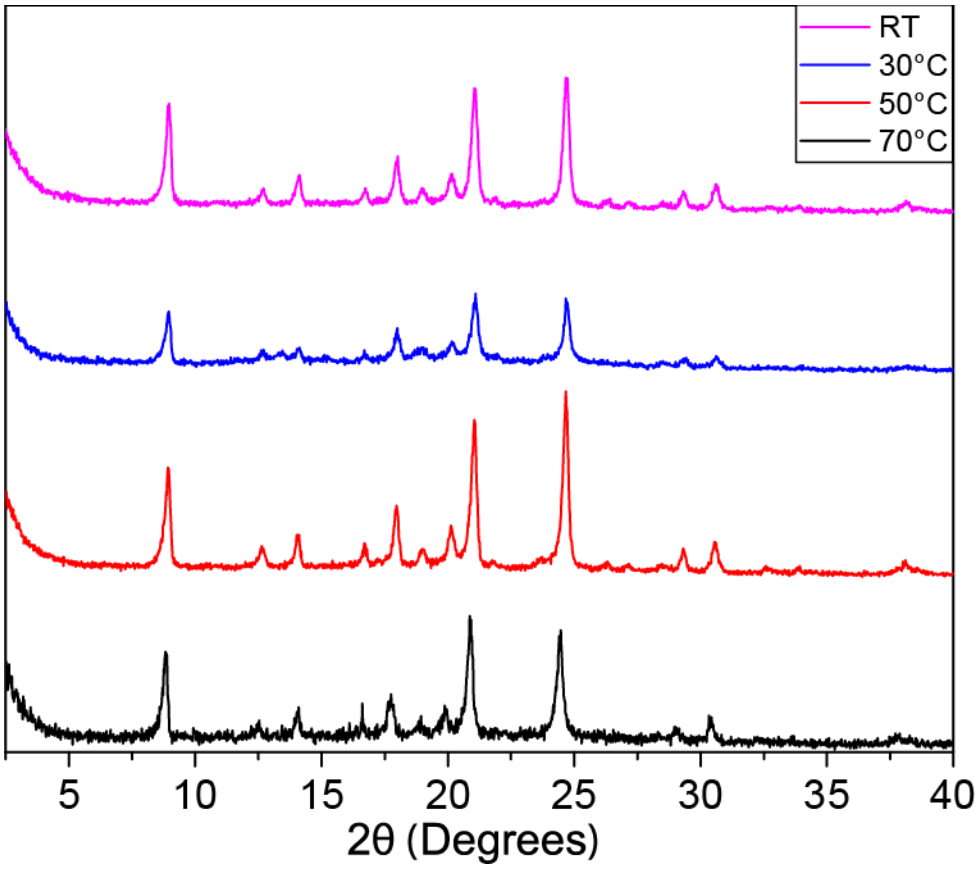

Figure 3.12. Comparison of PXRD spectra of COF-300 synthesized using $Sc(OTf)_3$ at each temperature at the optimal $Sc(OTf)_3$ loading and water content.

COF-300 synthesized utilizing $Sc(OTf)_3$ was further characterized by FTIR and solid-state ^{13}CP-TOSS NMR, and the resultant spectra are in good agreement with those of COF-300 synthesized from the conventional solvothermal method (Figure 3.13 and Figure 3.14). The PXRD spectra, shown in Figure 3.15, are essentially identical.

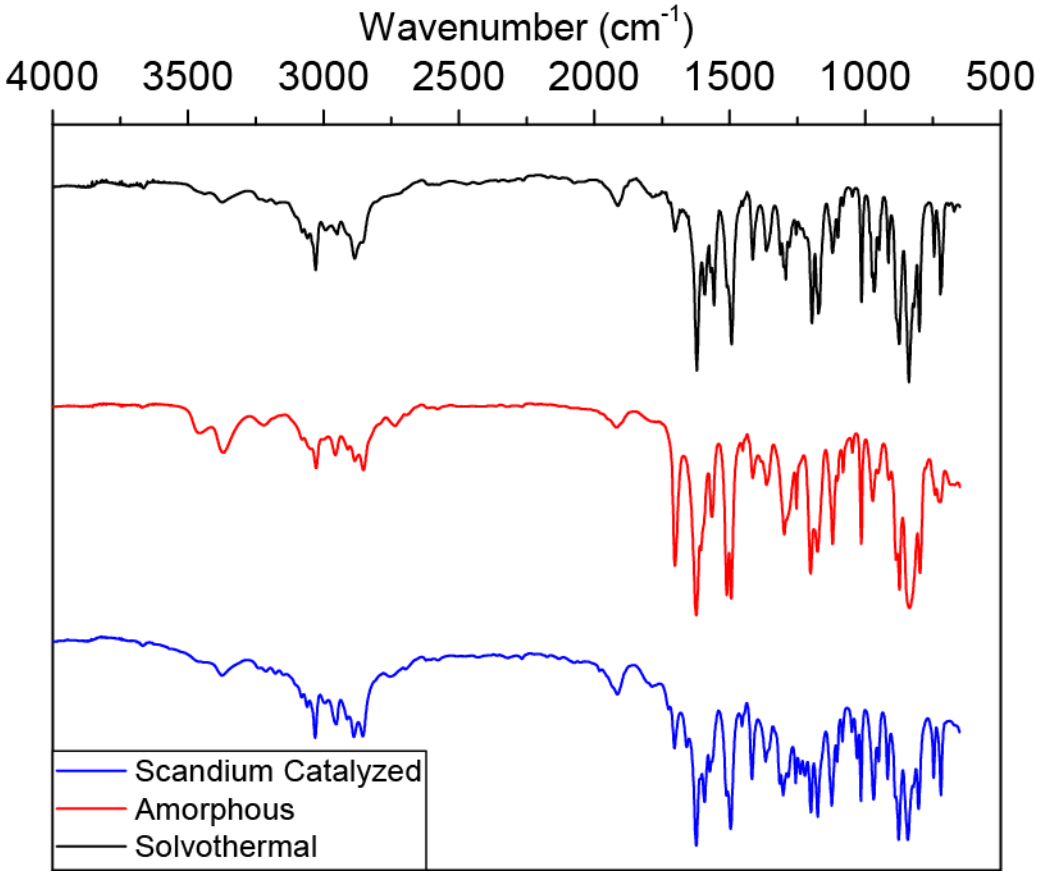

Figure 3.13. Comparison of FTIR spectrum of COF-300 synthesized using $Sc(OTf)_3$ compared to that synthesized *via* the solvothermal method and that of an amorphous sample.

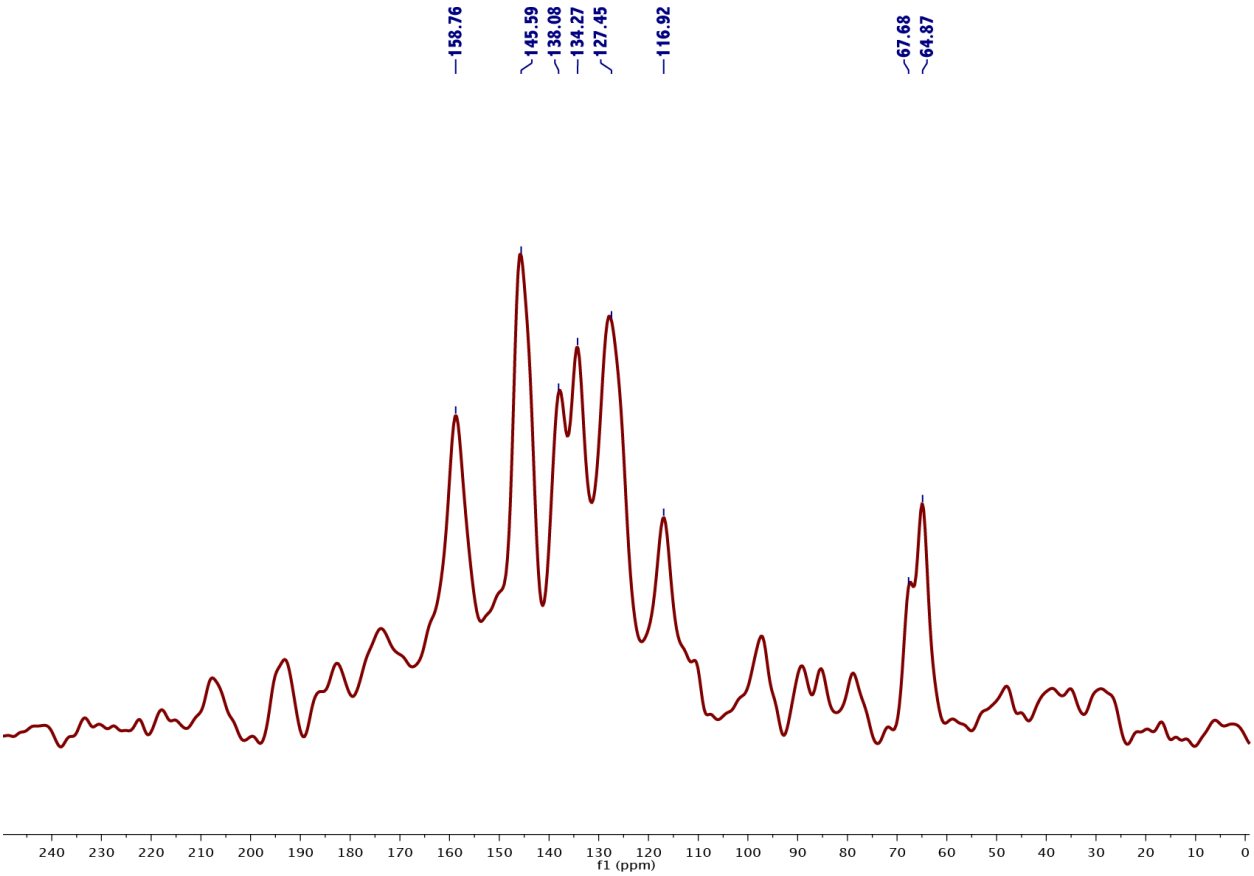

Figure 3.14. ^{13}CP-TOSS NMR spectrum of COF-300 synthesized using Sc(OTf)$_3$.

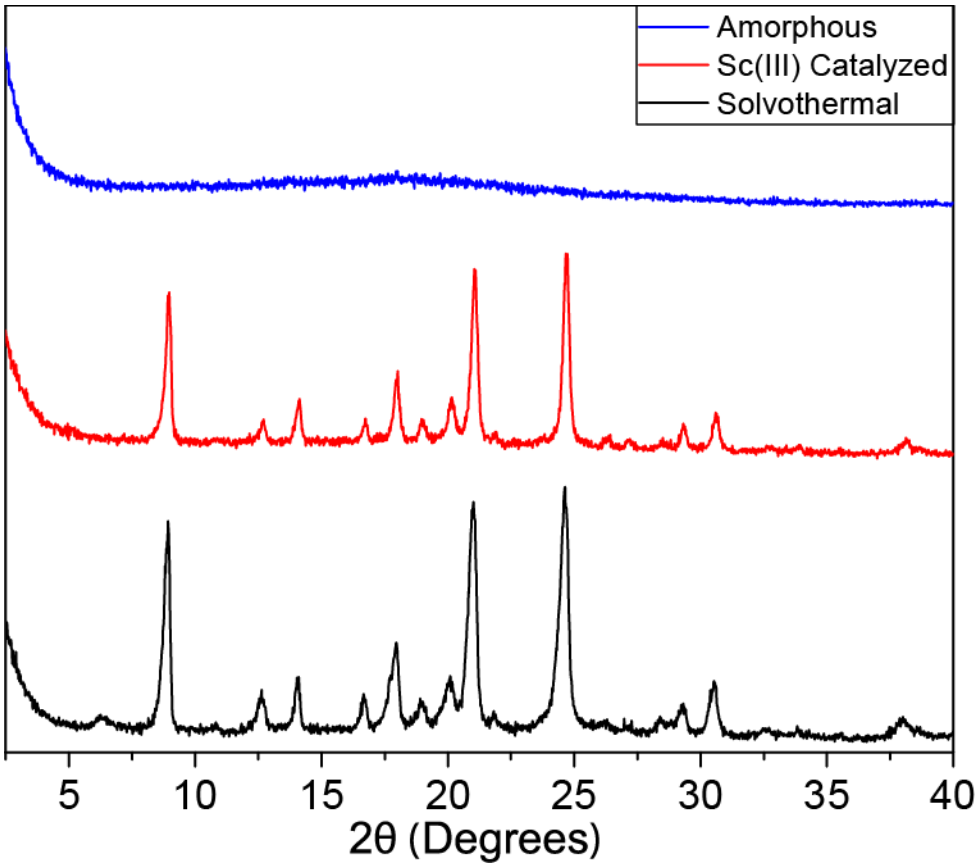

Figure 3.15. Comparison of PXRD spectrum of COF-300 synthesized using $Sc(OTf)_3$ compared to that synthesized *via* the solvothermal method and that of an amorphous sample.

N_2 adsorption-desorption isotherms were measured for COF-300 synthesized utilizing the solvothermal method and the $Sc(OTf)_3$ catalyzed method. The solvothermal isotherm (Figure 3.16) exhibits a lower degree of hysteresis than that originally reported for COF-300[10]. The isotherms for samples synthesized utilizing $Sc(OTf)_3$ (Figure 3.17 and Figure 3.18) exhibit a step-like behavior at $P/P_0 < 0.1$ which has similarly been observed in other reports on COF-300[11,12], and this phenomenon has been attributed to changes in pore structure during the adsorption-desorption process[11], possibly due to "guest-induced structural transformation and/or reorientation of the guest packing under increased pressure" [13]. The Brunauer-Emmett-Teller (BET) surface area was calculated in the range of $0.005 < P/P_0 < 0.065$ for the solvothermal sample, $0.12 < P/P_0 < 0.22$ for

the room temperature $Sc(OTf)_3$ sample, and $0.05 < P/P_0 < 0.095$ for the 50°C $Sc(OTf)_3$ sample to be 896 m^2/g, 982 m^2/g, and 907 m^2/g, respectively. These surface area values are very similar and fall within the range of reported BET surface area values of 756 – 1360 m^2/g for COF-300[10–12].

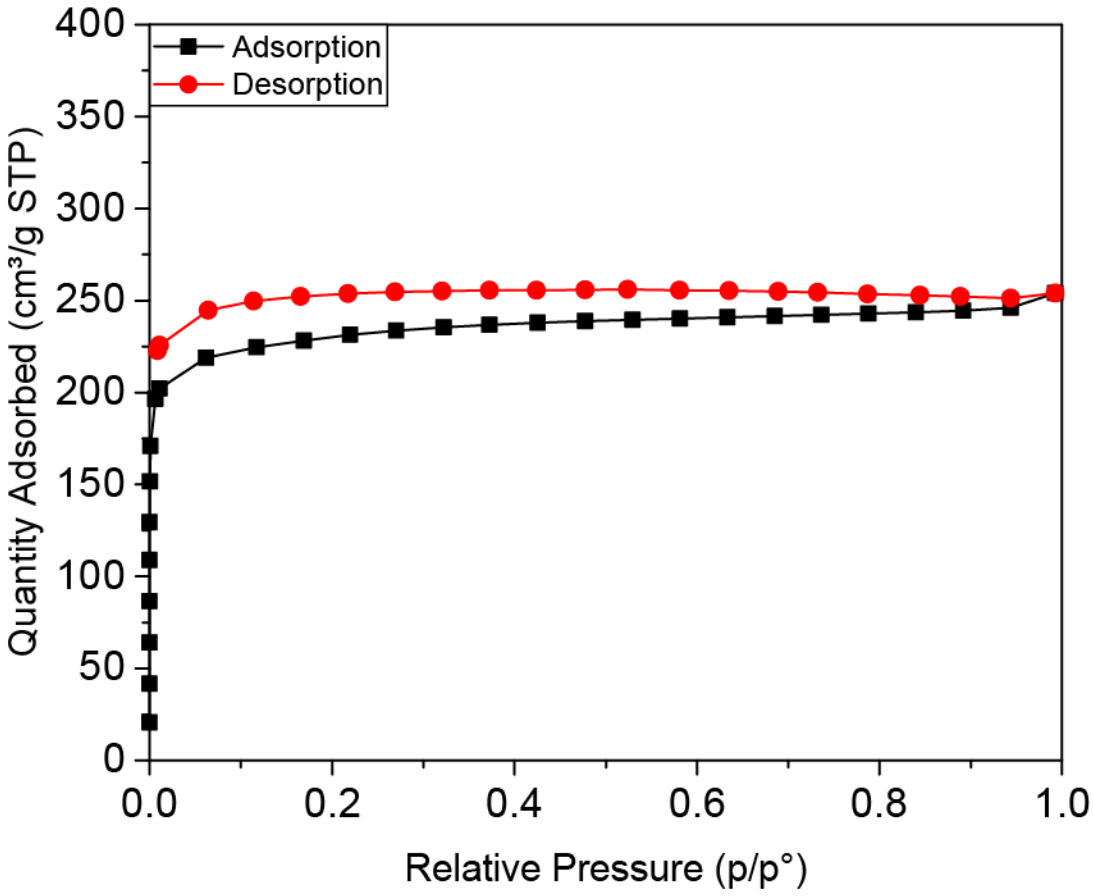

Figure 3.16. N_2 adsorption-desorption isotherms of COF-300 synthesized utilizing the solvothermal method.

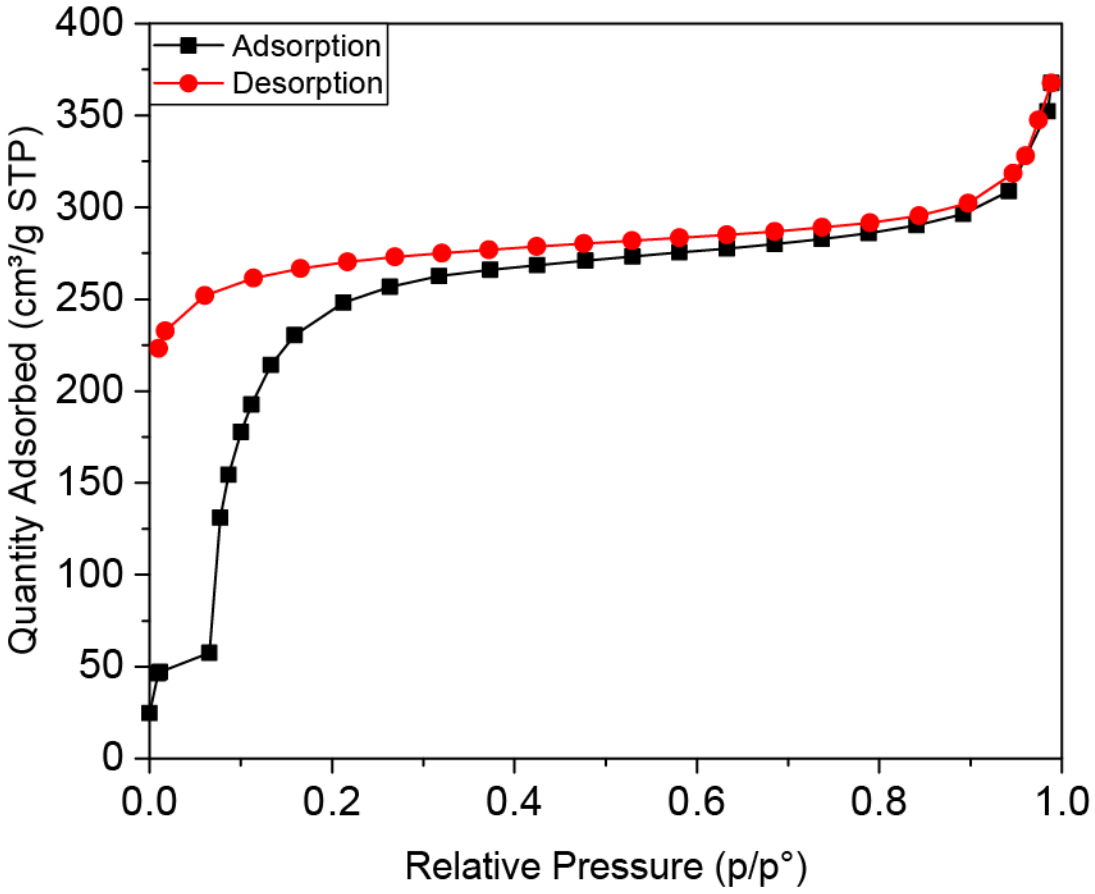

Figure 3.17. N_2 adsorption-desorption isotherms of COF-300 synthesized utilizing $Sc(OTf)_3$ at 50°C.

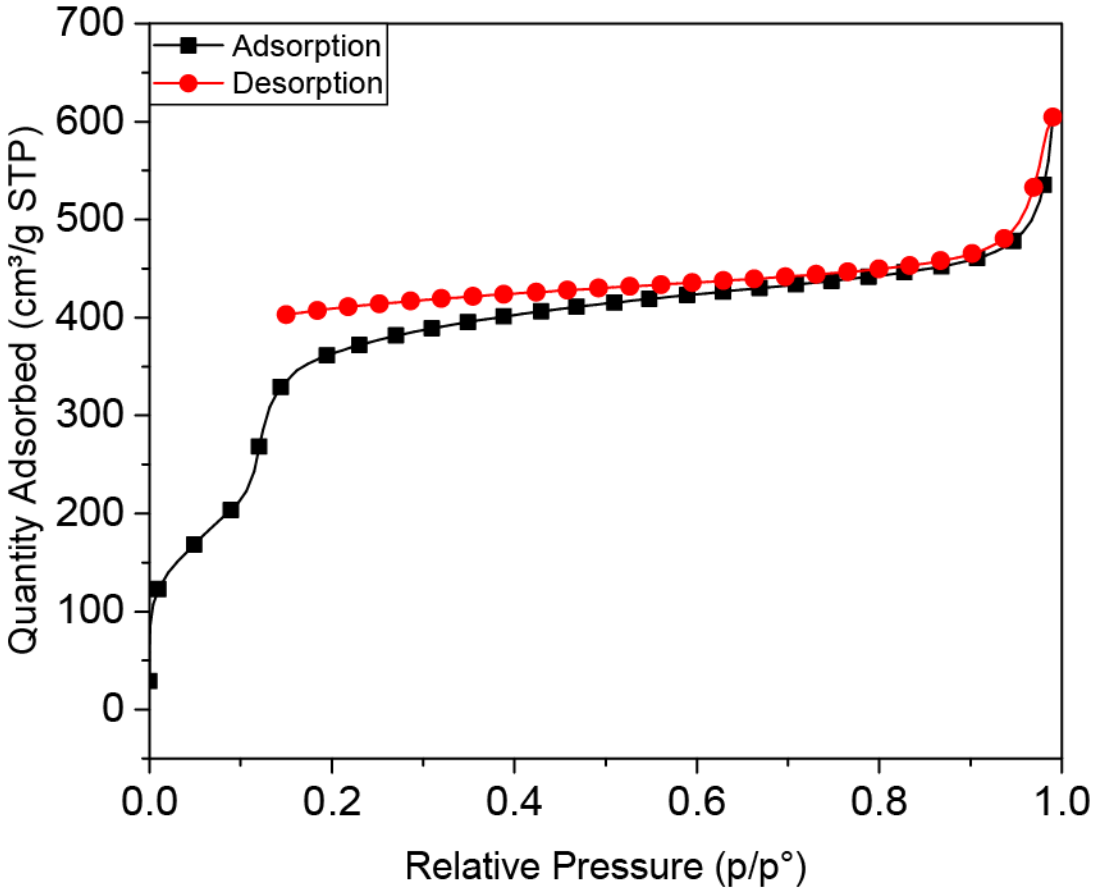

Figure 3.18. N_2 adsorption-desorption isotherms of COF-300 synthesized utilizing $Sc(OTf)_3$ at room temperature.

3.4.3 Ionothermal Synthesis of COF-300

Ionothermal synthesis of COF-300 was attempted following the procedures shown in Scheme 3.6. The product was characterized by PXRD and FTIR and compared to the spectra of COF-300 samples synthesized *via* the solvothermal method and $Sc(OTf)_3$ method as well as the reactants, as found in Figure 3.19 and Figure 3.20, respectively. The PXRD spectra of the ionic liquid catalyzed sample matches poorly with those of the two other COF-300 synthesis methods. Instead, many peaks match those found in the spectrum of TAPM, suggesting the presence of said reactants remained after the synthesis. Similarly, the FTIR spectrum of the ionic liquid catalyzed

sample exhibits a much stronger aldehyde stretching peak at 1700 cm^{-1} than those found in the $Sc(OTf)_3$ catalyzed and solvothermal spectra and comparable to that in the TA spectrum, indicating the presence of significant unreacted aldehyde functional groups in the structure. These two observations combined suggest that the reported success of the ionothermal synthesis method for imine-linked 3D COFs could not be replicated.

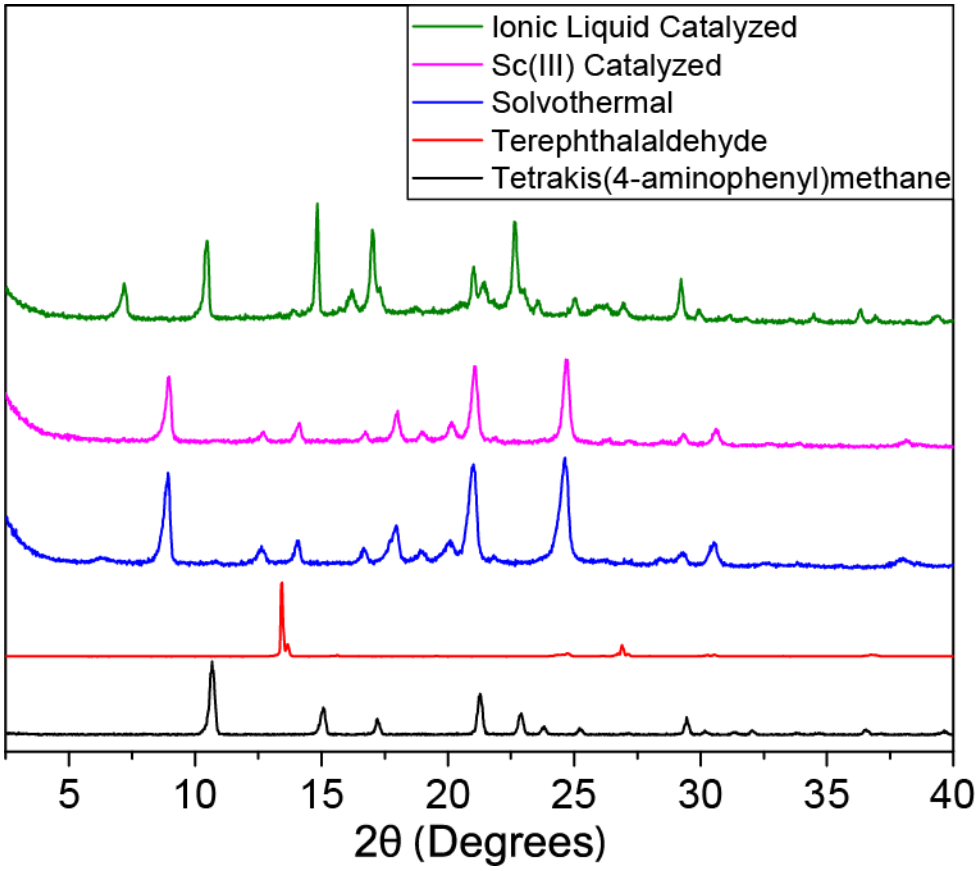

Figure 3.19. Comparison of PXRD spectra of COF-300 synthesized using the solvothermal method, $Sc(OTf)_3$ catalyzed method, and the ionothermal method with the reactants tetrakis(4-aminophenyl)methane and terephthalaldehyde.

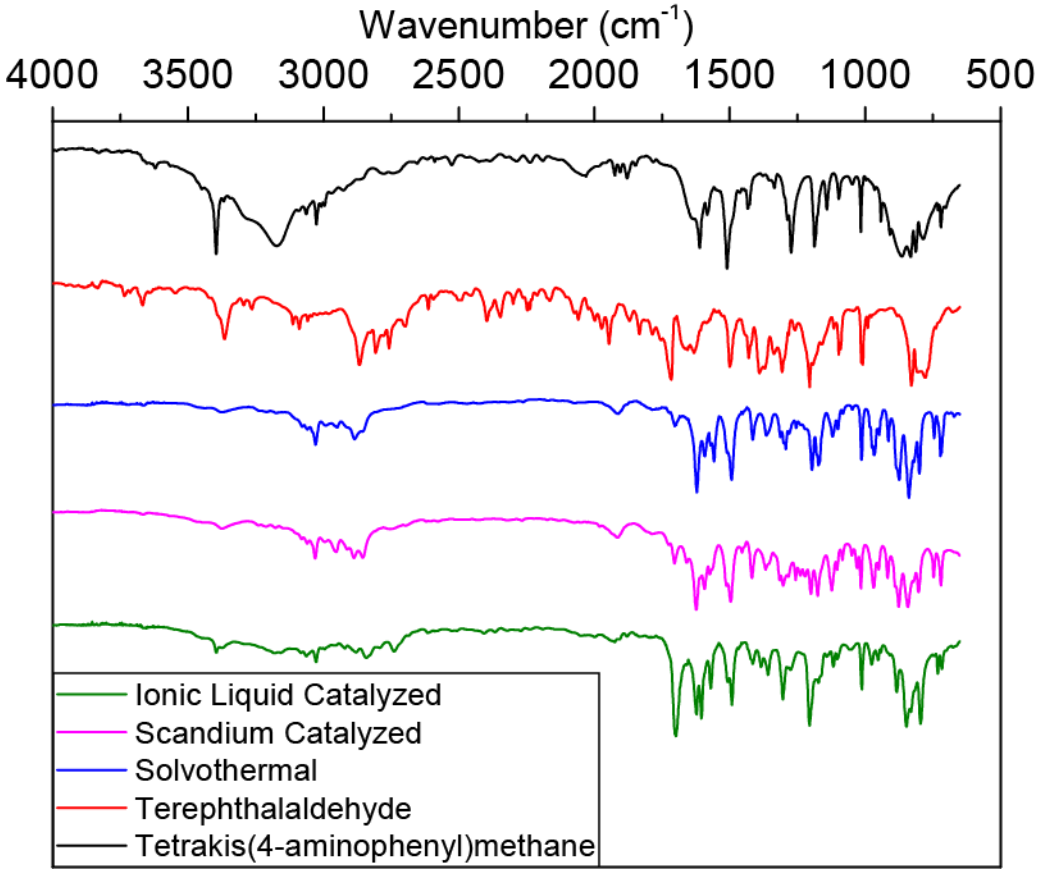

Figure 3.20. Comparison of FTIR spectra of COF-300 synthesized using the solvothermal method, $Sc(OTf)_3$ catalyzed method, and the ionothermal method with the reactants tetrakis(4-aminophenyl)methane and terephthalaldehyde.

3.5 Conclusions

COF-300 was synthesized at room temperature utilizing Sc(OTf)3 as the catalyst, demonstrating the first room temperature synthesis of a 3D COF utilizing rare earth metal triflate. Water was demonstrated to be crucial for obtaining a crystalline framework, and crystallinity at ambient temperature was optimized by adjusting water content and catalyst loading, with 53 equiv. water per amine and 0.04 Sc(OTf)3 per amine providing the most crystalline framework. Degassing of reaction vessel prior to synthesis was shown to be unnecessary, removing a time-consuming step from the COF synthesis procedure. Acetyl protection and subsequent *in situ*

deprotection of aldehyde groups was demonstrated to produce COFs with reduced crystallinity compared to conventional methods. Additionally, the ionothermal synthesis of imine-linked 3D COFs could not be reproduced. The synthesis procedures and reaction conditions identified in this chapter can be generalized to other imine-linked 3D COFs, and the insights obtained into different reaction parameters will contribute to improved understanding of 3D COF synthesis.

3.6 References

1. Ma, X. & Scott, T. F. Approaches and challenges in the synthesis of three-dimensional covalent-organic frameworks. *Commun. Chem.* **1**, 98 (2018).
2. Bisbey, R. P., DeBlase, C. R., Smith, B. J. & Dichtel, W. R. Two-dimensional Covalent Organic Framework Thin Films Grown in Flow. *J. Am. Chem. Soc.* **138**, 11433–11436 (2016).
3. Matsumoto, M. *et al.* Rapid, Low Temperature Formation of Imine-Linked Covalent Organic Frameworks Catalyzed by Metal Triflates. *J. Am. Chem. Soc.* **139**, 4999–5002 (2017).
4. DeBlase, C. R. & Dichtel, W. R. Moving Beyond Boron: The Emergence of New Linkage Chemistries in Covalent Organic Frameworks. *Macromolecules* **49**, 5297–5305 (2016).
5. Guan, X. *et al.* Fast, Ambient Temperature and Pressure Ionothermal Synthesis of Three-Dimensional Covalent Organic Frameworks. *J. Am. Chem. Soc.* **140**, 4494–4498 (2018).
6. Ma, T. *et al.* Single-crystal x-ray diffraction structures of covalent organic frameworks. *Science* **361**, 48–52 (2018).
7. Smith, B. J., Overholts, A. C., Hwang, N. & Dichtel, W. R. Insight into the crystallization of amorphous imine-linked polymer networks to 2D covalent organic frameworks. *Chem. Commun.* **52**, 3690–3693 (2016).
8. Ji, W., Sun, R., Geng, Y., Liu, W. & Wang, X. Rapid, low temperature synthesis of molecularly imprinted covalent organic frameworks for the highly selective extraction of cyano pyrethroids from plant samples. *Anal. Chim. Acta* **1001**, 179–188 (2018).

9. Wei, T., Furgal, J. C. & Scott, T. F. In situ deprotection and dynamic covalent assembly using a dual role catalyst. *Chem. Commun.* **53**, 3874–3877 (2017).

10. Uribe-Romo, F. J. *et al.* A Crystalline Imine-Linked 3-D Porous Covalent Organic Framework. *J. Am. Chem. Soc.* **131**, 4570–4571 (2009).

11. Ma, T. *et al.* Observation of Interpenetration Isomerism in Covalent Organic Frameworks. *J. Am. Chem. Soc.* **140**, 6763–6766 (2018).

12. Qian, H.-L., Yang, C. & Yan, X.-P. Layer-by-layer preparation of 3D covalent organic framework/silica composites for chromatographic separation of position isomers. *Chem. Commun.* (2018). doi:10.1039/C8CC06621C

13. Zhang, Y.-B. *et al.* Single-Crystal Structure of a Covalent Organic Framework. *J. Am. Chem. Soc.* **135**, 16336–16339 (2013).

Chapter 4
Synthesis of Functionalized Imine-linked 3D COFs

4.1 Abstract

Despite recent advances in 2D COF modification, investigation into the functionalization of imine-linked 3D COFs remains scarce. In this chapter, four different chemistries were pursued and evaluated for the synthesis of functionalized aldehyde linkers, and three different functionalized terephthalaldehyde species featuring dimethoxy, dihydroxy, and dibromide pendant groups were obtained. The functionalized aldehydes were employed for functionalized COF-300 synthesis utilizing both the conventional solvothermal approach and the $Sc(OTf)_3$ catalyzed approach described in Chapter 3. A systematic investigation of a wide range of reaction conditions was unsuccessful in producing crystalline frameworks with all three monomers, suggesting that steric hindrance rather than electronic hindrance was the root cause behind the inability to rearrange into crystalline structures.

4.2 Introduction

The chemical tunability and structural diversity of COFs, afforded by their organic nature, is one of their biggest strengths compared to other nanoporous materials[1]. Compared to 2D COFs, the diversity of 3D COFs is restricted by limited topologies and building blocks; therefore, modification and functionalization of existing 3D COF structure is crucial for producing tailored

structures and functionalities for applications[2]. The most common method for COF functionalization, post-synthetic modification (PSM), seeks to alter chemical features on the COF backbone, often adding reactive functionalities that would facilitate the intended application. However, the backbone of 3D COFs such as COF-300 lack the reactive sites needed for easy modification. As such, PSM usually involves embedding such reactive sites into the constituent monomers of the COF and applying necessary chemistry to said sites after the COF structure has been assembled.[2] Several such modifications have been carried out on the boron-oxygen linked COF-102[3–5], but only one instance has been reported for imine-linked 3D COFs, a demonstration of the carboxylation of hydroxy groups in a functionalized 3D COF[6]. Thus, further investigation into the synthesis of functionalized imine-linked 3D COFs and PSM of the embedded pendant groups in those COFs is vital for unlocking the full diversity of potential 3D COF applications.

Many reactive groups could be employed for monomer functionalization if they do not interfere with or participate in the imine chemistry. Hydroxy groups are well-suited for this purpose, as they do not interact with amines or aldehydes in any way and can be readily converted into a wide range of other functionalities. Figure 4.1 highlights a few examples of possible conversions and corresponding applications.

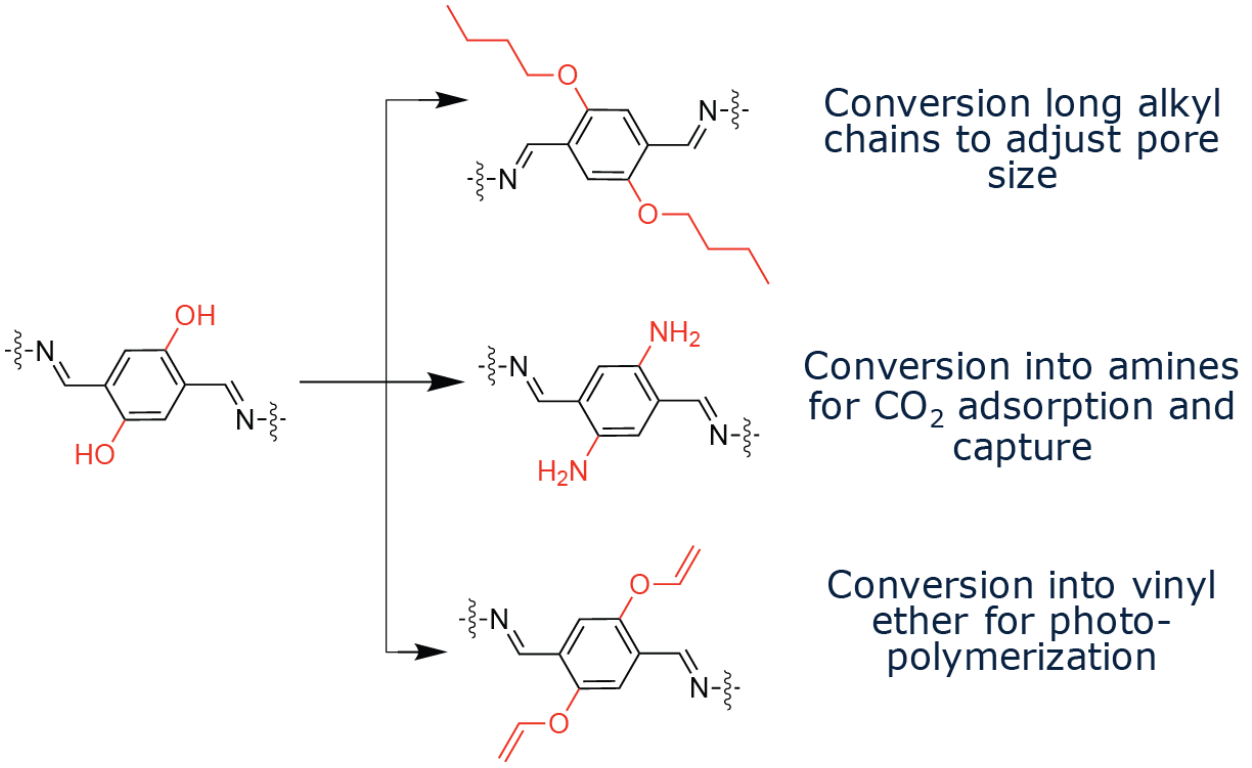

Figure 4.1. Sample conversion of hydroxy groups into long alkyl chains for pore size adjustment for size- and shape-based applications such as gas separation, into amines for CO_2 adsorption and capture, and into vinyl ether for photo-polymerization.

Aside from structural modification, another challenge that faces 3D COFs is interpenetration, where the empty space described by the crystalline framework accommodates one or more additional networks[16] and which can adversely affect pore volume and impact internal surface area[17]. Many 3D COFs reported to date have exhibited varying degrees of interpenetration, resulting in significant reductions in pore size and volume. Thus, establishing control over and reducing or preventing interpenetration in 3D COFs is key to fully realizing their potential as crystalline, controllably porous materials.

Whereas interpenetration in 3D COFs has typically been determined by structural modeling and unit cell indexing and is reported as an inherent characteristic, efforts to better understand, characterize, and even modify degrees of interpenetration have been recently reported. For

example, the synthesis of an interpenetration isomer was reported for COF-300, representing a preliminary attempt towards modifying the extent of interpenetration in a 3D COF[18]. More sophisticated approaches to control COF interpenetration might be derived from techniques successfully implemented in MOF syntheses, such as temperature and monomer concentration control[19], organic bond structure alteration[17], rational design of organic building blocks[20], and incorporation of space-filling protecting groups that could be post-synthetically cleaved[21], owing to their structural similarity. Of these, the usage of space-filling protecting groups affords the highest degree of tunability and control and would allow alteration of the degree of interpenetration by adjusting the size of the protecting groups.

There are a number of criteria governing the protecting group selection of these hydroxy moieties: 1) the protecting group should be of suitable size, large enough to fill space and prevent interpenetration and not too bulky as to hinder network formation; 2) the protection reaction must proceed to completion so that all hydroxy functionalities are protected and free space within the pores of the COF network is minimized; 3) the protected hydroxy group must not cleave under COF synthesis conditions, which could be either Lewis acidic[24] or weakly acidic at elevated temperatures of 120°C[25]; 4) deprotection would ideally proceed under non-acidic conditions, so the protection groups could be post-synthetically removed to clear the pores and increase pore volume.

In this chapter, four different chemistries are employed for the synthesis of functionalized aldehyde linkers containing vinyl ether, methoxy, hydroxy, and bromide functionalities. These functionalized aldehydes were utilized for 3D COF synthesis with tetrakis(4-aminophenyl)methane (TAPM) and the crystallinity of the product frameworks were characterized by powder X-ray diffraction. A systematic investigation of reaction conditions was conducted to

improve framework crystallinity. Additionally, the tert-butyldimethylsilyl (TBDMS) group was identified as the most promising for protecting hydroxy groups. The protection reaction using TBDMS chloride proceeds readily to 90%+ completion, and the TBDMS protection group can be removed using fluorinated compounds such as tetra-n-butylammonium fluoride (TBAF) at ambient temperature instead of the acidic conditions required to remove many other protection groups[26]. The protection of the hydroxy-functionalized aldehyde monomer was explored.

4.3 Experimental

4.3.1 General Experimental Procedure

All chemicals and reagents, unless specified, were purchased from commercial sources, including Fisher Scientific, Sigma-Aldrich, Alfa Aesar, and Oakwood Chemicals, and used as received without any further purification. ^{1}H NMR spectra were recorded on a Varian Inova 500 instrument (500 MHz). ^{13}C NMR spectra were recorded on a Varian MR400 instrument (400 MHz). Chemical shifts were measured in δ (ppm) relative to residual solvent signals as internal standards ($CDCl_3$: 7.24 for ^{1}H, 77.23 for ^{13}C; d^6-DMSO: 2.49 for ^{1}H). Powder X-ray Diffraction (PXRD) spectra were collected using a Rigaku 600 Miniflex XRD instrument and a 5 mm zero background sample holder.

4.3.2 Monomer Synthesis

4.3.2.1 Truncated Aldehyde

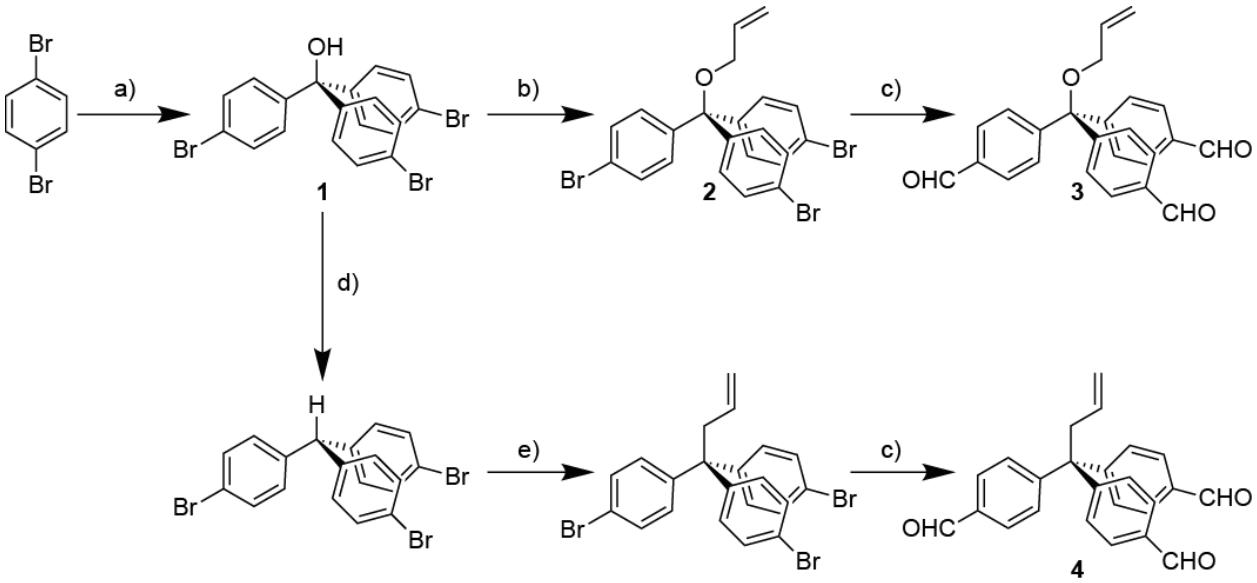

Scheme 4.1. 4,4',4''-((allyloxy)methanetriyl)tribenzaldehyde (2) and 4,4',4''-(but-3-ene-1,1,1-triyl)tribenzaldehyde (3). Reagents and conditions: a) n-BuLi/THF, $(EtO)_2CO$; b) NaH/Toluene, allyl bromide; c) n-BuLi/THF, DMF, -78°C; d) HCO_2H, 100°C; e) NAHDMS/THF, allyl bromide.

Tris(4-bromophenyl)methanol (1). 1,4-dibromobenzene (13.05 g, 55.3 mmol) was dissolved in anhydrous tetrahydrofuran (200 ml) in an oven-dried 500 ml 3-neck round bottom flask, which was then purged with N_2 equipped with a drying tube to remove air and moisture. The solution was cooled to -78°C, and n-butyllithium (30 ml, 2.5 M in hexanes, 75 mmol) was added dropwise. The solution was stirred at -78°C for 3 h. Meanwhile, diethyl carbonate (1.5 ml, 12.4 mmol) was sealed in a separate 50 ml round bottom flask and diluted with 4.5 ml of tetrahydrofuran. The flask was purged with N_2 to remove air and moisture, cooled to -78°C, and the mixture was added dropwise to the solution in the larger flask. The reaction mixture was warmed to room temperature, stirred for 6 h, and quenched with sat. ammonium chloride solution (75 ml). The mixture was extracted with ethyl acetate, washed with brine solution, dried over magnesium sulfate, and then

dried *in vacuo*. The product was isolated by column chromatography in a 1:3 dichloromethane/hexanes solvent system.

Characterization data: ^{1}H NMR ($CDCl_3$, δ ppm): 7.47 (d, 6H, Ar), 7.15 (d, 6H, Ar), 2.69 (s, 1H, -OH).

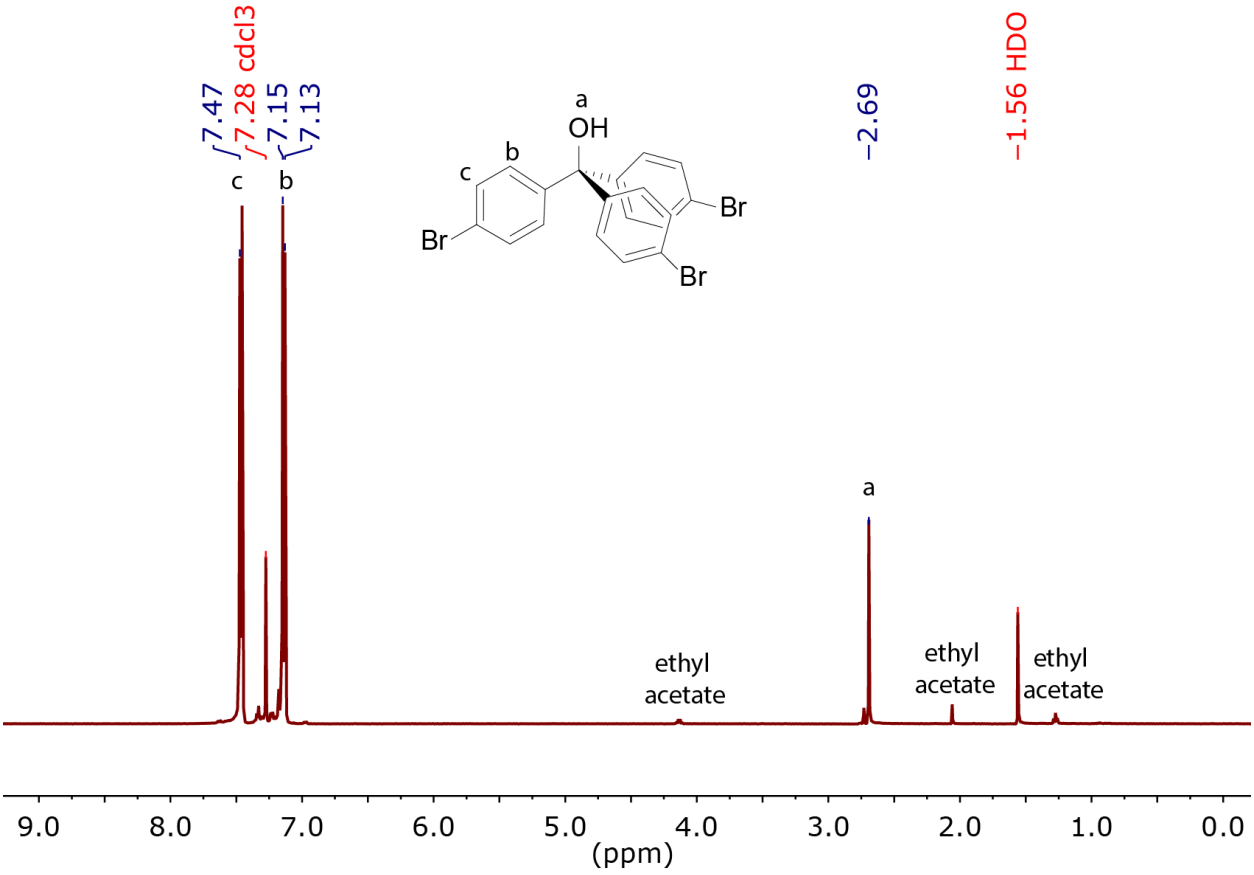

Figure 4.2. ^{1}H NMR spectrum of tris(4-bromophenyl)methanol.

4,4',4''-((allyloxy)methanetriyl)tris(bromobenzene) (2). Compound **1** (0.5 g, 1.0 mmol) was mixed with sodium hydride (0.24 g, 10.0 mmol), allyl bromide (1.0 ml, 11.6 mmol) and toluene (200 ml) in a 500 ml round bottom flask equipped with a magnetic stir bar. The reaction mixture was heated at 115°C for 48 h, during which time toluene and ally bromide were periodically

replenished. The solids were filtered out, and the filtrate was dried *in vacuo* to remove allyl bromide and solvent. The crude product was isolated by column chromatography (19:1 hexanes to ethyl acetate) to obtain compound **2**.

Characterization data: ^{1}H NMR (DMSO-d6, δ ppm): 7.57 (d, 6H, Ar), 7.31 (d, 6H, Ar), 5.91 (tt, 1H, -OCH$_2$-C*H*=CH$_2$), 5.41 (dd, 1H, -OCH$_2$-CH=C*H*$_2$), 5.37 (dd, 1H, -OCH$_2$-CH=C*H*$_2$), 3.50 (d, 2H, OC*H*$_2$-CH=CH$_2$).

`

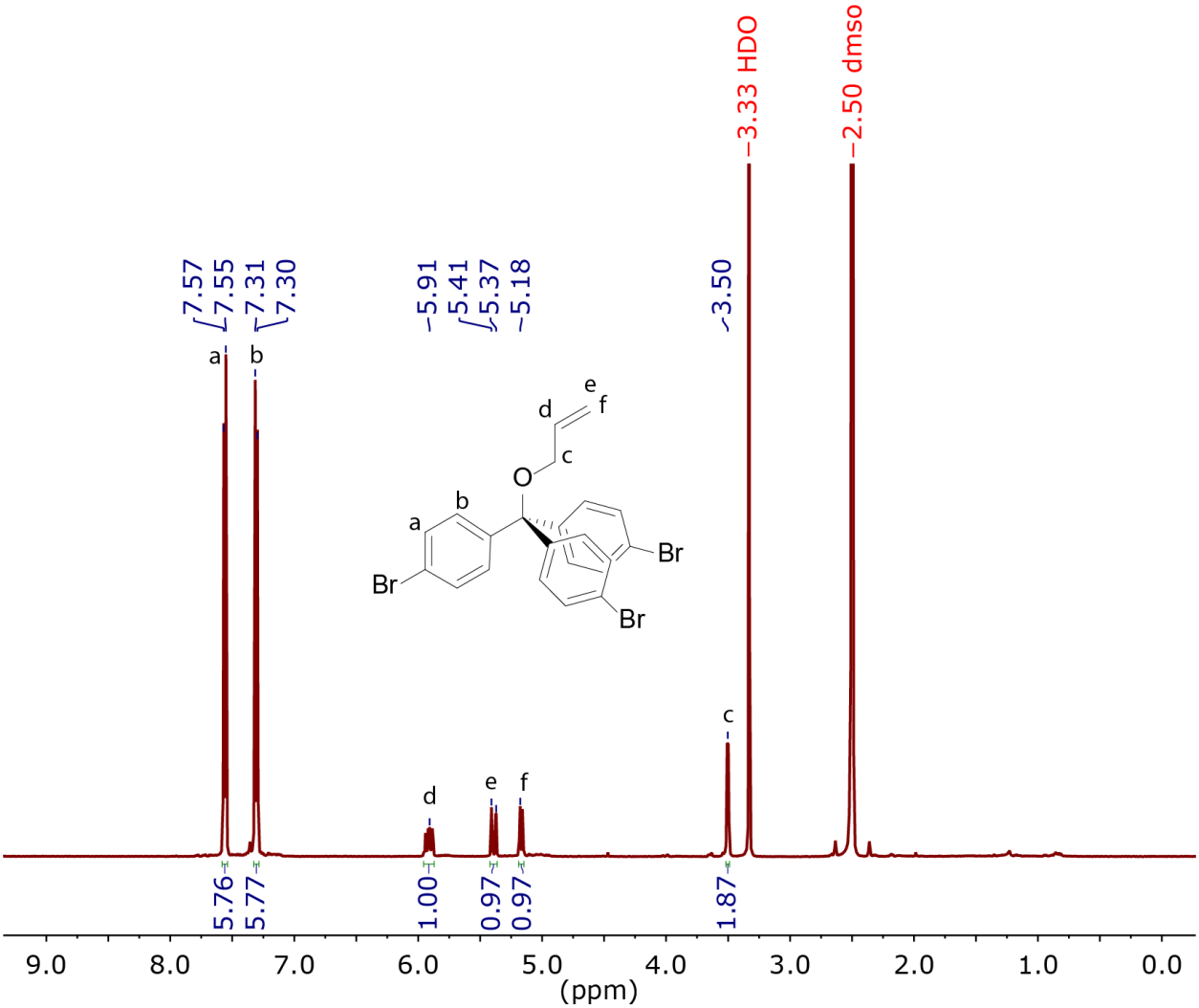

Figure 4.3. ^{1}H NMR spectrum of 4,4',4''-((allyloxy)methanetriyl)tris(bromobenzene).

4,4',4''-((allyloxy)methanetriyl)tribenzaldehyde (3). Compound **2** (133 mg, 0.25 mmol) was added to an oven-dried two-neck 100 ml round bottom flask equipped with magnetic stir bar and sealed. The flask was purged with an argon balloon equipped with a drying tube to remove air and moisture. Anhydrous tetrahydrofuran (10 ml) was added by syringe. The solution was cooled to -78°C, and n-butyllithium (0.5 ml, 2.5 M in hexanes, 1.25 mmol) was added dropwise using a syringe pump. The solution was stirred at -78°C for 1 h, and anhydrous dimethylformamide (0.9 ml, 11.6 mmol) was added by syringe. The reaction was warmed to room temperature, stirred overnight, and quenched with 1M aqueous hydrochloric acid solution (100 ml). The mixture was extracted with ethyl acetate, washed with brine solution, dried over magnesium sulfate, and then dried *in vacuo*.

Characterization data: ^{1}H NMR (DMSO-d6, δ ppm): 9.55 (d, 3H, -CHO), 7.55 (m, 6H, Ar), 7.36 (m, 6H, Ar), 5.91 (tt, 1H, -OCH_2-C*H*=CH_2), 5.41 (dd, 1H, -OCH_2-CH=C*H*$_2$), 5.38 (dd, 1H, -OCH_2-CH=C*H*$_2$), 3.51 (d, 2H, OC*H*$_2$-CH=CH_2).

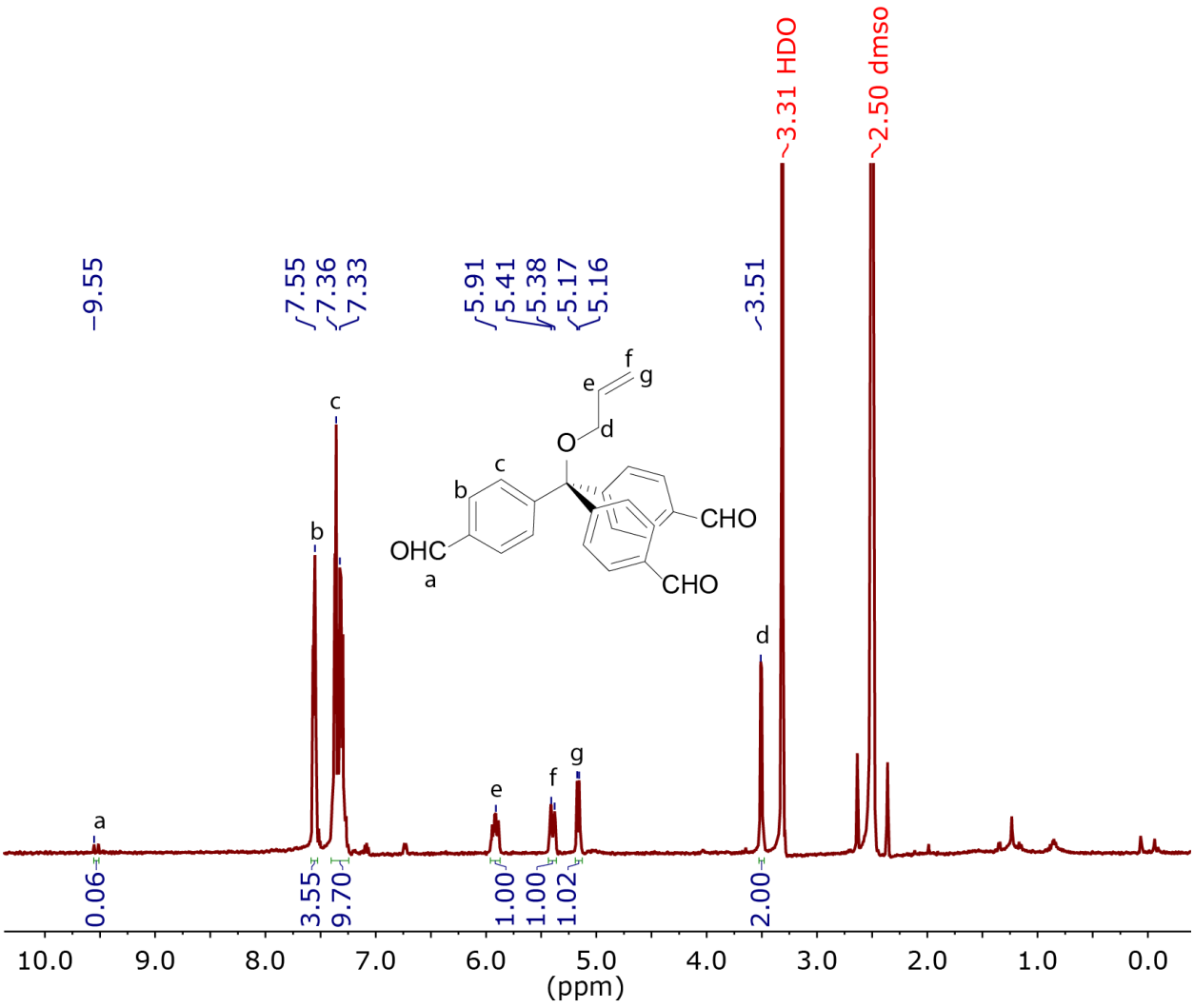

Figure 4.4. ^{1}H NMR spectrum of 4,4',4''-((allyloxy)methanetriyl)tribenzaldehyde.

4,4',4''-(but-3-ene-1,1,1-triyl)tribenzaldehyde (4). Unfortunately, due to the low yield and difficulty of attaining complete conversion and extreme complexity of the column chromatography purifications in the synthesis of **1** and its subsequent conversion into **2** and **3**, the synthesis of **4**, which follows a similar reaction pathway as that of compound **3**, was not further explored.

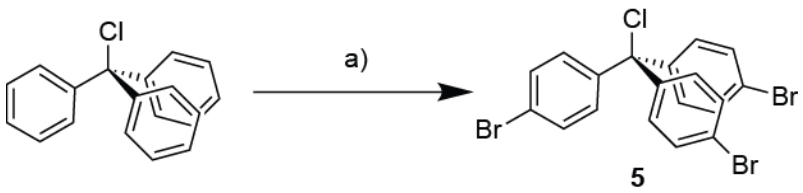

Scheme 4.2. Synthesis of 4,4',4''-(chloromethanetriyl)tris(bromobenzene) (5). Reagents and conditions: a) Br_2, EtOH, -78°C.

4,4',4''-(chloromethanetriyl)tris(bromobenzene) (5). Chlorotriphenylmethane (5.0 g, 17.9 mmol) was added to an oven-dried three-neck 500 ml round bottom flask equipped with magnetic stir bar and one neck connected to a sodium hydroxide quenching solution. Neat bromine (10 ml, 195 mmol) was added dropwise while stirred, and the mixture was stirred for 20 min. The mixture was cooled to -78°C, diluted with ethanol (100 ml), warmed to room temperature while stirring overnight, and quenched with sodium metabisulfite solution. The precipitates were filtered, dissolved in dichloromethane, washed with water, and dried over magnesium sulfate. A variety of solvent systems (3:1, 4:1, and 9:1 hexanes/ethyl acetate and 3:1 hexanes/dichloromethane) were evaluated for product isolation by column chromatography, but despite multiple attempts compound **5** could not be isolated.

4.3.2.2 Functionalized Dialdehyde Monomers

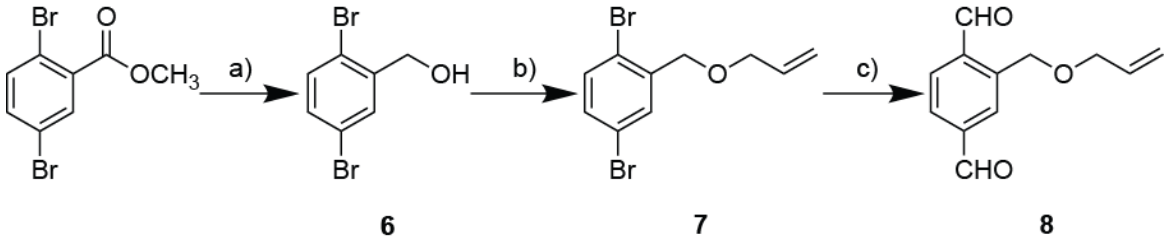

Scheme 4.3. Synthesis of 2-((allyloxy)methyl)terephthalaldehyde (8). Reagents and conditions: a) DIBAL, anhydrous DCM; b) NaH, toluene, allyl bromide; c) anhydrous THF, n-BuLi, anhydrous DMF.

(2,5-dibromophenyl)methanol (6). Methyl 2,5-dibromobenzoate (4.4 g, 15.0 mmol) was added to an oven-dried 250 ml round bottom flask equipped with a magnetic stir bar and sealed. Anhydrous dichloromethane (30 ml) was added by syringe, and the solution was cooled to 0°C. Diisobutylaluminium hydride (DIBAL, 30 ml, 0.17 mol) was added slowly *via* a syringe pump. The mixture was gradually warmed to room temperature and stirred overnight. The solution was then cooled to 0°C and quenched by slowly adding 15% aqueous citric acid solution. The product was extracted with dichloromethane and brine to induce separation, washed with brine, dried over magnesium sulfate and filtered. The filtrate was dried *in vacuo* to afford compound **6** as an analytically pure solid.

Characterization data: ^{1}H NMR ($CDCl_3$, δ ppm): 7.67 (d, 1H, Ar), 7.41 (d, 1H, Ar), 7.31 (dd, 1H, Ar), 4.74 (d, 2H, -CH_2-OH), 2.05 (t, 1H, -OH).

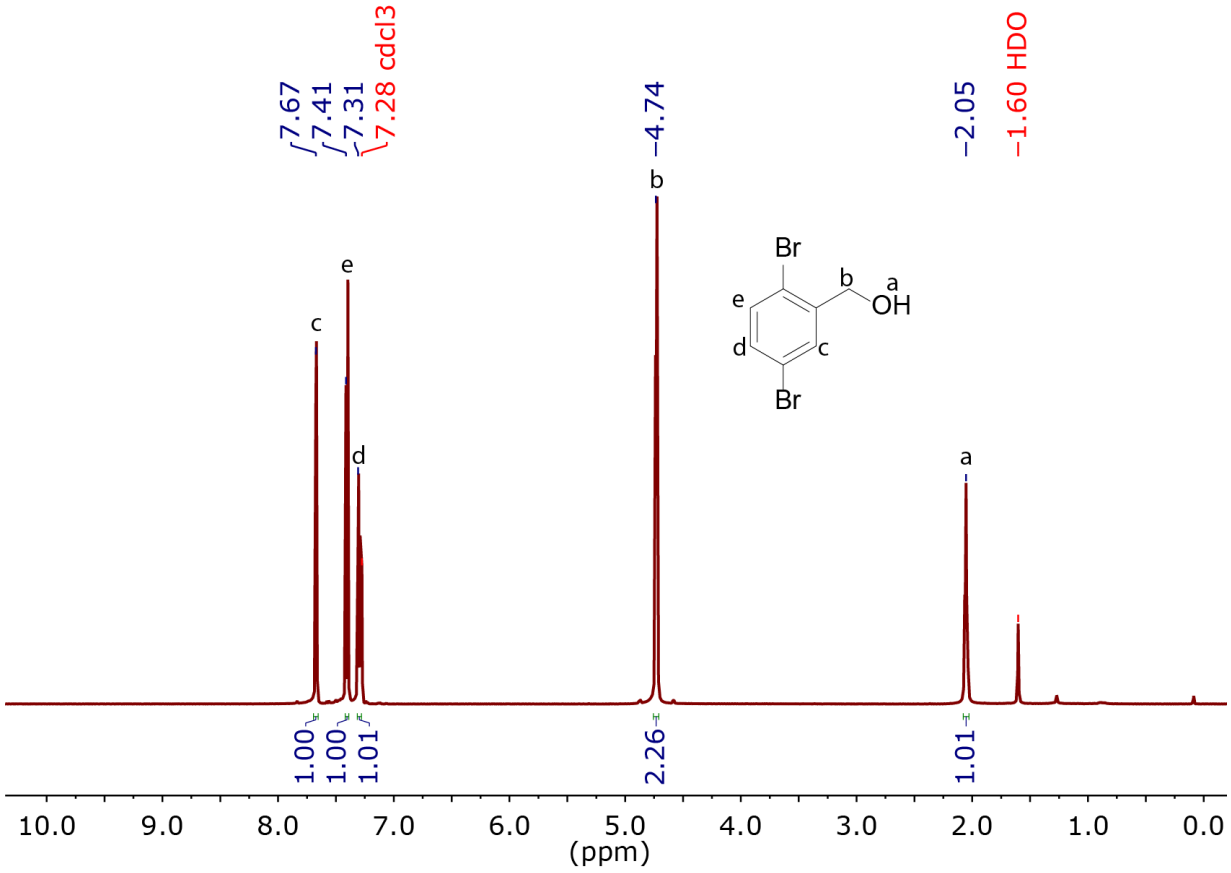

Figure 4.5. ^{1}H NMR spectrum of (2,5-dibromophenyl)methanol.

2-((allyloxy)methyl)-1,4-dibromobenzene (7). Compound **4** (1.0 g, 3.76 mmol), sodium hydride (0.9 g, 37.5 mmol), allyl bromide (3.5 ml, 40.2 mmol), and toluene (150 ml) were mixed together in a 250 ml round bottom flask equipped with a magnetic stir bar. The reaction mixture was heated to 65°C and stirred overnight. The mixture was filtered, and the filtrate was dried *in vacuo* to afford compound **7**.

Characterization data: ^{1}H NMR ($CDCl_3$, δ ppm): 7.67 (d, 1H, Ar), 7.38 (d, 1H, Ar), 7.25 (dd, 1H, Ar), 6.00 (tt, 1H, -OCH_2-C*H*=CH_2), 5.39 (dd, 1H, -OCH_2-CH=C*H*$_2$), 5.28 (dd, 1H, -OCH_2-CH=C*H*$_2$), 4.53 (s, 2H, -C*H*$_2$-O-), 4.14 (d, 2H, -O-C*H*$_2$-CH=CH_2).

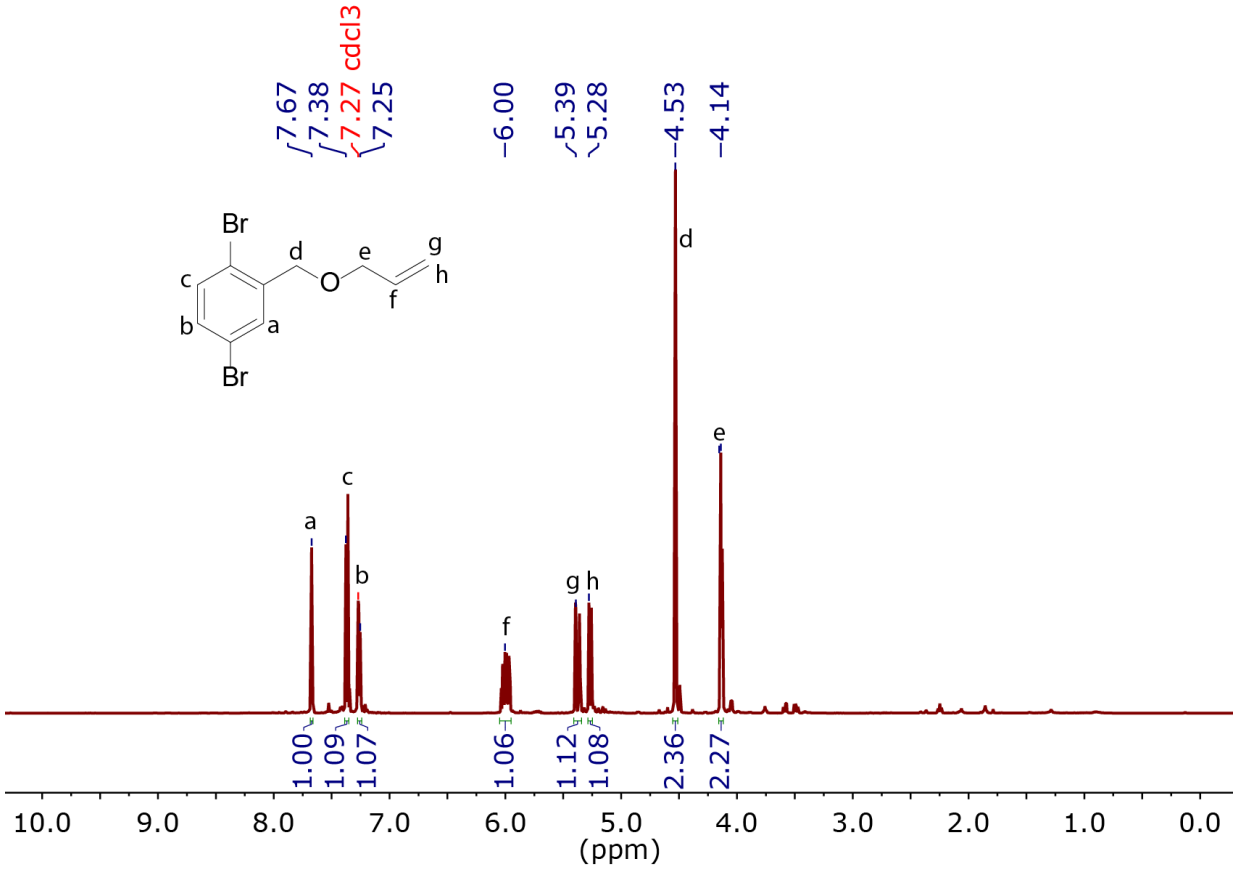

Figure 4.6. ^{1}H NMR spectrum of 2-((allyloxy)methyl)-1,4-dibromobenzene.

2-((allyloxy)methyl)terephalaldehyde (8). Compound **5** (0.3 g, 0.98 mmol) was added to an oven-dried two-neck 500 ml round bottom flask equipped with magnetic stir bar and sealed. The flask was purged with an argon balloon equipped with a drying tube to remove air and moisture. Anhydrous tetrahydrofuran (30 ml) was added by syringe. The solution was cooled to -78°C, and n-butyllithium (2 ml, 2.5 M in hexanes, 5 mmol) was added dropwise using a syringe pump. The solution was stirred at -78°C for 30 min, and anhydrous dimethylformamide (1 ml, 12.9 mmol) was added by syringe. The reaction was warmed to room temperature, stirred overnight, and quenched with 1 M aqueous hydrochloric acid solution (100 ml). The mixture was extracted with ethyl acetate, washed with brine solution, dried over magnesium sulfate, and dried *in vacuo*.

Despite many attempts, the reaction consistently yielded multiple products which would not be separated to obtain compound **8**.

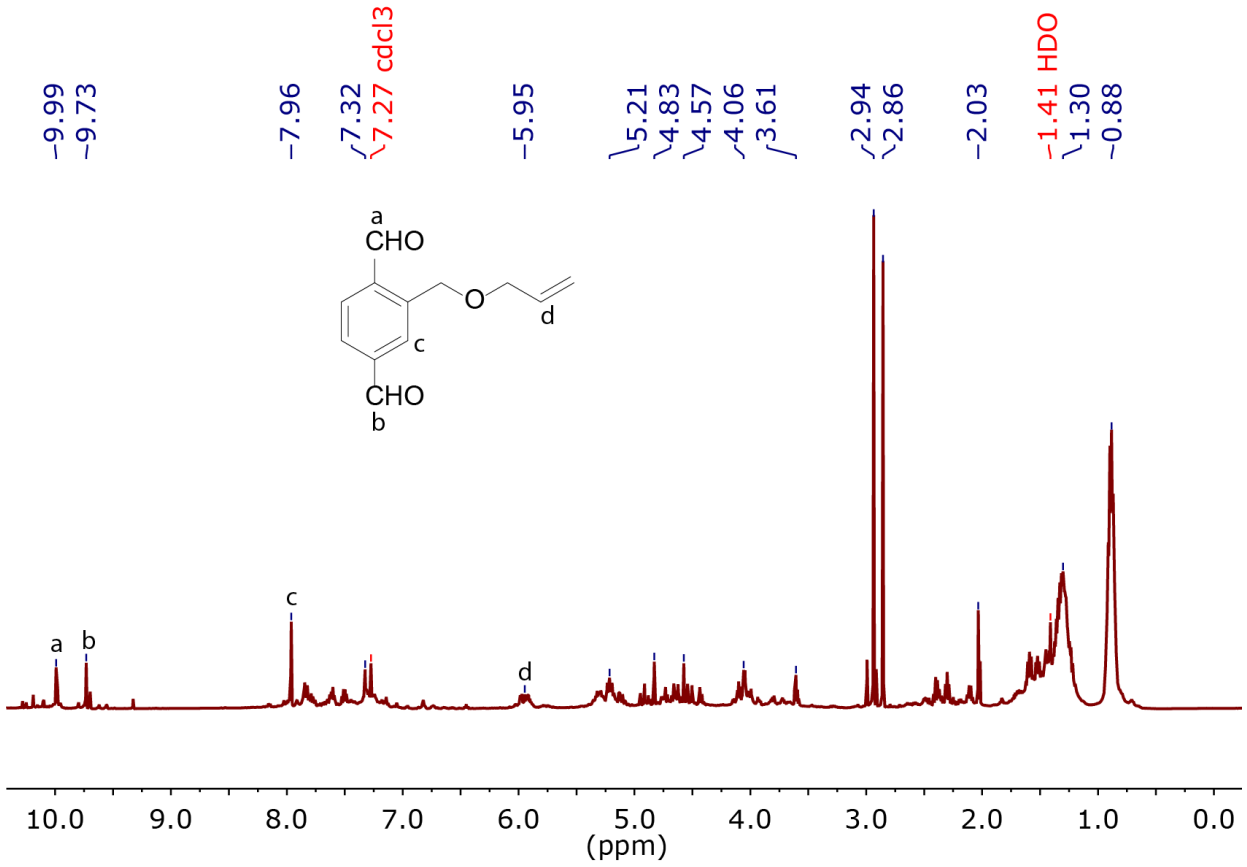

Figure 4.7. ^{1}H NMR spectrum of 2-((allyloxy)methyl)terephalaldehyde.

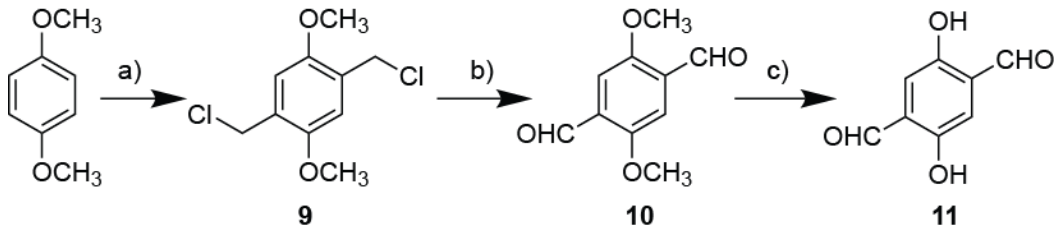

Scheme 4.4. Synthesis of 2,5-dihydroxyterephalaldehyde (11). Reagents and conditions: a) HCl (aq), 1,4-dioxane, CH_2O, HCl (g) b); $(CH_2)_6N_4$/anhydrous $CHCl_3$, H_2O/HCl (aq) c) AcOH, HBr.

1,4-bis(chloromethyl)-2,5-dimethoxybenzene (9). The synthesis procedures for **9** were adapted from a published approach[7]. 1,4-dimethoxybenzene (69.35 g, 0.50 mol), 1,4-dioxane (400 ml), and aqueous hydrochloric acid solution (37%, 65 ml) were mixed together in a 2L three-neck round bottom flask. Three equal portions of aqueous formaldehyde solution (37%; 100.5 ml, 1.35 mol) were added at intervals of 30 min with stirring at 0°C. During this time, aqueous hydrochloric acid solution was added dropwise to a separate 2L two-neck round bottom flask containing anhydrous calcium chloride powder to generate a consistent stream of hydrochloric acid gas, which was continuously bubbled into the reaction mixture in the three-neck flask and out into a quenching aqueous sodium bicarbonate solution. After the formaldehyde portions have been added, the reaction was stirred for 1 h at room temperature, and more aqueous hydrochloric acid solution was added (37%, 195 ml). The resulting solution was cooled to ~5°C overnight, and the white precipitate was collected in a glass frit and washed with chilled di-ionized water, recrystallized in acetone, and dried *in vacuo* to afford **9** as an analytically pure white solid.

Characterization data: ^{1}H NMR ($CDCl_3$, δ ppm): 6.94 (s, 2H, Ar), 4.65 (s, 4H, -CH_2Cl), 3.88 (s, 6H, -OCH_3).

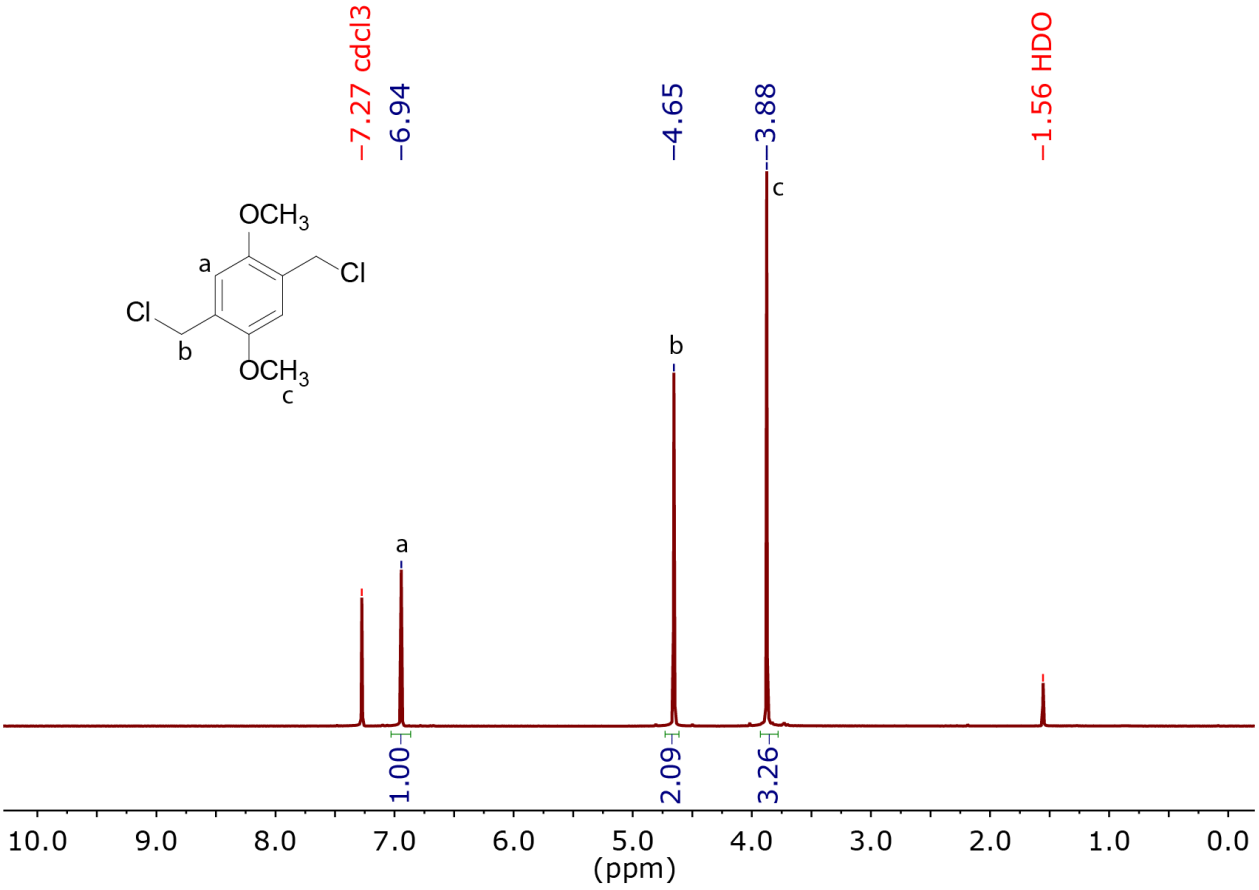

Figure 4.8. ^{1}H NMR spectrum of 1,4-bis(chloromethyl)-2,5-dimethoxybenzene.

2,5-dimethoxyterephthalaldehyde (10). The synthesis procedures for **10** were adapted from a published approach[7]. Compound **9** (10.00 g, 0.04 mol) and hexamethylenetetramine (11.2 g, 0.08 mol) were dissolved in anhydrous chloroform (150 ml) in an oven-dried and septum-sealed 500 ml two-neck round bottom flask equipped with magnetic stirrer. The flask was purged with an argon balloon equipped with drying tube to remove air and moisture. The reaction was heated to reflux for 3 h and cooled to 5°C. The cream-colored solids were filtered with a glass frit, re-dissolved in di-ionized water (130 ml) and heated to reflux for 2 h. After cooling to room temperature, aqueous hydrochloric acid solution (37%, 5 ml) was added, inducing the formation of yellow precipitates, which were collected on a glass frit. The aqueous filtrate was extracted

with chloroform, dried over magnesium sulfate, and evaporated to dryness *in vacuo* to yield a second crop of crude product. The crude product was purified *via* flash column chromatography (2:1 dichloromethane/ethyl acetate) and recrystallized in 1:1 dichloromethane/hexanes to obtain **10** as an analytically pure yellow needle-shaped crystals.

Characterization data: ^{1}H NMR ($CDCl_3$, δ ppm): 10.52 (s, 2H, -CHO), 7.47 (s, 2H, Ar), 3.96 (s, 6H, -OCH_3).

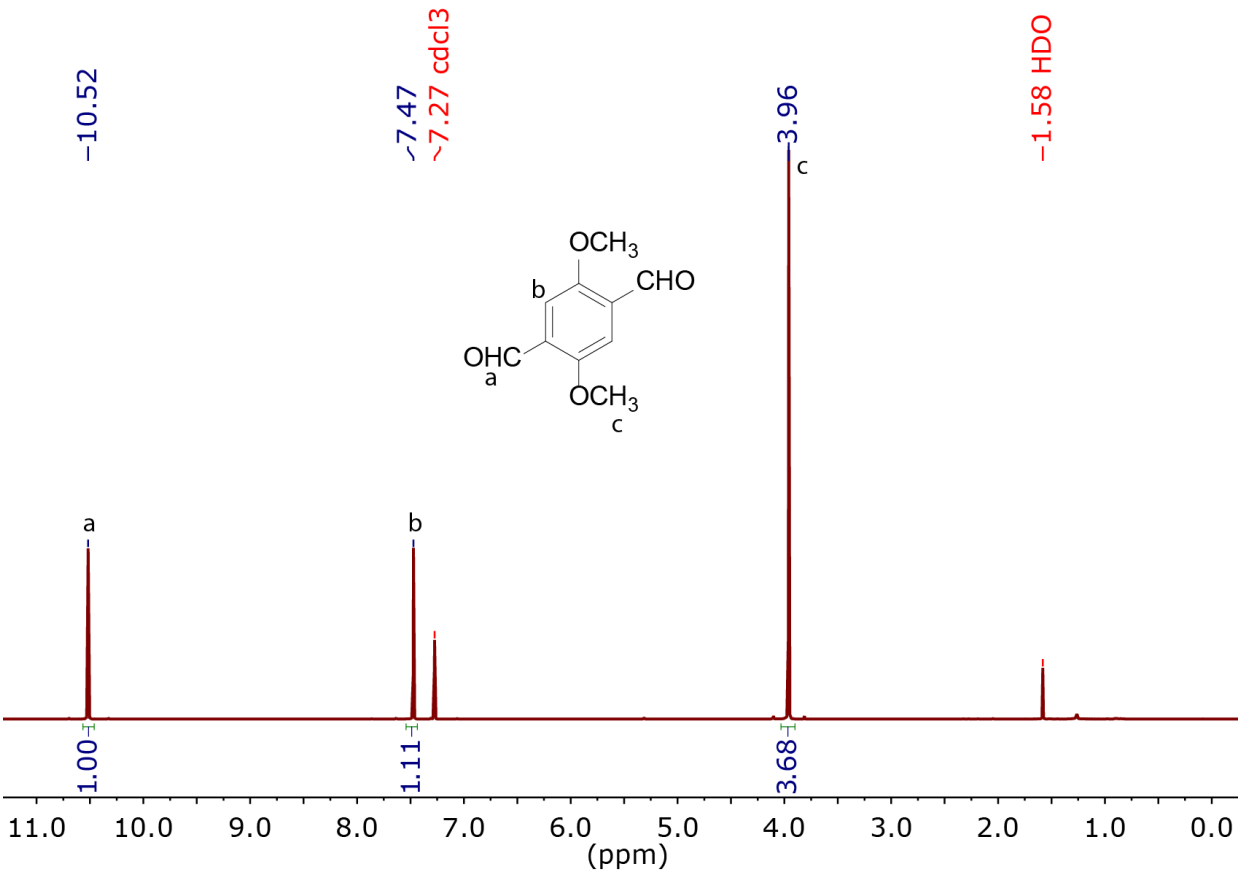

Figure 4.9. ^{1}H NMR spectrum of 2,5-dimethoxyterephthalaldehyde.

2,5-dihydroxyterephthalaldehyde (11). The synthesis procedures for **11** were adapted from a published approach[7]. Compound **10** (3.71 g, 0.02 mol), glacial acetic acid (99.5%, 190 ml), and aqueous hydrobromic acid (48%, 160 ml) were mixed together and heated to reflux for 14 h. Some

black particles formed during the reflux and were filtered out and washed with chloroform. The filtrate was extracted with chloroform and water. The aqueous layer was extracted repeatedly until the organic layer became clear and colorless. The organic layers were combined, evaporated to dryness under vacuum, and dried *in vacuo* to afford **11** as an analytically pure orange solid.

Characterization data: ^{1}H NMR ($CDCl_3$, δ ppm): 10.31 (s, 2H, -CHO), 7.88 (s, 2H, -OH), 7.22 (s, 2H, Ar).

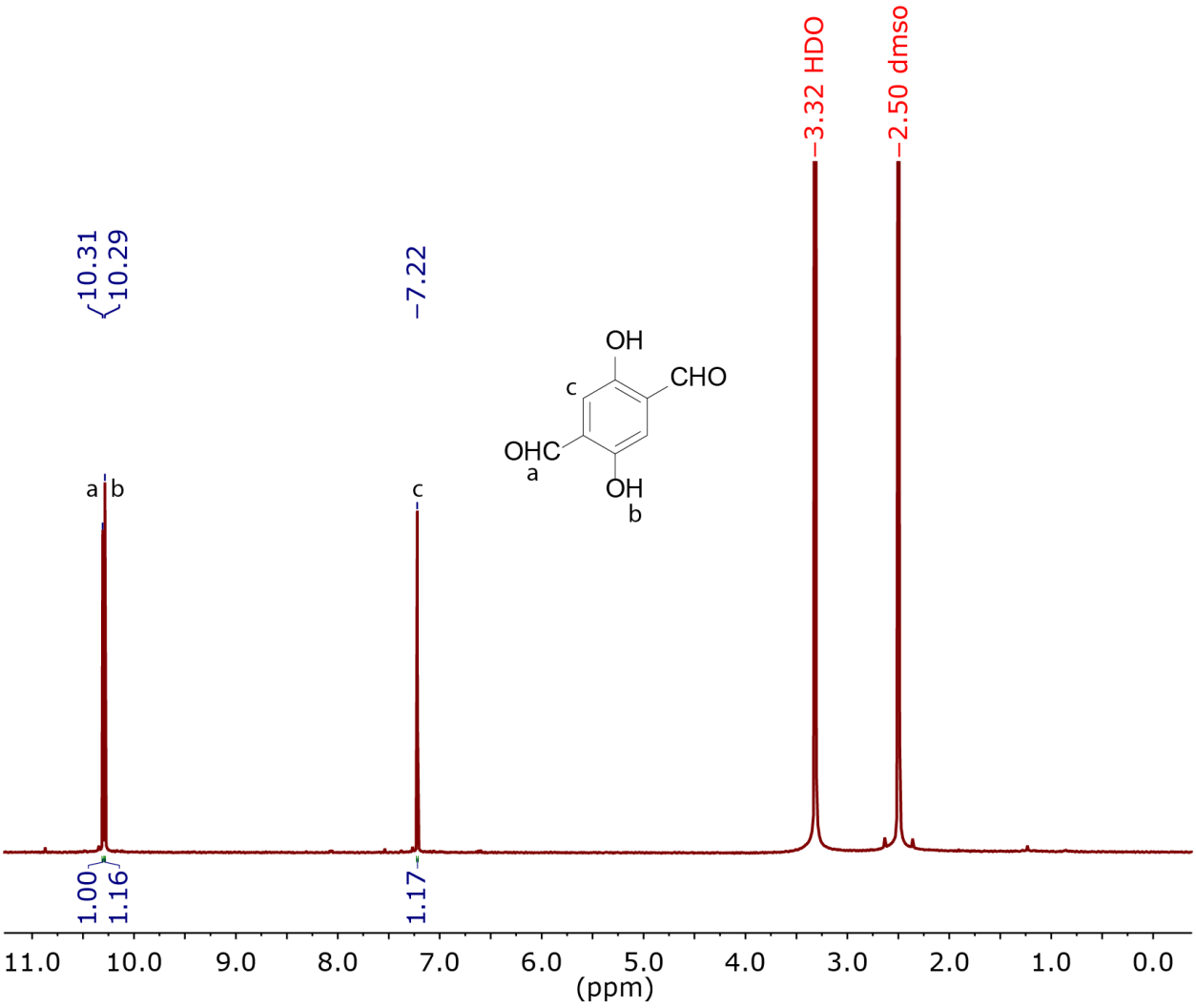

Figure 4.10. ^{1}H NMR spectrum of 2,5-dihydroxyterephthalaldehyde.

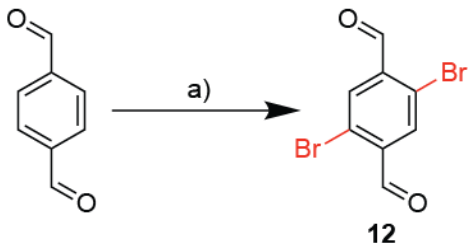

Scheme 4.5. Synthesis of 2,5-dibromoterephthalaldehyde (12). Reagents and conditions: a) NBS, H_2SO_4, 60°C, 3 h.

2,5-dibromoterephthalaldehyde (12). The synthesis of compound **12** was conducted following established procedure[8]. N-bromosuccinimide was purified by recrystallization in water prior to use in this reaction. Terephthalaldehyde (4 g, 30.0 mmol) was dissolved in concentrated sulfuric acid (40 ml) and heated to 60°C. N-bromosuccinimide (11.5 g, 65.0 mmol) was added portionwise over 15 minutes. The reaction mixture was heated at 60°C for 3 h. The solution was poured onto ice and the white precipitate was filtered off, dissolved in dichloromethane, and extracted with saturated sodium bicarbonate aqueous solution and brine. The organic layer was dried over sodium sulfate and the solvent was removed at reduced pressure. The crude product was recrystallized in ethyl acetate to obtain **12** as cream-colored crystals.

Characterization data: ^{1}H NMR ($CDCl_3$, δ ppm): 10.36 (s, 2H, -CHO), 8.17 (s, 2H, Ar).

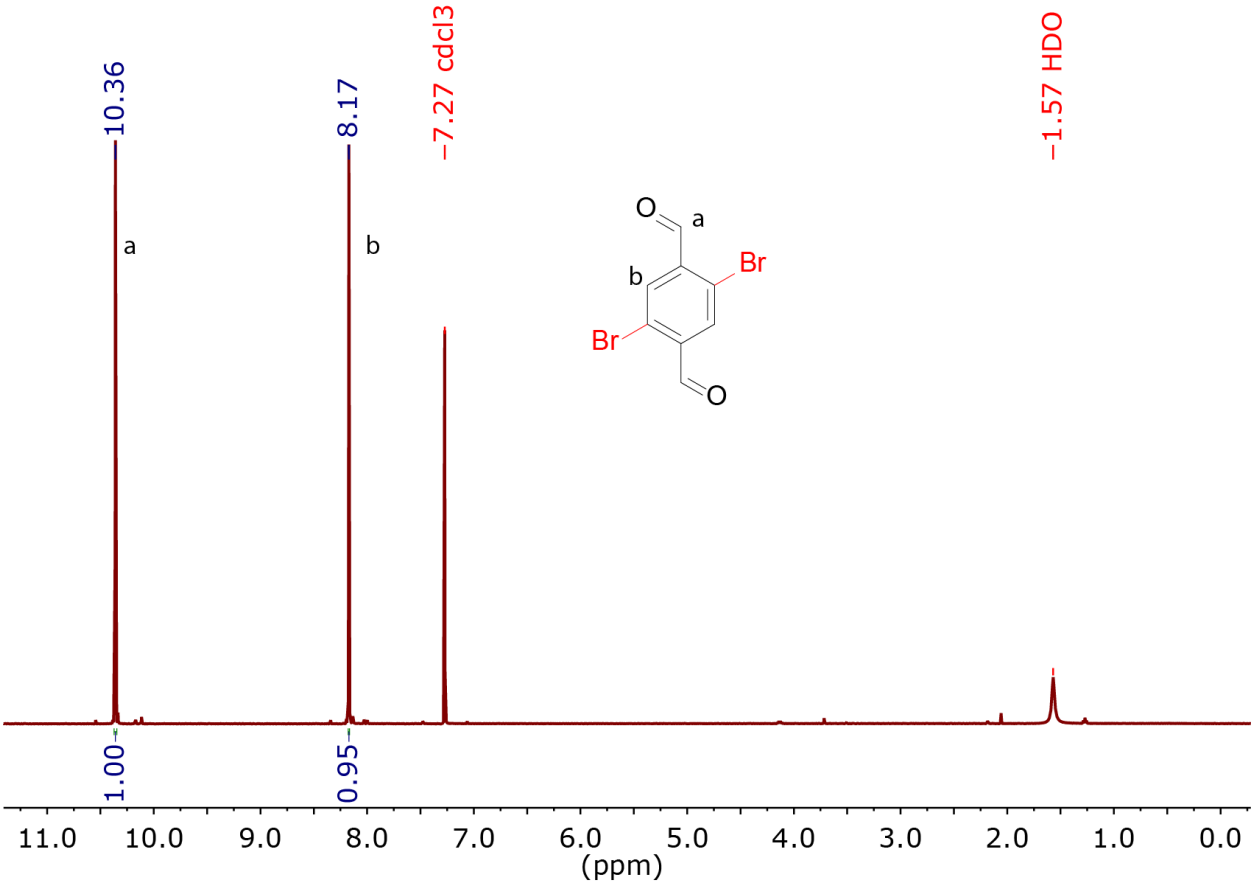

Figure 4.11. ^{1}H NMR spectrum of 2,5-dibromoterephthalaldehyde.

4.3.2.3 TBDMS Protection

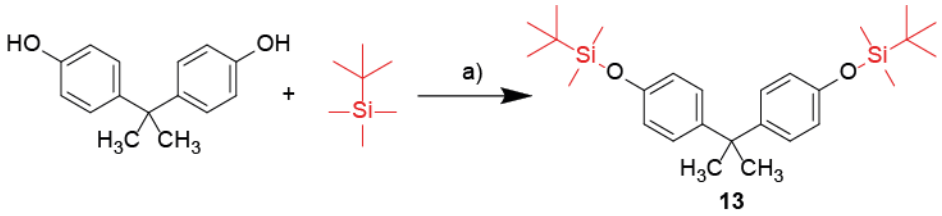

Scheme 4.6. Synthesis of ((propane-2,2-diylbis(4,1-phenylene))bis(oxy))bis(tert-butyldimethylsilane) (13) as model TBDMS protection reaction. Reagents and conditions: a) imidazole, DMF, 70°C, overnight.

((propane-2,2-diylbis(4,1-phenylene))bis(oxy))bis(tert-butyldimethylsilane) (13). 4,4'-(propane-2,2-diyl)diphenol (20 mg, 0.175 mmol), tert-butyldimethylsilyl chloride (31.7 mg, 0.210 mmol), imidazole (29.8 mg, 0.438 mmol), and dimethylformamide (10 ml) were mixed together and heated to 70°C overnight. The mixture was then diluted with a large amount of di-ionized water and extracted with 1:1 hexanes/ethyl acetate mixture. The organic layer was washed with brine solution, dried over magnesium sulfate, filtered, evaporated to dryness under reduced pressure, and dried *in vacuo* to afford compound **13**.

Characterization data: ^{1}H NMR ($CDCl_3$, δ ppm): 7.06 (d, 4H, Ar), 6.71 (d, 4H, Ar), 1.62 (s, 6H, --CH-(CH_3)$_2$), 0.98 (s, 18H, -Si(CH_2)$_2$-C(CH_3)$_3$), 0.19 (s, 12H, -Si(CH_2)$_2$-).

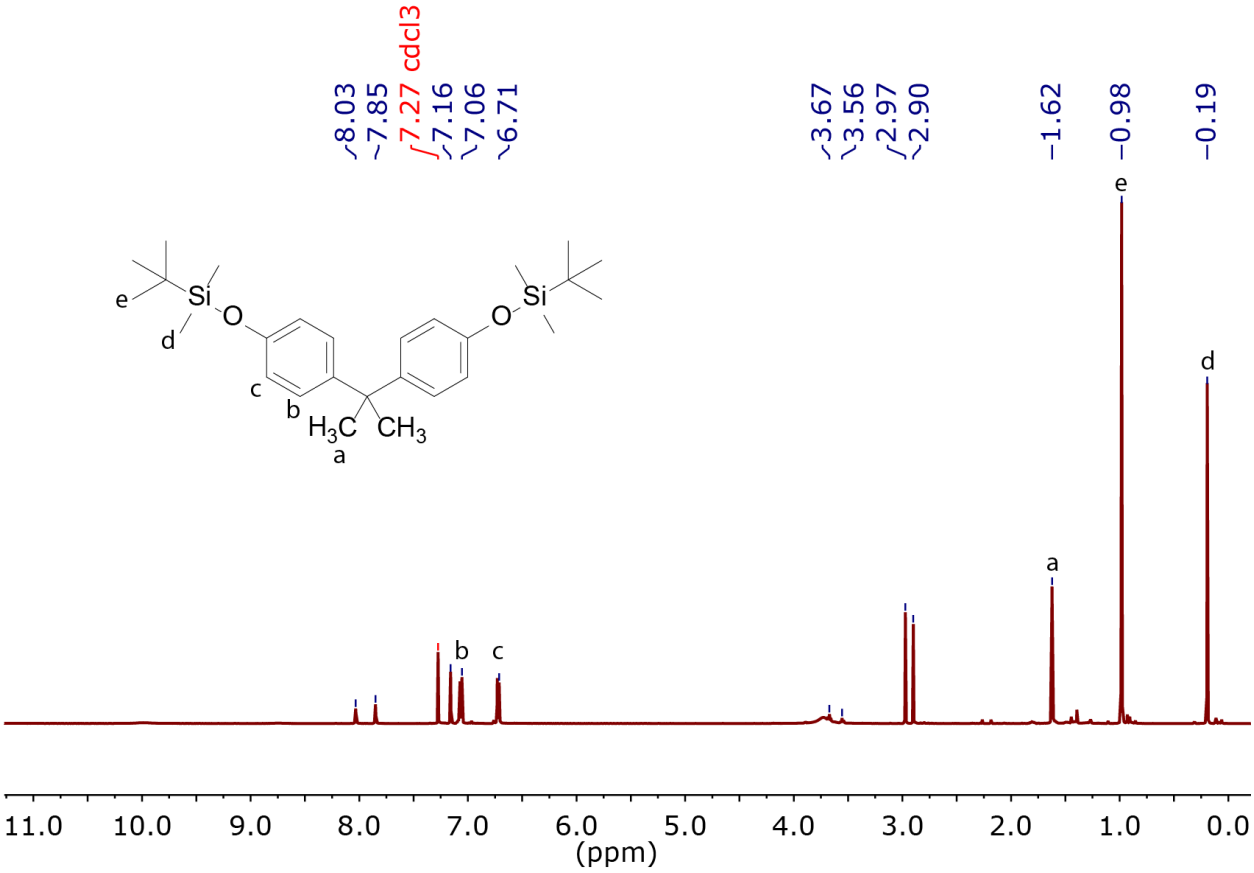

Figure 4.12. ^{1}H NMR of((propane-2,2-diylbis(4,1-phenylene))bis(oxy))bis(tert-butyldimethylsilane).

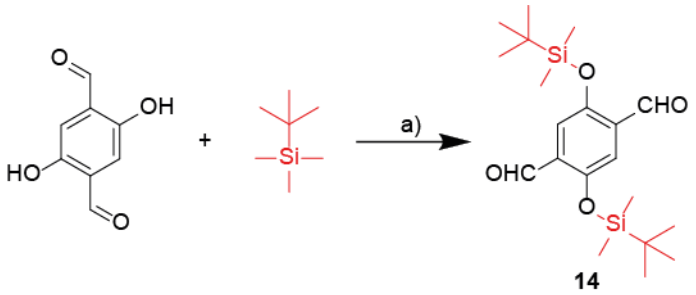

Scheme 4.7. Synthesis of 2,5-bis((tert-butyldimethylsilyl)oxy)terephthalaldehyde (14) through TBDMS protection. Reagents and conditions: a) imidazole, DMF, 100°C, overnight.

2,5-bis((tert-butyldimethylsilyl)oxy)terephthalaldehyde (14). 2,5-dihydroxyterephthal-aldehyde (50 mg, 0.301 mmol), tert-butyldimethylsilyl chloride (136.1 mg, 0.903 mmol),

imidazole (102.45 mg, 1.505 mmol), and dimethylformamide (25 ml) were mixed together and heated to 100°C overnight. The mixture was then diluted with large amount of de-ionized water and extracted with 1:1 hexanes/ethyl acetate mixture. The organic layer was washed with brine solution, dried over magnesium sulfate, filtered, evaporated to dryness under reduced pressure, and dried *in vacuo*.

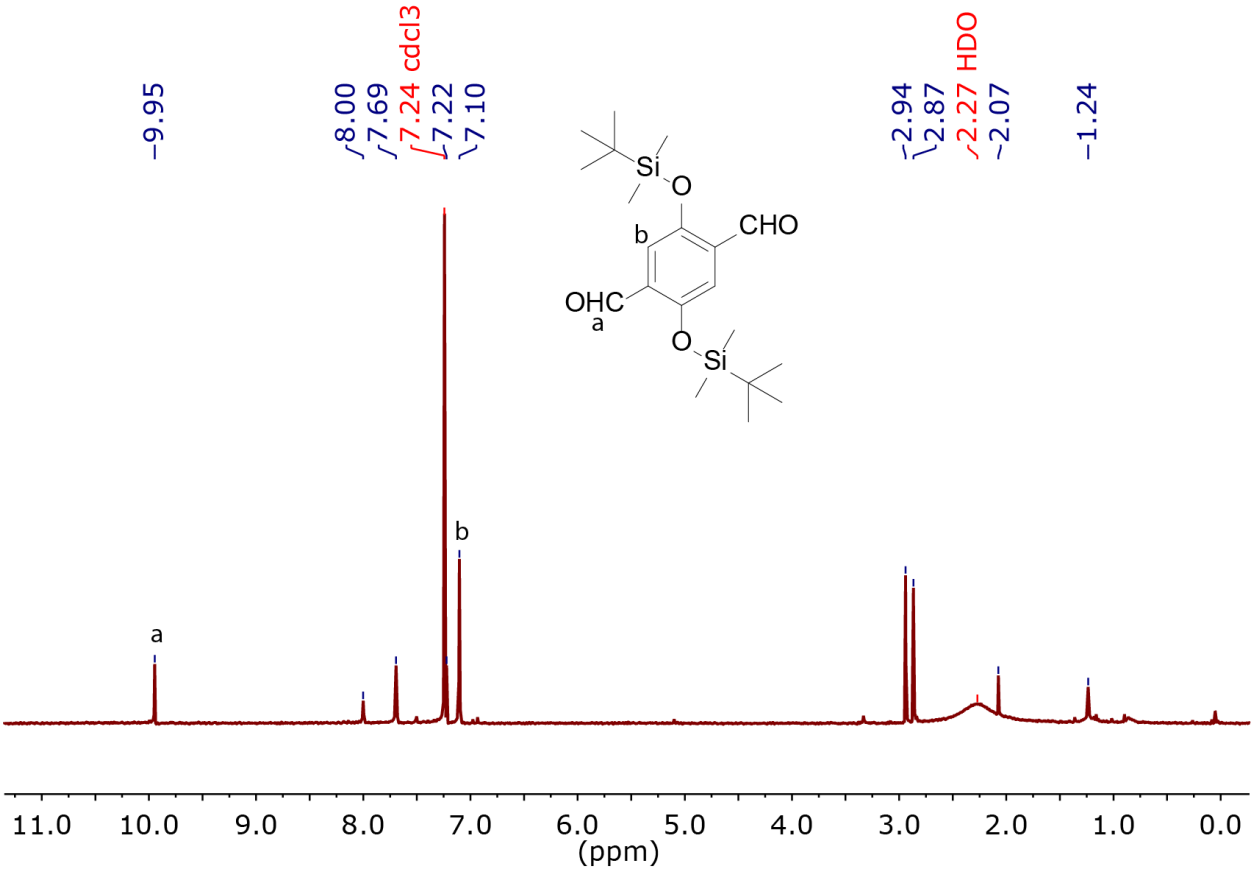

Figure 4.13. ^{1}H NMR of 2,5-bis((tert-butyldimethylsilyl)oxy)terephthalaldehyde.

4.3.3 Synthesis of Functionalized COFs

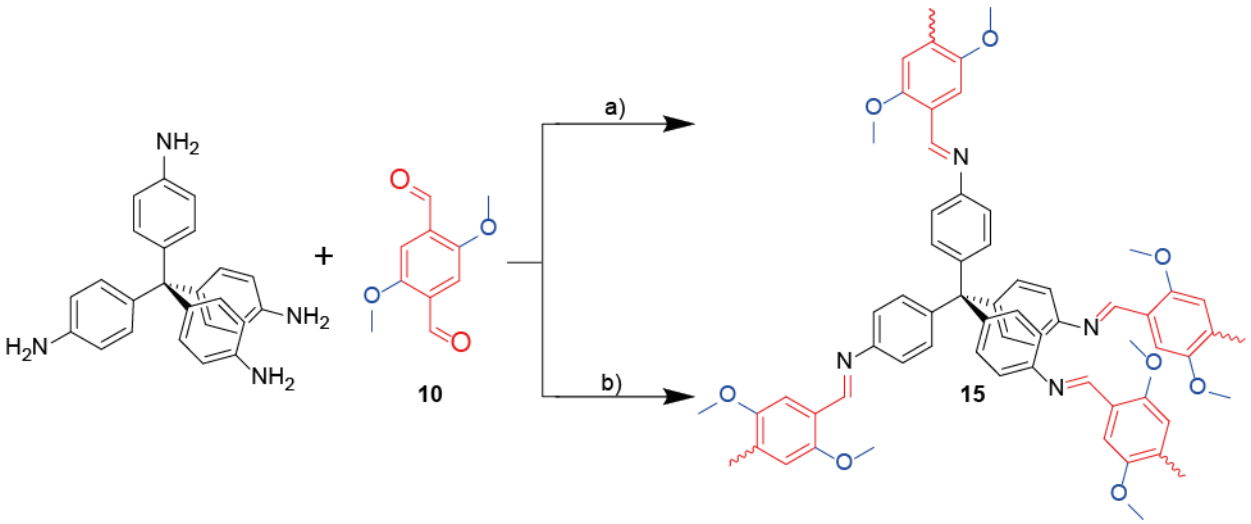

Scheme 4.8. Synthesis of dimethoxy-functionalized COF-300 (15). Reagents and conditions: a) 1,4-dioxane, AcOH (aq), 120°C, 72 h; b) 1,4-dioxane, $Sc(OTf)_3$, H_2O, 70°C, 72 h.

Solvothermal synthesis of dimethoxy-functionalized COF-300 (15). The synthesis procedure for compound **15** was adapted from the published approach for COF-300 refined in Chapters 2 and 3[9]. A 48 ml "glass bomb" heavy wall pressure vessel was charged with tetrakis(4-aminophenyl)methane (20 mg. 0.053 mmol), compound **10** (20.4 mg, 0.105 mmol), 1,4-dioxane (1 ml) and 3 M aqueous acetic acid solution (0.2 ml). The bomb reactor was sealed and heated to 120°C for 72 h. The solids were filtered, washed with 1,4-dioxane and tetrahydrofuran, and immersed in tetrahydrofuran for 24 h, during which the solvent was exchanged for fresh tetrahydrofuran several times. The solids were then isolated by filtration and dried *in vacuo* to afford **15** as an orange solid.

Scandium triflate catalyzed synthesis of dimethoxy-functionalized COF-300 (15). A 48 ml "glass bomb" heavy wall pressure vessel was charged with tetrakis(4-aminophenyl)methane (20

mg. 0.053 mmol), compound **10** (20.4 mg, 0.105 mmol), 1,4-dioxane (2.5 ml) and 42 µl of scandium triflate stock solution (0.2 M in acetonitrile, 0.084 mmol, 0.04 equiv. per amine). The reactor was capped, sealed, and heated to 50°C for 72 hours to yield a yellow powder, which was isolated by centrifugation and immersed and washed with tetrahydrofuran to remove residual solvent and guest. This was repeated several times until the solvent became colorless. The product was then washed with acetonitrile and water and lyophilized to give **15** as a yellow powder.

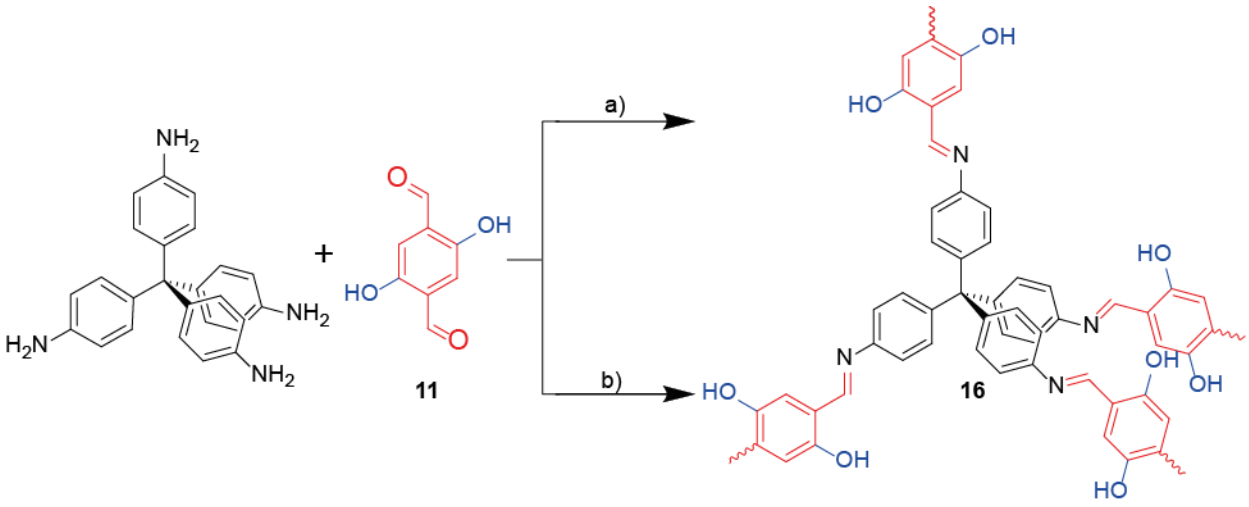

Scheme 4.9. Synthesis of dihydroxy-functionalized COF-300 (16). Reagents and conditions: a) 1,4-dioxane, AcOH (aq), 120°C, 72 h; b) 1,4-dioxane, $Sc(OTf)_3$, H_2O, 70°C, 72 h.

Solvothermal synthesis of dihydroxy-functionalized COF-300 (16). The synthesis procedure for compound **14** was adapted from the published approach for COF-300 refined in Chapters 2 and 3[9]. A 48 ml "glass bomb" heavy wall pressure vessel was charged with tetrakis(4-aminophenyl)methane (20 mg. 0.053 mmol), compound **11** (17.5 mg, 0.105 mmol), 1,4-dioxane (1 ml) and 3 M aqueous acetic acid solution (0.2 ml). The bomb reactor was sealed and heated to 120°C for 72 h. The solids were filtered, washed with 1,4-dioxane and tetrahydrofuran, and immersed in tetrahydrofuran for 24 h, during which the solvent was exchanged for fresh

tetrahydrofuran several times. The solids were then isolated by filtration and dried *in vacuo* to afford **16** as a yellow solid.

Scandium triflate catalyzed synthesis of dihydroxy-functionalized COF-300 (16). A 48 ml "glass bomb" heavy wall pressure vessel was charged with tetrakis(4-aminophenyl)methane (20 mg. 0.053 mmol), compound **11** (17.5 mg, 0.105 mmol), 1,4-dioxane (2.5 ml) and 42 µl of scandium triflate stock solution (0.2 M in acetonitrile, 0.084 mmol, 0.04 equiv. per amine). The reactor was capped, sealed, and heated to 50°C for 72 hours to yield a yellow powder, which was isolated by centrifugation and immersed and washed with tetrahydrofuran to remove residual solvent and guest. This was repeated several times until the solvent became colorless. The product was then washed with acetonitrile and water and lyophilized to give **16** as a yellow powder.

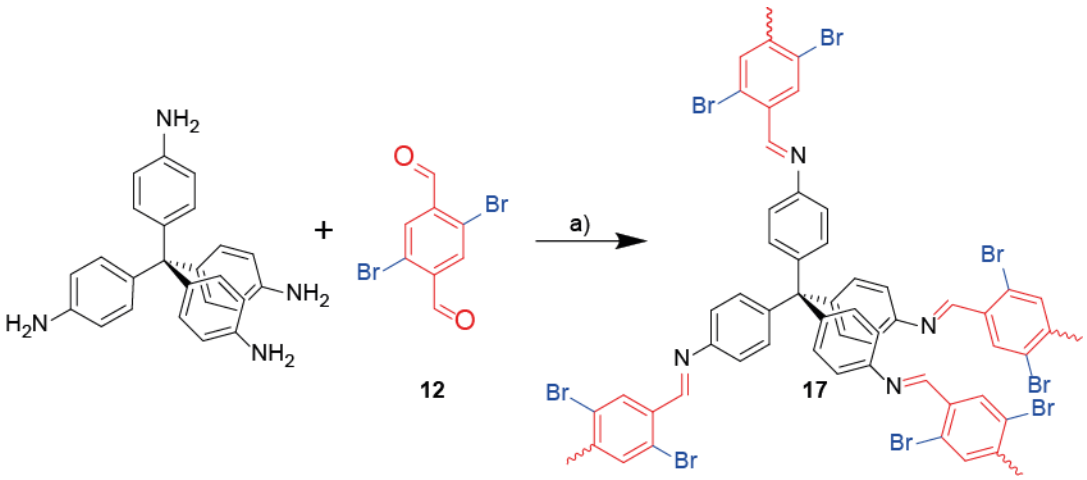

Scheme 4.10. Synthesis of dibromo-functionalized COF-300 (17). Reagents and conditions: a) 1,4-dioxane, $Sc(OTf)_3$, H_2O, 50°C, 72 h.

Dibromo-functionalized COF-300 (17). A 48 ml "glass bomb" heavy wall pressure vessel was charged with tetrakis(4-aminophenyl)methane (20 mg. 0.053 mmol), compound **10** (30.7mg, 0.105

mmol), 1,4-dioxane (2.5 ml) and 42 µl of scandium triflate stock solution (0.2 M in acetonitrile, 0.084 mmol, 0.04 equiv. per amine). The reactor was capped, sealed, and heated to 50°C for 72 hours to yield a yellow powder, which was isolated by centrifugation and immersed and washed with tetrahydrofuran to remove residual solvent and guest. This was repeated several times until the solvent became colorless. The product was then washed with acetonitrile and water and lyophilized to give **17** as a yellow powder.

4.4 Results and Discussion

4.4.1 Monomer Synthesis

4.4.1.1 Truncated Aldehyde Linker

The first synthesis attempt of a functionalized aldehyde linker, as shown in Scheme 2.1, was designed to produce a truncated tetrahedral aldehyde monomer as inspired by earlier work producing truncated tetrahedral boronic acid monomers for COF synthesis[3]. Compared to the tetrakis(4-formylphenyl)methane synthesized in Chapter 2, the products of this synthetic pathway, aldehydes **3** and **4** contain one fewer phenyl ring attached to the central carbon, which is replaced by a vinyl ether and an alkenyl group, respectively. Specifically, research efforts were focused on producing aldehyde **3**, as it required one fewer reaction step and should be similarly suitable for functionalized COF synthesis compared to aldehyde **4**. In the first step of this pathway, the conversion of 1,4-dibromobenzene to compound **1**, n-BuLi was employed to cleave exactly one of the two bromines attached to the starting materials, and subsequently exactly three of these bromobenzene radicals needed to attach to the central carbon in diethyl carbonate to form compound **1**. In addition, as observed in the synthesis of tetrakis(4-formylphenyl)methane synthesized in Chapter 2, the consistency of n-BuLi as a catalyst for the cleavage of bromines is poor. As such, the reproducibility of this reaction was quite low, and even when the correct product was formed, it was mixed with multiple side products that exhibited similar solubility and chromatographic mobility characteristics that rendered separation extremely difficult. Nevertheless, small amounts of analytically pure compound **1** were obtained through meticulous purification utilizing column chromatography, as shown by the ^{1}H NMR spectrum in Figure 2.1, while greater quantities of said product could not be separated from the side products despite repeated efforts.

The second step of this pathway, in which the hydroxy group in compound **1** was converted into the vinyl ether group in compound **2**, was much more consistent and effective than the first step, owing to the efficacy and consistency of sodium hydride as a catalyst. Though column chromatography was needed for purification, compound **2** was separated from the side products easily and was obtained in good yield and high purity, as shown by the ^{1}H NMR spectrum in Figure 4.3.

The final and most crucial step of this synthesis was the cleavage of the three aryl bromides and substitution by aldehyde groups to produce aldehyde **3** utilizing n-BuLi. This reaction was similar to the conversion of tetrakis(4-bromophenyl)methane to tetrakis(4-formylphenyl)methane shown in Chapter 2, and the results were similarly comparable. Although a relatively pure fraction of aldehyde **3** was obtained through many repeated attempts at synthesis and purification by column chromatography, as shown by the ^{1}H NMR spectrum in Figure 4.4, the inconsistencies and difficulties associated with n-BuLi reduced the yield and reproducibility to a degree at which it was infeasible to utilize the product for synthesis of functionalized COFs, which require vastly higher quantities of the functionalized aldehyde monomer than what could be obtained from many repeated syntheses, and the low reproducibility would have increased the required synthetic efforts to insurmountable levels. Ultimately, this truncated aldehyde linker was not utilized for functionalized COF synthesis, and the parallel pathway towards aldehyde **4** was not further pursued due to anticipation of similar difficulties.

To assess the possibility of reduced dependence on the inconsistent n-BuLi chemistry, an alternative method of synthesizing a truncated bromide linker **5** by directly brominating chlorotriphenylmethane, which was utilized for monomer synthesis in Chapter 2, as shown in Scheme 4.2. Unlike the bromination of tetraphenylmethane in Chapter 2, however, the asymmetry

and more complex molecular structure of chlorotriphenylmethane compared to tetraphenylmethane rendered this approach unsuccessful, and compound **5** could not be isolated.

4.4.1.2 Functionalized Dialdehyde Monomers

The cleavage of multiple bromides from complex aromatic structures utilizing n-BuLi had proven challenging in both the synthesis of tetrakis(4-formylphenyl)methane and the truncated aldehyde linker; however, n-BuLi chemistry was still the most common and widely adopted method for synthesizing aldehydes. As such, a synthesis pathway for obtaining a functionalized dialdehyde linker containing only one phenyl ring was designed and is shown in Scheme 2.2. Compared to prior aldehyde syntheses, the structure of the product was simpler and retained the desired vinyl ether functionality and only a single step required n-BuLi to cleave two bromides off the same phenyl ring. The first two reactions in the sequence relied on proven, simple, and consistent chemistries to convert the methyl ester group in the starting material to a vinyl ether group in compound **7**, and were completed without major issues, as evidenced by the clean ^{1}H NMR spectra of compounds **6** and **7** in Figure 4.5 and Figure 4.6, respectively. Unfortunately, the third and final reaction, the cleavage of bromides and substitution by aldehydes, was even more unsuccessful than the final reaction in the truncated aldehyde synthesis. Despite repeated attempts, aldehyde **8** could not be isolated in any quantity, and the ^{1}H NMR spectrum of the fraction that bore the closest resemblance to the desired product is shown in Figure 4.7. Two distinct aldehyde peaks can be observed at chemical shifts of 9.99 and 9.73, but the remainder of the spectrum is filled with peaks that do not match with either compound **7** or the product. Additional attempts to convert the bromides in starting material methyl 2,5-dibromobenzoate, compounds **6** and **7**, and 1,4-dibromobenzene to aldehyde groups were all similar unsuccessful. One possible cause for the

consistent inability to convert dihalides into dialdehydes could be the electronic structure of the phenyl ring. Aldehydes are stronger electron withdrawing functionalities than halides, and thus exert a stronger deactivation effect on the phenyl ring. As such, once the first bromide is replaced by an aldehyde, the second bromide becomes less reactive due to this change in reactivity.

Owing to the multitude of difficulties encountered in n-BuLi chemistry, it was highly desirable to design a reaction pathway that could produce a functionalized aldehyde linker without employing said chemistry. An extensive literature search provided the pathway shown in Scheme 4.4, which utilizes a Sommelet reaction to convert methyl chlorides into aldehyde groups, circumventing the need for n-BuLi[10]. The chloromethylation of 1,4-dibromobenzene was the first step and required the constant flow of hydrochloric acid gas through the reaction vessel for the duration of the reaction to ensure high yield and conversion rate. A constant source of hydrochloric acid gas was not readily available, so a two-stage reaction setup was designed to generate the hydrochloric acid gas as the reaction proceeded. As shown in Figure 4.14, concentrated aqueous hydrochloric acid solution was slowly added to anhydrous calcium chloride powder, which absorbed the water and released the hydrochloric acid gas. The gas was subsequently bubbled into the reaction mixture, providing the constant flow required by the reaction. An outlet from the main reaction vessel connected to a sodium carbonate solution to neutralize and quench the extraneous hydrochloric acid gas flowing through the system. This two-stage reactor facilitated the synthesis of analytically pure **9**, as shown by the ^{1}H NMR spectrum in Figure 4.8, with 90%+ yield.

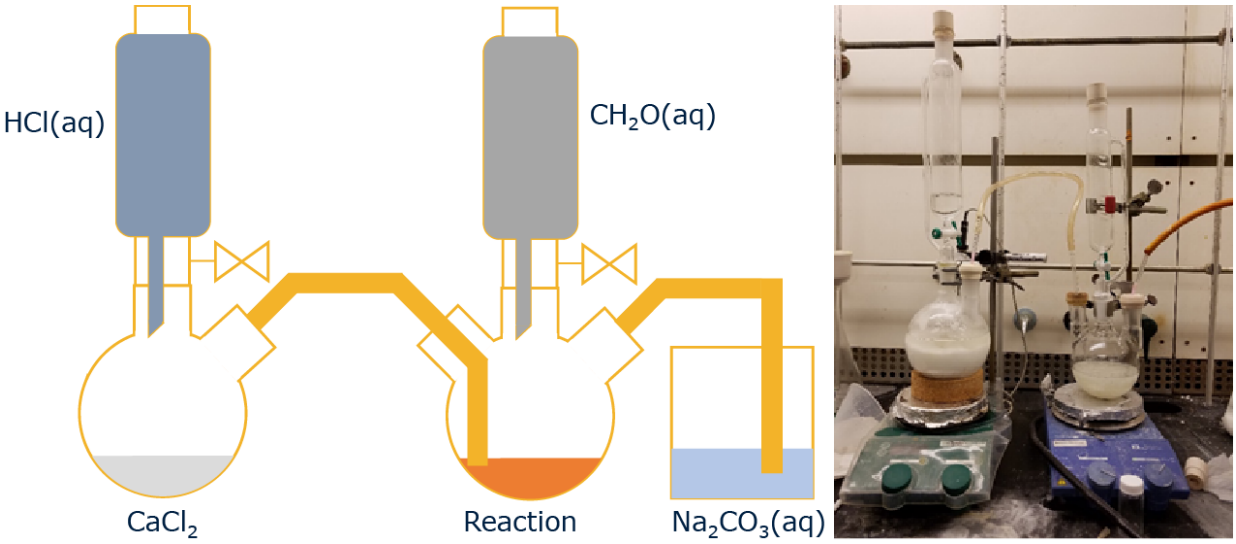

Figure 4.14. Schematic and photograph of the reaction setup for the in-situ generation of HCl gas and synthesis of 1,4-bis(chloromethyl)-2,5-dimethoxybenzene.

The conversion of the methyl chloride in compound **9** into the aldehydes in compound **10** through the Sommelet reaction had been reported to result in low yield (32%)[11]. An improved procedure was reported to increase the yield to 70%[7], but following said procedures consistently resulted in yields much lower than 70%. Attempts to improve the reaction procedures by repeating the reflux in water before isolation of the product, as well as adding another portion of hydrochloric acid solution to and refluxing the aqueous layer obtained from liquid-liquid extraction, yielded additional crops of crude product from which **10** was obtained, though the overall yield was still lower than 70%. Analytically pure **10**, as proven by the ^{1}H NMR spectrum in Figure 4.9, was isolated by a simple flash column, a marked departure from the complexity and difficulty of purification of prior aldehyde products obtained from n-BuLi chemistry.

Compound **10** is a dimethoxy-functionalized terephthalaldehyde (DMTA) and fits the requirements for utilization in functionalized COF synthesis; nevertheless, the two methoxy groups were further converted to hydroxy groups, which could then be modified into a wide array

of functionalities. Analytically pure compound **11**, the product of this reaction, was also isolated without issue, as shown by the ^{1}H NMR spectrum in Figure 4.10. This reaction produced dihydroxy-functionalized terephthalaldehyde (DHTA), which would also be employed for functionalized COF synthesis in Section 4.3.3.

In comparison to the methoxy and hydroxy groups, which were difficult to introduce but could be readily post-synthetically modified to many different functionalities, bromide groups were much easier to attach. As shown in Scheme 4.5, the synthesis of 2,5-dibromoterephthalaldehyde (DBTA, compound **12**) is a relatively straightforward one-pot reaction starting from the commercially available terephthalaldehyde. N-bromosuccinimide was recrystallized for purification purposes prior to use, and recrystallization of the crude product resulted in analytically pure **12**, the ^{1}H NMR of which is displayed in Figure 4.11. DBTA would also be utilized for functionalized COF synthesis in Section 4.3.3.

4.4.1.3 TBDMS Protection of DHTA

In order to establish interpenetration control over COF-300 using the space-filling tert-butyldimethylsilyl (TBDMS) protecting group, a model protection reaction was first conducted on commercially available 4,4'-(propane-2,2-diyl)diphenol following Scheme 4.6. While some impurities are present, as evidenced by the unidentified peaks in the ^{1}H NMR spectrum (Figure 4.12), protection of the hydroxy groups were successful, as every peak in the expected product was matched to their respective peaks. Subsequently, the same procedures for TBDMS protection were applied to DHTA in preparation for establishing interpenetration control following Scheme 4.7. Unfortunately, the same reaction procedures did not result in the successful protection of DHTA. As displayed in the ^{1}H NMR spectrum of the protection product in Figure 4.13, the two

prominent peaks which appeared at chemical shifts of 0.19 and 0.98 in the spectrum of the model protection product and were assigned to the tert-butyl and methyl groups in the TBDMS were conspicuously absent. Multiple attempts to modify the reaction conditions did not produce tangible improvements, and protection of functional groups and subsequent application of interpenetration control was not further pursued.

4.4.2 Functionalized COF-300 Synthesis

4.4.2.1 Dimethoxy-functionalized COF-300 Synthesis

The synthesis of functionalized COF-300 was attempted first utilizing DMTA in place of terephthalaldehyde (TA). The synthesis was first conducted following the solvothermal method and the reaction conditions conventionally used for COF-300 synthesis, namely 120°C and 3 M acetic acid. These conditions, which have been confirmed to produce crystalline COF-300, reliably gave amorphous products when utilizing DMTA. Adjustment of reaction temperature and acetic acid concentration (shown in Table 4.1) were carried out, but under no set of conditions was crystalline COF obtained. Representative XRD spectra of samples synthesized by the solvothermal method are shown in Figure 4.15.

Table 4.1. Summary of different reaction conditions attempted for the solvothermal synthesis of dimethoxy-functionalized COF-300.

Temperature (°C)	Acetic Acid Aqueous Solution Concentration (M)
120	3
120	6
120	9
160	9

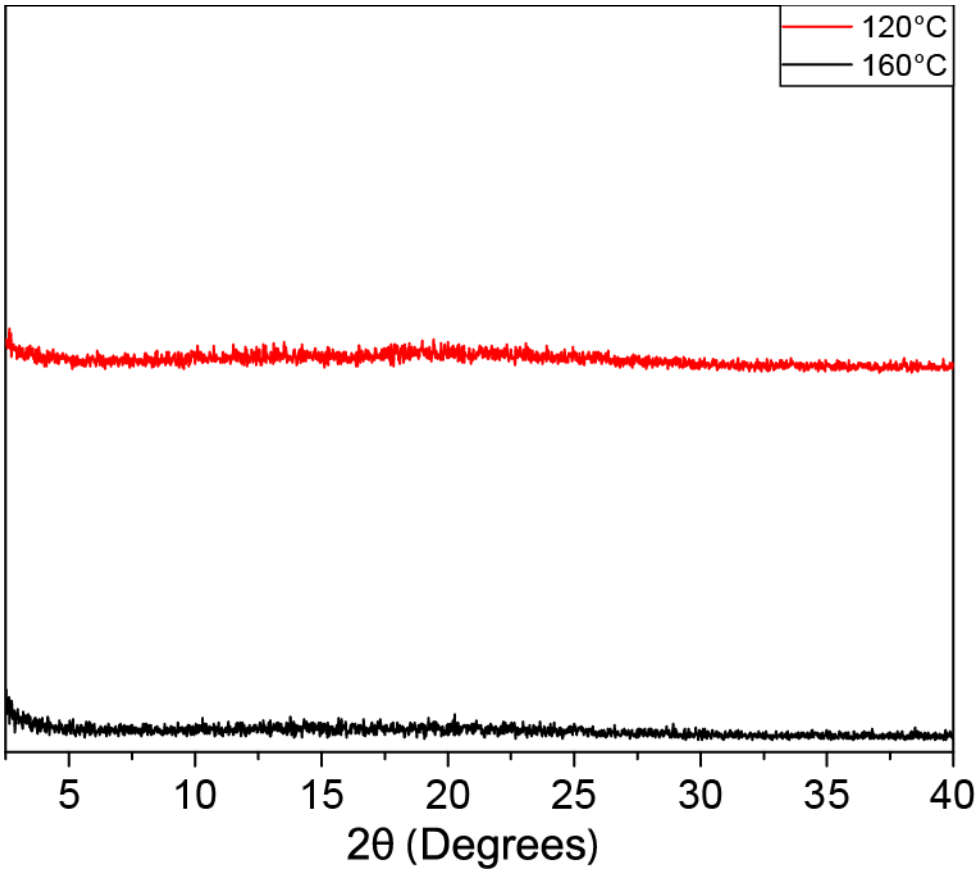

Figure 4.15. PXRD spectra of dimethoxy-functionalized COF-300 synthesized using 3 M acetic acid and the solvothermal method at different temperatures.

The dimethoxy-functionalized COF synthesis was then attempted utilizing scandium triflate ($Sc(OTf)_3$), which was demonstrated as a more effective catalyst then acetic acid for imine-linked COF synthesis in Chapter 3. Initial synthesis attempts using the optimal reaction conditions identified for COF-300 in Chapter 3 yielded amorphous products, so similar to the reaction condition optimization in Chapter 3, reaction temperatures, catalyst loading, and water content were varied independently to identify a set of conditions that facilitates the formation of crystalline dimethoxy-functionalized COF-300. A summary of the reaction conditions attempted is shown in Table 4.2. Unlike the results of Chapter 3, however, here no combination of reaction conditions even revealed a hint of crystallinity that could be observed by PXRD. Representative PXRD

spectra of $Sc(OTf)_3$ catalyzed dimethoxy-functionalized COF-300 synthesis carried out at a range of water content and catalyst loading are shown in Figure 4.16 and Figure 4.17, respectively.

Table 4.2. Summary of reaction conditions attempted for the $Sc(OTf)_3$ catalyzed synthesis of dimethoxy-functionalized COF-300.

Temperature (°C)	$Sc(OTf)_3$ Loading (equiv. per amine)	Water Content (equiv. per amine)
50	0.04	0
50	0.04	13
50	0.04	26
50	0.04	40
50	0.04	53
50	0.04	79
50	0.04	106
50	0.06	53
50	0.08	53
70	0.02	53
70	0.04	53
70	0.06	53
70	0.08	53
70	0.10	53
RT	0.04	53
RT	0.06	53
RT	0.08	53
RT	0.10	53
RT	0.12	53

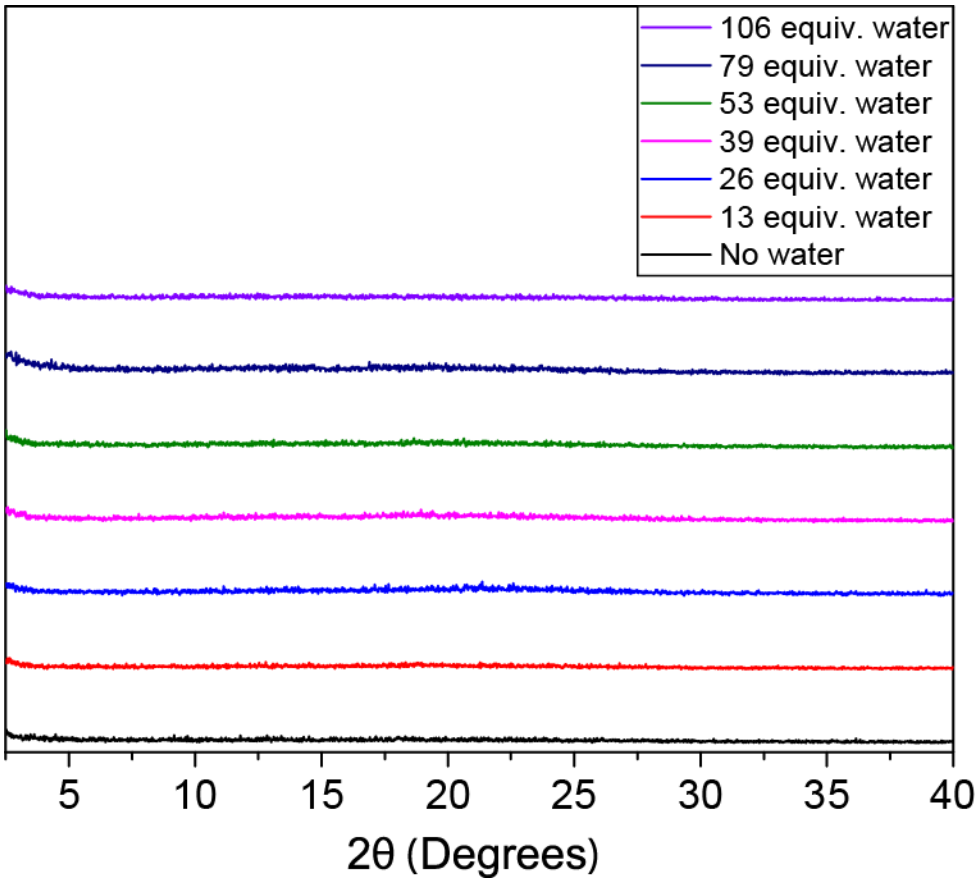

Figure 4.16. PXRD spectra of dimethoxy-functionalized COF-300 synthesized using 0.04 equiv. $Sc(OTf)_3$ at 50°C and a range of water content.

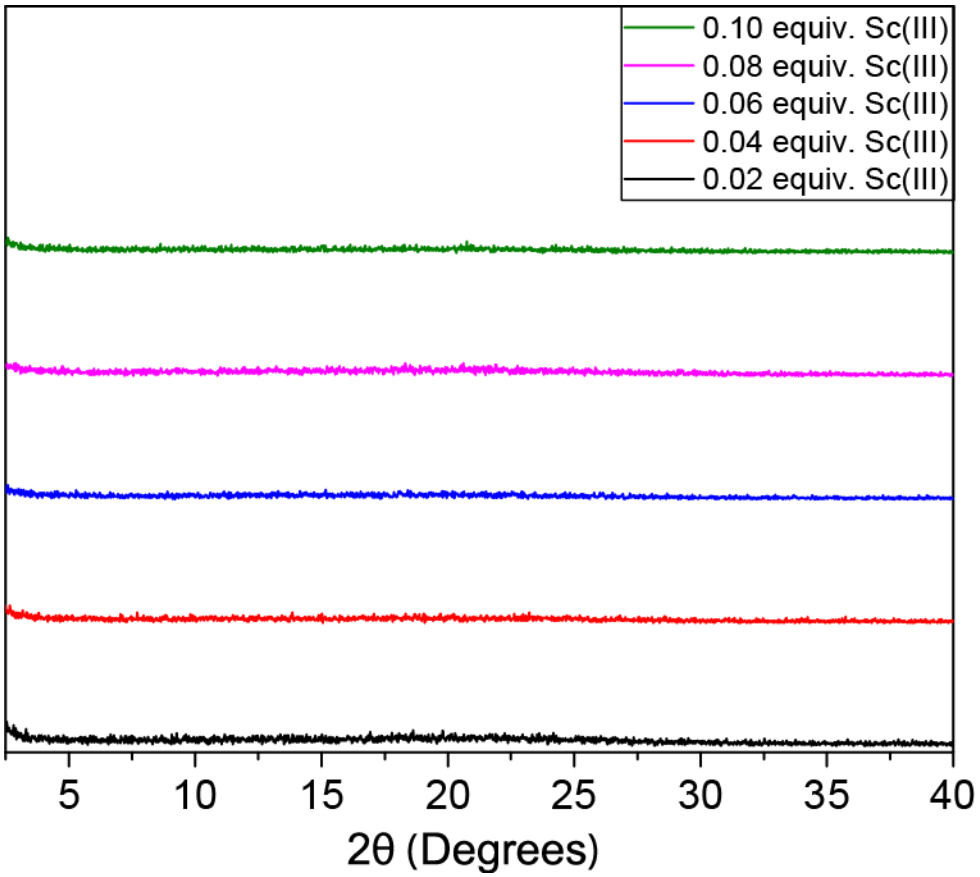

Figure 4.17. PXRD spectra of dimethoxy-functionalized COF-300 synthesized using $Sc(OTf)_3$ at 70°C and a range of catalyst loading.

Compared to the synthesis of COF-300, the sole difference in the synthesis of dimethoxy-functionalized COF-300 is the presence of methoxy groups attached to TA. As such, this difference is likely the cause of the amorphous products. To confirm the validity of this hypothesis, COF synthesis was carried out employing a range of ratios of DMTA/TA, and the crystallinity of the products were characterized by PXRD and displayed in Figure 4.18. At 100% TA, the product is simply COF-300, and as expected the spectrum is characterized by sharp and narrow peaks and a flat baseline, indicative of a crystalline structure. As the percentage of DMTA was increased to 60% in increments of 20%, a steady decrease in crystallinity could be observed as a function of the increase in DMTA. At 80% DMTA, the product was completely amorphous, with no signs of

any peaks throughout the spectrum. Overall, the correlation between increased amounts of DMTA and decreased crystallinity is clear and supports the hypothesis that the change in structure compared to TA was the cause of the loss of crystallinity.

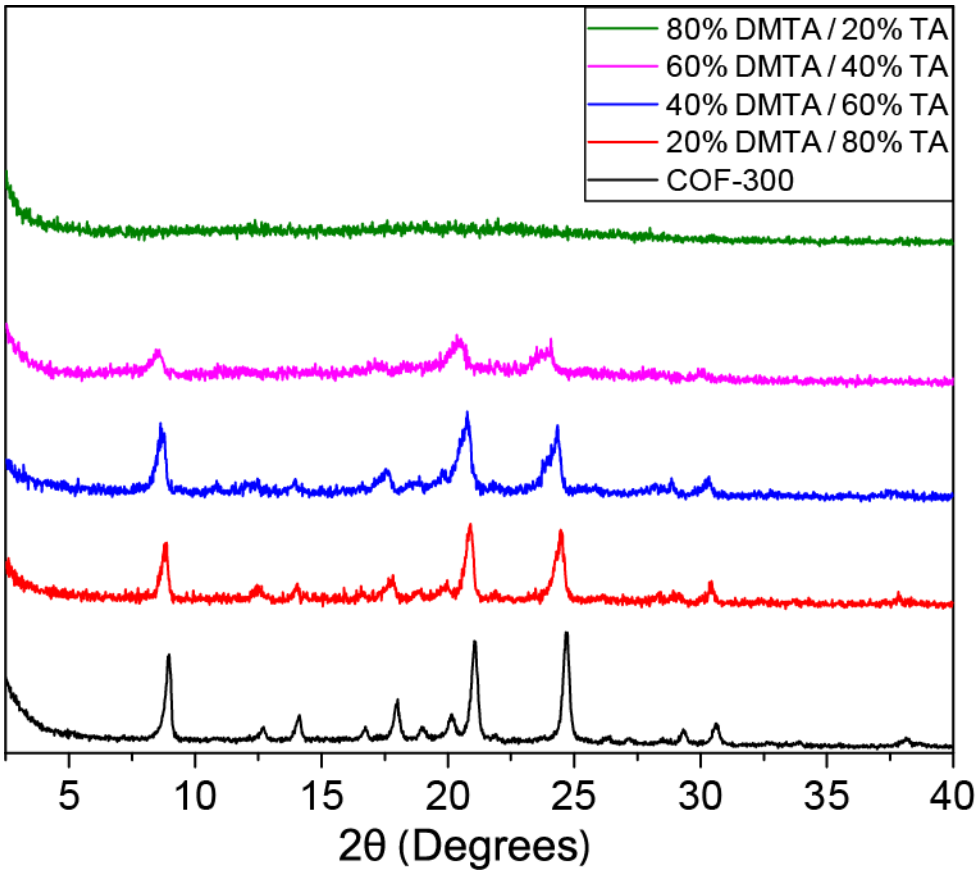

Figure 4.18. A comparison of XRD spectra of dimethoxy-functionalized COF-300 synthesized employing a range of ratios of dimethoxy-functionalized terephthalaldehyde to unfunctionalized terephthalaldehyde.

4.4.2.2 Dihydroxy-functionalized COF-300 Synthesis

Although dimethoxy-functionalized COF-300 could not be obtained in a crystalline state, there was another functionalized aldehyde monomer, DHTA, that could be employed for functionalized COF synthesis. Thus, the synthesis of dihydroxy-functionalized COF-300 was

investigated in a similar fashion, first utilizing the solvothermal method at different reaction temperatures and acetic acid concentrations, as shown in Table 4.3, and subsequently using $Sc(OTf)_3$ as the catalyst over an array of reaction temperatures, catalyst loading, and water content, the summary of which can be found in Table 4.4. The product crystallinity was characterized by PXRD, and once again every trial employing both synthetic methods produced amorphous material. Representative PXRD spectra of a comparison between the solvothermal method and the $Sc(OTf)_3$ method, a range of $Sc(OTf)_3$ loading, and a range of water content in the $Sc(OTf)_3$ catalyzed regime are shown in Figure 4.19, Figure 4.20, and Figure 4.21 respectively.

Table 4.3. Summary of different reaction conditions attempted for the solvothermal synthesis of dihydroxy-functionalized COF-300.

Temperature (°C)	Acetic Acid Aqueous Solution Concentration (M)
120	3
120	6
120	9
160	9

Table 4.4. Summary of reaction conditions attempted for the $Sc(OTf)_3$ catalyzed synthesis of dihydroxy-functionalized COF-300.

Temperature (°C)	**$Sc(OTf)_3$ Loading (equiv. per amine)**	**Water Content (equiv. per amine)**
50	0.04	26
50	0.04	53
50	0.04	106
50	0.06	53
50	0.08	53
70	0.04	53
70	0.06	53
70	0.08	53
RT	0.04	53
RT	0.06	53
RT	0.08	53

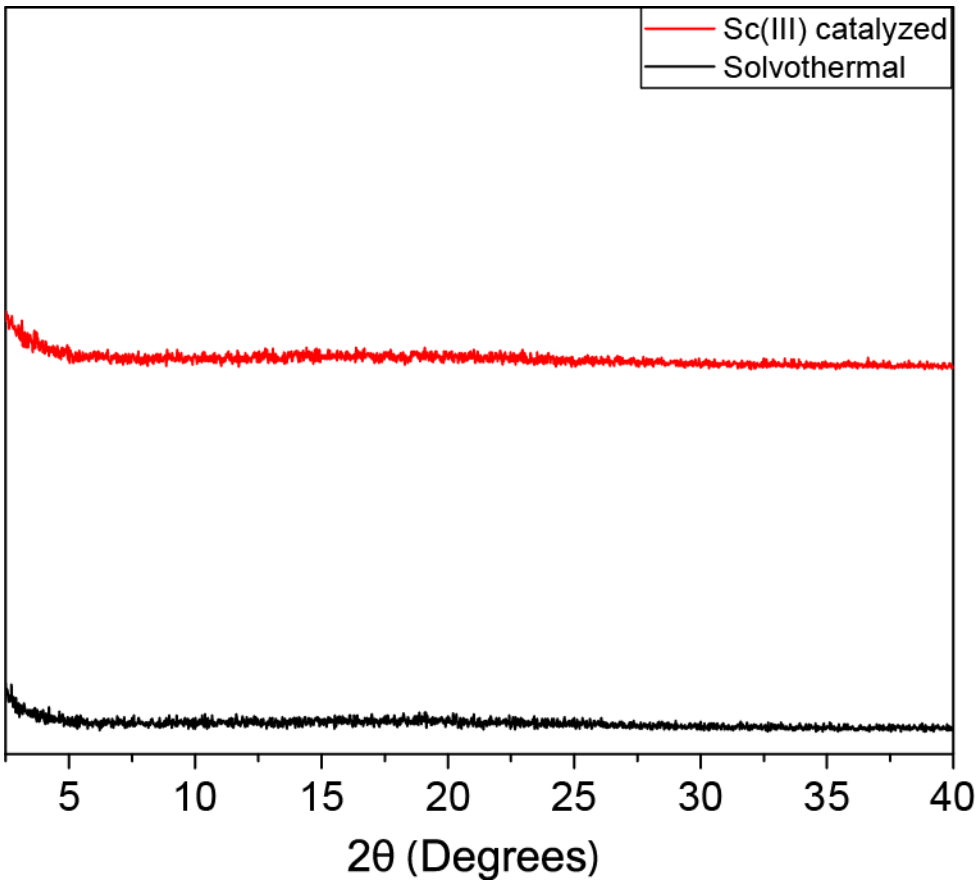

Figure 4.19. PXRD comparison of dihydroxy-functionalized COF-300 synthesized *via* the solvothermal method and the $Sc(OTf)_3$ method.

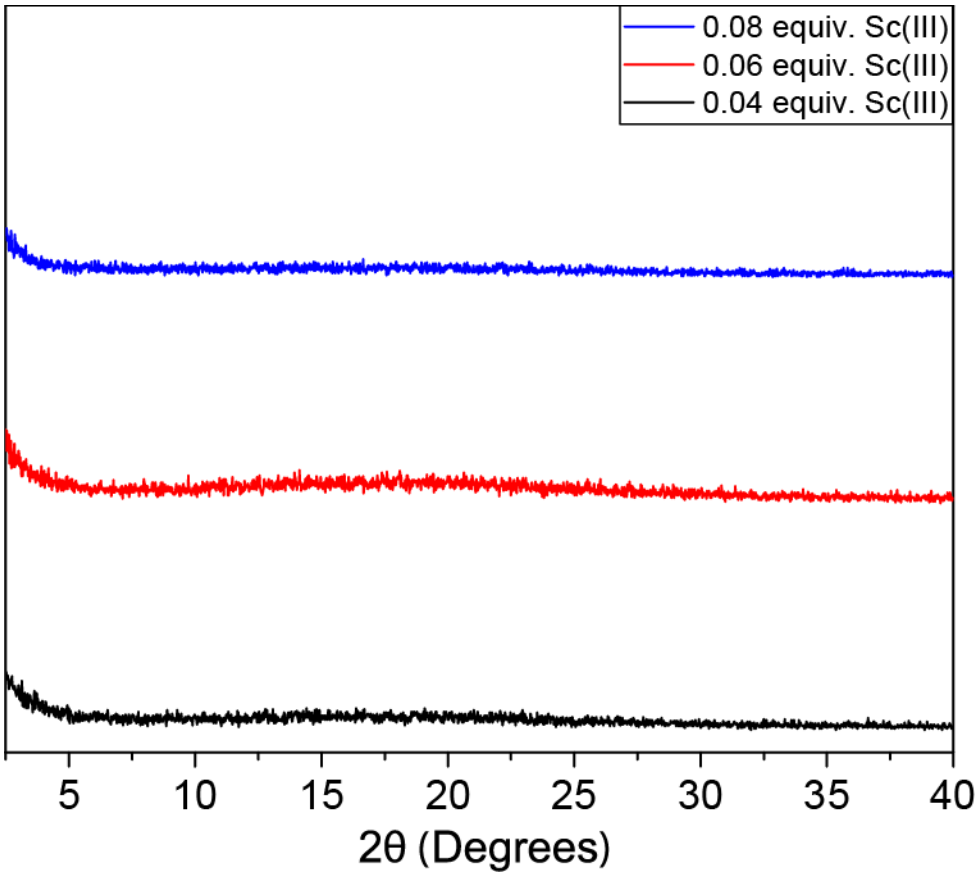

Figure 4.20. PXRD spectra of dihydroxy-functionalized COF-300 synthesized using $Sc(OTf)_3$ at 50°C, 53 equiv. water, and a range of catalyst loading.

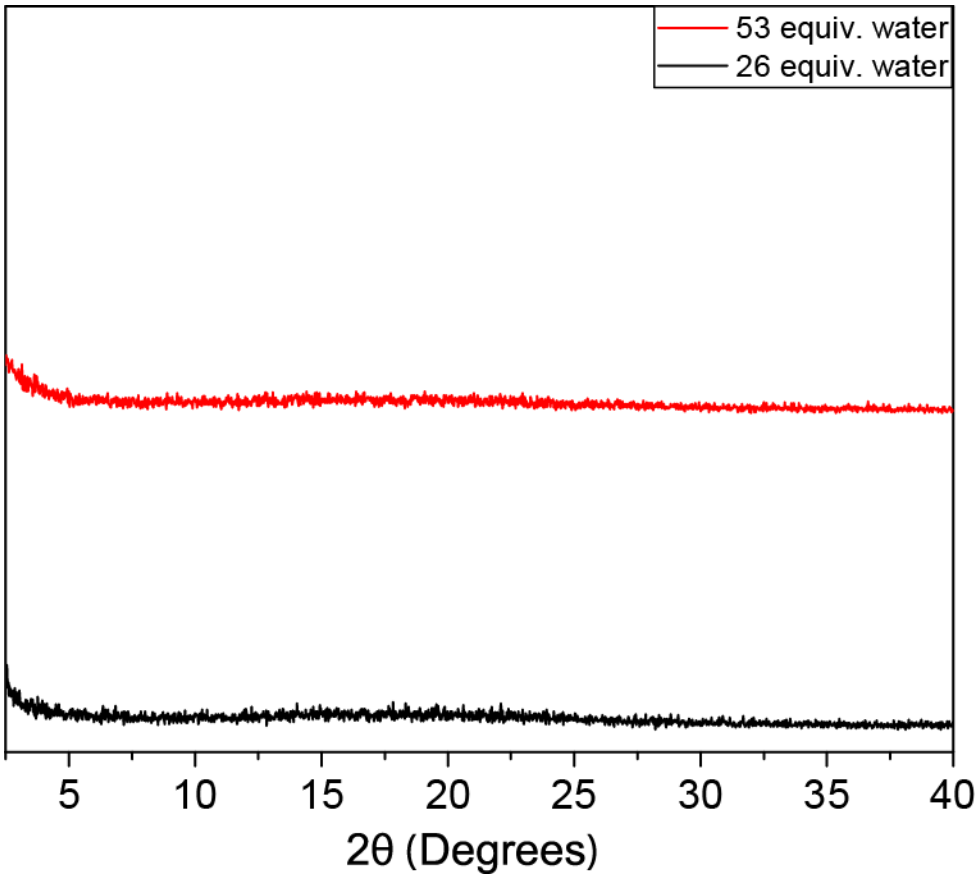

Figure 4.21. PXRD spectra of dihydroxy-functionalized COF-300 synthesized using 0.04 equiv. $Sc(OTf)_3$ at 50°C and a range of water content.

COF syntheses employing a range of ratios of DHTA/TA were conducted, and the crystallinity of the products were characterized by PXRD and shown in Figure 4.22. Similar to what was observed for dimethoxy-functionalized COF-300, crystallinity of the product clearly decreases as the percentage of DHTA increases, and at 80% DHTA the product becomes completely amorphous. This not only supports the hypothesis that the change in structure compared to TA is the cause of the loss of crystallinity, but also reveals that the loss of crystallinity was not due to the presence of a specific functional group, but rather some common feature of both the methoxy and hydroxy functionalities.

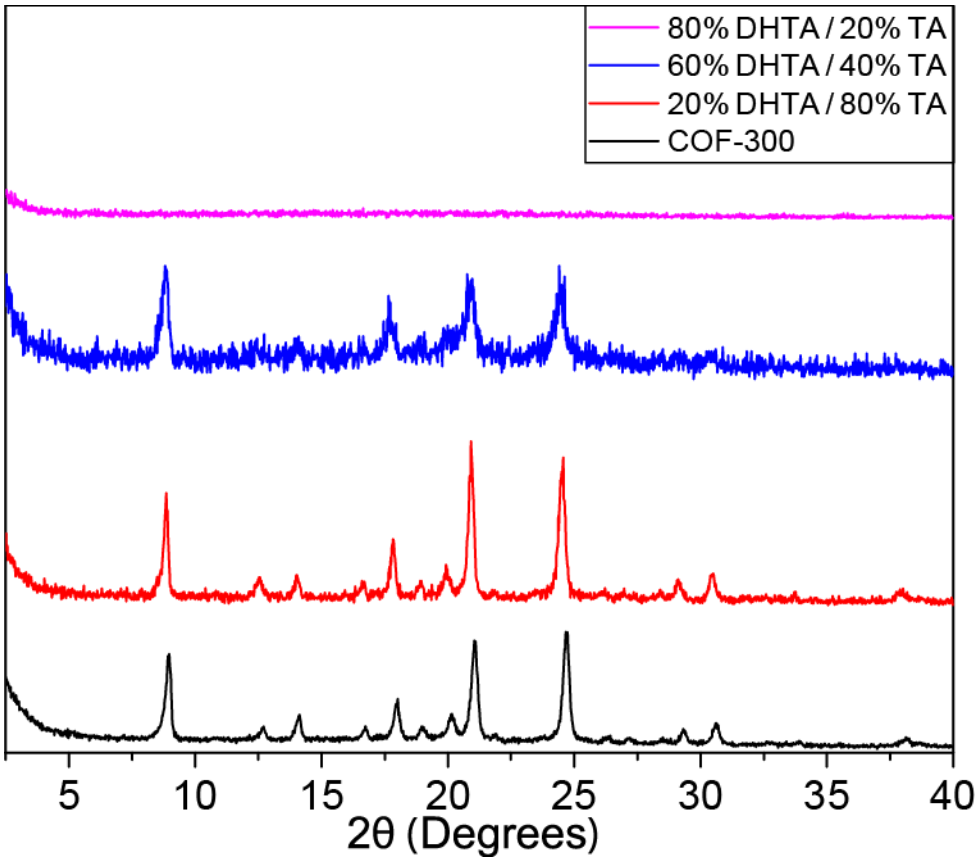

Figure 4.22. A comparison of XRD spectra of dihydroxy-functionalized COF-300 synthesized employing a range of ratios of dihydroxy-functionalized terephthalaldehyde to unfunctionalized terephthalaldehyde.

There are two potential explanations for this lack of crystallinity. The first is the alteration in the electronic structure of the ring. Both methoxy and hydroxy groups are strong electron donating groups and appending two methoxy or hydroxy groups to TA could have caused significant enough change to the reactivity of the two aldehydes on the same phenyl ring. The second possibility is reduced reaction site accessibility. Both methoxy and hydroxy groups are reasonably bulky, and these pendant groups could have sterically hindered the ability of the amines on tetrakis(4-aminophenyl)methane to access and react with the aldehydes located on the same ring, a concern exacerbated by the inherent tendency of 3D COFs to become kinetically trapped during synthesis due to lack of mobility and already bulky monomers. A combination of the two

factors is likely the cause for the inability to rearrange into a crystalline structure, but to gain some insight into which factor plays a more significant role, DBTA was employed for functionalized COF synthesis. In contrast with the strong electron donating effects of methoxy and hydroxy groups, bromides are weakly electron withdrawing and would exert a smaller and opposite effect on the reactivity of the aldehyde groups, which would allow for the assessment of the significance of electronic effects. As shown in Scheme 4.10, the synthesis was conducted utilizing $Sc(OTf)_3$ over a range of catalyst loading. PXRD characterization of the products show that they were consistently amorphous at each reaction condition attempted. Given that appending strong electron donating methoxy and hydroxy groups and weak electron withdrawing bromide groups to the phenyl ring resulted in comparable lack of product crystallinity, insufficient reaction site accessibility and steric hindrance was likely the key culprit in the inability of the constituent species to rearrange into an ordered crystalline structure.

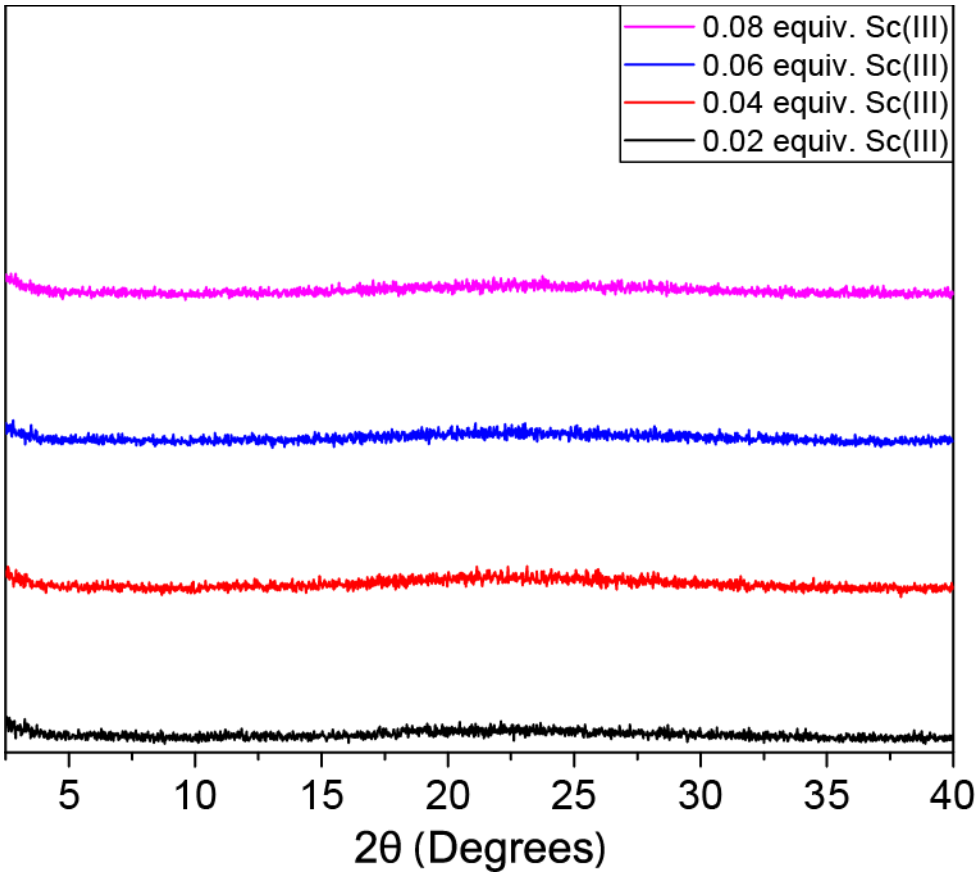

Figure 4.23. PXRD spectra of dibromo-functionalized COF-300 synthesized using 53 equiv. water and a range of $Sc(OTf)_3$ loading at 50°C.

4.5 Conclusions

Four different approaches to synthesizing functionalized aldehyde monomers for functionalized imine-linked 3D COF synthesis were explored. Two of the pathways were dependent on n-BuLi chemistry to introduce aldehyde functionalities, which has repeated proven to result in low yield, multiple side products, extremely difficult separation procedures, and low reproducibility. An alternative approach utilizing a Sommelet reaction was established and successfully produced two functionalized aldehyde linkers, DMTA and DHTA. Lastly, the one-pot conversion of commercially available TA to DBTA was successfully demonstrated, providing

a third monomer for functionalized COF synthesis. Both the solvothermal and the $Sc(OTf)_3$ catalyzed approaches were investigated for dimethoxy- and dihydroxy-functionalized COF-300, and despite testing a wide array of reaction conditions under both synthetic regimes, the products were consistently amorphous. Employing different ratio of DMTA/TA and DHTA/TA for functionalized COF synthesis revealed that product crystallinity decreased as the ratio of the functionalized monomers increased, and at 80% DMTA or DHTA the product became completely amorphous, indicating that these functional pendant groups were responsible for the lack of crystallinity. The synthesis of dibromo-functionalized COF-300 was conducted using DBTA, and again amorphous materials were obtained, suggesting that reaction site accessibility and steric hindrance, rather than the electron donating effects of the methoxy and hydroxy groups or the electron withdrawing effects of the bromide groups, resulted in the inability of the amorphous products to rearrange into a crystalline framework.

4.6 References

1. Feng, X., Ding, X. & Jiang, D. Covalent organic frameworks. *Chem. Soc. Rev.* **41**, 6010–6022 (2012).
2. Ma, X. & Scott, T. F. Approaches and challenges in the synthesis of three-dimensional covalent-organic frameworks. *Commun. Chem.* **1**, 98 (2018).
3. Bunck, D. N. & Dichtel, W. R. Postsynthetic functionalization of 3D covalent organic frameworks. *Chem. Commun.* **49**, 2457–2459 (2013).
4. Bunck, D. N. & Dichtel, W. R. Internal Functionalization of Three-Dimensional Covalent Organic Frameworks. *Angew. Chem. Int. Ed.* **51**, 1885–1889 (2012).
5. Brucks, S. D., Bunck, D. N. & Dichtel, W. R. Functionalization of 3D covalent organic frameworks using monofunctional boronic acids. *Polymer* **55**, 330–334 (2014).
6. Lu, Q. *et al.* Postsynthetic Functionalization of Three-Dimensional Covalent Organic Frameworks for Selective Extraction of Lanthanide Ions. *Angew. Chem.* **130**, 6150–6156 (2018).
7. Kretz, T., Bats, J. W., Lerner, H.-W. & Wagner, M. 2,5-Diformylbenzene-1,4-diol: A Versatile Building Block for the Synthesis of Ditopic Redox-Active Schiff Base Ligands. *Z. Für Naturforschung B* **62**, 66–74 (2014).
8. Prusinowska, N., Bardziński, M., Janiak, A., Skowronek, P. & Kwit, M. Sterically Crowded Trianglimines—Synthesis, Structure, Solid-State Self-Assembly, and Unexpected Chiroptical Properties. *Chem. – Asian J.* **13**, 2691–2699 (2018).

9. Uribe-Romo, F. J. *et al.* A Crystalline Imine-Linked 3-D Porous Covalent Organic Framework. *J. Am. Chem. Soc.* **131**, 4570–4571 (2009).

10. Zhao, S. *et al.* Channel-wall functionalization in covalent organic frameworks for the enhancement of CO2 uptake and CO2/N2 selectivity. *RSC Adv.* **6**, 38774–38781 (2016).

11. Angyal, S. J., Morris, P. J., Tetaz, J. R. & Wilson, J. G. 441. The Sommelet reaction. Part III. The choice of solvent and the effect of substituents. *J. Chem. Soc. Resumed* 2141–2145 (1950). doi:10.1039/JR9500002141

Chapter 5
Alternative Approaches to the Modification and Synthesis of 3D Imine-linked COFs

5.1 Abstract

This chapter details three alternative approaches to the modification and synthesis of 3D imine-linked COFs. Post-synthetic reduction of imine bonds to secondary amines employing sodium triacetoxyborohydride was explored. Multi-phase synthesis of COF-300 utilizing dual-phasic and tri-phasic interfacial synthesis as well as *in situ* aqueous extraction of scandium triflate was investigated. Additionally, the high-pressure transformation of COF powder possessing low to no crystallinity *via* pellet pressing is found to result in pellets that exhibit improved crystallinity, and the impact of pressing conditions as well as synthesis conditions on pellet crystallinity was evaluated.

5.2 Introduction

A major issue that plagues 3D COFs is the relative narrow range of synthesis and functionalization techniques. Synthetic methods are largely limited to the conventional solvothermal approach, despite recent demonstrations of ionothermal synthesis[1], room temperature single crystal synthesis[2], and scandium triflate ($Sc(OTf)_3$) catalyzed synthesis as demonstrated in Chapter 3. Examples of functionalization of 3D COFs, particularly those

constructed from imine linkages, remains sparse, and post-synthetic modification by embedding reactive functionalities into constituent monomers is the predominant method employed[3]. In this regard, 3D COFs lag 2D COFs significantly, and developing alternative methods of synthesis and modification is key to advancing the field of 3D COFs.

One modification method that was demonstrated in an imine-linked 2D COF was the reduction of the imine bonds to amides, which was found to alter the properties of the COF[4]. This methodology should be wholly transferrable to imine-linked 3D COFs, and the amides could serve as an interface for further modification. One example would be reaction with methacrylic anhydride to introduce double bonds, as shown in Figure 5.1. The double bonds can then be utilized for a variety of applications, such as photopolymerization.

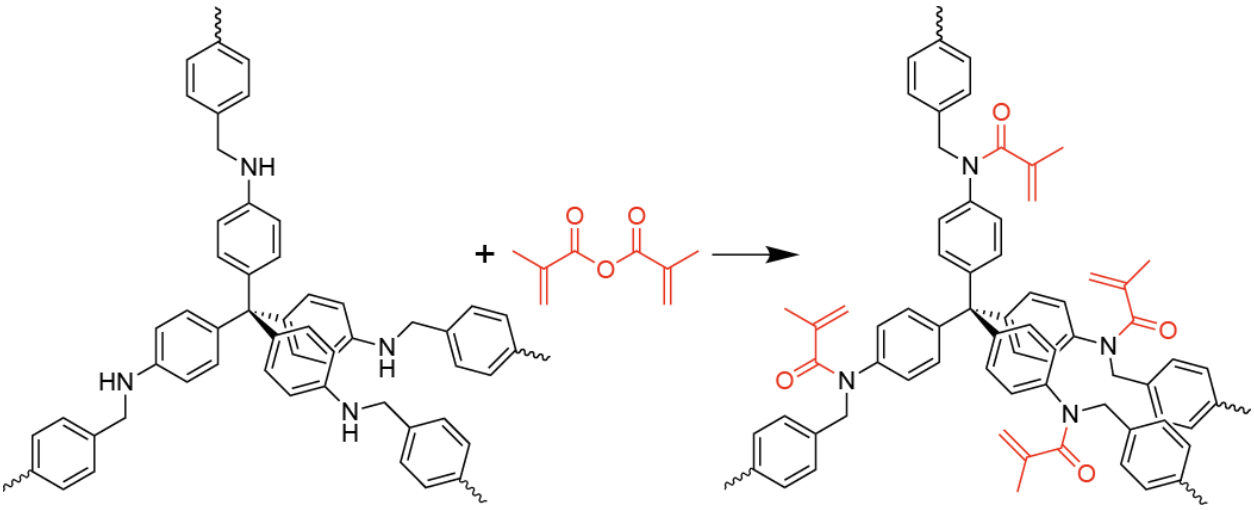

Scheme 5.1. Functionalization of amides within the pores of COF-300 utilizing methacrylic anhydride.

Many of the novel synthesis procedures that have been developed for 2D COFs, such as microwave synthesis[5], flow synthesis[6–8], and vapor-assisted synthesis[9,10], are still awaiting adaptation to 3D COFs. In particular, the $Sc(OTf)_3$ catalyzed interfacial synthesis of an imine-linked 2D COF was recently demonstrated[11]. Interfacial synthesis could serve as a method to

control or limit the availability of $Sc(OTf)_3$ or monomers, slow reaction kinetics, and mediate the reaction equilibrium to avoid kinetic trapping and overcome the "crystallization problem"[3]. Similarly, aqueous extraction of excess $Sc(OTf)_3$ from the reaction system could serve a similar function of limiting catalyst availability, a method that has been demonstrated for peptoid synthesis in this lab. In addition, one of the key contributors to the "crystallization problem" is the lack of additional strong driving forces. Compared to 2D COFs, whose self-assembly into crystalline structures is facilitated in part by the π-orbital overlap of stacking sheets, 3D COFs rely on only covalent interactions for rearrangement[12,13]. As such, the application of additional driving forces for forming ordered structures such as high pressure has the potential for facilitating increased crystallinity.

In this chapter, the reduction of imine bonds to amides in COF-300 is characterized. The interfacial $Sc(OTf)_3$ catalyzed synthesis of COF-300 is investigated in several different solvent systems and a number of different configurations. The aqueous extraction of excess $Sc(OTf)_3$ from the COF-300 synthetic system is explored as an alternative to interfacial synthesis. Lastly, the high-pressure processing of COF-300 and its corresponding impact on framework crystallinity is assessed.

5.3 Experimental

5.3.1 General Experimental Procedure

All chemicals and reagents, unless specified, were purchased from commercial sources, including Fisher Scientific, Sigma-Aldrich, Alfa Aesar, and Oakwood Chemicals, and used as received without any further purification. ^1H NMR spectra were recorded on a Varian Inova 500

instrument (500 MHz). ^{13}C NMR spectra were recorded on a Varian MR400 instrument (400 MHz). Chemical shifts were measured in δ (ppm) relative to residual solvent signals as internal standards ($CDCl_3$: 7.24 for ^{1}H, 77.23 for ^{13}C; d^6-DMSO: 2.49 for ^{1}H). X-ray Diffraction (XRD) spectra were collected using a Rigaku 600 Miniflex XRD instrument and a 5mm zero background sample holder.

5.3.2 Reduction and Functionalization of Imine Bonds

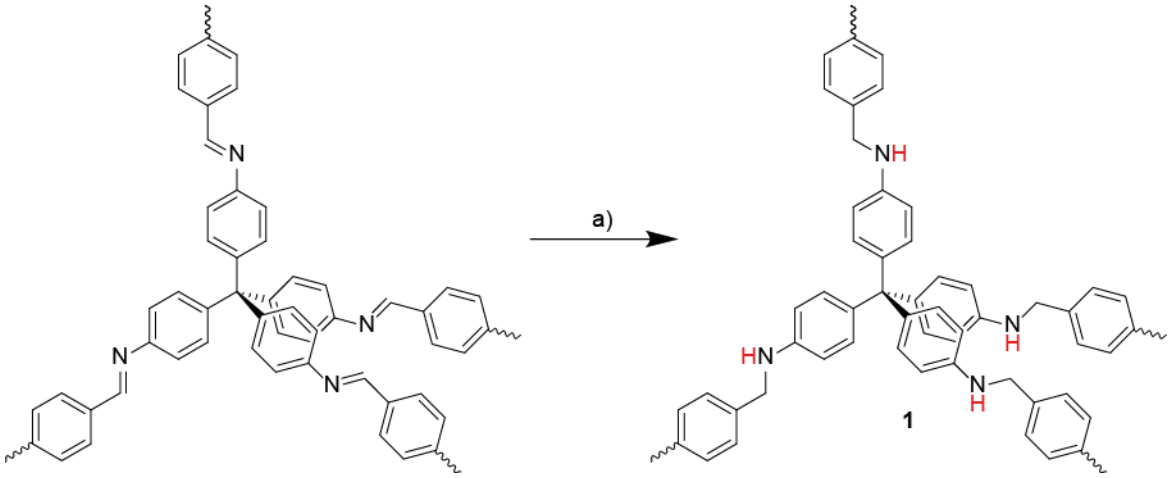

Scheme 5.2. Reduction of imine bonds in COF-300 (1). Reagents and conditions: a) $NaBH(OAc)_3$, THF, 50°C.

Reduced COF-300 (1). Sodium triacetoxyborohydride (1.12 g, 5.25 mmol) was dissolved in tetrahydrofuran (50 ml), and COF-300 (75 mg, 0.525 mmol imine bonds) was added. The mixture was stirred at 50°C for 48 h. The reaction was quenched with saturated aqueous sodium bicarbonate solution (15 ml). The solids were isolated by filtration, washed with saturated aqueous sodium bicarbonate solution and water, and dried *in vacuo* to afford reduced COF **1.**

5.3.3 Multiphase Synthesis of COF-300

5.3.3.1 Synthesis of COF-300 in Different Solvents

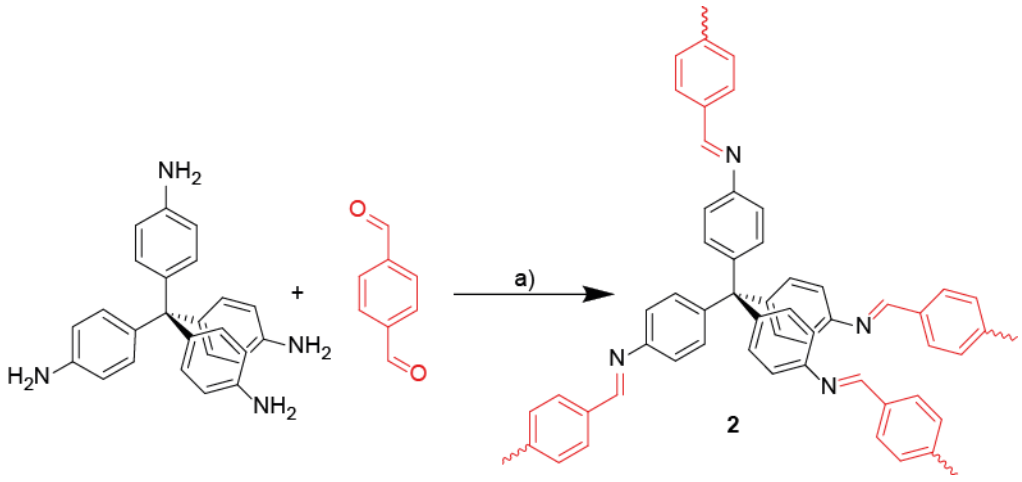

Scheme 5.3. Synthesis of COF-300 (2) in different solvents. Reagents and conditions: a) $Sc(OTf)_3$, H_2O, toluene/$CHCl_3$/DCM.

COF-300 (2). A 48 ml "glass bomb" heavy wall pressure vessel was charged with tetrakis(4-aminophenyl)methane (20 mg. 0.053 mmol), terephthalaldehyde (14.1 mg, 0.105 mmol), one of toluene/chloroform/dichloromethane (2.5 ml) and 42 µl of scandium triflate stock solution (0.2 M in acetonitrile, 0.084 mmol, 0.04 equiv. per amine). The reactor was capped, sealed, and left at room temperature for 144 h to yield a yellow powder, which was isolated by centrifugation and immersed and washed with tetrahydrofuran to remove residual solvent and guest. This was repeated several times until the solvent became colorless. The product was then washed with acetonitrile and water and lyophilized to give **2** as a yellow powder.

5.3.3.2 Interfacial Synthesis of COF-300

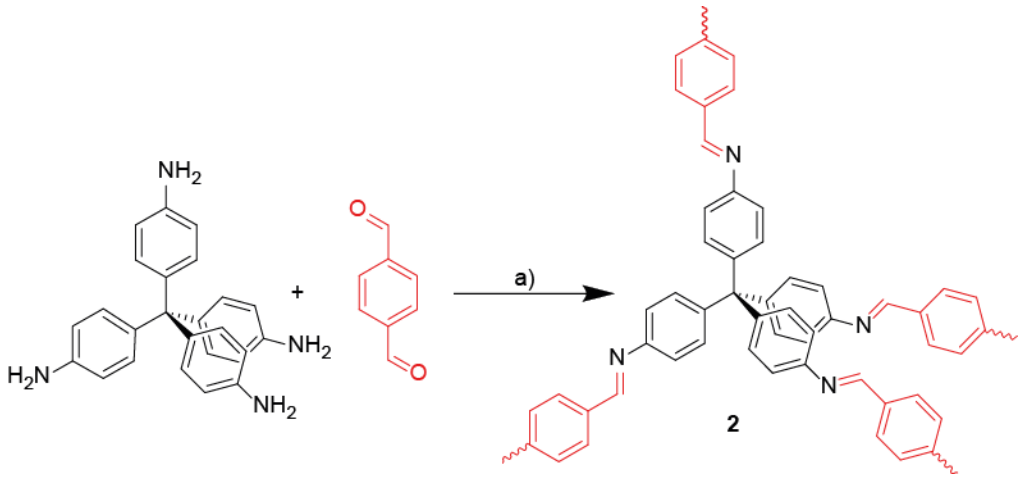

Scheme 5.4. Interfacial synthesis of COF-300 (2). Reagents and conditions: a) $Sc(OTf)_3$, H_2O, EA.

Interfacial synthesis of COF-300 (2). Tetrakis(4-aminophenyl)methane (10 mg, 0.026 mmol) and terephthalaldehyde (7.05 mg, 0.053 mmol) were dissolved in 15 ml ethyl acetate by heating to 60°C and rigorous stirring. The solution was gently deposited on top of aqueous $Sc(OTf)_3$ solution (0.03 M, 3 ml) in a 20 ml scintillation vial. The reaction was left at room temperature for 7 days to obtain a thin yellow layer at the interface of the two phases.

5.3.3.3 COF-300 Synthesis Utilizing Extraction of Scandium Triflate

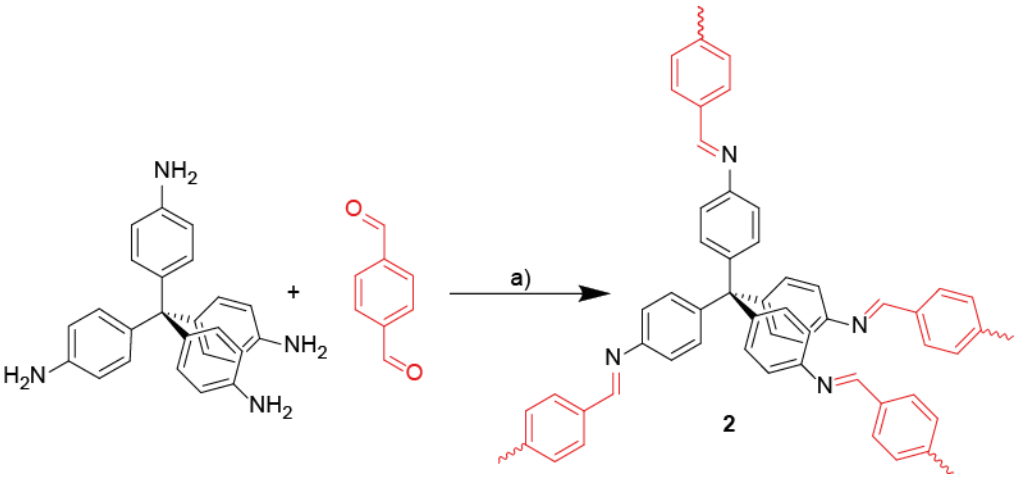

Scheme 5.5. Synthesis of COF-300 (2) utilizing extraction of $Sc(OTf)_3$. Reagents and conditions: a) $MeCN/CHCl_3$, $Sc(OTf)_3$, H_2O, 50°C.

Synthesis of COF-300 (2) utilizing extraction of $Sc(OTf)_3$. Tetrakis(4-aminophenyl)methane (10 mg, 0.026 mmol) was dissolved in chloroform (15 ml) by heating and stirring. To the solution, terephthalaldehyde (7.05 mg, 0.053 mmol), scandium triflate (51.7 mg, 0.105 mmol), and acetonitrile (15 ml) were added, and the solution was stirred at 50°C for two hours. The reaction was extracted with water to remove the scandium triflate, transferred to a "glass bomb" heavy wall pressure vessel and sealed, and subsequently heated to 50°C overnight. The reaction was extracted with water (150 ml) and brine solution (50 ml), and the yellow powder was isolated by centrifugation, washed with chloroform and acetonitrile, and dried by lyophilization.

5.3.4 High Pressure Transformation of COF-300

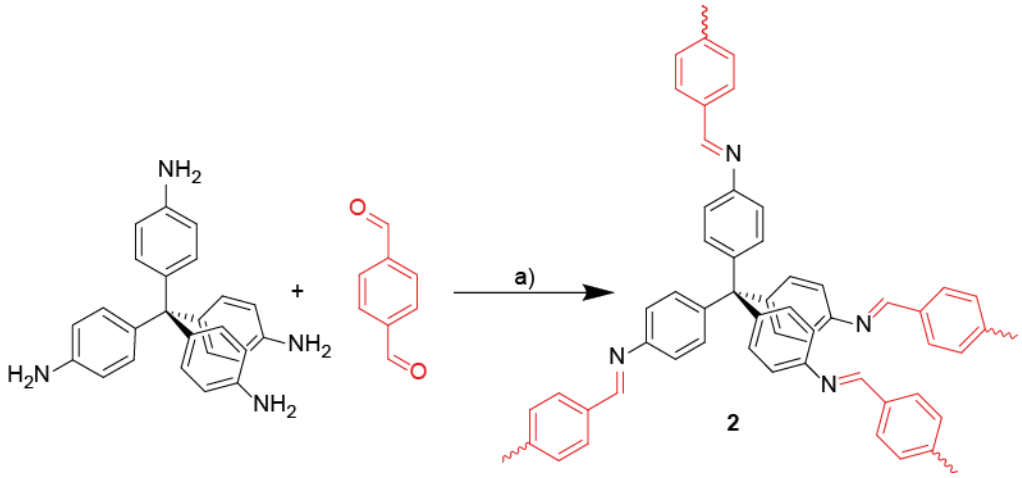

Scheme 5.6. Synthesis of COF-300 (2) for high pressure transformation. Reagents and conditions: a) $Sc(OTf)_3$, H_2O, 1,4-dioxane.

Synthesis of COF-300 (2) for high pressure transformation. A 48 ml "glass bomb" heavy wall pressure vessel was charged with tetrakis(4-aminophenyl)methane (80 mg. 0.21 mmol), terephthalaldehyde (56.4 mg, 0.42 mmol), 1,4-dioxane (10 ml), water (1.2 m, 79 equiv. per amine) and 168 µl of scandium triflate stock solution (0.2M in acetonitrile, 0.0336 mmol, 0.04 equiv. per amine). The reactor was capped, sealed, and heated to 50°C for 72 hours to yield a yellow powder. The solvent was removed under reduced pressure to give **2** with low crystallinity containing $Sc(OTf)_3$.

High pressure transformation of COF-300. The previously synthesized low crystallinity COF-300 containing $Sc(OTf)_3$ was placed in a pellet press. The powder was pressed at high pressures up to 10 metric tons, and elevated temperatures of 150°C were applied to certain samples. The high pressure was maintained for between 30 min and 5 days to obtain COF-300 pellets.

5.4 Results and Discussion

5.4.1 Reduction and Functionalization of Imine Bonds

The reduction of imine bonds in COF-300 was conducted utilizing sodium triacetoxyborohydride, a common imine reduction agent, following the procedures outlined in Scheme 5.2. FTIR characterization of the product, shown in Figure 5.1, revealed that reduction of imine bonds in COF-300, as the FTIR spectrum of the reduced COF-300 remains identical to that of the precursor COF-300. A second attempt at this reduction of the product from the first reduction reaction again did not produce tangible changes in the observed functional groups by FTIR. As such, this functionalization approach was not pursued further.

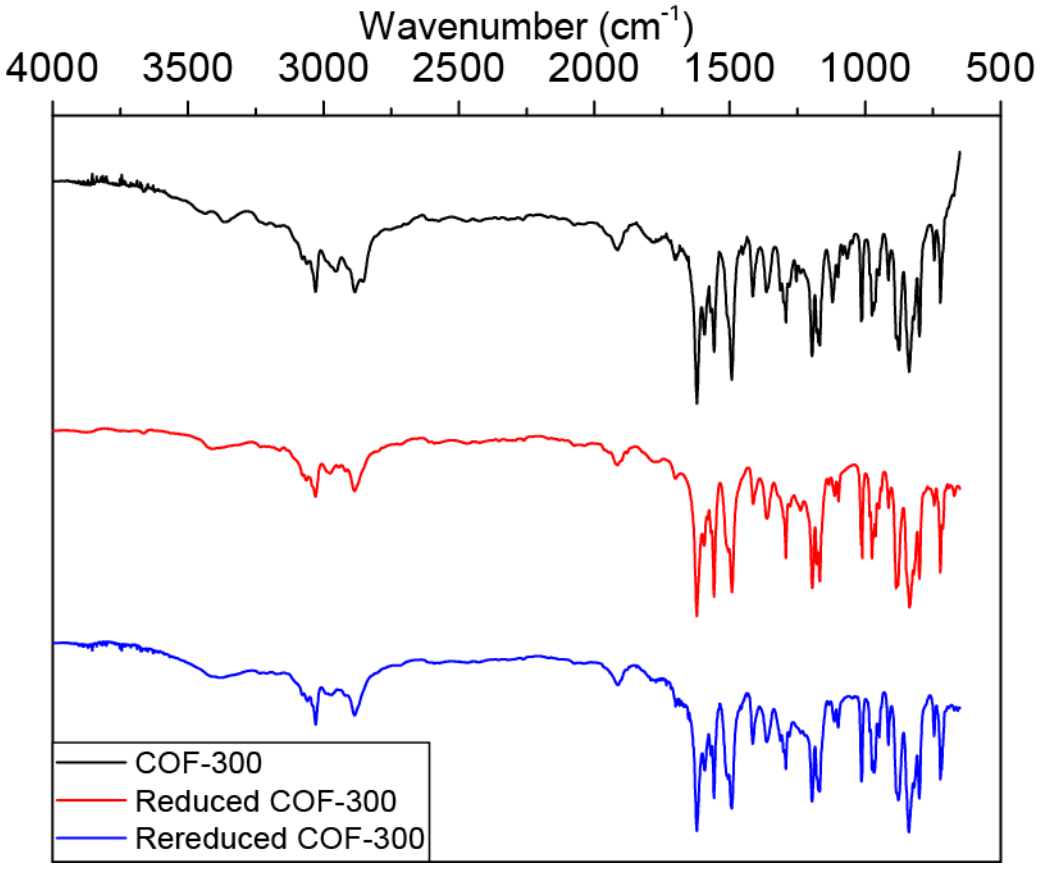

Figure 5.1. Comparison of FTIR spectra of normal COF-300, reduced COF-300, and twice-reduced COF-300.

5.4.2 Multiphase Synthesis of COF-300

5.4.2.1 Solubility and Synthesis Testing

For interfacial imine-linked 3D COF synthesis, there were two major considerations for solvent selection: 1) solubility of tetrakis(4-aminophenyl)methane (TAPM), whose bulky nature rendered its solubility poor in many common organic solvents; 2) immiscibility with water, necessary for the phase separation in interfacial synthesis. The miscibility with water of common organic solvents is mostly known, so the focus of the solvent screening process revolved around TAPM solubility, which was tested for every available organic solvent. The results are shown in Table 5.1. As expected, the general solubility of TAPM is quite poor and most of the solvents could not dissolve even a small quantity of TAPM. 1,4-dioxane, which is the solvent of choice of the synthesis of COF-300 and many other imine-linked 3D COFs, and acetonitrile were able to dissolve TAPM after rigorous mixing and leaving overnight. Unfortunately, 1,4-dioxane and acetonitrile are both miscible with water. Chloroform and ethyl acetate dissolved a small amount of TAPM upon heating and possess poor miscibility with water. No other solvents could dissolve TAPM to an observable extent. As such, chloroform and ethyl acetate were selected for further interfacial experimentation.

Table 5.1. Solubility of tetrakis(4-aminophenyl)methane in common organic solvents.

Solvent	Dissolved?
1,4-dioxane	Overnight
Acetonitrile	Overnight
Chlorobenzene	No
Chloroform	Heated
Dichloromethane	No
Diethyl ether	No
Ethyl acetate	Heated
Hexanes	No
Mesitylene	No
Toluene	No

5.4.2.2 Interfacial Synthesis

Chloroform and ethyl acetate were determined to be suitable candidates for interfacial synthesis owing to their low miscibility with water and ability to dissolve some TAPM at elevated temperatures. In addition, since the effectiveness of the 4:1 v/v 1,4-dioxane/mesitylene mixture was demonstrated for the interfacial synthesis of imine-linked 2D COFs[11], this solvent system was also employed for interfacial synthesis of 3D COFs. A summary of the solvent systems deemed suitable for interfacial synthesis is shown in Table 5.2.

Table 5.2. Solvent systems selected for interfacial synthesis and their water miscibility.

Solvent System	Water Miscibility
1,4-Dioxane/Mesitylene (4:1)	Partial
Ethyl acetate	Poor
Chloroform	Poor

For each solvent system, a simple dual-phase system in which TAPM and TA were dissolved in the organic phase and the scandium triflate ($Sc(OTf)_3$) was dissolved in the aqueous

phase would be conducive for interfacial synthesis, as illustrated in Figure 5.2. The monomer solutions were concentrated to increase availability at the interface, and $Sc(OTf)_3$ concentration was varied across a range of values. In addition, each interfacial synthesis was conducted in two approaches, a static approach in which the heavier phase was added first, and the lighter phase gently layered on top, and a phase diffusion approach in which the heavier phase was added second and slowly diffused through the lighter phase to reach the bottom to assess the impact of forming the interface more gradually. Summaries of static and phase diffusion dual-phase interfacial syntheses can be found in Table 5.3 and Table 5.4, respectively. Additionally, several heated interfacial syntheses were carried out utilizing the ethyl acetate system to assess the impact of elevated temperatures, as summarized in Table 5.5. All syntheses were conducted for a minimum of one week and were conducted at room temperature except those listed in Table 5.5.

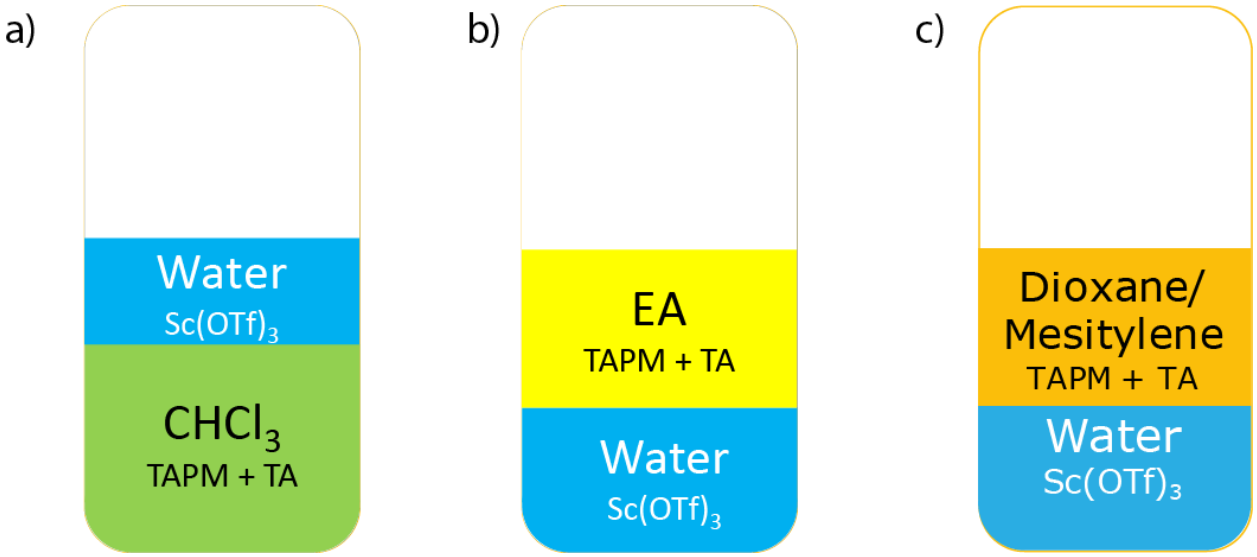

Figure 5.2. Illustration of dual-phase interfacial COF-300 synthesis setups utilizing a) chloroform; b) ethyl acetate, and c) dioxane/mesitylene as the organic phase.

Table 5.3. Summary of static dual-phase interfacial syntheses of COF-300.

Solvent	$Sc(OTf)_3$ (aq) Concentration (mM)	Water Volume (ml)	Moles of $Sc(OTf)_3$	$Sc(OTf)_3$ Amount (equiv. per amine)	Observation
Ethyl acetate	5	3	1.5E-05	0.143	Yellow sheet
Ethyl acetate	10	3	3.0E-05	0.285	Yellow sheet
Ethyl acetate	20	3	6.0E-05	0.571	Yellow sheet
Ethyl acetate	30	3	9.0E-05	0.856	Yellow sheet
Ethyl acetate	50	3	1.5E-04	1.427	Yellow sheet
Ethyl acetate	80	3	2.4E-04	2.283	Yellow sheet
Ethyl acetate	100	3	3.0E-04	2.854	Yellow sheet
Chloroform	10	3	3.0E-05	0.285	Yellow sheet
Chloroform	30	3	9.0E-05	0.856	Yellow sheet
Chloroform	50	3	1.5E-04	1.427	Yellow sheet
Chloroform	80	3	2.4E-04	2.283	Yellow sheet
Dioxane/Mesitylene	0.3	0.375	1.1E-07	0.001	Gelling in aqueous phase
Dioxane/Mesitylene	1.4	0.375	5.3E-07	0.005	Gelling in aqueous phase
Dioxane/Mesitylene	2.8	0.375	1.1E-06	0.010	Gelling in aqueous phase
Dioxane/Mesitylene	5.6	0.375	2.1E-06	0.020	Gelling in aqueous phase
Dioxane/Mesitylene	11.2	0.375	4.2E-06	0.040	Gelling in both phases
Dioxane/Mesitylene	16.8	0.375	6.3E-06	0.060	Gelling in both phases
Dioxane/Mesitylene	0.0	3	1.1E-07	0.001	Nothing
Dioxane/Mesitylene	0.2	3	5.3E-07	0.005	Yellow sheet
Dioxane/Mesitylene	0.7	3	2.1E-06	0.020	Yellow sheet
Dioxane/Mesitylene	2.1	3	6.3E-06	0.060	Yellow sheet

Table 5.4. Summary of dual phase interfacial syntheses of COF-300 utilizing phase diffusion.

Solvent	$Sc(OTf)_3$ (aq) Concentration (mM)	Water Volume (ml)	Moles of $Sc(OTf)_3$	$Sc(OTf)_3$ Amount (equiv. per amine)	Observation
Ethyl acetate	5	3	1.50E-05	0.143	Yellow sheet
Ethyl acetate	10	3	3.00E-05	0.285	Yellow sheet
Ethyl acetate	20	3	6.00E-05	0.571	Yellow sheet
Ethyl acetate	30	3	9.00E-05	0.856	Black sheet that collapsed
Ethyl acetate	50	3	1.50E-04	1.427	Black sheet that collapsed
Ethyl acetate	80	3	2.40E-04	2.283	Black sheet that collapsed
Dioxane/Mesitylene	0.3	0.375	1.05E-07	0.001	Yellow sheet
Dioxane/Mesitylene	1.4	0.375	5.26E-07	0.005	Yellow sheet
Dioxane/Mesitylene	5.6	0.375	2.10E-06	0.020	Yellow sheet
Dioxane/Mesitylene	16.8	0.375	6.31E-06	0.060	Yellow sheet

Table 5.5. Summary of heated dual-phase interfacial syntheses of COF-300.

Solvent	$Sc(OTf)_3$ (aq) Concentration (mM)	Water Volume (ml)	Moles of $Sc(OTf)_3$	$Sc(OTf)_3$ Amount (equiv. per amine)
Ethyl acetate	5	6	0.00003	0.04
Ethyl acetate	10	6	0.00006	0.07
Ethyl acetate	20	6	0.00012	0.14

For all of the syntheses listed in Table 5.3-Table 5.5, the trials which produced gelling or a thin sheet at the interface were characterized by XRD, and unfortunately these products were consistently amorphous across the entire range of solvents, $Sc(OTf)_3$ concentrations, and temperatures. The representative XRD spectra shown for the ethyl acetate system in Figure 5.3 and for the chloroform system in Figure 5.4, are completely flat, with not even a hint of a peak. Additionally, many of the trials in dioxane/mesitylene resulted in gelling in the aqueous phase or both phases, attributable to the miscibility between the aqueous and organic phases that provided

ample availability of water and $Sc(OTf)_3$ throughout the organic phase, thus satisfying all of the reaction conditions necessary for imine-linked network formation away from the interface. This was in stark contrast to the literature report for interfacial synthesis of 2D COFs, which stated that a crystalline COF thin film formed cleanly the interface between these two phases[11].

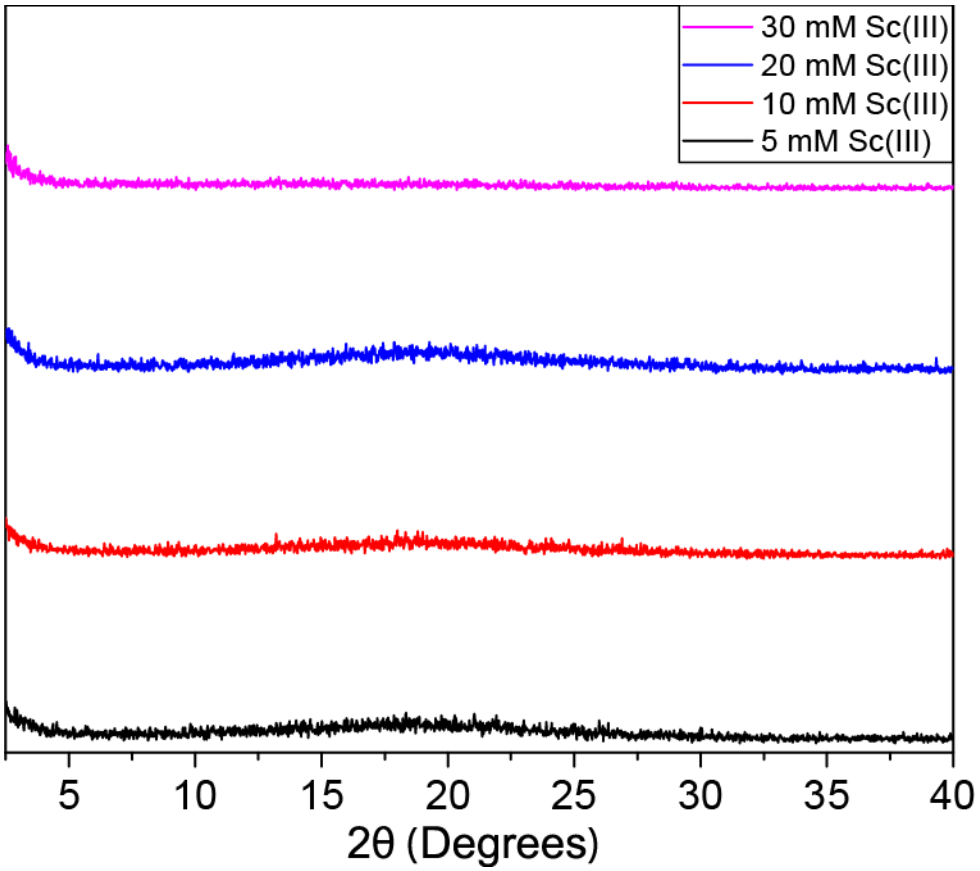

Figure 5.3. Representative XRD spectra of COF-300 interfacially-synthesized employing ethyl acetate as the organic layer in a dual-phase system.

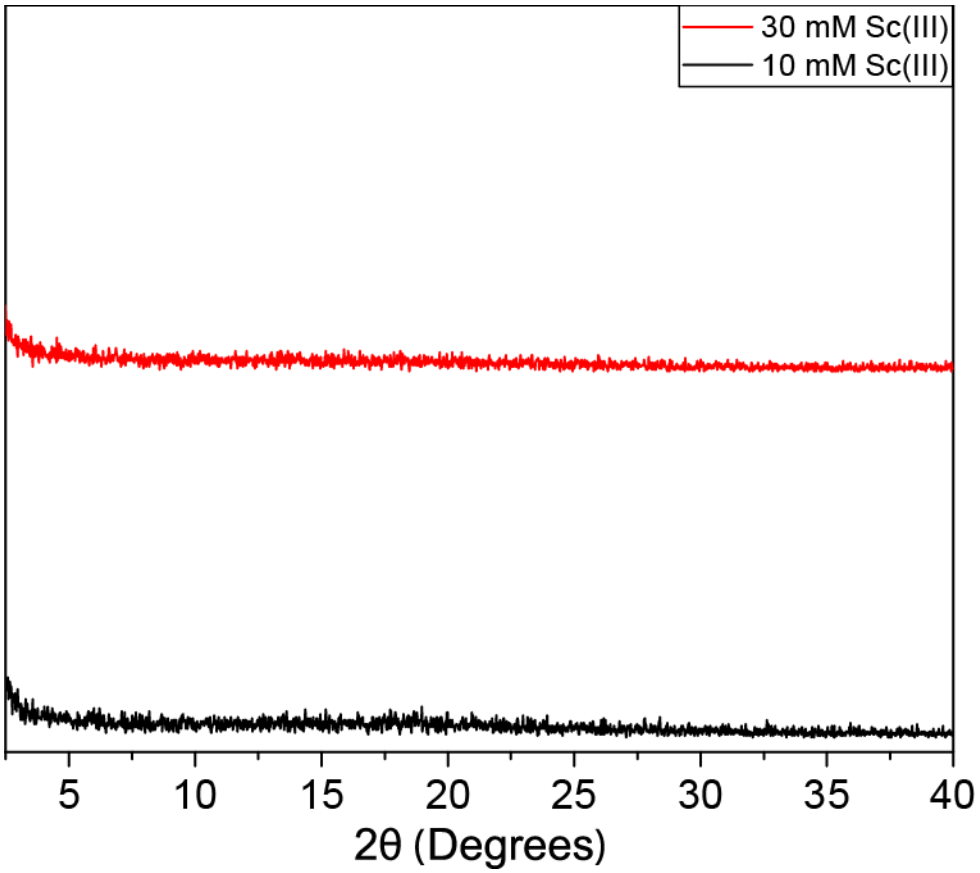

Figure 5.4. Representative XRD spectra of COF-300 interfacially-synthesized employing chloroform as the organic layer in a dual-phase system.

To better utilize the the relatively high solubility of TAPM in dioxane and circumvent the lack of clearly defined interface, a tri-phase system was designed, as shown in Figure 5.5, the first organic layer consisted of TAPM dissolved in a 4:1 v/v dioxane/mesitylene mixture, and the second organic layer was a solution of TA in chloroform. A thin aqueous layer containing $Sc(OTf)_3$ separated the two organic layers, forming a tri-phase system in which the expected mixing of dioxane/mesitylene and water would lead to the presence of all necessary reaction components (TAPM, TA, $Sc(OTf)_3$, and water) at the water-chloroform interface. The trials were performed at room temperature across a range of $Sc(OTf)_3$ concentrations and several different aqueous layer thicknessesfor one week, as summarized in Table 5.6. A yellow sheet at the water-

chloroform interface was obtained in all syntheses, but as highlighted by the representative XRD spectra in Figure 5.6, the products were once again consistently amorphous.

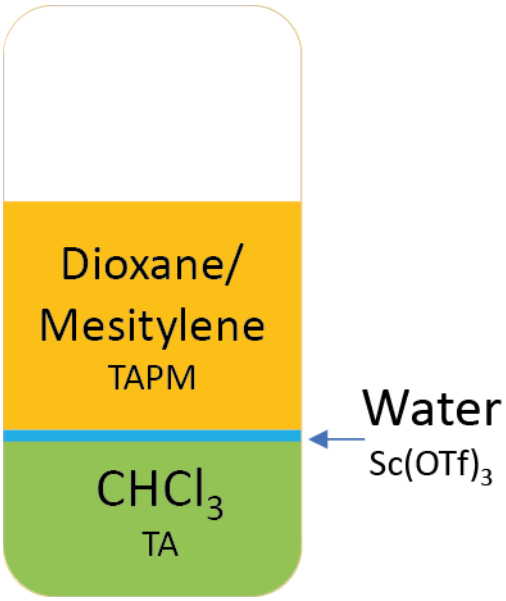

Figure 5.5. Illustration of tri-phase interfacial COF-300 synthesis setup.

Table 5.6. Summary of tri-phase interfacial syntheses of COF-300.

$Sc(OTf)_3$ (aq) Concentration (mM)	Water Volume (ml)	Moles of $Sc(OTf)_3$	$Sc(OTf)_3$ Amount (equiv. per amine)	Observation
1.1	0.1	1.05E-07	0.001	Yellow sheet
5.3	0.1	5.26E-07	0.005	Yellow sheet
21.0	0.1	2.10E-06	0.020	Yellow sheet
63.1	0.1	6.31E-06	0.060	Yellow sheet
1.8	0.3	5.26E-07	0.005	Yellow sheet
0.5	1	5.26E-07	0.005	Yellow sheet

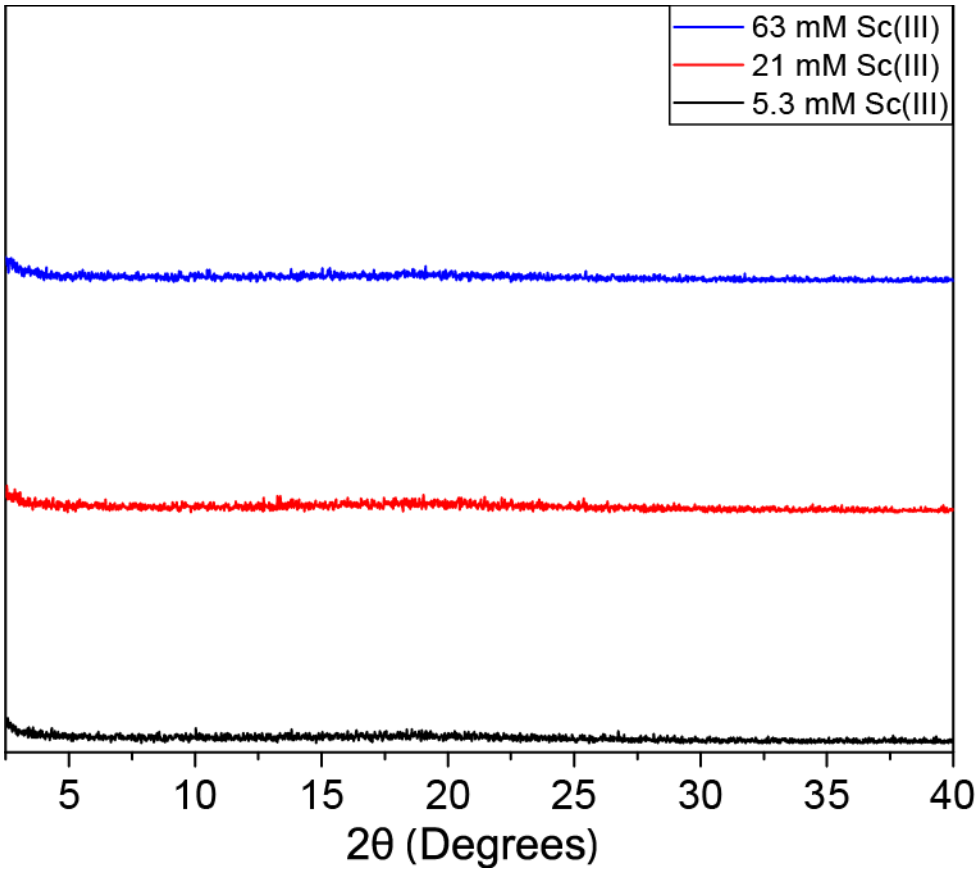

Figure 5.6. Representative XRD spectra of COF-300 interfacially-synthesized employing the tri-phase system.

5.4.2.3 Scandium Triflate Extraction

Extraction of $Sc(OTf)_3$ from COF-300 synthesis was initially performed utilizing chloroform, which is more hydrophobic than ethyl acetate, following the procedures outlined in Scheme 5.5, which yielded only amorphous material. It was hypothesized that the high hydrophobicity of chloroform was a hindrance rather than a boon, resulting in insufficient water content, which was identified as a crucial component of imine-linked 3D COF synthesis in Chapter 3. In contrast, ethyl acetate is partially miscible with water, and could be a promising alternative to provide sufficient water after the extraction. Utilizing the ternary phase diagram in Figure 5.7, an extraction system for ethyl acetate was designed such that the solvent system would separate

into two heterogeneous phases, one water phase rich to be extracted away and one water poor phase to remain as the reaction solvent. Unfortunately, several attempted reliably produced amorphous products, as shown by the representative XRD spectra in Figure 5.8.

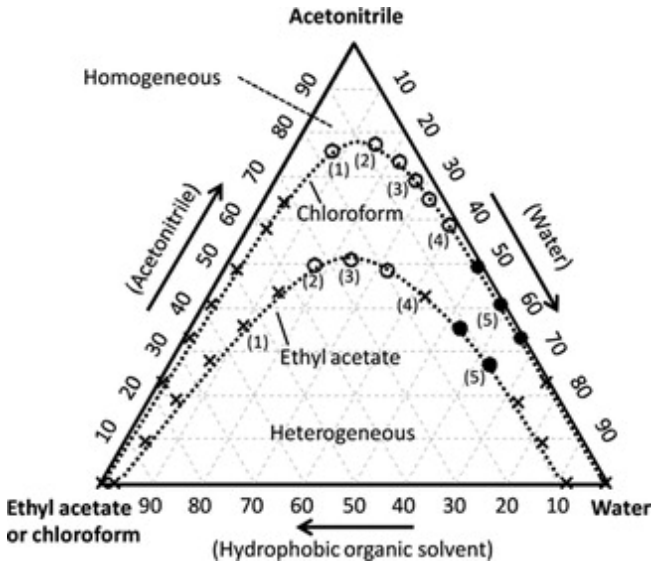

Figure 5.7. Ternary phase diagram for ethyl acetate/acetonitrile/water and chloroform/acetonitrile/water systems at 20°C[14].

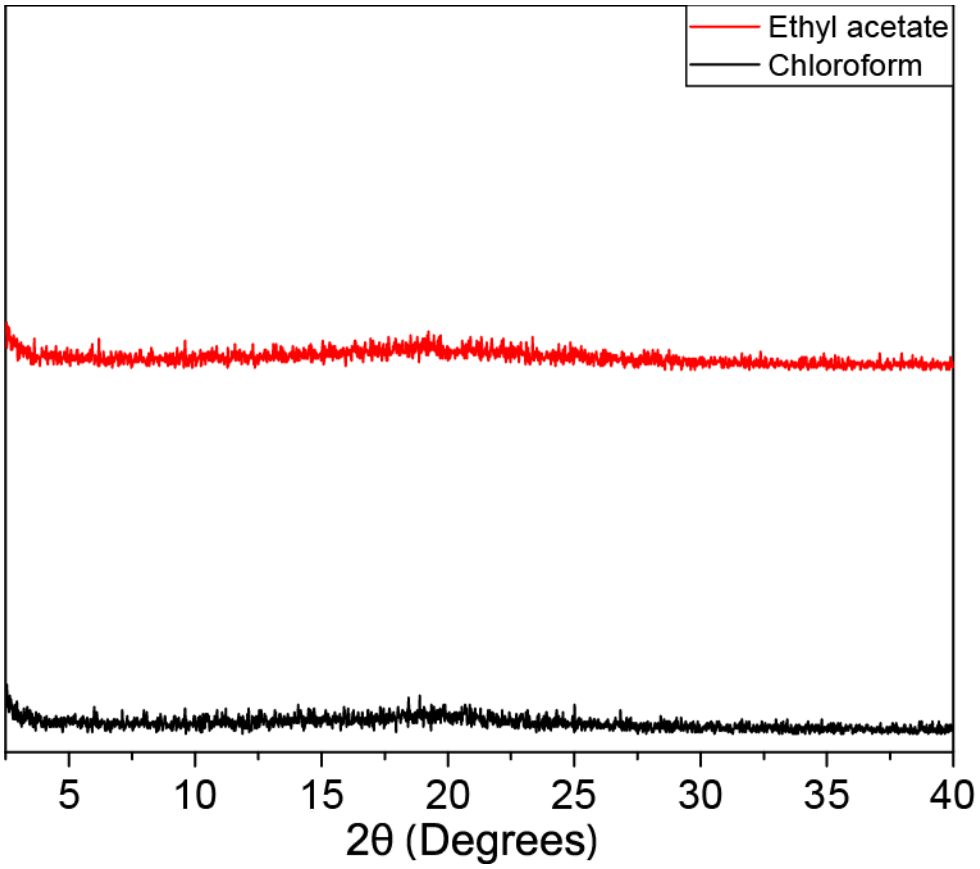

Figure 5.8. Representative XRD spectra of COF-300 synthesized *via* the extraction of $Sc(OTf)_3$.

5.4.3 High Pressure Transformation of COF-300

COF samples with low or no observed crystallinity were prepared following the procedures outlined in Scheme 5.6, and subsequently subject to an array of pressures, temperatures, and processing durations on a pellet press. The crystallinity of the obtained pellets was characterized by XRD and compared to the spectrum of COF-300 in Figure 5.9. The application of high-pressure processing revealed peaks of varying height and width, but consistently at angles matching those of the peaks in the COF-300 spectrum, suggesting that some extent of crystallinity had been introduced into these pellets.

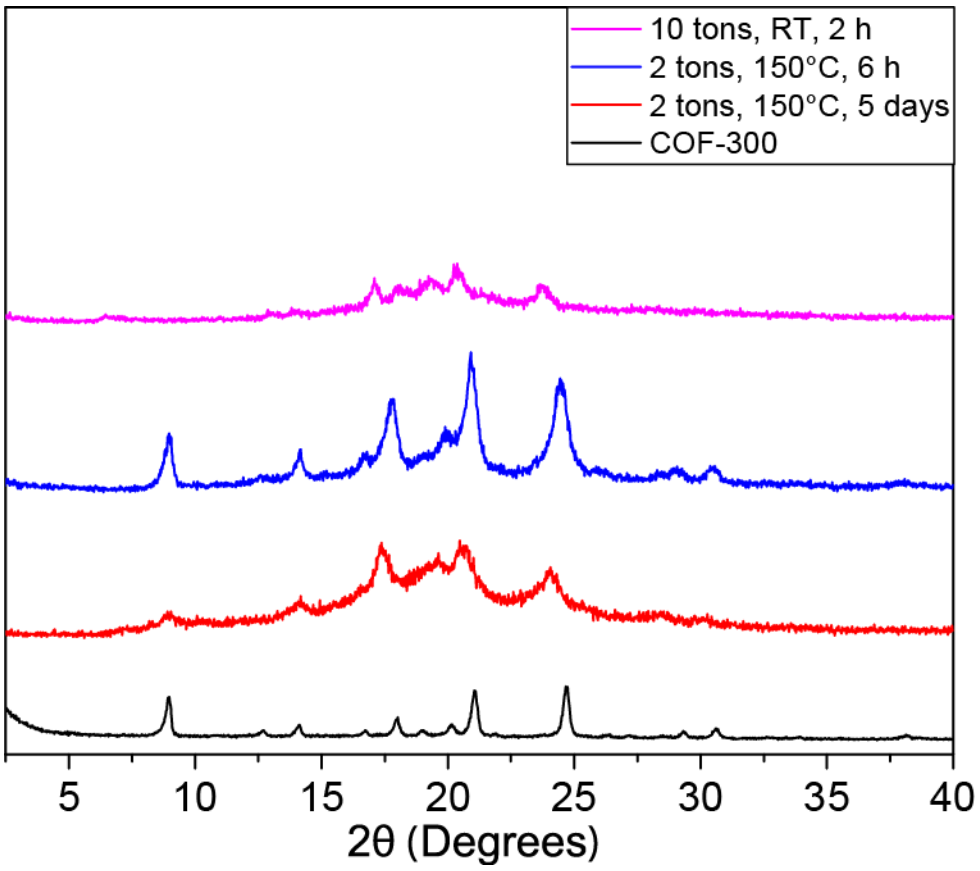

Figure 5.9. XRD spectra of COF pellets processed at various conditions compared to COF-300.

As the pellets characterized in Figure 5.9 were processed at quite different conditions but produced XRD spectra that exhibited similar peak positions, it was unclear whether pressing conditions exerted an impact on the crystallinity of the pellet. The similarity of the two spectra in Figure 5.10 and Figure 5.11, which show comparison of the same COF samples processed at different pressing conditions, suggest that varying pressure, temperature, and/or pressing duration exerts no effect on the crystallinity of the obtained COF pellet.

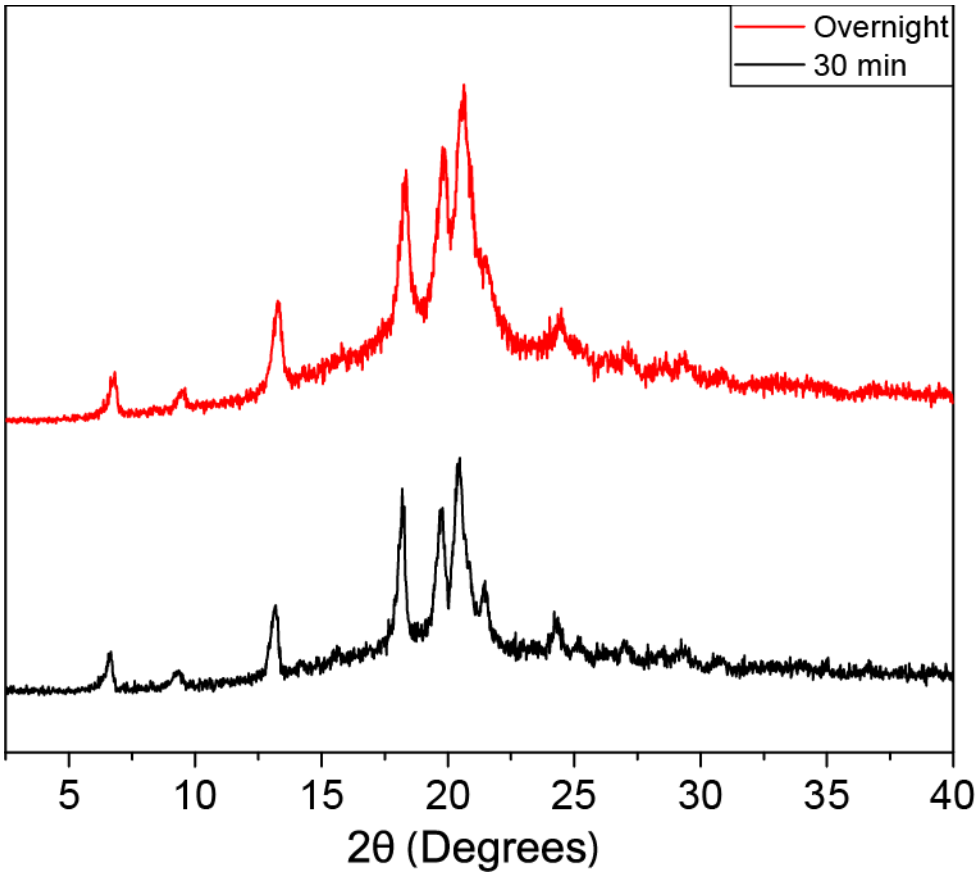

Figure 5.10. Comparison of XRD spectra of the same COF sample pressed at 5 metric tons of pressure for 30 minutes and overnight.

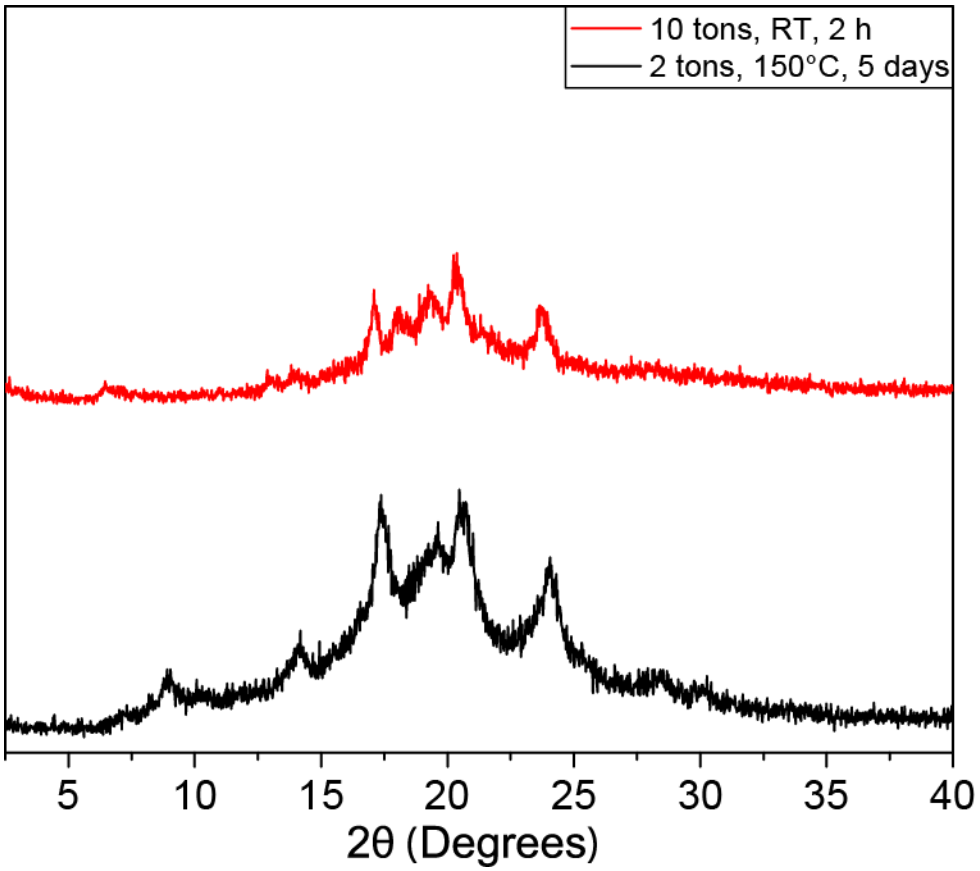

Figure 5.11. Comparison of XRD spectra of the same COF sample pressed at 2 metric tons of pressure and 150°C for 5 days and 10 metric tons of pressure and room temperature for 2 hours.

Additionally, the reversibility of the observed crystallinity changes was investigated by repeatedly pressing and grinding up the same COF sample, and the crystallinity of the pellets and powders were characterized by XRD and are shown in Figure 5.12. The crystallinity imbued by pressing the powder into a pellet was not permanent and grinding the pellet into powder reverted it completely to its original amorphous state. The results of a second cycle of pellet pressing and grinding produced results consistent with the first cycle. The only literature report of pellet pressing of COFs was focused on 2D COFs and found that directional orientation of the 2D COF pellets relative to the X-ray beam affected the XRD spectra[15]. The authors also conducted a single

trial on a 3D COF, and found that pressing a crystalline 3D COF removed all traces of crystallinity, which is directly opposite what has been observed here. Nevertheless, the reversibility of the crystallinity changes displayed in Figure 5.12 suggest the possibility that the pellet pressing may be imparting some form of directional or orientational change in the structure of the COF pellet compared to the powder that is conducive for showing up in XRD characterization.

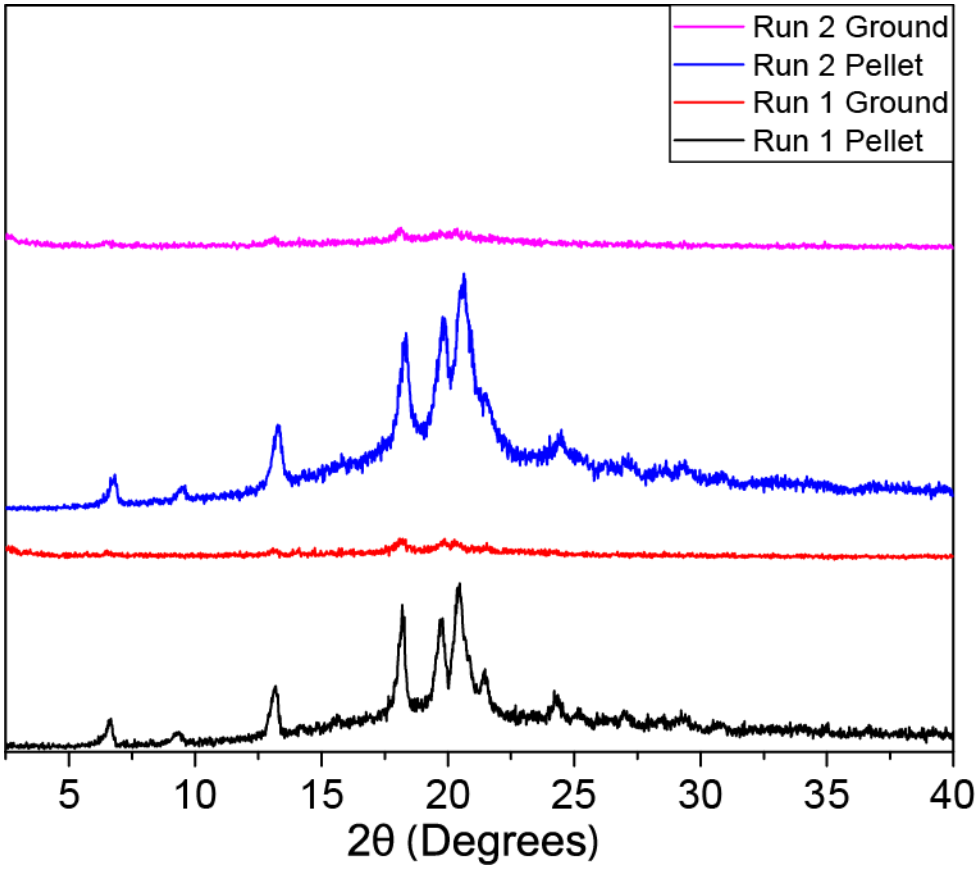

Figure 5.12. Comparison of XRD spectra of the same COF sample pressed into pellet and ground up repeatedly.

As described in the Experimental Procedures, the COF powders utilized for pellet press processing retained their the $Sc(OTf)_3$ during post-synthesis work-up as a means to imbue additional driving forces for rearrangement during pellet pressing. As such, the amount of

$Sc(OTf)_3$ could also influence the crystallinity of the pellets. COF samples synthesized with different $Sc(OTf)_3$ loading were subject to pellet pressing, and the XRD spectra of the obtained pellets are shown in Figure 5.13. There does not seem to be an obvious correlation between $Sc(OTf)_3$ loading and the shape of the resultant XRD spectrum.

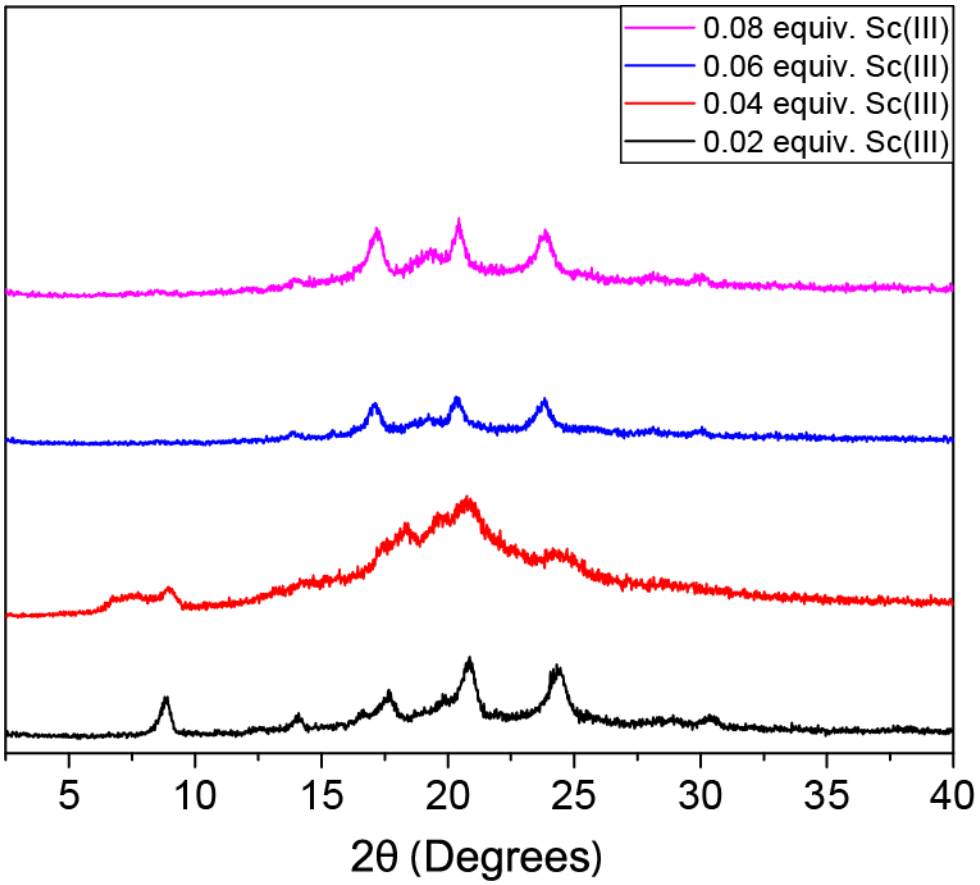

Figure 5.13. Comparison of XRD spectra of COF-300 pellets pressed from amorphous powder containing different amounts of $Sc(OTf)_3$.

5.5 Conclusions

The reduction of the imine bonds in COF-300 to secondary amines was explored as an alternative method of functionalizing COF-300, but unfortunately the successful reduction of the imine bonds could not be confirmed by FTIR after repeated reduction reactions. The multiphase

synthesis of COF-300 was extensively investigated as an alternative synthetic method. Dual-phase interfacial syntheses utilizing chloroform, ethyl acetate, and dioxane/mesitylene as well as a dioxane/mesitylene-water-chloroform tri-phase system were attempted, and extraction of $Sc(OTf)_3$ was also shown. Unfortunately, all of these efforts ultimately led to amorphous products with no hint of crystallinity.

The high-pressure transformation of amorphous frameworks by pellet pressing was also investigated, and it was found that varying the pressure, temperature, and duration at which the pressing occurred did not impact pellet crystallinity, and that pellet pressing and grinding the pellet into powder was a reversible process. As such, it was theorized that pellet pressing imparted some form of orientation change in the pellet compared to the powder that revealed crystalline peaks in the XRD spectra. In addition, the effect of $Sc(OTf)_3$ loading in the amorphous powder on crystallinity of the pellet was assessed, and no direct correlation between the two factors was observed.

5.6 References

1. Guan, X. *et al.* Fast, Ambient Temperature and Pressure Ionothermal Synthesis of Three-Dimensional Covalent Organic Frameworks. *J. Am. Chem. Soc.* **140**, 4494–4498 (2018).
2. Ma, T. *et al.* Single-crystal x-ray diffraction structures of covalent organic frameworks. *Science* **361**, 48–52 (2018).
3. Ma, X. & Scott, T. F. Approaches and challenges in the synthesis of three-dimensional covalent-organic frameworks. *Commun. Chem.* **1**, 98 (2018).
4. Han, X., Huang, J., Yuan, C., Liu, Y. & Cui, Y. Chiral 3D Covalent Organic Frameworks for High Performance Liquid Chromatographic Enantioseparation. *J. Am. Chem. Soc.* **140**, 892–895 (2018).
5. Ritchie, L. K., Trewin, A., Reguera-Galan, A., Hasell, T. & Cooper, A. I. Synthesis of COF-5 using microwave irradiation and conventional solvothermal routes. *Microporous Mesoporous Mater.* **132**, 132–136 (2010).
6. Singh, V., Jang, S., Vishwakarma, N. K. & Kim, D.-P. Intensified synthesis and post-synthetic modification of covalent organic frameworks using a continuous flow of microdroplets technique. *NPG Asia Mater.* **10**, e456 (2018).
7. Bisbey, R. P., DeBlase, C. R., Smith, B. J. & Dichtel, W. R. Two-dimensional Covalent Organic Framework Thin Films Grown in Flow. *J. Am. Chem. Soc.* **138**, 11433–11436 (2016).

8. Peng, Y. *et al.* Room Temperature Batch and Continuous Flow Synthesis of Water-Stable Covalent Organic Frameworks (COFs). *Chem. Mater.* **28**, 5095–5101 (2016).

9. Jiang, Y. *et al.* Green, scalable and morphology controlled synthesis of nanofibrous covalent organic frameworks and their nanohybrids through a vapor-assisted solid-state approach. *J. Mater. Chem. A* **2**, 8201–8204 (2014).

10. Medina, D. D. *et al.* Room Temperature Synthesis of Covalent–Organic Framework Films through Vapor-Assisted Conversion. *J. Am. Chem. Soc.* **137**, 1016–1019 (2015).

11. Matsumoto, M. *et al.* Lewis-Acid-Catalyzed Interfacial Polymerization of Covalent Organic Framework Films. *Chem* **4**, 308–317 (2018).

12. Feng, X., Ding, X. & Jiang, D. Covalent organic frameworks. *Chem. Soc. Rev.* **41**, 6010–6022 (2012).

13. Baldwin, L. A., Crowe, J. W., Pyles, D. A. & McGrier, P. L. Metalation of a Mesoporous Three-Dimensional Covalent Organic Framework. *J. Am. Chem. Soc.* **138**, 15134–15137 (2016).

14. Fujinaga, S., Hashimito, M. & Tsukagoshi, K. Investigation of the Composition for a Ternary Solvent System in Tube Radial Distribution Chromatography. *J. Liq. Chromatogr. Relat. Technol.* **38**, 600–606 (2015).

15. Vazquez-Molina, D. A. *et al.* Mechanically Shaped Two-Dimensional Covalent Organic Frameworks Reveal Crystallographic Alignment and Fast Li-Ion Conductivity. *J. Am. Chem. Soc.* **138**, 9767–9770 (2016).

Chapter 6
Concluding Remarks and Future Directions

6.1 Summary of Research

Three-dimensional (3D) covalent organic frameworks (COFs) possess huge potential for a variety of applications due to their unique combination of crystalline and organic traits compared to conventional nanoporous materials such as zeolites and exceptionally high internal surface areas and pore sizes compared to two-dimensional (2D) COFs[1]. Unfortunately, the challenges in 3D COF development, namely the "crystallization problem", deficient systematic understanding, limited diversity in synthetic approaches, and dearth of functionalization and application have significantly hindered the progress in the field compared to that of 2D COFs. Therefore, this dissertation focused on addressing these hurdles through the development of a novel synthetic method utilizing an alternative catalyst addressed the crystallization problem and improved fundamental understanding of COF synthesis, investigation of functionalization and modification of 3D COFs for future applications, and exploration of alternative methods of synthesis and modification.

The synthesis of 3D COFs has been an opaque process since such the first reports of such structures[2,3], and subsequent investigations of 3D COFs mostly followed the solvothermal approach from these earlier reports that were mostly established empirically with no deeper insights into the mechanisms, kinetics, or equilibrium of the reactions. In Chapter 2, tetrakis(4-aminophenyl)methane (TAPM), the amine monomer that many imine-linked 3D COFs are

constructed from, as well as tetrakis(4-formylphenyl)methane (TFPM), the tetra-aldehyde analog of TAPM, were successfully synthesized. An improved degassing procedure was developed for solvothermal synthesis that allowed simple degassing, vessel sealing, and product retrieval without destroying the reaction vessel utilizing heavy wall glass pressure vessels and reverse septum sealing. Utilizing this technique, the solvothermal syntheses of COF-300 and COF-320 were successfully conducted, providing frameworks with comparable characteristics as those reported, which was confirmed by powder X-ray diffraction (PXRD), Fourier transform infrared spectroscopy (FTIR), and scanning electron microscopy (SEM) characterization[3,4]. The synthesis of a novel COF constructed from TAPM and TFPM was explored. COF-300, as an archetypal imine-linked 3D COF, would serve as the platform of subsequent synthesis and functionalization studies in later chapters. The insights gained and difficulties encountered from solvothermal synthesis informed later efforts to develop alternative methods of synthesis.

3D COFs suffer extensively from the "crystallization problem", which states that the constituent species of the system quickly react and form strong covalent bonds owing to fast kinetics and lack the driving force towards bond breakage and mobility for rearrangement necessary to self-assemble into the desired crystalline structure[5]. In addition, little fundamental understanding has been offered for the synthesis of 3D COFs. In Chapter 3, an alternative method of synthesis for imine-linked 3D COF-300 was developed utilizing scandium triflate ($Sc(OTf_3)$, a significantly more effective catalyst for imine formation and exchange than the acetic acid that was used in solvothermal synthesis. A systematic investigation of relevant reaction parameters temperature, $Sc(OTf)_3$ loading, and water content identified the ideal combination of reaction conditions at each temperature for optimal product crystallinity, demonstrated the capability of synthesizing highly crystalline COF-300 at room temperature, and elucidated the role of these

parameters on the reaction equilibrium and product crystallinity. In addition, the degassing procedure in the established solvothermal synthesis method was demonstrated to be wholly unnecessary. The $Sc(OTf)_3$ catalyzed synthesis method and insights gained in this chapter will serve to inform future studies in the space of imine-linked 3D COFs.

One advantage COFs offer over conventional nanoporous materials is chemical tunability and structural diversity. As the entire structure is an organic polymer, chemistry can be applied to the COF structure to modify its properties and characteristics according to the intended application. The most common method of alteration is post-synthetic modification (PSM) of the COF backbone to introduce desired features; however, the backbones of most COFs such as COF-300 lack the reactive sites needed to easily conduct PSM. As such, embedding these reactive sites into the constituent monomers prior to COF synthesis has found practical utility in 2D COFs[6–8], but has not seen extensive investigation in 3D COFs. In Chapter 4, the synthesis of several functionalized aldehyde monomers was conducted utilizing a variety of chemistries. n-Butyllithium (n-BuLi) chemistry proved impractical for this purpose, whereas a Sommelet reaction and bromination utilizing N-bromosuccinimide produced functionalized terephthalaldehyde monomers containing methoxy, hydroxy, and bromide functionalities. These monomers were subsequently employed for functionalized COF-300 synthesis utilizing both the solvothermal and the $Sc(OTf)_3$ catalyzed methods. Unfortunately, no combination of reaction conditions and functionalized aldehyde was able to produce a crystalline framework. Additionally, the protection of the hydroxy groups in 2,5-dihydroxyterephthalaldehyde (DHTA) with the bulky tertbutyldimethylsilyl (TBDMS) protecting group was conducted to explore the reduction of interpenetration within the COF pores, but unfortunately the protection reaction did not proceed as anticipated. The likely culprit responsible for the difficulties in assembling a crystalline framework and protecting the hydroxy

groups was the additional steric hindrance from the presence of pendant groups on the same phenyl ring.

Compared to 2D COFs, which have been synthesized *via* a range of new methods such as microwave synthesis[9], flow synthesis[10–12], and vapor-assisted synthesis[13,14], 3D COF syntheses have been limited to more conventional chemistry. Therefore, expanding the 3D COF synthesis portfolio was imperative in advancing progress in the field to match its 2D counterpart. In Chapter 5, three alternative methods of synthesis and functionalization were explored. The post-synthetic reduction of imines to amides in COF-300 was attempted, though FTIR analysis did not reveal any change in the imine functionalities present in COF-300. The multiphase $Sc(OTf)_3$ synthesis of COF-300 was investigated. Four different organic solvents or solvent systems for interfacial synthesis were employed based on solubility and water miscibility, and a variety of conditions were examined. Although thin films were obtained at the interface in many trials, they were consistently amorphous. The extraction of excess $Sc(OTf)_3$ from ethyl acetate and chloroform was performed as an alternative multi-phase synthesis method, but the product was once again amorphous. Lastly, high pressure was applied to COF powder which were amorphous or moderately crystalline utilizing a pellet press, and the resultant pellets exhibited PXRD features that resembled peaks to various extents that were not previously present and matched well with the peak positions of COF-300. This emergent crystallinity was reversible and disappeared when the pellet was ground into powder. Additionally, there were no observable trends in the shapes of PXRD spectra of the pellets as a function of alterations in the pressing conditions or COF synthesis conditions.

In conclusion, this dissertation has attempted to address the most pressing challenges facing 3D COFs today. The development of the $Sc(OTf)_3$ catalyzed synthesis, which allows the synthesis

of COF-300 at room temperature, provides a much needed alternative to the conventional solvothermal method and unlocks potential applications which were not possible at reaction temperatures of 120°C. The insights into how reaction parameters impact the equilibrium and framework crystallinity improves the fundamental understanding of 3D COF synthesis that is currently lacking, and this method should find broad applicability in the realm of imine-linked 3D COFs. Subsequent attempts at synthesizing functionalized 3D COFs and alternative synthesis and modification methods, although unsuccessful, will as a baseline for future investigation.

6.2 Future Work

The research in this dissertation has advanced the progress of the field of 3D COFs and revealed new opportunities for investigation. These potential future directions are briefly discussed in this section.

In Chapter 2, the synthesis of imine-linked 3D COFs COF-300 and COF-320 were synthesized according to literature procedure, and improved degassing procedures were developed for the solvothermal synthesis method, establishing the imine-linked COFs that would be used for the subsequent chapters. Aside from the imine linkage, there are several linkages that have been utilized for 2D COF construction that have yet to see similar usage for 3D COFs. One such linkage is the azine linkage, which is formed by the reaction of a hydrazine with an aldehyde. As the chemistry bears similarities to imine chemistry, the solvothermal approach utilizing acetic acid has been demonstrated to be conducive for crystalline 2D framework formation[15]. A proposed pathway for synthesizing two variations of the hydrazine analog of TAPM can be found in Scheme 6.1. These tetra-hydrazines can subsequently be employed for the synthesis of the first azine-

linked 3D COF, as shown in Scheme 6.2, and would propel the field of 3D COFs towards parity with 2D COFs.

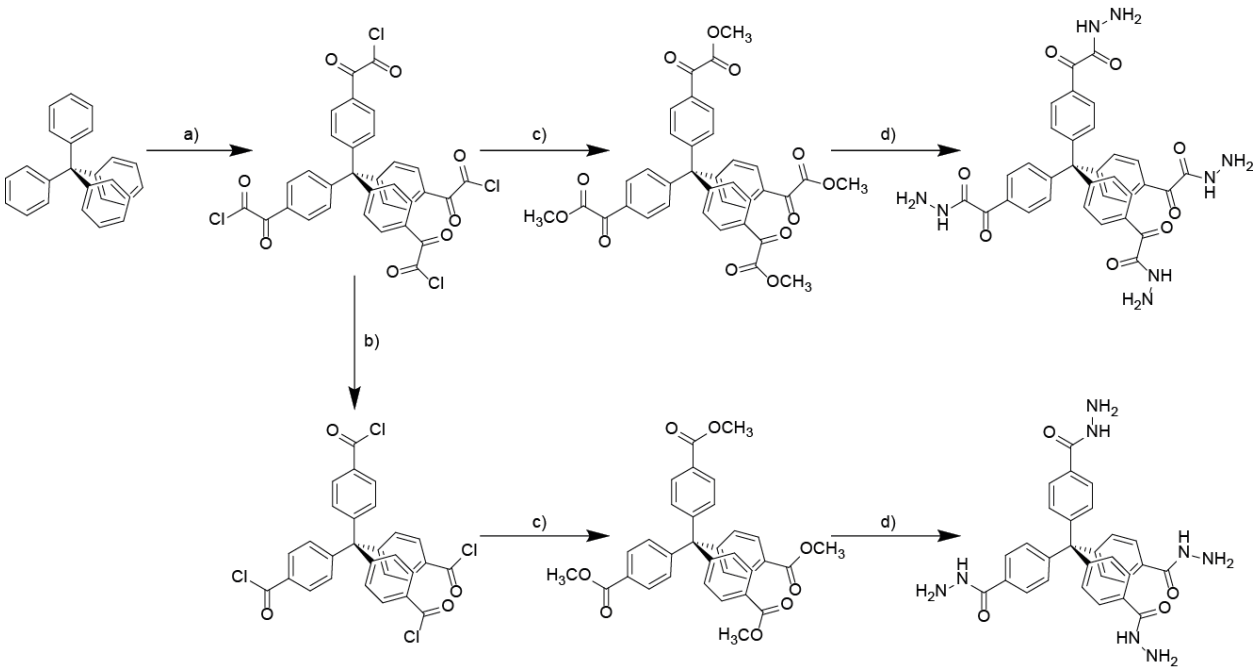

Scheme 6.1. Synthesis pathway for tetra-hydrazine monomers. Reagents and condition: a) $AlCl_3/(COCl)_2$; b) heat; c) CH_3OH; d) hydrazine hydrate, EtOH, reflux.

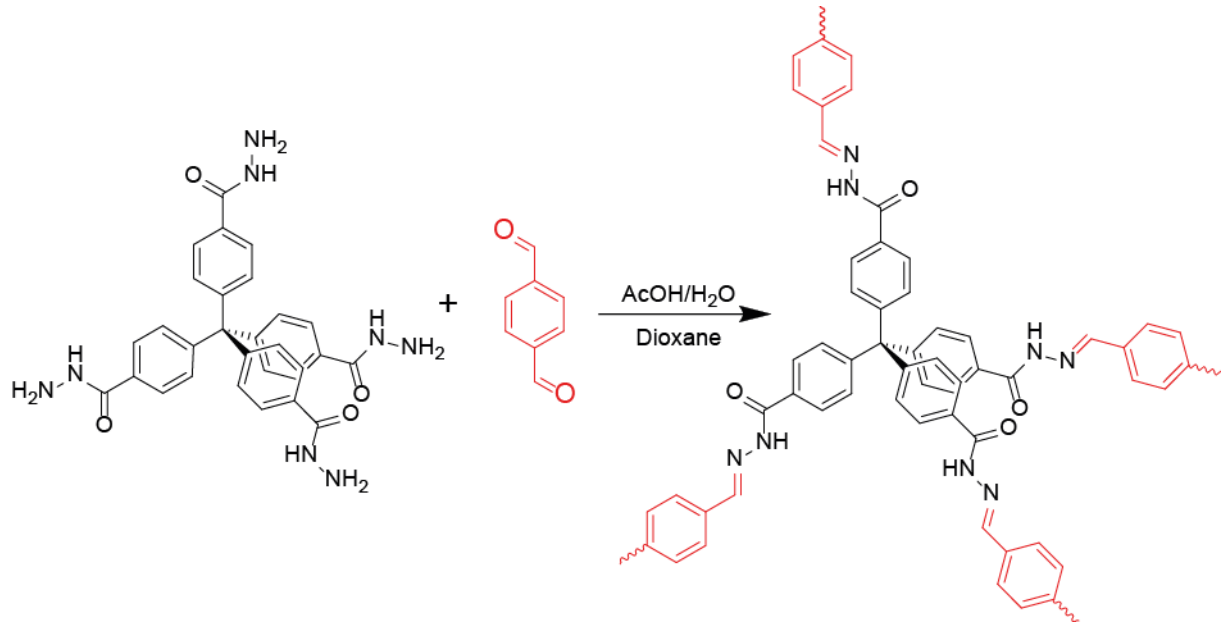

Scheme 6.2. Synthesis of azine-linked 3D COF utilizing tetra-hydrazine monomers.

The $Sc(OTf)_3$ catalyzed synthesis method for imine-linked 3D COFs developed in Chapter 3 is a significant achievement, but its effectiveness has only been demonstrated for COF-300. Further investigation should be conducted into its utility for other imine-linked 3D COFs such as COF-320 to demonstrate its general applicability to all imine-linked 3D COFs. Additionally, this method should be more than just an alternative to solvothermal synthesis. The significantly higher effective of $Sc(OTf)_3$ compared to acetic acid may enable the synthesis of bulkier and more complex frameworks such as the tetraamine-tetraaldehyde COF briefly explored in Chapter 2, which previously suffered from kinetic trapping. Elevated temperatures can be applied in conjunction with $Sc(OTf)_3$ to facilitate more difficult syntheses.

The synthesis of functionalized COF-300 in Chapter 4 was largely unsuccessful owing to steric hindrance of bulky pendant groups, which were uniformly attached to the same phenyl ring as the two aldehyde groups. As such, extension of the linear aldehyde linker by adding an additional phenyl ring may ameliorate the steric hindrance enough to overcome the kinetic trapping observed in Chapter 4. This was demonstrated in the only example of post-synthetic modification of a 3D COF, which utilized a biphenyl diamine linker with a single hydroxy group attached to each phenyl ring[16]. Although the tert-butyldimethylsilyl (TBDMS) protection of the hydroxy groups was unsuccessful, the concept of interpenetration control is vital to fully realizing the potential of 3D COFs as crystalline, controllably porous materials. Similar protection of a more extended linker may prove more successful due to reduced steric and electronic hindrance. In addition, the extension of the linear linker would allow for the incorporation of bulkier protecting groups, such as the photolabile group shown in Scheme 6.3. This group can be photolytically

cleaved post synthesis and its effectiveness in eliminating metal-organic framework (MOF) interpenetration has been demonstrated[17]. More sophisticated approaches to control COF interpenetration might also be derived from techniques successfully implemented in MOF syntheses, such as temperature and monomer concentration control[18], organic bond structure alteration[19], and rational design of organic building blocks[20].

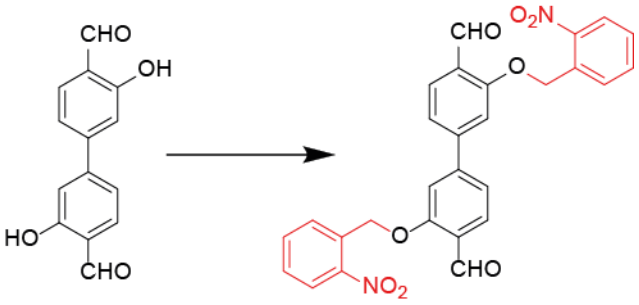

Scheme 6.3. Protection of hydroxy groups in extended aldehyde linker with photolabile protecting group.

6.3 References

1. Ma, X. & Scott, T. F. Approaches and challenges in the synthesis of three-dimensional covalent-organic frameworks. *Commun. Chem.* **1**, 98 (2018).
2. El-Kaderi, H. M. *et al.* Designed Synthesis of 3D Covalent Organic Frameworks. *Science* **316**, 268–272 (2007).
3. Uribe-Romo, F. J. *et al.* A Crystalline Imine-Linked 3-D Porous Covalent Organic Framework. *J. Am. Chem. Soc.* **131**, 4570–4571 (2009).
4. Zhang, Y.-B. *et al.* Single-Crystal Structure of a Covalent Organic Framework. *J. Am. Chem. Soc.* **135**, 16336–16339 (2013).
5. Waller, P. J., Gándara, F. & Yaghi, O. M. Chemistry of Covalent Organic Frameworks. *Acc. Chem. Res.* **48**, 3053–3063 (2015).
6. Huang, N., Chen, X., Krishna, R. & Jiang, D. Two-Dimensional Covalent Organic Frameworks for Carbon Dioxide Capture through Channel-Wall Functionalization. *Angew. Chem. Int. Ed.* **54**, 2986–2990 (2015).
7. Huang, N., Krishna, R. & Jiang, D. Tailor-Made Pore Surface Engineering in Covalent Organic Frameworks: Systematic Functionalization for Performance Screening. *J. Am. Chem. Soc.* **137**, 7079–7082 (2015).
8. Chen, X. *et al.* Locking Covalent Organic Frameworks with Hydrogen Bonds: General and Remarkable Effects on Crystalline Structure, Physical Properties, and Photochemical Activity. *J. Am. Chem. Soc.* **137**, 3241–3247 (2015).

9. Ritchie, L. K., Trewin, A., Reguera-Galan, A., Hasell, T. & Cooper, A. I. Synthesis of COF-5 using microwave irradiation and conventional solvothermal routes. *Microporous Mesoporous Mater.* **132**, 132–136 (2010).

10. Singh, V., Jang, S., Vishwakarma, N. K. & Kim, D.-P. Intensified synthesis and post-synthetic modification of covalent organic frameworks using a continuous flow of microdroplets technique. *NPG Asia Mater.* **10**, e456 (2018).

11. Bisbey, R. P., DeBlase, C. R., Smith, B. J. & Dichtel, W. R. Two-dimensional Covalent Organic Framework Thin Films Grown in Flow. *J. Am. Chem. Soc.* **138**, 11433–11436 (2016).

12. Peng, Y. *et al.* Room Temperature Batch and Continuous Flow Synthesis of Water-Stable Covalent Organic Frameworks (COFs). *Chem. Mater.* **28**, 5095–5101 (2016).

13. Jiang, Y. *et al.* Green, scalable and morphology controlled synthesis of nanofibrous covalent organic frameworks and their nanohybrids through a vapor-assisted solid-state approach. *J. Mater. Chem. A* **2**, 8201–8204 (2014).

14. Medina, D. D. *et al.* Room Temperature Synthesis of Covalent–Organic Framework Films through Vapor-Assisted Conversion. *J. Am. Chem. Soc.* **137**, 1016–1019 (2015).

15. Dalapati, S. *et al.* An Azine-Linked Covalent Organic Framework. *J. Am. Chem. Soc.* **135**, 17310–17313 (2013).

16. Lu, Q. *et al.* Postsynthetic Functionalization of Three-Dimensional Covalent Organic Frameworks for Selective Extraction of Lanthanide Ions. *Angew. Chem.* **130**, 6150–6156 (2018).

17. Jiang, H.-L., Makal, T. A. & Zhou, H.-C. Interpenetration control in metal–organic frameworks for functional applications. *Coord. Chem. Rev.* **257**, 2232–2249 (2013).

18. Zhang, J., Wojtas, L., Larsen, R. W., Eddaoudi, M. & Zaworotko, M. J. Temperature and Concentration Control over Interpenetration in a Metal−Organic Material. *J. Am. Chem. Soc.* **131**, 17040–17041 (2009).

19. Prasad, T. K. & Suh, M. P. Control of Interpenetration and Gas-Sorption Properties of Metal–Organic Frameworks by a Simple Change in Ligand Design. *Chem. – Eur. J.* **18**, 8673–8680 (2012).

20. Farha, O. K., Malliakas, C. D., Kanatzidis, M. G. & Hupp, J. T. Control over Catenation in Metal−Organic Frameworks via Rational Design of the Organic Building Block. *J. Am. Chem. Soc.* **132**, 950–952 (2010).